The role of ATMIN in regulating ATM signalling

Tianyi Zhang

A thesis submitted for the degree of Doctor of Philosophy

University College London

January 2014

Supervisor: Axel Behrens

Mammalian Genetics Laboratory

Cancer Research UK London Research Institute

Declaration

I confirm that the work presented in this thesis is my own. Where information has been derived from other sources, I confirm that this has been indicated in the thesis.

Abstract

Ataxia telangiectasia-mutated (ATM), the protein kinase that is mutated in patients with ataxia telangiectasia (A-T), is a central player in the cellular response to DNA damage. ATM is activated following double-strand breaks by MRE11-RAD50-NBS1 complex (MRN), which acts as an initial sensor of DSB. ATM is also activated by stimuli that change chromatin structure such as chloroquine and hypotonic shock, which depends on the ATM-interactor protein (ATMIN) as a cofactor.

In this study, I show that there exists competition between ATMIN and NBS1 for ATM binding and this can regulate ATM signalling. The absence of one cofactor can lead to enhanced signalling through the alternative pathway. Furthermore, I also characterise the role of an E3 ligase that regulate the interaction between ATMIN and ATM by mediating ATMIN mono-ubiquitination. Thus ATMIN ubiquitination could be an important step in ensuring robust ATM activation after IR.

In addition, I also show that ATMIN is required for ATM signalling after replication stress to protect against genomic instability in the form of anaphase bridges and aberrant chromosome segregations. ATM is activated by replication stress and is required for the formation of 53BP1-containing nuclear bodies, which protect fragile sites. ATMIN interacts with WRNIP and RAD18 in a complex that is required to activate ATM at sites of stalled replication forks.

Furthermore, using a genome-wide screening approach, I identified additional factors that regulate ATM signalling after replication stress. The 8-oxo-guanosine repair pathway could represent a link between ATM signalling and genomic instability. I show that the components of base excision repair pathway are required for the activation of ATM and formation of 53BP1 nuclear bodies that protect fragile sites in the maintenance of genome stability.

Acknowledgements

I would like to thank my supervisor, Axel Behrens, for giving me the opportunity to work in his laboratory and for his guidance and support throughout the PhD. I have learned tremendously from his insight and knowledge, and benefitted greatly from the opportunities to learn many skills and techniques. I am also grateful for his patience and understanding during my PhD.

I am also very grateful to the Axel Behrens lab members for all their guidance, support, encouragement and friendship through these four years. I am thankful to Nnennaya Kanu for introducing me to ATMIN and DNA damage and shared with me her knowledge and experience. I am grateful to Rocio Sancho, who has been a great friend and teacher both in and out of the lab. As the Chinese saying goes, even the most talented cook cannot cook without rice, I am also indebted to Clive Da Costa for taking good care of the lab and ensuring that things ran smoothly. Thank you to all present and past members of the lab who taught me many things, especially Clare Davis, Cristina Aguilera, Sophia Blake, Markus Diefenbacher, Atanu Chakraborty, Catherine Cremona and Janet Cronshaw. I am thankful to Catherine for proof-reading my thesis and teaching me about scientific writing skills. I have been very fortunate to have supportive colleagues who made the work atmosphere cheerful and enjoyable everyday.

I am thankful to Sally Leevers for her guidance throughout the PhD process and my thesis committee, Julie Cooper and Mark Petronzcki for their advice and comments. Thank you to the CRUK High-throughput screening facility, Microscopy facility, FACS lab, Equipment park and other core facilities for their help.

Last but not least, I would like to thank my family and friends for their support and understanding. I am immensely grateful to my families in Singapore, China and France for always being there for me during the ups and downs. Also, it would not have been possible without my loving and understanding husband, Yann Le Gentil, who has been a constant source of positive energy to me. Thank you also to my beautiful daughter, Elise Luxin (Lele), for being the little angel and bringing much laughter and happiness to our lives.

Table of contents

Abbreviations

53BP1	p53 binding protein 1
8-oxoG	8-oxoguanine
A-T	Ataxia telangiectasia
AID	Activation-induced cytidine deaminase
AIM	ATM interaction motif
Aph	Aphidicolin
ASCIZ	Chk2-interacting Zn^{2+}-finger protein
ATLD	Ataxia telangiectasia like disorder
ATM	Ataxia telangiectasia mutated
ATMIN	ATM interacting protein
ATR	ATM and Rad3-related protein
ATRIP	ATM and Rad3-related protein interacting protein
BER	Base excision repair
BLM	Bloom syndrome, RecQ helicase-like
BRCA1	Breast cancer 1
BRCA2	Breast cancer 2
BRCT	BRCA1 C-terminal
CDC	Cell division cycle
CDK	Cyclin-dependent kinase
CSR	Class switch recombination
DAPI	4-6-diamidino-2-phenylindole
DDR	DNA damage response
DMEM	Dulbecco's Modified Eagle's Medium
DMSO	Dimethylsulfoxide
DNA-PKcs	DNA dependent protein kinase catalytic subunit
DSB	Double strand break
DSBR	Double strand break repair
DUB	Deubiquitinase
DYNLL1	L8 Dynein light chain
FANCD2	Fanconi anemia, complementation group D2
FAT	FATC. ATM and TRRAP domain
FATC	FAT C-terminal domain
FCS	Fetal calf serum
FHA	Forkhead associated
GFP	Green fluorescent protein
GSTM	Glutathione S transferase mu
H3K4	Histone 3 lysine 4
H4K16	Histone 4 lysine 16
H4K20	Histone 4 lysine 20
HAT	Histone acetyltransferase
HR	Homologous recombination
HUWE1	HECT, UBA and WWE domain containing 1

IF	Immunofluorescence
Ig	Immunoglobulin
IP	Immunoprecipitation
IR	Ionising radiation
IRIF	IR-induced foci
KAP1	KRAB-associated protein 1
MDC1	Mediator of DNA damage checkpoint 1
MRE11	Meiotic recombination 11
MUTYH	mutY homolog
NBS1	Nijmegen breakage syndrome1
NCS	Neocarzinostatin
NHEJ	Non-homologous end joining
NUDT1	nudix (nucleoside diphosphate linked moiety X)-type motif 1
OGG1	8-oxoguanine DNA glycosylase
PBS	Phosphate buffered saline
PCNA	proliferating cell nuclear antigen
PFA	Paraformaldehyle
pH3	phospho-Histone H3
PI	Propidium Iodide
PI3K	Phosphatidylinositol-3 kinase
PICH	Polo like kinase 1 interacting checkpoint helicase
PIKK	Phosphatidylinositol-3 kinase related kinase
POSH	Plenty of SH3s
ROS	Reactive oxygen species
RPA	Replication protein A
SDS	Sodium dodecylsulphate
SDS-PAGE	Sodium dodecylsulphate-polyacrylamide gel electrophoresis
SH3MD2	SH3 domain containing ring finger 1
SMC1	Structural maintenance of chromosome protein 1
SSB	Single-strand break
TCR	T cell receptor
TEMPOL	4-hydroxy-2,2,6,6-tetramethylpiperidin-1-oxyl
TERF1	Telomere-repeat binding factor 1
TRIM	Tripartite motif protein
TRRAP	transformation/transcription domain-associated protein
UBR5	ubiquitin protein ligase E3 component n-recognin 5
UFB	Ultrafine bridge
V(D)J	Variable (Diversity) Joining
WRNIP1	Werner helicase interacting protein 1

Chapter 1. Introduction

1.1 Canonical ATM signalling after double-strand breaks is mediated by the MRN complex

1.1.1 The role of PIKKs in DNA damage and disease

The ability to maintain genome integrity is fundamental to cell survival and a key contributor to preventing oncogenesis. Cells suffer a wide range of genotoxic insults, such as those generated endogenously by reactive oxygen species from the mitochondria, and by external agents such as UV, drugs that interfere with DNA replication and chemical clastogens. The most severe form of DNA damage is double-strand breaks (DSBs), which are formed as a result of cellular events such as V(D)J and class switch recombination in lymphocytes or meiotic recombination, or a deleterious consequence when a replication fork collapses or telomeres become uncapped. DSBs can also be induced by γ-irradiation and radiomimetics, such as neocarzinostatin and bleomycin. It is estimated that the DSB occurs at a spontaneous rate of approximately 50 per cell cycle per cell in replicating human cells (Vilenchik and Knudson, 2003), which is equivalent to the number of DSBs induced by 2Gy of irradiation. By impeding cellular replication, DSBs could lead to cell death or genomic rearrangements that can predispose the cell for further DNA aberrations and oncogenesis.

Three kinases of the phosphatidylinositol 3 kinase-related (PIKK) kinases family, ATM, ATR and DNA-PK, play central roles in the cellular defence against DNA damage. While ATM and ATR primarily respond and transduce upstream signals following DSBs and ssDNA breaks respectively, DNA-PK regulates downstream DNA repair via the nonhomologous end-joining pathway (Figure 1). Mutations or loss of these kinases lead to radiosensitivity and DNA repair defects, seen in patients as well as in mouse models.

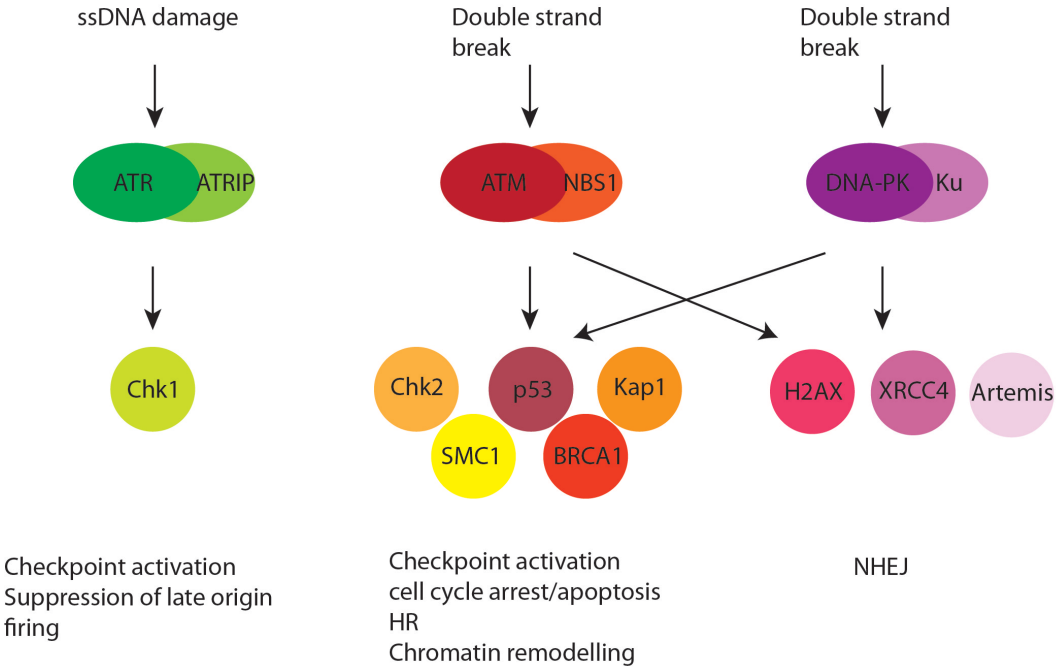

Figure 1: ATM, ATR and DNA-PK activation in response to DNA damage in the presence of their cofactors.

ATR-ATRIP is activated upon ssDNA breaks and phosphorylates Chk1 in order to execute cell cycle checkpoints and suppress late origin firing. ATM is activated by DSB and phosphorylates many downstream substrates to halt the cell cycle and leads to DNA repair, chromatin decondensation and apoptotic responses. DNA-PK is also activated by DSB and promotes NHEJ repair by phosphorylating Artemis and XRCC4. Some substrates are common between the PIKKs such as H2AX and p53.

The Ataxia-Telangiectasia syndrome (A-T) is an inherited autosomal recessive disorder characterised by clinical features such as early onset progressive cerebellar ataxia, ocular telangiectasia, growth retardation, immunodeficiency, neurodegeneration, radiosensitivity and susceptibility to cancer, especially lymphoid tumours (Lavin et al., 2005). The gene responsible for A-T was identified to be *ataxia-telangiectasia mutated* (*ATM*)(Savitsky et al., 1995) that encodes a large protein of 350kDa. Over four hundred mutations in *ATM* have been so far identified, mostly resulting in truncations (Gilad et al., 1996, Byrd et al., 1996). The *Atm* knockout mouse model also shows similar phenotypes of growth retardation, neurologic dysfunction, radiosensitivity and tumour predisposition. In addition, the *Atm* mouse also displays male and female sterility (Barlow et al., 1996).

Other related disorders that have overlapping phenotypes with A-T are due to mutations in the MRN complex (Mre11-Rad50-Nbs1), which functions as a cofactor in recruiting ATM to DSB sites. Nijmegen breakage syndrome occurs due to a mutation in *NBS1*, where most patients harbor a hypomorphic 5bp deletion in exon 6 (657∆5). This results in the generation of 2 truncation proteins, p26 and p70 that encode FHA-BRCT domains and ATM phosphorylation sites respectively. NBS patients have microcephaly, dysmorphic facial features, mild growth retardation, ovarian dysgenesis, immunodeficiency, increased cancer predisposition and radiosensitivity (Digweed and Sperling, 2004). While the clinical phenotypes closely overlap with A-T, there is no cerebellar degeneration. As NBS1 knockout is embryonic lethal, several murine models with truncation mutations have been established to reproduce the human disease. In the $nbs1^{\Delta B/\Delta B}$ model, the BRCT domain of NBS1 was deleted to produce a N-terminal 80kDa truncation protein. This mimics some aspects of NBS, such as radiosensitivity, intra-S checkpoint defect and synthetic lethality with ATM deficiency (Williams et al., 2002). However, there is no cancer predisposition, immunodeficiency or female infertility as observed in humans. Another NBS1 mouse model with N-terminal truncation ($nbs1^{m/m}$) produces more similar phenotypes to human NBS such as thymic lymphoma and female sterility, but does not produce the p70 NBS1 protein found in NBS cells (Kang et al., 2002). Finally, in a humanised NBS1 mouse model, human $hNBS1^{(657\Delta5)}$ was able to rescue the lethality of *NBS1-/-* mice and fully recapitulate the human NBS phenotypes (Difilippantonio et al., 2005).

A single case of NBS-like disorder has been reported as a result of heteroallelic mutation in *Rad50* gene, giving rise to low levels of RAD50 protein. Similar to NBS syndrome, the characteristics are microcephaly, mental retardation, 'bird-like' face, and short stature. Fibroblasts derived from the patient are also characterised by defective ATM signalling after IR, impaired checkpoint responses post IR and radiosensitivity. However, unlike NBS syndrome, there is no immunodeficiency and or cancer incidence. Moreover, the phenotypes of RAD50-deficient cells were rescued by overexpressing wildtype RAD50 (Waltes et al., 2009).

A related, milder form of A-T, AT-like disorder (ATLD) is caused by mutation in *Mre11.* While these patients exhibit similar but milder characteristics of A-T like

cerebellar ataxia and immunodeficiency, there is no known predisposition to cancer (Theunissen et al., 2003). Similarly, *Mre11*$^{ATLD1/ATLD1}$ mice, while having defect in ATM-mediated checkpoint functions, are not prone to lymphoma like *atm-/-* mice (Taylor et al., 2004).

1.1.2 ATM kinase structure and domains

As a member of the PIKK family, ATM is a large protein of 3056 amino acids and shares similarities with related kinases such as ATR, DNA-PKcs (DNA dependent protein kinase catalytic subunit), mTOR (mammalian TOR) and hSMG1(suppressor of mutagenesis in genitalia 1) in its domain structure, with a C-terminal kinase domain flanked by a FAT domain (conserved in FRAP, ATM and TRRAP) and a FAT-C domain, as well as its roles in signalling after cellular stress. TRRAP (transformation/transcription domain-associated protein) is the only member of FAT proteins that lacks catalytic activity. The N-terminus of ATM contains a region (amino acids 91-97) required for binding to substrates such as NBS1, p53 and BRCA1 (Fernandes et al., 2005). The FAT-C domain, on the other hand, is required for interaction with the acetyltransferase TIP60, whose acetylation of ATM on Lys3016 is a crucial step in its activation (Jiang et al., 2006). Recently, it has been shown that damage-induced phosphorylation of Tyr44 of TIP60 promotes the latter binding to chromatin and triggers the ATM acetylation (Kaidi and Jackson, 2013). (Figure 2).

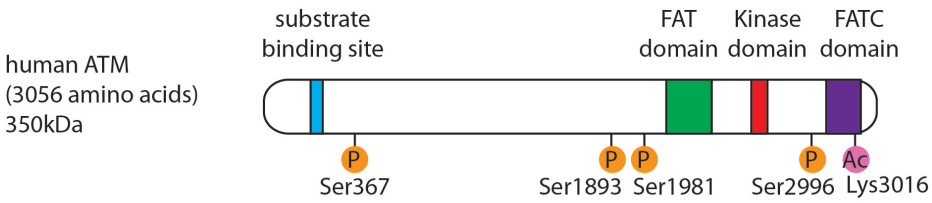

Figure 2. Scheme of ATM major protein domains

ATM has several domains conserved with other PIKK family members such as FAT and FATC domains. Some of the posttranslational modifications on ATM are also indicated.

ATM phosphorylates substrates and itself on Ser/Thr residues that precede a Glu (SQ/TQ motif). Several autophosphorylation sites have been characterised on ATM

that are important for its activation and regulation discussed below. These are Ser367, Ser1893 (Kozlov et al., 2006), Ser1981 (Bakkenist and Kastan, 2003), Ser2996 (Kozlov et al., 2011). While other phosphorylation sites have been identified in large-scale proteomic studies, their exact roles in regulating ATM function have not been elucidated (Matsuoka et al., 2007, Daub et al., 2008, Oppermann et al., 2009).

1.1.3 Mechanism of MRN-dependent ATM activation following IR

1.1.3.1 The roles of the MRN complex and interaction with ATM

The canonical pathway of ATM activation following a DSB involves the upstream sensor MRN complex. MRE11 has both N-terminal phosphoesterase activity and C-terminal DNA binding ability; this enables it to act as a ssDNA endonuclease as well as a 3' to 5' dsDNA exonuclease. Rad50, on the other hand, forms an ABC type ATPase domain with a long antiparallel coiled-coiled domain. MRE11 and RAD50 form a complex that is conserved across all kingdoms that plays an important role in DNA repair (Aravind et al., 1999), through homology directed repair (HDR) and non-homologous end-joining (NHEJ) pathways. The Mre11-Rad50 complex can tether the DNA ends and carry out resection of DSB ends to promote repair (Mimitou and Symington, 2009). Structural studies show that the Mre11-Rad50 forms a heterotetrameric complex with the Rad50 ATPase activity catalysing conformation changes that bind DNA and modulating the exonuclease activity of Mre11 (Hopfner et al., 2001, de Jager et al., 2001). Recent data from small-angle X-ray scattering (SAXS) showed that MRE11 dimers adopt a four-lobed U-shaped structure that is crucial for its assembly and DNA binding (Williams et al., 2008). Using an ATP analog-sensitive mutant of ATM, Lee et al. showed that a "closed," ATP-bound state of MRN is essential for ATM stimulation as well as for NBS1 binding to the complex (Lee et al., 2013).

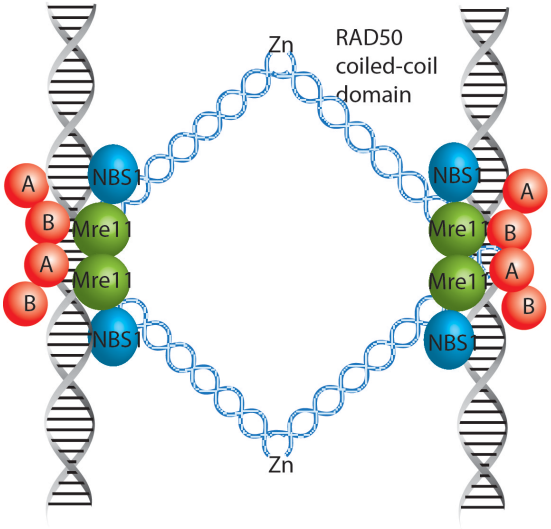

Figure 3. Structure of MRN complex binding to DSB.

The coiled-coil domain of RAD50 mediates dimerisation and formation of the MRN complex, while the Walker A and Walker B domains bind the DSB ends. Mre11 interacts with both NBS1 and RAD50 and can promote resection to facilitate HR repair.

NBS1, unlike the Mre11-Rad50 complex, is conserved only in Eukaryotes and forms a signalling adaptor and regulatory component to recruit signalling proteins such as ATM to site of DNA damage and localises the MRN complex in the nucleus. NBS1 has an FHA (forkhead associated) domain and a BRCT (Breast cancer carboxy-terminal) domain in the N-terminus, which mediates binding to phosphoproteins such as CTIP (Lloyd et al., 2009) and MDC1 (Chapman and Jackson, 2008). NBS1 also has a C-terminal motif that is required for interaction with Mre11 (Desai-Mehta et al., 2001, Tauchi et al., 2001, Williams et al., 2009) and ATM (You et al., 2005) (Falck et al., 2005). Complementation studies using NBS-deficient cell lines and NBS1 constructs that lack the ATM interaction motif (AIM) show that while the AIM is required for ATM phosphorylation of its substrates and rescue of intra-S and G2/M checkpoint functions, it is not required for ATM autophosphorylation, which is the marker of active ATM. Moreover, in vitro studies also showed that NBS1 is dispensable for ATM activation in vitro stimulated by only purified MRE11 and RAD50 (Lee and Paull, 2004). The discrepancy as to whether the NBS1 AIM is required for ATM activation could be due to differences in species and systems used. The current evidence suggests that NBS1 AIM is not absolutely required for ATM autophosphorylation and activation, but is required for recruiting the active ATM and bridging it with other ATM substrates in vivo. Together, the

MRN complex acts as an early, upstream sensor that recruits ATM to the site of a DSB (Carson et al., 2003) (Kitagawa et al., 2004).

The recruitment of MRN complex to DSB is independent of ATM (Mirzoeva and Petrini, 2001). ATM autophosphorylation, DSB retention and target phosphorylation were all impaired in the absence of the MRN complex (Uziel et al., 2003), hence the MRN complex is upstream of ATM in DSB detection and facilitates full ATM activation. Activated ATM, in turn, can phosphorylate MRE11 and NBS1 to stimulate their activity. It was shown in *S.cerevisiae* that MRE11 and the NBS1 homologue, XRS2, are phosphorylated after DNA damage in a manner that depends on TEL1, the yeast homologue of ATM (D'Amours and Jackson, 2001). Several proteomics studies have also provided evidence of phosphorylation on MRE11 by ATM and/or ATR (Matsuoka et al., 2007) (Beausoleil et al., 2004, Kim et al., 1999, Olsen et al., 2006). Evidence also shows that processing of DNA breaks by the MRN complex produce oligonucleotides that stimulate ATM activity in vitro and in vivo (Jazayeri et al., 2008). Hence, the cooperation between ATM and MRN has been shown to contribute to the full activation of ATM signalling.

1.1.3.2 ATM dimer dissociation and autophosphorylation

A crucial step in ATM activation upon DSB involves the dissociation of the ATM dimer into monomers, which coincides with its autophosphorylation of S1981 by the kinase domain (Bakkenist and Kastan, 2003). Bakkenist et al. showed an increase of ^{32}P radioactive label in ATM after IR, in a manner that depended on the kinase activity of ATM. This phosphorylated residue was identified to be S1981, conserved in human, mouse and *Xenopus.* Using phospho-specific antisera, it was shown that the phosphorylation on S1981 (pS1981) increases after IR. Biochemical evidence also showed that S1981 is also important in binding the kinase domain, and transfected wildtype ATM loses binding to wildtype ATM but still interacts with kinase dead or S1981A mutant forms of ATM. Hence, the auto-phosphorylation is a switch in triggering monomerisation of ATM and is important for ATM checkpoint function *in vivo* (Bakkenist and Kastan, 2003). Recently, other ATM phosphorylation sites have been identified by mass spectrometry at Ser367, S1893 and Ser2996. IR induces these phosphorylations in a manner that depends on

ATM kinase activity, and with the exception of Ser2996, immunofluorescence staining using phosphoantibodies shows that they all localise to DSBs like Ser1981. Mutants in these sites fail to rescue IR-induced apoptosis and cell cycle defects in A-T cells and show defective ATM signalling after IR (Kozlov et al., 2006, Kozlov et al., 2011).

However, there has been considerable debate over the requirement for autophosphorylation on ATM. While S1981A ATM has dominant negative activity over wild-type ATM and cannot reconstitute ATM activity in A-T cells (Bakkenist and Kastan, 2003), the S1981A mutant still displays kinase activity *in vitro* (Lee and Paull, 2005). You et al. showed that ATM loading onto DNA fragments could occur prior to autophosphorylation(You et al., 2007). Furthermore, a transgenic mouse model that expresses only S1987A (corresponding to human S1981) mutant ATM showed normal checkpoint responses to IR, ATM recruitment to DSBs and phosphorylation of substrates. Even a triple mutant (Ser367A, Ser1893A, Ser1987A) mouse model retains normal ATM kinase activity and ATM functions in vivo (Daniel et al., 2008). To reconcile these data, it has been shown that ATM autophosphorylation, while not required for initial recruitment to DSB and early signalling, is required for sustained retention of ATM at DSBs (So et al., 2009). An alternative hypothesis suggests that ATM activation follows a two-step model, whereby ATM can first bind DNA and dissociate into monomers without autophosphorylation, followed by MRN-dependent activation and autophosphorylation of ATM (Dupre et al., 2006).

The discrepancy between *in vitro* data and *atm* mouse models could be attributed to species differences in ATM activation or contribution by other factors such as phosphatases and chromatin remodellers *in vivo* that influence ATM activation. Arguably, the differences in results could also stem from different systems and techniques used, such as in vitro DNA fragments for some and high intensity microlaser to generate DSB for others, which could elicit different cellular responses owing to the factors such as chromatin structure, cellular components present and the extent of damage generated.

1.1.3.3 Additional players in the canonical ATM activation

In addition to autophosphorylation, ATM activation also requires the acetylation at Lys3016 by TIP60 histone acetyltransferase (HAT) (Sun et al., 2005, Sun et al., 2007). Mutation of Lys3016 or inactivation of TIP60 HAT activity prevents ATM activation and phosphorylation of substrates, and sensitises cells to IR.

Upon full ATM activation, ATM phosphorylates a number of substrates to further amplify the signalling cascade. H2AX is phosphorylated (γH2AX) along both sides of the break to serve as a platform for the recruitment of downstream factors such as MDC1 (Stucki et al., 2005) that amplifies the DSB signal and induces chromatin modifications. Other substrates such as p53 and CHK2 cause cell cycle arrest at the G1/S and S phase checkpoint respectively, while phosphorylation of SMC1 (Schar et al., 2004) and KAP1 (Noon et al., 2010) regulates chromatin modifications to facilitate access by other DNA repair proteins, and phosphorylation of BRCA1 up-regulates DNA repair (Zhang et al., 2004). The DNA damage response (DDR) is accompanied by many post-translational modifications including phosphorylation, ubiquitination, sumoylation, methylation, acetylation and poly-(ADP)ribosylation as well as epigenetic changes to facilitate the detection and repair of damage. While the canonical pathway is evident after DSB, evidence is mounting that ATM can also be activated by other stimuli in an MRN-independent manner.

1.1.4 Alternative models of ATM activation by chromatin modifications

Recently, it has been shown that oxidative stress can directly activate ATM independently of DNA damage and the MRN complex. Cells that lack ATM display sensitivity to reactive oxygen species (Barzilai et al., 2002). Paull et al. showed that ATM could phosphorylate a subset of its substrates such as p53 and CHK2 after oxidative stress induced by H_2O_2 that does not cause DSB *per se*. They found that oxidation could induce ATM activation by the formation of an intermolecular disulphide bond on C2991 (Guo et al., 2010b). Mutation of this residue abrogated ATM signalling after oxidative stress but does not affect MRN and DNA-dependent

ATM activation. Hence, this finding suggests that ATM could also be activated by dimer formation that is independent of the MRN complex.

Recently, Soutoglou et al. showed, using an elegant system of tethering individual DDR factors via fusion with a fluorescently tagged *E. coli* lacR protein to a stably integrated lacO array in mammalian genome, that ATM-dependent DDR can be activated in the absence of DNA lesions. By tethering NBS1, MRE11 or a fragment of ATM that contains the kinase domain, γH2AX foci formed at the site in an ATM-dependent manner and cells also showed an increase in ATM- and Chk2-dependent G2/M arrest (Soutoglou and Misteli, 2008). Hence, ATM activation can be activated independently of DSBs and the MRN complex, provided that ATM is recruited to the chromatin. In another study, the induction of senescence was shown to trigger pan-nuclear ATM activation and γH2AX formation in the absence of DSBs, although it was unclear what was the molecular stimulus and whether the MRN complex was required (Pospelova et al., 2009).

In addition, ATM can also be activated by hypoxia (<0.1% oxygen), which has been shown to induce replication stress and activation of ATR and ATM (Hammond et al., 2007, Bencokova et al., 2009, Olcina et al., 2010). Under hypoxic conditions, ATM is auto-phosphorylated in a manner that is independent of the MRN complex as well as DNA-PK and ATR. While γH2AX formed foci reminiscent of DSB signalling, neither ATM, pATM nor 53BP1 formed foci after hypoxia (Bencokova et al., 2009). MDC1 was shown to be required for ATM-mediated KAP1 phosphorylation in hypoxia conditions. Moreover, ATM can be activated by UV or hydroxyurea (HU) treatment in an ATR-dependent manner (Stiff et al., 2006). Under these conditions, ATM autophosphorylation and H2AX phosphorylation were unaffected by the ATM inhibitor KU-55933, and ATM activation does not require the C-terminus of NBS1, suggesting a non-canonical, ATR-mediated mode of ATM activation.

1.1.5 DNA repair

Following DSB formation, there are two pathways of repair; the error-prone NHEJ pathway that promotes direct ligation at the DSB ends, and HR that involves resection of DSBs and subsequent error-free repair by using the homologous DNA as a template. While NHEJ is active throughout the cell cycle and is the favoured mechanism in G1 cells, HR predominantly occurs after DNA replication in S and G2 phase when an identical sister chromatid is available.

1.1.5.1 Non-homologous end joining pathway of DNA repair

During NHEJ, the Ku70-Ku80 heterodimer is rapidly recruited to DSBs and encircles the broken DNA ends via its symmetrical ring topology. The crystal structure of Ku heterodimer bound to DNA revealed that Ku does not make specific contacts with DNA bases and backbone, but is positioned to fit into the major and minor grooves of DNA to support the broken ends during end processing and ligation (Walker et al., 2001). Furthermore, Ku has 5'dRP (5'-deoxyribose-5-phosphatase)/AP lyase activity, which facilitates the removal of abasic sites near DSBs and favour NHEJ pathway over HR (Roberts et al., 2010).
The binding of Ku to DNA is required for recruitment of DNA-PKcs, which in turn facilitates the translocation of Ku to the extreme DNA termini (Yoo and Dynan, 1999) (Calsou et al., 1999). Subsequent assembly of the XRCC4-ligase IV complex, which is responsible for the ligation step, is also dependent on the Ku and DNA-PKcs as well DNA-PKcs-mediated phosphorylation (Chen et al., 2000, Calsou et al., 2003, Nick McElhinny et al., 2000). In addition, XLF4 (XRCC4-like factor) is also recruited by Ku and stimulates the activity of XRCC4-ligase IV (Hentges et al., 2006) (Tsai et al., 2007). Artemis endonuclease is an additional described NHEJ component that is mutated in radiosensitive severe combined immunodeficiency (RS-SCID) sydrome (Moshous et al., 2001). Artemis is required during end-processing for the repair of a subset of IR-induced DSBs (10%) in an ATM- and DNA-PK dependent manner (Riballo et al., 2004, Lobrich and Jeggo, 2005).

Another pathway of error-prone end joining is the microhomology-mediated end joining (MMEJ) which involves limited resection (4-6 nucleotides) and the use of 5-25bp of microhomologous sequence for annealing prior to the rejoining of broken

ends, thereby resulting in a deletion of the flanking sequence. There are evidence for the inhibitory effects of NHEJ proteins on MMEJ, such as Ku and DNA-PK, hence MMEJ might serve as an alternative repair mechanism when NHEJ fails to complete or when DNA ends are not compatible with NHEJ repair (McVey and Lee, 2008).

1.1.5.2 DNA repair by homologous recombination

In comparison, HR is initiated by extensive 5'-3' resection of DNA ends by the MRN complex aided by Sae2/CtIP to generate 3' ssDNA tails. DNA resection is regulated in a cell-cycle dependent manner by phosphorylation of CtIP Ser847 by CDK2 (Huertas and Jackson, 2009), which is required for effective ssDNA generation, RPA recruitment, and RPA phosphorylation at DSBs. Following resection, the ssDNA ends are rapidly coated by RPA and replaced by RAD51 faciliated by RAD52. The formation of RA51 nucleofilaments allows homology search and strand invasion. BRCA2 interacts with RAD51 via its BRC repeat and the C-terminus to facilitate the Rad52 recombinase activity (Xia et al., 2001, Moynahan et al., 2001). A double holliday junction intermediate is generated, which could be either resolved by resolvases including Mus81-EME1, SLX1/SLX4 and GEN1 (Wyatt et al., 2013) to form crossover products, or undergo dissolution by BLM-TOPOIIIα-RMI1/2 to form non-crossover products (Wu and Hickson, 2006).

1.1.5.3 ATM is required for the repair of DSBs in heterochromatin

Whilst the majority of DSBs are repaired rapidly within 4-6 hours in a manner that is independent of ATM and its downstream substrates, a slower repair is observed (>8hours) for a subset heterochromatin-associated, which is refractory to repair and requires ATM and KAP1 (Murray et al., 2012). Kap1, a transcriptional corepressor that associates with heterochromatin, is phosphorylated by ATM at Ser847 after IR (Ziv et al., 2006) and its rentention on heterochromatin also decreases after IR (Goodarzi et al., 2008). The knockdown of Kap1 rescues the DSBR defect after ATM inhibition, and also alleviates a similar defect after the knockdown of 53BP1, RNF168 and RNF8. Hence, Kap1 plays a role in the ATM- and 53BP1-dependent repair of DSBs in heterochromatin. Using immunofluorescence readouts, Noon et al showed that pKap1 was pan-nuclear at early time point post-IR, but localised to

discrete foci that colocalised with heterochromatin markers at 4-8 hours post-IR. The formation of late pKap1 foci was dependent on 53BP1, which was proposed to act by promoting MRN accumulation and thereby concentrating ATM activity at late-repairing DSBs (Noon et al., 2010).

1.2 ATMIN defines an NBS1-independent pathway of ATM activation

1.2.1 ATMIN as a novel interactor of ATM

Other forms of chromatin modifications which do not cause DSB *per se*, such as hypotonic shock and chloroquine which causes chromatin decondensation (Kobliakova Iu et al., 2001) (Mahut et al., 2012), can also activate ATM without the requirement of NBS1, as shown by Nbs1-null cells which can still activate ATM following these stimuli (Difilippantonio et al., 2005).

ATMIN was recently identified as an ATM interacting protein that stabilises ATM and which is required for ATM signalling after these chromatin modification stimuli but not after IR-induced DNA damage (Kanu and Behrens, 2007). While a truncated version of the protein was firstly identified as ASCIZ (ATM/ATR-substrate CHK2-interacting Zn^{2+} finger protein) (McNees et al., 2005), the full protein was subsequently found to contain two additional N-terminal exons. ATMIN has a C-terminal ATM interaction motif that is homologous to that of NBS1, a putative PEST sequence associated with ubiquitin-mediated proteolysis, and 18 SQ/TQ ATM phosphorylation motifs (Figure 4). As shown by immunofluorescence and co-IP, ATMIN interacts with ATM under basal conditions but not after IR. Moreover, the dissociation of ATMIN from ATM post-IR was also shown to be dependent upon NBS1, suggesting a non-overlapping role of ATMIN with NBS1. An ATMIN knockout mouse model was generated by using PGK-cre and lox P sites flanking exon 4, which encode most of the protein (amino acids 209-818), from germline stage (Kanu and Behrens, 2007). MEFs derived from these mice with a homozygous germline deletion of *atmin* exon 4 do not express detectable ATMIN protein, hence resulting in a null mutation. ATMIN knockout is embryonic lethal but heterozygotes are viable and fertile. Moreover, ATMINΔ/Δ MEFs shows impaired ATM signalling after hypotonic shock and replication stress. Hence ATMIN is required for ATM activation under these non-canonical stimuli.

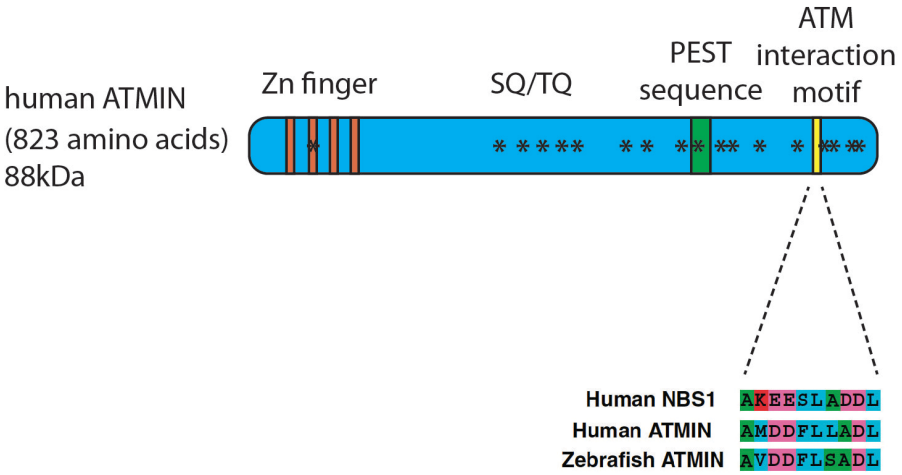

Figure 4. ATMIN domains showing N-terminal zinc fingers, putative PEST domain and C-terminal ATM interaction motif that is homologous to that of NBS1.

Another report suggested a function for ATMIN in DNA repair of DNA alkylating damage. ATMIN was reported to form foci after methylmethane sulphonate (MMS), that colocalise with Rad51 (McNees et al., 2005). Moreover, in the absence of ATMIN, Rad51 foci formation after MMS is impaired and this is accompanied by increased cell death. The increased apoptosis in ATMIN depleted cells was dependent on the presence of MLH1, a DNA endonuclease that functions in mismatch repair. Since mismatch repair involves the formation of a ssDNA gap intermediate, the data suggests that ATMIN is downstream of MLH1 and is recruited to form foci at ssDNA gaps. However, there is a lack of evidence that ATMIN colocalises with RPA, a protein that coats ssDNA, or biochemical data to support the hypothesis that ATMIN binds preferentially to ssDNA. While the colocalisation of ATMIN and RAD51 foci implies a role of ATMIN in DNA repair, there is insufficient evidence to show the effect of ATMIN on homologous recombination (HR) and other repair pathways such as non-homologous end joining (NHEJ). Indeed, another study used ATMIN knockout chicken DT40 cell line to study Immunoglobulin (Ig) gene conversion, which leads to the diversification of Ig V segments initiated by activation-induced deaminase (AID) and repair by HR or translesion synthesis-dependent hypermutation. While the loss of ATMIN increased Ig conversion, the efficiency of DSB repair by HR or BER-dependent hypermutation was not affected. Hence, ATMIN does not directly control homologous recombination or formation of abasic sites (Oka et al., 2008).

In addition to a possible role in DNA repair, ATMIN is also required for ATM signalling triggered by oxidative stress. *atmin*$^{\Delta/\Delta}$ MEFs are more susceptible to oxidative damage and show impaired recruitment of ATM to basal ROS-induced DNA damage (Kanu et al., 2010). Using an *atmin*$^{f/f}$; *nestin-cre* model to conditionally delete ATMIN in the mouse brain, our laboratory observed increased loss of neurons associated with aging and impaired ATM activation in spite of greater accumulation of γH2AX in aging ATMINΔN mouse brains.

While ATMIN acts as a cofactor for ATM activation under specific stimuli, the ATMIN-ATM pathway seems to activate similar downstream ATM phosphorylation substrates as NBS1-dependent ATM signalling, such as KAP1, SMC1 and p53. Hence, these substrates shall be used in assessing ATM pathway activation in this thesis. It is not clear whether ATMIN directs ATM to additional substrates, as this awaits further studies using results from ATMIN genome screen (Section 6) and other proteomic analysis.

1.2.2 Role of ATMIN as a transcription factor

ATMIN has been implicated as a transcription factor from evidence that tethering ATMIN to yeast Gal4-DNA binding domain or luciferase reporters can transactivate reporter genes (Jurado et al., 2010). Two studies further showed *Dynll1* as a transcriptional target of ATMIN as identified from yeast-two-hybrid screens (Jurado et al., 2012a) (Rapali et al., 2011). As a regulator of protein dimerisation, DYNLL can interact with ATMIN and regulate its foci formation after MMS, and was also identified as a target in a siRNA screen for loss of ATMIN foci formation. Interestingly, the binding of DYNLL dampens the transcription activation by ATMIN, thereby forming an auto-feedback loop that limits DYNLL expression (Jurado et al., 2012a). However, while the SQ/TQ cluster on ATMIN was shown to be sufficient for activation of yeast and luciferase promoters, in the latter study transcription was dependent on ATMIN zinc fingers in mammalian cells. It is also not clear whether the DYNLL-ATMIN interaction is important for cell viability and whether it is DNA damage-dependent. While Rapali et al. reported that the overexpression of DYNLL also blocked ATMIN foci formation, Jurado et al. observed that overexpressed DYNLL colocalised with overexpressed ATMIN and knockdown of DYNLL impairs

ATMIN foci formation. Hence, more evidence is needed to understand the physiological role of ATMIN as a transcription factor.

1.2.3 Role of ATMIN in the development of the immune system and other organs

ATMIN also plays a role in the maturation and safeguarding of the genomic stability of immune cells. Using *CD19-cre; atmin*$^{f/f}$ to delete ATMIN from the pro-B cell stage (*atmin*$^{\Delta B/\Delta B}$), previous work from our laboratory showed that loss of ATMIN impaired B cell maturation and class switch recombination (CSR) (Loizou et al., 2011). Moreover, *atmin*-null B cells displayed reduced ATM signalling in response to hypotonic shock. More strikingly, the physiological importance of ATMIN is highlighted by the high frequency of B cell lymphoma (40% of cohort after 6 months of age) in *atmin*-null animals. This is further supported by transcriptional profiling data from human patients with B cell acute lymphoblastic leukemia (B-ALL) that *atmin* expression was reduced in B-ALL compared to normal B cells. Hence, ATMIN could be a tumour suppressor in the development of human B cell lymphomas.

A similar finding was reported that showed the loss of ATMIN resulted in defect in B cell development (Jurado et al., 2012b). An *atmin*$^{f/f}$*; Mx1-cre* model was used, which activates *cre* upon interferon or polyinosinic:polycytidylic acid injection. However, the authors did not observe B cell lymphoma due to loss of ATMIN but a reduction in mature B cell numbers. The basis of the phenotype was attributed to ATMIN transcription factor function in regulating DYNLL, which attenuates the pro-apoptotic effect of Bim, since the B cell lymphopenia was rescued by crossing with Bim knockout. Bim has been shown to induce apoptosis in auto-reactive B cells, but the physiological role and expression level of Bim in normal, non-autoreactive B cells is not clear. Hence, whether the effect of ATMIN on B cell maturation is via ATM signalling or DYNLL transcription regulation will require more data for elucidation. However, since the phenotype of *atmin*$^{\Delta B/\Delta B}$ mice closely resemble that of *atm*-/-, such as normal mature B cell numbers, defective CSR and genomic instability, and both *atmin*$^{\Delta B/\Delta B}$ mice and human A-T patients have increased

lymphoma susceptibility, these suggests that ATMIN's role in DNA damage signalling could be more relevant, but at this stage we cannot rule out the possibility that its transcriptional function also plays a role.

In addition to the immune system, ATMIN is also essential for normal development of the lungs and brain. *atmin* -null embryos fail to develop lung and trachea even though they are able to initially specify the respiratory endoderm. However, they are unable to remodel the endoderm required for initiation of lung budding and trachea formation (Jurado et al., 2010). ATMIN null embryos also display exencephaly (25% of embryos), which indicate that ATMIN is required for neural tube development. Deletion of ATMIN in the central nervous system (CNS) using *nestin-cre* also leads to greater neurodegeneration in old mice compared to controls animals (Kanu et al., 2010).

1.3 The functions of ubiquitination in ATM signalling

Post-translational modifications play an important role in regulating protein activity, interaction and stability. One of the most prevalent modifications, ubiquitination, has been identified as a key modulator of the DDR. As well as the DDR following DSBs, the Fanconi anemia pathway for the repair of interstrand crosslinks during DNA replication, and DNA damage bypass by translesion synthesis also rely on ubiquitination in their activation and signalling cascade. While the primary function of the ubiquitin system is the regulation of proteasome-dependent proteolysis, increasing evidence points towards the importance of non-degradative ubiquitination in the context of DNA damage signalling.

1.3.1 Components of the ubiquitin system

The ubiquitin system comprises of three key enzymes and the 76-amino acid ubiquitin moiety. An ubiquitin activating enzyme (E1) first uses ATP to covalently attach the ubiquitin moiety to itself via a cysteine to form E1~Ub thioester intermediate. Then the ubiquitin is transferred onto a cysteine residue on a ubiquitin conjugating enzyme (E2), before being passed onto a substrate by a ubiquitin ligase enzyme (E3). RING domain E3 ligases, such as the SCF (Skp, Cullin, F-box containing) complex usually form large, multi-protein complexes that bridges between the E2 and the substrate. Moreover, the E2 usually dictates the substrate specificity and chain linkage type, whether it is K63, K48, K11 linkage etc. HECT domain E3s, on the other hand, contain an active site cysteine that gets charged with the ubiquitin from E2 before transferring it to the substrate acceptor lysine residue. Hence, HECT domain E3s need to recognise both the E2 and the substrate and usually determine the substrate specificity (Komander and Rape, 2012) (Figure 5). In mammals, ubiquitination involves two E1s, over 35 E2s, and over 600 E3s (Jackson and Durocher, 2013). Given the large number of E2s and E3s identified so far, it is likely that there are many more substrate selection and ubiquitin linkage topologies possible. Ubiquitin chain formation can occur at any of the seven internal lysine residues of ubiquitin, and result in different topologies and functions, such as mono-, multi-mono- and polyubiquitination. Polyubiquitin chains can be homotypic (a single type of linkage, such as Lys6) or heterotypic (more than one linkage type). The latter can also take on a linear or

branched topology. While Lys48 chain formation targets the substrate for proteolysis, Lys63 plays a role amplifying DDR signal at DSB. Recently, other atypical ubiquitin chains have also been identified. Lys6-chains are made by BRCA1/BARD1 E3 ligase during DDR, Lys11-chains have been implicated in proteasome degradation and endocytosis, Lys27 plays a role in autophagy of the mitochondria, Lys29 functions together with Lys48 chain linkage in ubiquitin fusion degradation, and Lys33 linkage plays a role in regulating protein interaction in the T cell receptor signalling (Kulathu and Komander, 2012).

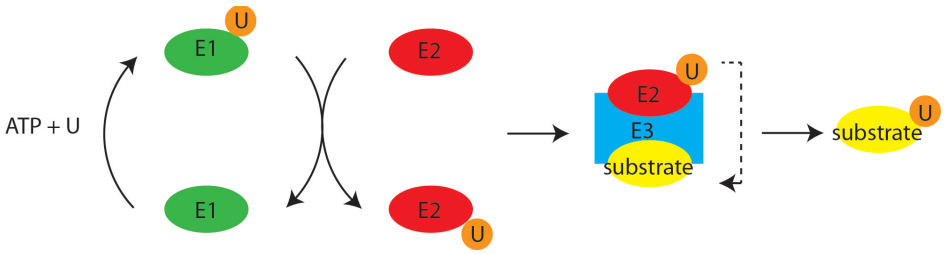

Figure 5. HECT domain E3 ligase-mediated ubiquitination reaction.

The ubiquitination reaction is initiated by an E1 enzyme that uses ATP to form a charged E1-Ubi intermediate. Then the ubiquitin is transferred onto a cysteine residue on an ubiquitin conjugating enzyme (E2), before being passed onto a substrate by an ubiquitin ligase enzyme (E3). HECT domain E3s need to recognise both the E2 and the substrate in order to accept the charged ubiquitin from the E2 before transferring it to the substrate acceptor lysine.

Another aspect of ubiquitination is the reversibility of signalling; the ubiquitin code can be removed by deubiquitinases (DUBs). Human cells contain approximately 100 DUBs that reverse the activity of E3s; these include ubiquitin C-terminal hydrolases (UCHs), ubiquitin-specific proteases (USPs), ovarian tumour proteases (OTUs), Josephin domain DUBs and JAMM (JAB1/MPN/MOV34) family DUBs (Komander et al., 2009). While it is still unclear how the specificity of linkage recognition by DUBs is achieved, DUBs can be highly specific for their substrates, for instance POH1 shows Lys63 linkage specificity towards its substrate histone H2A (Cooper et al., 2009). In addition to simply reversing the activity of E3s, DUBs add another level of regulation and control; DUBs may bind an E3 that auto-ubiquitinates itself and thereby stabilise the E3, DUBs may help to switch off activated signalling pathways, DUBs can also fine-tune ubiquitination of a substrate by acting on both the substrate and E3 (such as in the case of USP7 acting on MDM2 and p53 (Brooks et al., 2007), and by coupling E3 and DUB

activity on a single protein allow concomitant regulation of many substrates (Wertz et al., 2004).

Here, I shall focus on the functions of ubiquitin in regulating the DDR, especially in response to DSBs that are sensed by the MRN complex and trigger ATM signalling.

1.3.2 Ubiquitin-Based DSB Signalling by RNF8 and RNF168

Upon the formation of a DSB, ATM activation by the MRN complex leads to a myriad of phosphorylation and ubiquitination events, which serve to amplify the signal and increase retention of DNA repair factors at the damage site. ATM phosphorylates H2AX, which in turn recruits MDC1 via the latter's BRCT domain (Stucki et al., 2005). MDC1 is also a substrate of ATM phosphorylation, and has been shown by biochemical and structural studies to interact and recruit RNF8 to the site (Mailand et al., 2007, Kolas et al., 2007, Huen et al., 2007). RNF8 is a RING domain E3 ligase that works with UBC13 to add Lys63 linked ubiquitin chains on target proteins such as H2A (Wang and Elledge, 2007). The activity of RNF8 is facilitated by HERC2 (HECT domain and RCC1-like domain-containing protein 2), a HECT domain-containing protein whose recruitment to DSBs is itself dependent on RNF8 and MDC1. HERC2 interacts with RNF8 and enhances the RNF8-UBC13 interaction, such that RNF8 is stabilised and its Lys63-type ubiquitination of substrates is increased (Bekker-Jensen et al., 2010). Contributing to the ubiquitination signal, RNF168 also works with UBC13 to amplify Lys63-type ubiquitination at DSBs. RNF168 is recruited by ubiquitinated products of RNF8, such as ubiquitinated H2A, and also by its own ubiquitination products. Interestingly, while an RNF8-UBC13 fusion protein can rescue the recruitment of 53BP1 foci that arise due to loss of RNF8 or UBC13 alone, it cannot rescue the same phenotype after knockdown of RNF168, suggesting that RNF168 is crucial for boosting the ubiquitination signal in order to retain repair factors at DSBs. Bilallelic mutations in *rnf168* result in the recessive RIDDLE syndrome (Radiosensitivity, immunodeficiency, dysmorphic features, and learning difficulties), that results from failure to localise 53BP1 to DSB sites (Stewart et al., 2007) (Stewart et al., 2009). Recently, the site of RNF168 ubiquitination on H2A and H2AX was identified to be primarily Lys13 and Lys15 (Gatti et al., 2012,

Mattiroli et al., 2012). Together, RNF8 and RNF168 E3 activity creates a Lys63- and mono-ubiquitin signalling platform that functions in the recruitment and retention of downstream repair factors such as 53BP1 and the RAP80/BRCA1 complex.

In addition to RNF8 and RNF168, the Polycomb E3 ligase RING1B/BMI1 can also monoubiquitinate H2A, but on residue Lys119 located away from the Lys13/15 site. (Wu et al., 2011a, Pan et al., 2011, Ismail et al., 2010, Ginjala et al., 2011). This modification could provide an additional independent mechanism to facilitate transcriptional silencing around the damage site (Shanbhag et al., 2010, Chagraoui et al., 2011). (Figure 6)

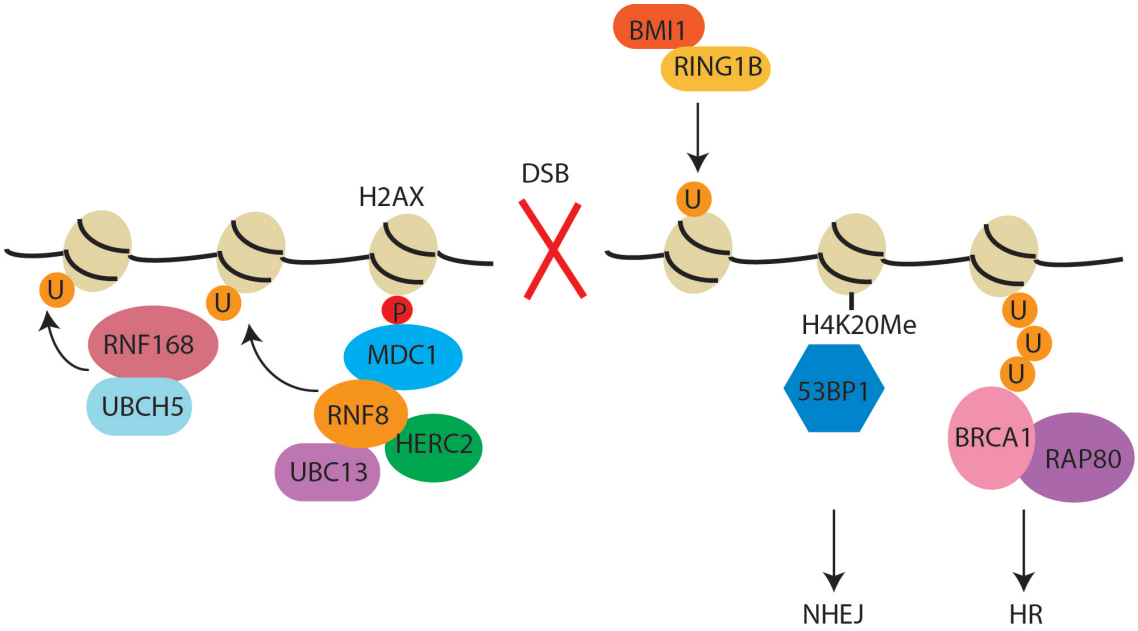

Figure 6. Ubiquitin cascade in the DSB response.

Upon DSB formation, ATM phosphorylates H2AX, which recruits MDC1. ATM-dependent phosphorylation of MDC1 creates a signalling platform to recruit RNF8. Together with UBC13 and facilitated by HERC2, RNF8 ubiquitinates H2A and H2AX via K63 linkage. The initial ubiquitination is further amplified by the recruitment of RNF168 to ubiquitinated H2A. RNF168, together with its E2 UBCH5, further amplifies the K63 ubiquitin linkage on flanking chromatin. In addition, BMI1/RING1B also ubiquitinates H2A independently on the C-terminus. DSB-induced chromatin ubiquitination, in addition to other chromatin modifications such as H4K20 methylation, is necessary for the recruitment of 53BP1 and BRCA1-RAP80 complex, which promotes NHEJ and HR respectively.

1.3.3 Role of ubiquitination in recruitment of 53BP1

53BP1 is a downstream mediator of MRN-dependent ATM signalling and also forms foci that colocalise with γH2AX in response to DSBs. The loss of 53BP1 leads to mild defects in ATM signalling, such as slightly reduced KAP1 phosphorylation (Noon et al., 2010) and checkpoint function (Shibata et al., 2010). By contrast, 53BP1 has a prominent role in DNA repair. It has been suggested that 53BP1 amplifies ATM signalling by concentrating more MRN-ATM complex via its BRCT domain (Noon et al., 2010, Lee et al., 2010). As such, 53BP1 is required for pKAP1 foci formation at late-repairing heterochromatic sites (Noon et al., 2010). The ATM-dependent phosphorylation of KAP1 is required to disperse CHD3 from heterochromatin and thereby facilitate chromatin relaxation and repair of damage (Goodarzi et al., 2011). 53BP1 is also required for NHEJ of uncapped telomeres by increasing the mobility of chromatin ends, which in turn move through larger nuclear territories (Dimitrova et al., 2008). In a similar way, 53BP1 promotes long range synapsis of DNA ends during V(D)J recombination and class switch recombination (CSR). *53bp1*-/- mice have reduced B and T lineage cells and thymocytes display more genomic aberrations, a loss of TCR (T-cell receptor) loci and increased apoptosis (Difilippantonio et al., 2008), due to defective long range V(D)J recombination. 53BP1 oligomerisation that occurs independent of DNA damage is thought to be important in bridging DNA ends together during synapsis. *53bp1*-/- mice also have defective CSR over long distances: this was supported by evidence that 53BP1 promotes intra-chromosomal end joining of I-SceI induced DSB ends separated by 96kb, but not proximal or trans-chromosomal ends (Bothmer et al., 2011). 53BP1 also protects DNA ends from resection (Bothmer et al., 2010, Bunting et al., 2010), and the loss of 53BP1 can rescue the embryonic lethality of *brca1-/-* by blocking HR, albeit with a resulting high level of genomic instability (Cao et al., 2009). Recently, RIF1 was identified as the downstream target of 53BP1 that counteracts BRCA1-mediated HR. (Chapman et al., 2013, Di Virgilio et al., 2013, Escribano-Diaz et al., 2013, Feng et al., 2013, Zimmermann et al., 2013).

The evidence that *rnf168*-/- mice share a similar phenotype as *53bp1-/-* mice in defective long range V(D)J recombination, and that RNF168 is required for 53BP1 foci localisation onto DNA, strongly suggests that ubiquitination plays an important

role in 53BP1 recruitment. Its recruitment to foci was shown to be dependent on its tandem Tudor domains, which bind dimethylated Histone4 Lys20 (H4K20me2) (Botuyan et al., 2006). Accumulating evidence suggests that the ubiquitination of H2A and H2AX by RNF8 and RNF168 allows the histone methylation marks to become more accessible, thereby facilitating 53BP1 recruitment (Stewart et al., 2009, Doil et al., 2009, Bekker-Jensen et al., 2010, Mailand et al., 2007, Huen et al., 2007). RNF8 has been shown to act synergistically with CHFR (checkpoint protein with FHA and Ring domain) to allow H4K16 acetylation, which leads to chromatin relaxation and is required for ATM signalling after IR (Wu et al., 2011b). More biochemical data will be required to fully elucidate the mechanism by which 53BP1 is recruited to DSB.

1.3.4 Role of ubiquitination in the regulation of BRCA1

BRCA1 is required for efficient repair of DSB by HR, as well as transcription-coupled DNA repair, DNA crosslink repair and checkpoint control. BRCA1 has a N-terminal RING domain, a central SQ/TQ cluster, and two C-terminal BRCT domains. BRCA1 is phosphorylated post-IR in an ATM-dependent manner (Gatei et al., 2000a), but its recruitment into foci was not changed in A-T cells or after ATM inhibitor treatment. BRCA1 activation also requires phosphorylation by CHK2 (McGowan, 2002) or interaction with CHK1 (Joughin et al., 2005). In addition, chromatin ubiquitination set up by RNF8 and RNF168 is also crucial for BRCA1 recruitment (Lukas et al., 2011b).

BRCA1 associates with its partner BARD1, forming a dimeric RING-domain E3 ligase. This interaction stabilises both proteins *in vivo* and enhances BRCA1 E3 activity *in vitro* (Xia et al., 2003). BRCA1 retention on DSBs requires interaction with the RAP80 complex, but the latter is dispensable for the initial recruitment of BRCA1 (Yin et al., 2012, Hu et al., 2011). Hence, it remains unclear how BRCA1 docks onto ubiquitin conjugates. Another open question is whether the E3 activity of BRCA1 is required for HR and tumour suppression. Using a RING mutant knock-in, Shakya et al. showed that *Brca1*^{I26A} mice display normal HR with no elevated tumour predisposition (Reid et al., 2008, Shakya et al., 2011). A similar mutation in chicken DT40 cells, however, results in hypersensitivity to DNA damage induced by camptothecin (Sato et al., 2012). On the other hand, another

BRCA1 RING mutant (C61G) does lead to embryonic lethality and DNA repair defects, but it could be due to the disrupted interaction with BARD1 rather than loss of BRCA1 E3 activity (Drost et al., 2011). Hence, more evidence is required to ascertain the role of BRCA1 E3 activity in its function.

Downstream, BRCA1 interacts with CtIP via its BRCT domain and promotes the resection ability of CtIP to generate longer tracks of ssDNA for HR. On the other hand, RAP80 associates with BRCA1 and restrains excessive resection of ssDNA (Coleman and Greenberg, 2011, Hu et al., 2011). CtIP has been shown to be a target of BRCA1 E3 activity, which adds Lys6-ubiquitin chains but does not seem to target CtIP for degradation (Yu et al., 2006). Rather, CtIP ubiquitination could be required for recruitment and colocalisation with BRCA1 into IR-induced foci (IRIF). As another important negative regulator of BRCA1 resection, 53BP1 has been identified to restore HR and viability after PARP inhibition in *Brca1-/-* cells (Cao et al., 2009, Bunting et al., 2010) (Bouwman et al., 2010) (Figure 7).

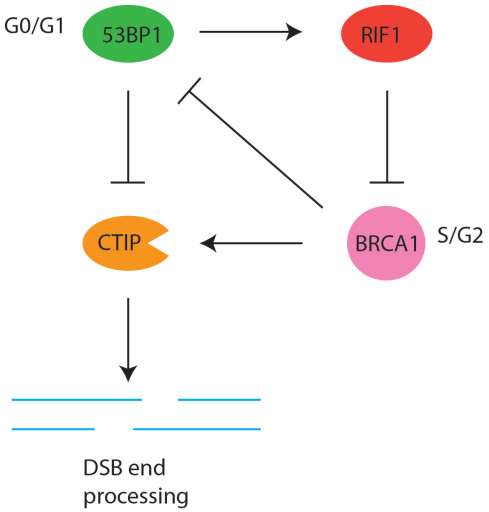

Figure 7. 53BP1 and BRCA1 regulates the balance between NHEJ and HR modes of DNA repair.

During G0/G1, where BRCA1 is not normally present, 53BP1 inhibits the end-resection function of CtIP. RIF1, a downstream target of 53BP1, also blocks BRCA1-mediated HR. During S phase, BRCA1, by an unknown mechanism, inhibits this function of 53BP1 at DNA breaks, while also promoting CTIP-mediated end resection activity to facilitate HR.

1.3.5 UBR5 as a new player in the DNA damage response

UBR5 (Ubiquitin protein ligase E3 component n-recognin 5, also known as EDD or HYD) was first identified in mammalian cells, by differential display, as a progestin-regulated gene (Callaghan et al., 1998) and a potential HECT domain E3 ligase with the ability to bind ubiquitin *in vitro*. It is also a homolog of the tumour suppressor gene in *Drosophila, Hyperplastic discs (hyd)* (Mansfield et al., 1994). Temperature-sensitive mutation of UBR5 in *Drosophila* leads to the overgrowth of imaginal discs, suggesting that it is required for the regulation of cell proliferation (Figure 8).

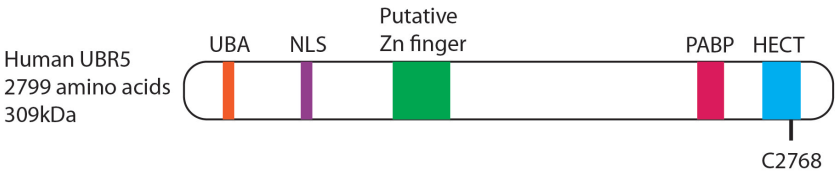

Figure 8. Domain structure of UBR5.

UBR5 has a N-terminal ubiquitin-associated domain (UBA) which can binds mono- as well as poly-ubiquitin chains, a nuclear localisation signal (NLS), and a putative zinc finger in N-recognin family, a recognition component of the N-end rule pathway. It has a C-terminal HECT domain with a catalytic cysteine residue at C2768. Moreover, UBR5 has a poly-(A) binding protein domain (PABP) that mediates binding to and regulation of mRNA.

The first link of UBR5 to DDR came from a yeast-two-hybrid study that showed UBR5 interacted with TOPBP1, and the interaction required two BRCT domains of TOPBP1. Moreover, UBR5 can ubiquitinate TOPBP1 in vitro in the presence of E1 and UbcH4 (Honda et al., 2002). The evidence for direct ubiquitination of TOPBP1 in vivo was less convincing, as the authors showed separately that Flag-HYD overexpression results in the formation of ubiquitination substrates, and Flag-TOPBP1 can be ubiquitinated *in vivo*. The ubiquitination of TOPBP1 was augmented by proteasome inhibition (MG132), suggesting a degradative form of ubiquitination, and was seemingly strongly reduced upon IR, even in the presence of MG132. However, one cannot distinguish whether IR prevents the ubiquitination of TOPBP1 in the first place, or accelerates the DUB activity.

UBR5 was also shown to regulate CHK2 phosphorylation after IR and interacts with the FHA domain of CHK2 (Henderson et al., 2006). Loss of UBR5 led to

decreased CHK2 T68 phosphorylation but did not affect other substrates including ATM autophosphorylation. Moreover, the knockdown of UBR5 resulted in increased colony formation after treatment with radiomimetic drugs and defective G2/M checkpoint post IR. However, it is not clear whether this depended on its E3 ligase activity (Henderson et al., 2006). In addition, UBR5 has also been reported to negatively regulate ATM-dependent p53 Ser15 phosphorylation and target gene expression after DSBs (Ling and Lin, 2011), in a manner that is independent of its E3 ligase activity. Hence, while UBR5 affected DSB-induced CHK2 and p53 phosphorylation, the mechanism remains enigmatic, as it did not regulate their protein stability.

UBR5 also contains a PABP domain in the C-terminus, which suggest a possible role in mRNA metabolism. The X-ray structure of the C-terminus also suggests a homology to PABP (Poly-A binding protein) (Deo et al., 2001). PABP binds to the 5' end of mRNA and is required for translation initiation. Paip1 and 2 (PABP-interacting protein) negatively regulate PABP and UBR5 was shown to target Paip2 for degradation (Yoshida et al., 2006). In mouse, UBR5 is required for yolk sac vascularization and chorioallantoic fusion and UBR5 knockout is embryonically lethal at E10.5 (Saunders et al., 2004). In human, UBR5 was found overexpressed and amplified in a number of cancers including breast and ovarian cancers, thereby highlighting its importance in tumourigenesis (Clancy et al., 2003).

1.3.6 Switching off the damage-induced ubiquitination cascade

To ensure the reversibility of signalling, damage-induced ubiquitination is also highly regulated. A recent study identified TRIP12 and UBR5 in a siRNA-based screen that is responsible for suppressing RNF168 chromatin loading and retention (Gudjonsson et al., 2012). While the knockdown of these E3 ligases leads to expanded 53BP1 and RNF168 foci, it is not clear how they exert their inhibitory effect on RNF168, whether by proteolysis or other mechanisms. Several other DUBs also regulate the ubiquitin response, such as BRCC36, which is directed by the ubiquitin-recruited RAP80 itself, and acts against RNF8-UBC13 dependent Ly63-ubiquitin synthesis (Shao et al., 2009). OTUB1 also negatively regulate the ubiquitin response by directly binding UBC13 and prevents the

ubiquitin transfer (Juang et al., 2012, Wiener et al., 2012), thereby suppressing RNF168 activity in vivo and in vitro (Nakada et al., 2010). Another DUB, USP3, acts specifically on monoubiquitinated H2A and H2B and in turn regulates the DSB response as well as S phase checkpoint responses (Nicassio et al., 2007).

1.4 The role of ATM and ATR in replication stress

Replication stress is the interference of replication fork progression caused by DNA damage, depletion of deoxyribonucleotide pools, and DNA sequences and structures that are inherently difficult to replicate such as repetitive sequences, DNA interstrand crosslinks, G-quadruplex structures and others. Drugs such as aphidicolin can also block replication by inhibiting DNA polymerase α and δ, while hydroxyurea inhibits ribonucleotide reductase and thereby block the production of deoxyribonucleotides. ATR is the primary kinase that responds to replication stress by stabilising the replication fork, suppressing late origin firing and inhibiting mitotic entry (Cimprich and Cortez, 2008, Flynn and Zou, 2011).

1.4.1 Mechanism of ATR activation and its downstream functions

Replication stress generates ssDNA through the uncoupling of DNA polymerase and helicase at the replication fork (Byun et al., 2005) or through resection by nucleases at DSBs (Huertas, 2010). ssDNA is rapidly coated by Replication Protein A (RPA) and the ssDNA-RPA acts as the initial signal that recruits ATR, as the depletion of RPA impairs ATR activation and foci formation in *Xenopus* egg extracts and human cells (Costanzo and Gautier, 2003, Zou and Elledge, 2003, Dart et al., 2004). ATR activation also requires the cofactor ATRIP (ATR interacting protein), which interacts stoichoimetrically with ATR independently of damage and stabilises the latter (Cortez et al., 2001). ATR and ATRIP colocalise at DNA damage foci after inhibition of replication and ATRIP directly binds RPA in promoting the recruitment of ATR (Zou and Elledge, 2003, Ball et al., 2005). ATRIP has an N-terminal RPA binding domain, a C-terminal ATR interacting domain, and a central coiled-coil domain that mediates dimerization and which is required for stable interaction with ATR (Ball and Cortez, 2005, Itakura et al., 2005).

ATR activation requires the activator TOPBP1, which binds to both ATR and ATRIP via its PIKK regulatory domain (PRD), stimulates ATR kinase activity in vitro and in vivo and is required for its checkpoint functions (Mordes et al., 2008, Kumagai et al., 2006). TOPBP1 recruitment, in turn, depends on the 9-1-1 complex (RAD9-HUS1-RAD1), which is loaded onto the 5' resected DNA junction by the RFC-like clamp loader RAD17 (Zou et al., 2002, Bermudez et al., 2003,

Ellison and Stillman, 2003). The phosphorylated C-terminus of RAD9 interacts with the BRCT domains of TOPBP1, enabling the latter to associate with and activate ATR (Furuya et al., 2004, Delacroix et al., 2007, Lee et al., 2007). The 9-1-1 complex and TOPBP1 are recruited independently of ATR-ATRIP, thus providing additional layers of control in DDR activation in sensing replication fork stalling (Melo et al., 2001, Kondo et al., 2001). It is unclear how TOPBP1 activates ATR, possibly by a change in conformation that increases the affinity for ATR substrates (Cimprich and Cortez, 2008). Recently, the MRN complex has been implicated in the recruitment of TOPBP1 to ds-ssDNA junctions and is required for ATR activation (Duursma et al., 2013), hence highlighting the potential crosstalk between ATM and ATR pathways.

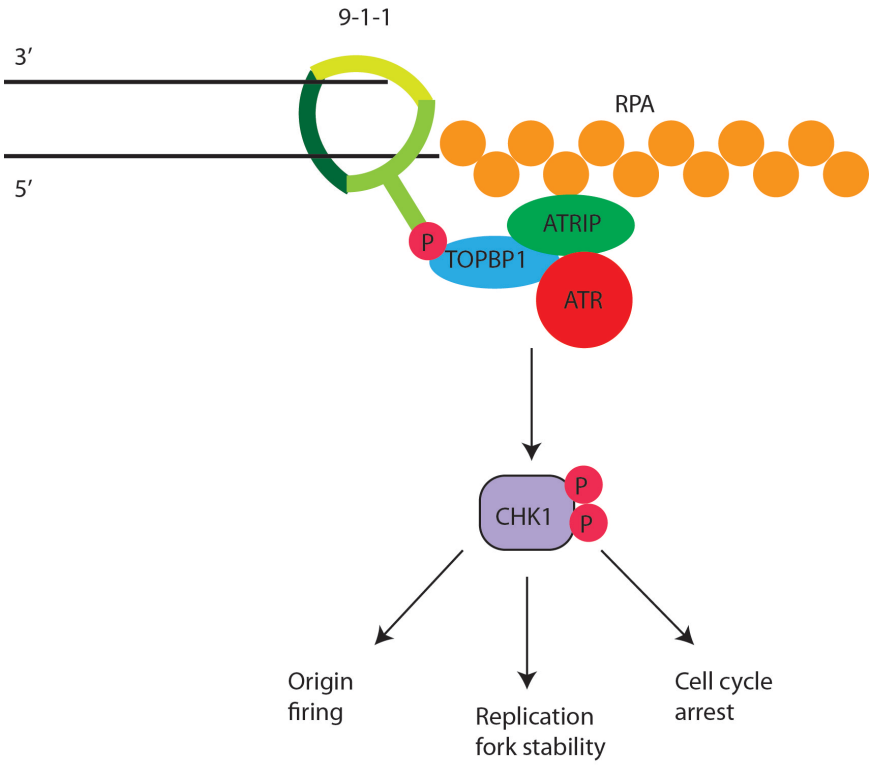

Figure 9. Mechanism of ATR activation.

ssDNA is rapidly coated by RPA, which serves as a signal to recruit ATR via ATRIP. ssDNA-RPA also triggers recruitment of a checkpoint clamp, the 9-1-1 complex, which is loaded onto the resected dsDNA junction by the clamp loader RAD17 (not shown). Phosphorylated 9-1-1 complex facilitates the recruitment of TOPBP1, a coactivator of ATR, which binds to both ATR and ATRIP and stimulates ATR kinase activity. Activated ATR phosphorylates downstream substrates such as Chk1, which executes checkpoint responses.

Upon activation, ATR phosphorylates its downstream substrates, CHK1 on sites Ser317 and Ser345, which has been used as markers of ATR signalling (Liu et al., 2000) (Zhao and Piwnica-Worms, 2001). Recently, ATR autophosphorylation at T1989 has been shown to be a marker of active ATR and required for ATR function (Liu et al., 2011). The auto-phosphorylation was induced by UV, IR and HU, and was abolished by T1989A mutation. Reconstitution of ATR-null cells with T1989A ATR resulted in defective substrate phosphorylation. Moreover, phospho-T1989 was shown to be required for TOPBP1 phosphorylation, but not vice versa, suggesting that ATR autophosphorylation is upstream of TOPBP1 recruitment. Several companies have made commercial antibodies against another site, Ser428, but the S428A mutant does not impair CHK1 phosphorylation. Hence, in contrast to the multiple autophosphorylation sites on ATM, T1989 is the only site identified so far that marks ATR activation.

As the effector substrate of ATR, CHK1 mediates many of its downstream functions such as intra S phase checkpoint and G2/M arrest (Feijoo et al., 2001, Liu et al., 2000). ATR-mediated phosphorylation of CHK1 promotes the dissociation of the latter from chromatin and facilitates the transmission of DNA-damage signals to downstream targets (Smits et al., 2006). CHK1 and ATR are both required for UVC-induced inhibition of replication, which does not depend on ATM, NBS or MRE11 (Heffernan et al., 2002). Recently, ATR also been shown to phosphorylate MLL (Lysine methyltransferase) after replication stress, which protects it from degradation by SKP2 E3 ligase and leads to the stabilisation of MLL. As a result, the increase in H3K4 methylation at origins can impair the binding of CDC45 and suppress replication initiation (Liu et al., 2010).

CHK1 activation also halts the cell cycle to allow replication block or DNA damage to be repaired. CHK1 phosphorylates CDC25A upon its activation by ATR (Sorensen et al., 2003), and promotes the proteasome-dependent degradation of CDC25A phosphatase. The resulting increase in CDK (cyclin-dependent kinase) phosphorylation at Tyr15 residue inhibits CDK activity and induces S phase arrest (Zhou and Elledge, 2000) (Bartek and Lukas, 2003).

Another key function of ATR in the protection of genome integrity is the maintenance of stalled replication fork. Inhibition of ATR kinase activity induces

cell death, defective replication initiation and collapse of replication forks due to excessive deregulated activity of SMARCAL1 DNA translocase. ATR phosphorylation of SMARCAL1 on Ser652 limits its aberrant processing of replication fork, thereby maintaining fork integrity (Couch et al., 2013). Similar findings were reported on the role of ATR in preventing fork collapse and breakage in SV40 chromatin replication (Sowd et al., 2013).

In addition, ATM was also shown to play an important role in suppressing excessive recombination intermediates and promoting bidirectional fork progression (Sowd et al., 2013). Hence, ATM and ATR could cooperate in the protection of stalled replication forks. Recently, ATM was shown to be required for the formation of 53BP1 G1 nuclear bodies at fragile sites (Harrigan et al., 2011, Lukas et al., 2011a), which are caused by replication fork collapse after partial inhibition of DNA replication (Durkin and Glover, 2007). The 53BP1 nuclear bodies were proposed to protect fragile sites and unrepaired DNA from erosion and sequester them until the next cell cycle for repair. While ATR is required to maintain fragile site stability in mammalian cells (Casper et al., 2002), it is not required for the formation of 53BP1 nuclear bodies (Harrigan et al., 2011). Hence, while ATR is activated to transduce checkpoint responses immediately following replication stress in an early step, ATM could also play a role in preserving replication fork integrity and preventing accumulation of DNA damage during prolonged replication fork stalling.

1.5 ROS-induced DNA damage and the base excision repair pathway

Reactive oxygen species (ROS) are generated endogenously as by-products of oxidative respiration in mitochondria, in macrophages and neutrophils, and in peroxisomes. ROS can also be induced by exogenous exposure to IR, by the presence of heavy metals and drugs such as barbiturates or phorbol esters (Klaunig and Kamendulis, 2004). Regardless of the source, free radicals such as O_2^-•, •OH and H2O2 are generated, the latter being the most damaging given its ability to diffuse rapidly through membranes and target DNA (Boveris et al., 2006). The first line of defence against ROS is the intracellular pool of antioxidants, such as superoxide dismutase, catalase and glutathione peroxidase enzymes and nonenzymatic compounds such as vitamins C, E and glutathione. However, when oxidants are in excess, ROS induced damage can occur to nucleic acids, lipids and proteins, which may affect cellular function and viability.

Amongst the different types of oxidative DNA damage, 7,8-dihydro-8-oxo-guanine (8-oxoG) is the most abundant and occurs at a frequency of 1000 per human cell per day (van Loon et al., 2010). This also makes it a good biomarker of oxidative stress (Klaunig and Kamendulis, 2004). In addition, 8-oxoG is also the most highly mutagenic due to its ability to mispair with adenine, leading to G:C to T:A transversions if left unrepaired at DNA replication. Other base oxidation products include 2,6-diamino-4-hydroxy-5-formamidopyrimidine (faPy-G) and 7,8-dihydro-8-oxo-adenine (8-oxo-A). Increasing evidence attributes the loss of BER as a cause of tumourigenesis; G:C to T:A transversions constitute the most predominant form of somatic mutations in many cancers(Greenman et al., 2007), germline mutations in *MUTYH* are associated with MUTYH-associated polyposis (Mazzei et al., 2013), polymorphism in OGG1 has been implicated in increased susceptibility to lung cancer (Sugimura et al., 1999), and reduced activity of 8-oxoguanine DNA glycosylase (OGG1) is a risk factor in lung and head and neck cancer (Paz-Elizur et al., 2008). Given the mutagenic potential of damaged bases, they need to be efficiently detected and repaired by the base excision repair pathway.

1.5.1 Base excision repair pathway

As the primary repair system for damaged bases, the base excision repair (BER) pathway is initiated by specific DNA glycosylases that recognise damaged bases and catalyses base cleavage to form an apurinic/apyrimidinic (AP) site. This is followed by cleavage to form an ssDNA break at the site by AP endonuclease I (APEI). Further processing by DNA polymerase β generates a one-nucleotide gap, which is subsequently filled by short-patch or long-patch repair. During short-patch BER, DNA pol β synthesises a one-nucleotide repair patch, which is ligated by DNA ligase III/XRCC1 heterodimer (Kubota et al., 1996, Srivastava et al., 1998). Long-patch BER involves the repair of two to 12 nucleotides, which is initiated by DNA pol β (Podlutsky et al., 2001), and then elongated by DNA pol δ and ε. Additional factors are required to facilitate strand displacement synthesis including RFC, PCNA and FEN1 which cleaves the displaced nucleotides. Unlike short-patch repair, the final ligation step in long-patch repair is mediated by DNA ligase I (van Loon et al., 2010). An alternative, APE1-independent mode of BER by DNA glycosylase/AP lyase NEIL1/NEIL2 has been identified, which acts on 5-hydroxyuracil (5-OHU), thymine glycol, 8-oxo-G, and uracil. In this pathway, NEIL1 and polynucleotide kinase (PNK) act in concert to remove the 3' terminal phosphate group after the ssDNA break, and can also carry out repair initiated by other DNA glycosylases (Wiederhold et al., 2004).

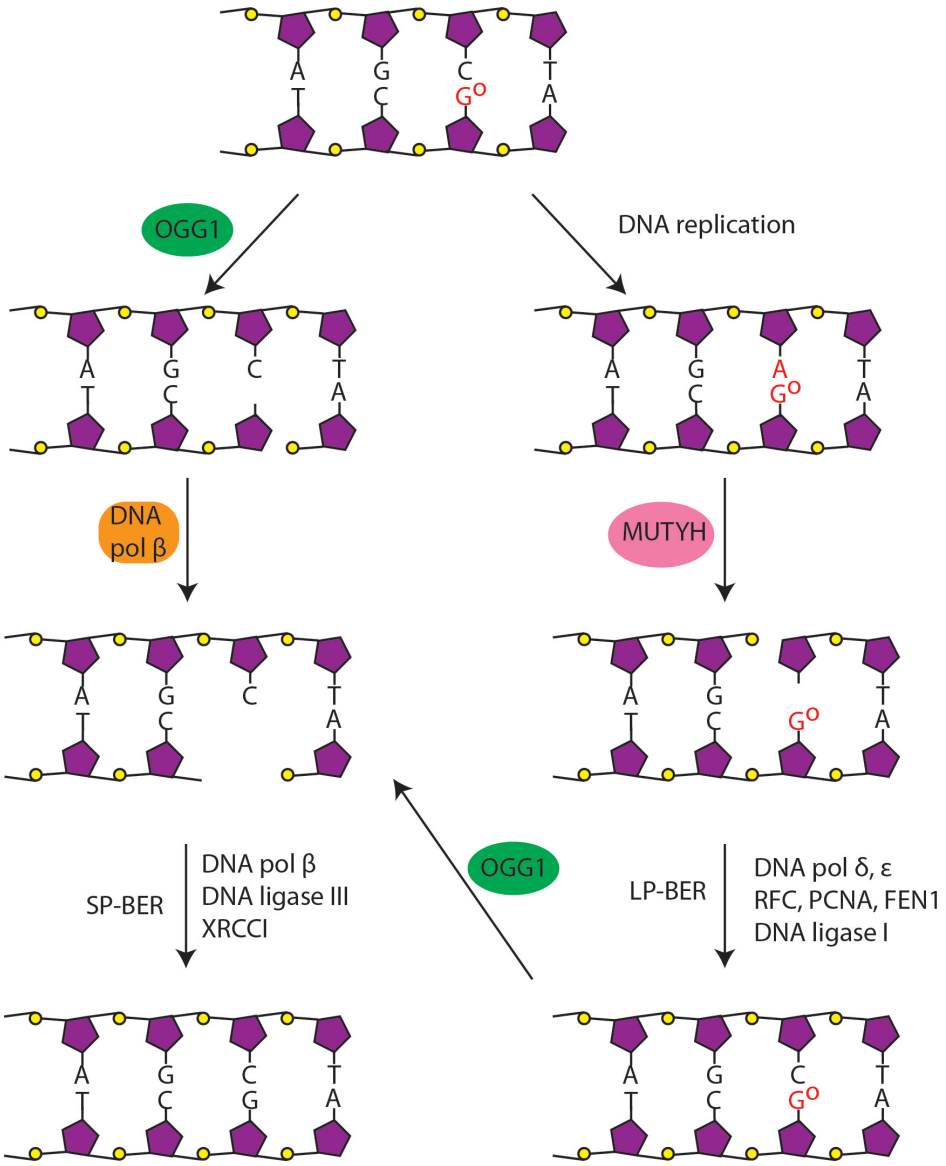

Figure 10. Mechanism of BER pathway.

Oxidative damage to DNA results in the formation of 8-oxoG, which is recognised and excised by OGG1, followed by SP-BER mediated by DNA pol β and ligated by DNA ligase III/XRCC1 to restore to C:G base pair. However, if DNA replication occurs before the 8-oxoG is repaired, replicative polymerases misincorporate dAMP opposite 8-oxoG, resulting in G:C to T:A transversion in the following cell cycle. A:8-oxoG mispair is recognised by MUTYH, which cleaves the adenine and initiates LP-BER via DNA pol δ, ε, RFC and PCNA. DNA pol ƛ further elongates the newly synthesised strand and the resulting flap is removed by FEN1, before ligation by DNA ligase I. The C:8oxoG base pair is subsequently targeted by OGG1 and SP-BER to restore to the original C:G base pair.

In order to counteract the mutagenic effect of 8-oxo-G, cells have conserved DNA glycosylases that can detect and cleave the oxidised base from the genome. In humans cells, the 8-oxoG system consists of NUDT1 (Nucleoside diphosphate linked moiety X type motif 1), OGG1 and MUTYH. NUDT1 is a nucleoside phosphatase that hydrolyses oxidised guanine nucleosides and prevents their incorporation into the DNA (Furuichi et al., 1994) (Kakuma et al., 1995). NUDT1 or MTH1 (MutT homolog 1) was identified from human tumour cell lines that possessed 8oxo-dGTPase activity (Mo et al., 1992). Additional homologues, MTH2 (NUDT15) and MTH3 (NUDT18) have also been identified (Cai et al., 2003, Takagi et al., 2012). NUDT1 has greater activity towards 8-oxo-dGTP, MTH2 hydrolyses both 8-oxo-dGTP and dGDP with lower affinity, and MTH3 is specific towards 8-oxo-dGDP (Takagi et al., 2012).

Once the oxidised nucleotide has been incorporated into the genome, the 8-oxo-G is recognised by OGG1, a bifunctional enzyme with both DNA glycosylase and AP lyase activity (Figure 10). OGG belongs to the Helix-hairpin-helix (HhH) family of BER DNA glycosylases, and was initially identified by its ability to suppress the mutagenicity of the *fpg muty* E.coli mutant and to act towards an 8-oxo-G substrate (van der Kemp et al., 1996). Structural data of the free enzyme and OGG1-DNA complex demonstrated induced-fit conformational changes upon 8-oxoG binding, that allows the flipping of the 8-oxoG out of the DNA base pair (Bruner et al., 2000, Bjoras et al., 2002). Using a trapped enzyme-DNA intermediate, Fromme et al were able to show that the cleaved 8-oxoG acts as a cofactor in the subsequent lyase step (Fromme et al., 2003). However, if the 8-oxoG is not removed before DNA replication, the DNA polymerase may incorporate adenine opposite 8-oxoG. In this case, cells rely on MUTYH to remove the mismatched adenine, followed by OGG1 mediated cleavage of 8-oxoG to revert to the G: C base pair. Another member of the endonuclease III (Nth) family, NTH1, has also been found to be active against 8-oxoG, as well as other substrates such as thymine glycol (Tg), 5-hydroxycytosine, dihydrouracil (DHU), urea and other oxidized pyrimidine derivatives (Ikeda et al., 1998, Hilbert et al., 1997, Aspinwall et al., 1997, Liu and Roy, 2002). A similar mechanism of base flipping occurs in MUTYH-mediated recognition of mismatched A in an A: 8-oxoG mispair (Fromme et al., 2004), which ensures specific binding only to

adenine opposite an oxidised G. While the AP site generated by OGG1 is predominantly repaired by SP-BER, as shown by reduced repair efficiency in DNA pol β deficient cell line (Fortini et al., 1999) and from in vitro reconstitution of 8-oxoG BER with human purified proteins (Pascucci et al., 2002), that generated by MUTYH is most likely repaired via LP-BER, due to the involvement of replicative polymerase δ that is sensitive to aphidicolin and followed by a PCNA-dependent mechanism (Weiser et al., 1991) (Einolf and Guengerich, 2001).

1.5.2 Mouse models of BER pathway

Despite the mutagenicity and susceptibility to tumourigenesis in the absence or reduction in base excision repair in human patients, mouse models lacking the 8-oxoG genes have not been reported to have a severe phenotype. *Ogg1* knockout mice were generated by two approaches, either by targeted deletion of exon 2 and 3 (Minowa et al., 2000) or deletion of the genomic DNA including the conserved helix-hairpin-helix motif of OGG1 required for DNA glycosylase/AP lyase activity (Klungland et al., 1999). However, despite the increase in 8-oxoG in the tissue of mutant animals and elevated spontaneous mutation rate, there were no overt phenotypes or malignancies in these mice from the early reports. The *ogg1-/-* mice also did not show increased tumorigenesis in response to long-term potassium bromate induced carcinogenesis despite accumulation of 8-oxoG in vivo (Arai et al., 2006). Only one report showed that *ogg1*-/- animals developed spontaneous lung adenoma and carcinoma after 1.5 year and this could be somehow suppressed by the double knockdown of MTH1 (Sakumi et al., 2003).

Similarly, *mutyh-/-* mice also display no severe phenotype, with one report of increased intestinal tumours at 18 months of age (Sakamoto et al., 2007). However, when combined with the $APC^{min/+}$ model, $APC^{min/+}$; *mutyh-/-* accelerated intestinal tumourigenesis compared with $APC^{min/+}$ *; mutyh+/+* or $APC^{min/+}$ *; mutyh+/-* and three Apc mutations in polyps from $APC^{min/+}$ *; mutyh-/-* mice were found to be G:C to T:A transversions which resulted in termination codons (Sieber et al., 2004). While *mutyh-/-* mice have no apparent increase in 8-oxoG in tissues, *mutyh-/-; ogg1-/-* double knockout animals accumulated more 8-oxoG (Russo et al., 2004) and was reported to have shorted lifespan (10 months) and increased lung tumour incidence (Xie et al., 2004). Moreover, most lung tumours were also

found to harbor G to T transversions in codon 12 of K-ras, in line with a defect in base excision repair.

Mth1 knockout mice show no difference in survival due to spontaneous tumourigenesis compared to wildtype, but were found to have increased tumour incidence(Tsuzuki et al., 2001b, Tsuzuki et al., 2001a). Hence, MTH1 could likely confer protection against early tumour initiation events, but its loss is not sufficient alone to accelerate tumourigenesis. In addition, MTH1 has been found to play a protective role against the mutagenicity and cytotoxicity of 8-oxoG accumulation in neurons, which contribute to neurodegeneration in a mouse model of Parkinson's Disease (Nakabeppu et al., 2006).

1.5.3 Regulation of BER pathway

Given the prevalence of 8-oxoG in the genome, the activities of MUTYH and OGG1 must also be regulated to correct for these errors in the timely manner. MUTYH activity has been proposed to correlate with DNA replication, since its activity needs to be targeted to the newly synthesised DNA. MUTYH directly interacts with PCNA and RPA in human and yeast cells, and colocalises with BrdU and PCNA in replication foci (Parker et al., 2001, Boldogh et al., 2001). Using an in vivo repair system, it was shown that DNA replication increased the activity of MUTYH, in a manner that depends on the interaction with PCNA (Hayashi et al., 2002). In addition, MUTYH could be regulated by PKC (Protein kinase C) mediated phosphorylation, which augments its activity (Parker et al., 2003).

In contrast, OGG1 protein level does not seem to change appreciably with the cell cycle, and induction of its activity after oxidative stress is also variable, possibly due to cell type differences (Dhenaut et al., 2000). OGG1 activity can be boosted in liver by regular exercise (Nakamoto et al., 2007), as well as by ischemic preconditioning in the brain of rats in order to enhance repair of reperfusion-induced oxidative damage (Li et al., 2006, Lan et al., 2003). Following the kinetics of GFP-OGG1 fusion protein, Amouroux et al showed that OGG1 is recruited to euchromatic regions upon oxidative stress and this does not involve binding and recognition of 8-oxoG, as a OGG1 F319A mutant which cannot recognise 8-oxoG

is still able to localise to open chromatin (Amouroux et al., 2010). Hence, there must be additional factors that regulate OGG1 localisation.

OGG1 has been shown to interact with RAD52 in vitro and in vivo, specifically after oxidative stress but not after IR. Rad52 mediates HR by facilitating RAD51 nucleoprotein filament formation on ssDNA and annealing of RPA-coated ssDNA (Sung, 1997, New et al., 1998, Shinohara and Ogawa, 1998). While OGG1 inhibits the strand annealing activity of RAD52, the latter boost the activity of OGG1 and colocalises with OGG1 in nuclear foci after H_2O_2 treatment (de Souza-Pinto et al., 2009). It was speculated that since OGG1 removes 8-oxoG less effectively closer to DNA ends, RAD52 cooperates to enhance OGG1 activity. It might also be a way to couple the completion of BER to HR once the template DNA has been restored to its original state. OGG1 also interacts with PARP1, and the interaction is increased by oxidative stress. While OGG1 stimulates poly(ADP-ribosyl)ation, PARP1 inhibits OGG1 activity, suggesting that PARP1 could regulate OGG1 activity. OGG1 has also been shown to be regulated by posttranslational modifications. Dantzer et al reported that OGG1 could be potentially phosphorylated by PKC on a serine residue, although it is unclear what physiological effect this has on OGG1 activity (Dantzer et al., 2002). Subsequently, OGG1 was also found to be phosphorylated by CDK4 and acetylated by p300, both of which increase its cleavage activity (Hu et al., 2005, Bhakat et al., 2006).

While MUTYH and OGG1 have been linked to the replication and DSB pathway through interactions with DDR factors, it is not clear whether these interactions influence the crosstalk between DDR and base excision repair. It is plausible that ATM or ATR could help to direct the activity of MUTYH1 and OGG1 to DNA damage sites after oxidative stress, but a direct interaction has not been reported so far. Moreover, it would be of interest to understand whether base excision repair also affects ATM and ATR signalling. This will be further discussed in chapter 6.

Chapter 2. Materials and Methods

2.1 Materials

2.1.1 Reagents

Acetone	Sigma-Aldrich
Acrylamide	Sigma-Aldrich
Agarose	Bioline
Ammonium persulphate	Sigma-Aldrich
Ampicilin	Sigma-Aldrich
Aphidicolin	Sigma-Aldrich
ATM inhibitor	Calbiochem
β-mercaptoethanol	Sigma-Aldrich
Bovine serum albumin	Sigma-Aldrich
BrdU	Sigma-Aldrich
Calcium phosphate	CRUK
Calf intestinal phosphatase	New England Biolabs
Cell strainer (45μm)	BD falcon
Coverslips	Menzel-Glaeser
Cuvettes	Fisher scientific
DAKO fluorescent mounting medium	DAKO
DAPI	Sigma-Aldrich
Dharmafect 1	Life Technologies
Direct PCR Lysis reagent	Viagen Biotech
Dithiothretol	Sigma-Aldrich
DMEM	Life Technologies
DMSO	Sigma-Aldrich
DNA ladder (1kb)	Life Technologies
DyeEx® 2.0 Spin kit	QIAGEN
Dynabeads M-280 Strepavidin	Life Technologies
ECL western blotting detection reagent	GE healthcare
EDTA	CRUK
Eppendorf tubes	Eppendorf
Ethanol	Fisher scientific

Ethidium bromide	Sigma-Aldrich
Falcon tubes (15ml, 50ml)	Corning
Fuji X-ray film	Fisher scientific
Glycerol	Sigma-Aldrich
GoTaq PCR DNA polymerase	Promega
Harris's haematoxylin	CRUK
Hydrogen peroxide	Sigma-Aldrich
Illustra ^{TM} GFX ^{TM} DNA Purification kit	GE healthcare
Industrial methylated spirit (IMS)	CRUK
Isopropanol	Sigma-Aldrich
Kanamycin	Sigma-Aldrich
LB medium	CRUK
Lipofectamine-2000	Life Technologies
Lullaby transfection reagent	OZ Biosciences
Luperox	Sigma-Aldrich
Magnesium chloride	CRUK
Methanol	Sigma-Aldrich
Microscope slides	Menzel-Glaeser
Needles	BD Microlance
Neutral buffered formalin (NBF)	CRUK
Nitrocellulose transfer membrane	Whatman
NP-40	Sigma-Aldrich
Nucleofactor transfection reagent	Lonzo AG
Opti-MEM	Life Technologies
Paraformaldehyde	Sigma-Aldrich
PBS	CRUK
Penicillin/streptomycin	CRUK
Phenylmethylsulfonyl fluoride (PMSF)	Sigma-Aldrich
Ponceau S	Sigma-Aldrich
Propidium iodide	Sigma-Aldrich
Protease inhibitor cocktail	Sigma-Aldrich
Protein A-sepharose	Sigma-Aldrich
Protein Assay Dye Reagent	Bio-Rad
Protein G-sepharose	Sigma-Aldrich
Proteinase K	Melford Laboratories

QIAGEN plasmid Maxi Kit	QIAGEN
QIAprep Spin miniprep kit	QIAGEN
Rainbow protein marker	GE healthcare
Restriction endonucleases	New England Biolabs
RIPA buffer	New England Biolabs
Rnase-free Dnase	QIAGEN
serological pipettes (5ml, 10ml, 25ml)	Corning
	A1 Laboratory supplies
Skimmed milk powder	Ltd
Sodium azide	Sigma-Aldrich
Sodium chloride	CRUK
Sodium dodecyl sulphate	Sigma-Aldrich
Sodium fluoride	Sigma-Aldrich
Sodium orthovanadate	New England Biolabs
Superscript III cDNA synthesis kit	Life Technologies
SYBR green	Life Technologies
Syringes (5ml, 10ml, 25ml)	BD Plastipak
T4 DNA ligase	New England Biolabs
Taq PCR kit	QIAGEN
TEMED	Sigma-Aldrich
Tissue culture dishes (6cm, 10cm)	Corning
Tissue culture flasks (25cm^2, 75cm^2, 150cm^2)	Corning
Tissue culture plates (6-well, 24-well, 96-well)	Corning
Triton X-100	Sigma-Aldrich
Trypan Blue	Sigma-Aldrich
Trypsin	Life Technologies
Tween-20	Sigma-Aldrich
Urea	Sigma-Aldrich

2.2 Buffers and solutions

ATM IP buffer

RIPA buffer	1x
NaF	50mM

Na_3VO_4	1mM
β-glycerophosphate	1mM
Complete Protease inhibitor cocktail	1% (v/v)

ATM IP wash buffer

Tris (pH7.5)	100mM
LiCl	0.5M

Blocking buffer (Immunofluorescence)

FCS	10%
Triton X-100	0.10%
PBS	89.90%

Blocking buffer (Immunohistochemistry)

Goat serum	10%
BSA	1%
PBS	89%

Cell lysis buffer

Tris-HCl (pH7.2)	80mM
NaCl	150mM
NP-40	0.2% (v/v)
Glycerol	10% (v/v)
NaF	50mM
Na_3VO_4	1mM
β-glycerophosphate	1mM
Complete Protease inhibitor cocktail	1% (v/v)

10% Denaturing urea PAGE gel

40% Acrylamide (29:1)	12.5ml
Urea	24g
30% APS	166ul
TEMED	20ul
10x TBE	5ml
ddH2O	make up to 50ml

DMEM (complete media)

DMEM (4.5g/l glucosse, +L-glutamine,+pyruvate)	445ml
FCS	50ml
1% penicillin/streptomycin	5ml

DNA IP buffer DW

Tris-HCl 1M pH8.0	20mM
NaCl	2M
EGTA	0.5mM
NP-40	0.03%

DNA IP Buffer B

HEPES (pH 7.9)	20mM
BSA	0.05mg/ml
glycogen	0.05ml/ml
KCl	300mM
NP-40	0.02%
DTT	2.5mM
Polyvinylpyrrolidone	5mg/ml

DNA IP Buffer G

Tris (pH 7)	10mM
MgCl2	1.5mM
NaCl	100mM
EGTA	0.2mM
Potassium glutamate	10mM
NP-40	0.02%
DTT	10mM
PMSF	0.2mM

DNA oxidation buffer

H2O2	3mM
CuCl2	100uM
Sodium ascorbate	100uM

PBS	50mM

Fixing solution (Immunofluorescence-UFB)

TritonX-100 (10%)	0.5ml
PIPES 1M	0.5ml
EGTA (0.5M)	0.5ml
MgCl2 (0.5M)	50ul
Formaldehyde (37.8%)	2.7ml
ddH2O	make up to 25ml

GST protein purification buffer

Tris (pH8)	50mM
NaCl	200mM
Triton-X	0.10%
β-mercaptoethanol	5mM
Glycerol	10%

Hypotonic buffer

NaCl	50mM
FCS	1% (v/v)
Glucose	0.45% (v/v)

Kinase buffer

HEPES (pH7.5)	10mM
Glycerolphosphate	50mM
NaCl	50mM
MgCl2	10mM
MnCl2	10mM
ATP	5uM
DTT	1mM

Laemmli buffer

Tris-HCl (pH6.8)	63mM
SDS (w/v)	2% (w/v)
Glycerol	10% (v/v)

Bromophenol blue	0.0025% (v/v)
β-mercaptoethanol	2.5% (v/v)

Nuclear/cytoplasmic fractionation buffer A

HEPES (pH7.9)	10mM
MgCl2	1.5mM
KCl	10mM
DTT	1mM
NP-40	0.2% (v/v)

Nuclear/cytoplasmic fractionation buffer C

HEPES (pH7.9)	20mM
NaCl	420mM
MgCl2	1.5mM
DTT	1mM
EDTA	0.2mM
Glycerol	25% (v/v)

RPMI media (complete)

RPMI-1640 media (0.3g/L L-glutamine, 0.001g/L folic acid, 2g/L sodium bicarbonate	445ml
FCS	50ml
1% penicillin/streptomycin	5ml

10x SDS-PAGE running buffer

Tris	300g
Glycine	1400g
20%SDS (v/v)	250ml
ddH2O	make up to 10L

5% SDS Stacking gel

30% Acrylamide (37.5:1)	1.7ml
Tris (1M pH6.8)	1.25ml
10% SDS (w/v)	100ul

10% Ammonium persulphate	100ul
TEMED	10ul
ddH2O	make up to 10ml

6% SDS resolving gel

30% Acrylamide (37.5:1)	4ml
Tris (1M pH8.8)	5ml
10% SDS (w/v)	200ul
10% Ammonium persulphate	200ul
TEMED	16ul
ddH2O	make up to 20ml

8% SDS resolving gel

30% Acrylamide (37.5:1)	5.3ml
Tris (1M pH8.8)	5ml
10% SDS (w/v)	200ul
10% Ammonium persulphate	200ul
TEMED	12ul
ddH2O	make up to 20ml

Transfer buffer

Tris	24mM
Glycine	192mM
Methanol (v/v)	20%
SDS (v/v)	0.01%

50x TAE buffer

Acetic acid	57.1ml
EDTA (0.5M)	100ml
Tris base	242g
ddH2O	make up to 1L

20x TBST

NaCl (5M)	3L
Tris (1M, pH 7.5)	2L
Tween-20	200ml
ddH2O	up to 10L

10x TBE

Tris base	108g
Boric acd	55g
EDTA	7.5g
ddH2O	make up to 1L

Ubiquitin wash buffer A

NaH2PO4	0.1M
Na2HPO4 (pH8)	0.1M
Imidazole	10mM
Tris (pH8)	0.01M
Guanidium chloride (6M)	400ml

2.3 Oligonucleotides

Sequencing primers

Gene	Use	Sequence	
atmin	forward	TCAGCATCTTCTCCAGAGAG ACAG	Wildtype430bp
	reverse	CACATGTGTACAGCACATTCA TTG	floxed 515bp
	delta	CTCAGGGTACACATACTATG CTTGC	deleted 400bp
Cre	forward	CGGTCGATGCAACGAGTGAT GAGG	Cre 600bp
	reverse	CCAGAGACGGAAATCCATCGCTCG	
nbs1	forward	CAGGGCGACATGAAAGAAAA C	wildtype 320bp

	reverse	AATACAGTGACTCCTGGAGG	floxed 380bp
	delta	ATAAGACAGTCACCACTGCG	delta 590bp
LSL-	forward	GGAGCGGGAGAAATGGATAT	wildtype 600bp
ROSA26-	wiltype	G	
YFP			
	forward	AAGACCGCGAAGAGTTTGTC	mutant 320bp
	mutant		
	reverse	GGAGCGGGAGAAATGGATATG	
ogg1	forward	CTGAATGAACTGCAGGACGA	
	neo		
	reverse	CTCTTCGTCCAGATCATCCT	
	neo		
	forward	ACTGCATCTGCTTAATGGCC	
	wiltype		
	reverse	CGAAGGTCAGCACTGAACAG	
	wildtype		

QPCR primers

Gene	**Use**	**Species**	**Sequence**
Trim38 (Pair 1)	QPCR F	Human	ACGTATGCCAGGGCTACAAG
Trim 38 (Pair 1)	QPCR R	Human	TCAAGTTGCTTCAGTTTTGTC AC
Trim 38 (Pair 2)	QPCR F	Human	TGAGAGGAAAACAGCCTACC C
Trim 38 (Pair 2)	QPCR R	Human	CACCTGCACCTCTATGTGATG
Huwe1 (Pair 1)	QPCR F	Human	AGAGAGCGGCTGACAGAGG
Huwe1 (Pair 1)	QPCR R	Human	CACTAACCCACTCAGGTCAG G
Huwe1 (Pair 2)	QPCR F	Human	TGAATGCTCTGGCTGCATAC
Huwe1 (Pair 2)	QPCR R	Human	CCCCAGGTTTAGGATCAGATT
Trim67 (Pair 1)	QPCR F	Human	GCCAAGCACGAGGTGAAG
Trim67 (Pair 1)	QPCR R	Human	CCATTTAAGGCCTGAGATAGT TGT
Trim67 (Pair 2)	QPCR F	Human	AGGCAAAGGAAGCAAAGGA
Trim67 (Pair 2)	QPCR R	Human	CGTAGTCCAGTCCGTTTTCC
SH3RF2 (Pair 1)	QPCR F	Human	AGACCTGTCGTTTGTGAAAGG
SH3RF2 (Pair 1)	QPCR R	Human	GTTCAAGTTCTGCCTCACTCT G
SH3RF2 (Pair 2)	QPCR F	Human	CATCAGATGTTCCCTACCAAG C
SH3RF2 (Pair 2)	QPCR R	Human	CAGTGGCAGCCAGGAGAG
ATMIN (set4)	QPCR F	Human	TGGCCTGGAATACGATGGA
ATMIN (set4)	QPCR R	Human	GACATGCGCAGAGCTGCA

ATMIN (set5)	QPCR F	Human	CAAGCACTCGGTGTCAATGG
ATMIN (set5)	QPCR R	Human	CACAGTGCGCAGGCATCT
UBR5 Pair1	QPCR F	Mouse	CACCGAGGACCAGCTCAA
UBR5 Pair2	QPCR R	Mouse	GTAGCCTGCTCCAGTACATTCA
UBR5 pair 2	QPCR F	Mouse	GCCCAGAAGATTGCCAAAG
UBR5 pair 2	QPCR R	Mouse	GGCAAACCATTCCCATGA
UBR5 pair 3	QPCR F	Mouse	TTCACTTCTTTCAATGATGAGTCAG
UBR5 pair 3	QPCR R	Mouse	ATTGACCAGAACCACCGTTT
OGG1 pair1	QPCR F	Mouse	TTATCATGGCTTCCCAAACC
OGG1 pair1	QPCR R	Mouse	GGCCCAACTTCCTCAGGT
OGG1 pair2	QPCR F	Mouse	TTATGAAGAGGCCCACAAGG
OGG1 pair2	QPCR R	Mouse	TCAAGGGCCATTAAGCAGAT
OGG1 pair1	QPCR	Human	CTGCATCCTGCCTGGAGT
OGG1 pair1	QPCR	Human	CCTGGGGCTTGTCTAGGG
OGG1 pair2	QPCR	Human	CCAACAAGGAACTGGGAAAC
OGG1 pair2	QPCR	Human	AGGTCGGCACTGAACAGC
Nbs1 (Pair1)	QPCR F	Human	ACCGATGTGGAAACTGCTG
Nbs1 (Pair1)	QPCR R	Human	CAACGCCAGTCAAAAGTCTG
Nbs1 (Pair2)	QPCR F	Human	GCATAAATGATGATTATGGTCAACTAA
Nbs1 (Pair2)	QPCR R	Human	CCTCCAATGATGTGTGGAAGT
NBs1 (pair1)	QPCR F	Mouse	ACCACATACGTAGCTGACACAGA
NBs1(pair 1)	QPCR R	Mouse	GGTCTTTCACTCAAAGGCATACA
NBs1 (Pair 2)	QPCR F	Mouse	TGAATTTCTCAAAGCAGTTGAATC
NBS1 (Pair2)	QPCR R	Mouse	TCATCAATGGGTGGGTAAAAA
RNA Pol II (Pair 1)	QPCR F	Mouse	AATCCGCATCATGAACAGTG
RNA Pol II (Pair 1)	QPCR R	Mouse	TCATCCATTTTATCCACCACCT
RNA Pol II (Pair 2)	QPCR F	Mouse	CAGTGATGAAAACAAGATGCAAG
RNA Pol II (Pair 2)	QPCR R	Mouse	ATCGCAGGAAGACATCATCA
NUDT1	QPCR F	Human	GAAGGAGAGACCATCGAGGA
NUDT1	QPCR R	Human	CACTGTCAGACCGCTCTCC
GSTM5	QPCR F	Human	AGGACTTCATCTCCCGCTTT
GSTM5	QPCR R	Human	AAACAAAAGACCTCGGAGGAA
MutYH	QPCR F	Human	ATGACACCGCTCGTCTCC
MutYH	QPCR R	Human	GCTTCTGCCTCCCTTCCT
NUDT1	QPCR F	Mouse	GACGCCCACAGAAAGTGAAG
NUDT1	QPCR R	Mouse	GGGAACCAGTAGCTGTCATCC
GSTM5	QPCR F	Mouse	GCTATGAGGAGAAACGGTAC

			ATC
GSTM5	QPCR R	Mouse	CCATGAGGTAGGGCAGGTT
MutYH	QPCR F	Mouse	AGAACACGTGCCCTTAGCA
MutYH	QPCR R	Mouse	AACTCCTCTCTCTTCTGCTTG G
ATM	QPCR F	Human	TGATAGTAGTGTTAGTGATGC AAACG
ATM	QPCR R	Human	CAGCTAAAGGATTAATGGCAC CT
UBR5 Pair1	QPCR F	Human	GGATGATACAGCCAGCGAAT
UBR5 Pair1	QPCR R	Human	TCGGCATCAAGGAGAGACAT
UBR5 pair 2	QPCR F	Human	GCATTTGCAATTGACCTGTG
UBR5 pair 2	QPCR R	Human	CCATTAGGAATGAGTTCAACC TG
ATM pair 1	QPCR F	Mouse	TCTCAAGCAGATGATCAAGAA GTT
ATM pair 1	QPCR R	Mouse	TGACTTTGAGACCTGCATCAT T
ATM pair 2	QPCR F	Mouse	TGCAGTCATCATGCAGACCTA
ATM pair 2	QPCR R	Mouse	TCTCTGCTGTTGCCATCGT

DNA IP oligoes (Tsuji et al., 2008)

DNA oligo 1	AGCTACCATGCCTGCACGAATTCGTATCAGCGTAATCA TGGTCATAGCT
DNA oligo 2	GCATCCTCACCATCAACTCACAGCCCAACATCAACGGG AAGCCGTCCTCCGACCCCATCGTGGGCTGGGGCAGCT ACCATGCCTGCACGAATTCGTATCAGCGTAATCATGGT CATAGCT
DNA oligo 3	AGCTATGACCATGATTACGCTGATACGAATTCGTGCAG GCATGGTAGCT
DNA oligo 6	TTCCCGTTGATGTTGGGCTGTGAGTTGATGGTGAGGAT GC

siRNA sequences

Gene	Catalogue number	Sequence
mouse UBR5	D-048858-01	CGAGAAGACUGAAAUACUA
	D-048858-02	GGGUGUACAUUCUUUAAUA
	D-048858-03	GAAGCUCAAUUACGUUAUG
	D-048858-04	AGACAAAUCUCGGACUUGA
Human UBR5	J-007189-09	GGUCGAAGAUGUGCUACUA
(ONTARGET	J-007189-08	GAUCAAUCCUAACUGAAUU

PLUS)

	J-007189-07	GAUUGUAGGUUACUUAGAA
	J-007189-06	GCACUUAUAUACUGGAUUA
siGenome	D-007189-18	GGUAAAUGGCUGCGGUGAA
	D-007189-19	AGUUUGAGAUUACGGGAAA
	D-007189-03	CAACUUAGAUCUCCUGAAA
	D-007189-02	GGACAGGAAUCUCCCAUUA
Human ATMIN	D-020304-04	GUAAGUGCAGCAAUUCGUA
siGenome	D-020304-03	UUAAUGCCCUUGUCAGUAG
	D-020304-02	GAGAUAUCCUCAGAAGUUG
	D-020304-01	GCAGAGACAGUAACUCAUA
Human OGG1	D-005147-01	GAUCAAGUAUGGACACUGA
siGenome	D-005147-04	AGAGGUGGCUCAGAAAUUC
	D-005147-23	GGUUCUGCCUUCUGGACAA
	D-005147-24	GGAGCAAAGUCCUGCACAC
Human MUTYH	D-012806-03	UAUAUGGGCUGGCCUUGGA
siGenome	D-012806-05	GAUCAACUACUAUACCGGA
	D-012806-18	CAGAGCAGCUUCAGCGCAA
	D-012806-19	CCAUCUAUUCAGAGACGUA
Human NUDT1	D-005218-01	GACGACAGCUACUGGUUUC
siGenome	D-005218-02	GAAAUUCCACGGGUACUUC
	D-005218-03	CGACGACAGCUACUGGUUU
	D-005218-04	AGACGUGGCUGCUGAACAG
Human GSTM5	D-011178-01	GAAAGUCAGCUACAUGGAA
siGenome	D-011178-02	UGACAUGAAGCGUAUAUUU
	D-011178-03	UGGAUUUCCUUGCCUAUGA
	D-011178-04	ACAUGAAGCGUAUAUUUGA
Human RNF168	J-007152-08	GAAAUUCUCUCGUCAACGU
ONTARGETplus	J-007152-07	AGAAGAACAGGACAGGUUA
	J-007152-06	CAAAGUAAGGCCUGGUAAA
	J-007152-05	GACACUUUCUCCACAGAUA
Mouse GSTM5	D-049356-04	CCGCAUGCUUCUGGAGUUU
siGenome	D-049356-03	GUUCGCCUCUGCUACAAUU
	D-049356-02	GCUAUGAGGAGAAACGGUA
	D-049356-01	GUAACGCCAUCCUGAGAUA
Mouse MUTYH	D-048516-04	ACAUCAAACUGACGUAUCA
siGENOME	D-048516-03	CAUAUCAUCUCUUCAGCGA
	D-048516-02	GAACUUAGCCCAGCAGCUC
	D-048516-01	CCACAGUGAUCGACUAUUA
Mouse NUDT1	D-042056-04	GAAAGUGGUCUGAGCGUGG
siGENOME	D-042056-03	UGCGAGAGGUGGACUCAUU
	D-042056-02	GAAGAAAUGCGCCCUCAGU
	D-042056-01	CCACAUCUCGUUUGAAUUU
Human Chk1	J-003255-10	CAAGAUGUGUGGUACUUUA
ONTARGETplus	J-003255-11	GAGAAGGCAAUAUCCAAUA
	J-003255-12	CCACAUGUCCUGAUCAUAU

	J-003255-13	GAAGUUGGGCUAUCAAUGG
Human NBS1	J-009641-06	CCAACUAAAUUGCCAAGUA
ONTARGETplus	J-009641-07	GCAGAUACAUGGGAUUUGA
	J-009641-08	GAAUAGAAACGUCUUGUUC
	J-009641-09	AACAAUAUGUGCACUCAUU
Human RAD18	D-004591-04	GCAGUUUGCUUUAGAGUCA
siGenome	D-004591-03	GAUAAUAUGACCUCAGUAA
	D-004591-02	GCAGGUUAAUGGAUAAUUU
	D-004591-01	CAUAUUAGAUGAACUGGUA
MOUSE OGG1	D-048121-01	CAACAUUGCUCGCAUUACU
siGenome	D-048121-02	UGGAAACCCUACACAAGUA
	D-048121-03	GACUACGGCUGGCAUCCUA
	D-048121-04	CUUAAUGGCCCUUGACAAA
Human SH3MD2	J-007037-05	GAUCGUAGGUUCUCGAAAU
ONTARGETplus	J-007037-06	AAAGGGACAUCCAUGCAUA
	J-007037-07	AAAGGCACAUUACAACGUA
	J-007037-08	GGAUGAAUCAGCCUUGUUG
Human TRIM38	J006929-05	GGCCCUAUUUCCAGGUUUA
ONTARGETplus	J006929-06	CGGAUGGGAUUUAGGAGUU
	J006929-07	CAGCAAUGCGAAUAACUAA
	J006929-08	GUGUAUAACAGACUUCUUU
Human HUWE1	J-007185-07	GCUUUGGGCUGGCCUAAUA
ONTARGETplus	J-007185-08	GCAGUUGGCGGCUUUCUUA
	J-007185-09	GAGCCCAGAUGACUAAGUA
	J-007185-10	UAACAUCAAUUGUCCACUU
Human Trim67	J-032288-05	GCACAAGGCACAACUAUCU
ONTARGETplus	J-032288-06	GGUAAGGAGACUUUGUGUA
	J-032288-07	UAACCUGGCUUUAAUAGUG
	J-032288-08	GAAGGUGGCGUGUGCAAGG

Antibodies

Primary antibody	**Species**	**Usage**	**Supplier**
53BP1	rabbit	IF 1:400 IHC 1:200	Santa cruz
Actin	rabbit	WB1:1000	Sigma
ATM	mouse	WB 1:500 IP 1ug	Santa cruz
ATR	goat	WB 1:1000 IF 1:400	Santa cruz
pS1981-ATM	mouse	WB 1:1000	Epitomics
pS1981-ATM	mouse	WB 1:1000 IF	Cell signalling

		1:400	
pS1981-ATM	sheep	WB1:1000	Rockland
ATMIN/ASCIZ	rabbit	WB1:1000	Chemicon
pS317-Chk1	rabbit	WB 1:1000	Cell signalling
Chk1	mouse	WB 1:1000	Cell signalling
UBR5	rabbit	WB 1:1000	Bethyl labs
FANCD2	rabbit	IF:1:400	Novus
Flag M2	mouse	WB 1:5000	Sigma
GFP	mouse	WB 1:1000	Sigma
pS139-H2AX	mouse	WB 1:1000	Upstate
		IF1:400	
pS139-H2AX	rabbit	WB 1:1000	Upstate
		IF1:401	
HA	rabbit	WB 1:1000	Sigma
Kap1	rabbit	WB 1:1000	Bethyl labs
Kap1	rabbit	WB 1:1000	Abcam
pS824-Kap1	rabbit	WB 1:1000	Bethyl labs
MCM6	goat	IHC 1:200	Santa cruz
Myc	rabbit	WB 1:1000	Sigma
NBS1	rabbit	WB 1:1000 IF	Novus
		1:400	
p53	mouse	WB 1:1000	Santa cruz
pS15-p53	mouse	WB 1:1000	Cell signalling
PICH	mouse	IF:1:400	Millipore
RAD18	rabbit	WB 1:1000	Epitomics
		IF1:400	
SMC1	rabbit	WB 1:1000	Abcam
pS957-SMC1	mouse	WB 1:1000	Millipore
pS966-SMC1	rabbit	WB 1:1000 IF	Bethyl labs
		1:400	
tubulin	mouse	WB 1:1000	Abcam
WRNIP1	goat	WB 1:1000 IF	Santa cruz
		1:400	
Secondary antibody	**Species**	**Usage**	**Supplier**
Alexa fluor 488	donkey	IF 1:400	Life technologies

	anti-mouse		
	donkey anti-rabbit	IF 1:401	Life technologies
	donkey anti-goat	IF 1:402	Life technologies
	Goat anti-mouse	IF 1:403	Life technologies
	Goat anti-rabbit	IF 1:404	Life technologies
Alexa fluor 546	donkey anti-mouse	IF 1:405	Life technologies
	donkey anti-rabbit	IF 1:406	Life technologies
Alexa fluor 647	donkey anti-mouse	IF 1:407	Life technologies
	donkey anti-rabbit	IF 1:408	Life technologies
	donkey anti-goat	IF 1:409	Life technologies
HRP-conjugated anti-mouse	goat	WB 1:5000	Jackson
HRP-conjugated anti-rabbit	mouse	WB 1:5001	Jackson
HRP-conjugated anti-goat	mouse	WB 1:5002	Jackson

2.4 Plasmids

The FlagATMIN construct was cloned into pCMVFlag2B using HindIII (N) and blunted XhoI (C) sites and XhoI site was destroyed after ligation. Flag-ATMIN N-terminus (1-354) and C-terminus (625-818) were cloned by PCR into pCMVFlag2B using StuI and EcoRI respectively. The Flag-ATMIN wildtype and K238R mutant was cloned by PCR into pCMVFlag2B and pMSCV-IRES GFP.

The MycNBS1 construct was a kind gift from Simon Boulton. The GFP-ATM contruct (in pSG5plus) vector was a kind gift from Kum Kum Khanna. The GST-p53 contruct was a kind gift from Tanya Paull. The Flag-UBR5 expression construct (in pSG5 vector) was a kind gift from Colin Watts. The Flag-UBR5 C2768A mutant was cloned by PCR mutagenesis in the same vector.

2.5 Methods

2.5.1 Molecular biology

2.5.1.1 DNA preparation and sequencing

For DNA amplification, DH5α bacteria were used for transformation. 50ng of DNA was added to an aliquot of competent bacteria and incubated on ice for 30 minutes. The bacteria were heat-shocked at 42°C for 30 seconds and placed on ice for another two minutes. 1ml of pre-warmed LB media was added and the bacteria was incubated at 37°C for one hour, prior to plating or inoculation in antibiotic selection media. From an overnight bacteria culture, the cell pellet was obtained by centrifugation and DNA extracted using a Plasmid Maxi Kit (Qiagen).
For the amplication of large plasmids such as GFP-ATM and FlagUBR5, SURE-2 competent cells (Agilent) were used and bacteria culture was grown at 30°C for two days with gentle agitation.

DNA sequencing was performed by the Equipment Park facility at LRI.

Sequencing reaction:

BigDye Terminator reaction mix	8ul
Sequencing primer (10uM)	0.32ul
DNA	300ng
DMSO	1ul
ddH2O	make up to 20ul

Sequencing PCR:

Step	Temperature (°C)	Time
1	95	1min
2	95	10sec
3	55	5sec
4	60	4 minutes
5	Go to step 2 for 24 cycles	
6	4	end

Sequencing reaction was purified using the DyeEx 2.0 spin kit (Qiagen) prior to sequencing.

2.5.1.2 Extraction of genomic DNA and genotyping

To extract genomic DNA for genotyping, mouse ear snips were incubated in 95ul of DirectPCR Lysis Reagent (Viagen) and 5ul of Proteinase K at 56°C overnight with shaking. The following day samples were heated at 85°C for 45 minutes to inactivate proteinase K. Samples were allowed to cool briefly and centrifuged at 5000rpm for five minutes. The supernatant was used for genotyping reactions.

Genotyping reaction (Qiagen):

Coralload PCR buffer (10x)	2ul
Solution Q	4ul
dNTPs (25mM)	0.2ul
Primer (100uM)	0.2ul each
Taq-Polymerase	0.2ul
DNA	2ul
ddH2O	make up to 20ul

Genotyping PCR reaction cycle:

Step	Temperature (°C)	Time
1	94	3min
2	94	30sec
3	60	45sec
4	72	45sec
5	Go to step 2 for 30 cycles	
6	72	10min
7	4	

PCR products were resolved on a an agarose gel (2-3%) dissolved in 1xTAE with 1: 10000 ethidium bromide. Electrophoresis was run at 120V for one hour with 100bp DNA ladder used as a reference of band size. Resolved DNA bands were visualised by UV illumination using a UV transluminator.

2.5.1.3 RNA isolation and quantitative PCR

The RNeasy mini kit (Qiagen) was used for extraction of total RNA from cells. Cell pellets were passed through a 19-gauge needle at least five times for homogenisation. The RNase-free DNase kit (Qiagen) was used for on-column DNA digest. Extracted RNA concentration and quality were assessed using a Nanodrop Spectrophotometer.

750ng of RNA was used for cDNA synthesis using Superscript III First-Strand cDNA synthesis kit (Life Technologies). Random hexamers were used for cDNA synthesis and a negative control without reverse transcriptase was included in parallel to check for presence of genomic DNA.

For QPCR, cDNA was first diluted in ddH20 (1:5). Each reaction was performed in triplicate in a 96 well plate.

QPCR reaction mix:

Primers (10uM)	0.5ul each
Platinum SYBR green	12.5ul
DNA	2ul
ddH2O	9.5ul

SYBR binding to newly synthesised double-stranded DNA emits fluorescence, measured using a real-time thermal cycler (Applied Biosystems). The fluorescence over background (C_T) was used to measure relative amount of cDNA compared to a control gene such as actin. In order to eliminate unspecific PCR products, primer dimer formation and contamination, a dissociation curve was also performed as well as a 'no DNA' control reaction for each primer set. Average of three Ct values for each sample that differ by not more than 0.2 was used to calculate relative mRNA levels.

Relative mRNA levels = $2^{-(\text{sample CT-control CT})}$

2.5.2 Biochemistry

2.5.2.1 Cell lysis for protein extraction

Cells were washed once with cold PBS and gently scraped into 3ml of cold PBS and centrifuged. After aspirating the PBS, the cell pellet was resuspended by pipetting in cold cell lysis buffer and incubated for 20 minutes on ice. The suspension was then sonicated with 4x 8 second pulses at 25% power in a sonicator. The whole cell lysate (WCL) was centrifuged at 4°C for ten minutes at 13K rpm. The supernatant was removed and placed into a new tube for western blot analysis.

2.5.2.2 Determination of protein concentration using Bradford assay

Bradford reagent (Bio-rad) was diluted in ddH_2O (1:5). In order to prepare a standard curve, 1, 2, 4 and 8ul of 1mg/ml BSA were each diluted into 1ml of diluted Bradford reagent, mixed thoroughly by pipetting and absorption measured at 595nm in a spectrophotometer. The absorption value was plotted against protein concentration to obtain a standard curve. Similarly, 1ul of WCL was mixed with 1ml of Bradford reagent and the absorption value used to determine the protein concentration based on the BSA standard curve. Equal amounts of WCL was calculated and used for western blotting by SDS-PAGE.

2.5.2.3 Western blotting

Western blots were performed using standard procedures. Whole cell lysates were separated by SDS–PAGE, and subsequently transferred onto nitrocellulose membranes by wet transfer. After transfer, the membrane was stained with Ponceau S staining and then blocked in 5% milk for 1 hour prior to incubation with primary antibodies overnight.

2.5.2.4 In vivo ubiquitylation

293T cells in 100-mm plates were transfected with His-ubiquitin, Flag-tagged ATMIN and Flag-tagged UBR5 using a calcium phosphate protocol (Profection). After 48 hours, cells were harvested and 1/10th volume of the lysate was used for standard western blotting to equalise the amount of protein used for pulldowns (since ATMIN and UBR5 appear to stabilise each other when overexpressed) and

the rest used for pulldown with Ni-NTA beads (Qiagen). For the IP, cells were lysed in ubiquitin wash buffer A and incubated with Ni-NTA beads at 4°C overnight. Beads were washed three times with buffer A, twice with buffer B (1:5 dilution of buffer A in 25mM Tris-HCl, pH 6.8, 20mM imidazole) and twice in buffer C (25mM Tris-HCl, pH 6.8, 20mM imidazole). The IP mixture was boiled in 2X SDS loading buffer in the presence of 200mM imidazole). The eluted proteins were analysed by western blot for the ATMIN ubiquitination by probing with Flag-HRP (Sigma).

2.5.2.5 Nuclear/cytoplasmic fractionation

Cells were harvested by trypsin, washed once with cold PBS and spun down by centrifugation. Cell pellet was resuspended gently in fractionation buffer A supplemented with protease inhibitors by pipetting 8 times and left on ice for 5 minutes. Cells were then spun at 13K rpm for 10 seconds and the supernatant (cytoplasmic extract) was removed and transferred into a fresh tube. The nuclear pellet was washed at least 3 times with fractionation buffer and resuspended in fractionation buffer C supplemented with protease inhibitors. The nuclear pellet is sonicated for 15 seconds at 25% max power and spun at 13K rpm for 10 minutes. Finally the supernatant, which contains the nuclear extract is transferred into a new tube.

2.5.2.6 Immunoprecipitation

For ATM immunoprecipitation, 293T cells were transfected and irradiated prior to lysis for 30 min at 4°C in 500 µl of ATM IP buffer and sonication for 4x 8seconds at 25% power. After centrifugation, supernatants were pre-cleared using IgG beads and incubated overnight at 4°C with ATM antibody prior to binding of Protein G-Sepharose beads for 3-4 hours.

2.5.2.7 In vitro kinase assay

ATM immunoprecipitates were washed thrice with ATM IP buffer, once with ATM wash buffer, and twice with kinase buffer. Kinase reactions were initiated by resuspending washed beads in 30 µl of kinase buffer containing 5uM ATP and 1 µg GSTp53 and incubated for 30 min at 30°C. The mixture was subsequently boiled in Laemmli buffer and analysed by SDS-PAGE.

2.5.2.8 Mass spectrometry

For the identification of ATMIN ubiquitylation site in Chapter 2, Flag-ATMIN was pulled down after an in vivo ubiquitination experiment using FlagM2 beads and separated by SDS-PAGE. Gel slices were isolated and subjected to automated in-gel trypsin digestion using a Perkin Elmer Janus Workstation. Extracted peptides were acidified to 0.1% TFA and analysed using a LC-MS system consisting of a Ultimate 3000 RSLC coupled to a LTQ-Orbitrap Velos (both Thermo Fisher Scientific). Peak lists were extracted from the raw data using Mascot distiller and searched with Mascot v.2.4.1 (Matrix Science). Ubiquitinated peptides were identified by searching for a variable mass addition of 114.042927Da on non- C-terminal lysines, corresponding to the glycine-glycine remnant remaining after trypsin digestion of an ubiquitinated protein.

2.5.3 Cell biology

2.5.3.1 Cell Culture, Transfection and Infection

Primary Murine Embryonic Fibroblasts (MEF) cells were derived from E12.5 embryos. 293 and primary MEF cells were cultured in DMEM supplemented with 10% FCS, at 37 °C with 5% CO_2 and 3% O_2. For in vitro deletion of ATMIN, *$ATMIN^{F/F}$; cre-ERT* MEFs was incubated with DMEM supplemented with 25nM of 4-hydroxytamoxifen for consecutive 7 days, with daily replacement media.

HEK293T, 293A, HeLa Ohio, HCT116 cell lines were cultured in DMEM supplemented with 10% FCS, at 37 °C with 5% CO_2 and 20% O_2. ATM wildtype and null lymphoblastoid cell lines were cultured in RPMI media supplemented with 10% FCS, at 37 °C with 5% CO_2 and 20% O_2.

2.5.3.2 Cell transfection

Transient plasmid transfections of 293 cells were performed using Lipofectamine 2000 (Invitrogen) according to manufacturer's protocol. Namely, 1 million cells were seeded onto 10cm dishes at sub-confluent density 24 hours prior to transfection. DNA and Lipofectamine 2000 were separately diluted in pre-warmed Opti-MEM (500ul each) and then mixed gently and allowed to incubate at room temperature for 30 minutes. Cells were washed once with pre-warmed PBS prior

to addition of transfection mixture and Opti-MEM to a total volume of 5ml. After 4-6 hours, the Opti-MEM was aspirated from the cells and replaced with pre-warmed DMEM and cells allowed at least 24 hours before harvest. siRNA SMARTpools and RISC-free control siRNA were obtained from Thermofisher. siRNA transfection of 293 cells and HeLa Ohio were performed using Dharmafect 1 (Invitrogen) and Lullaby reagent (Ozbiosciences) respectively, using the same method as Lipofectamine 2000 transfection. siRNA transfection of immortalised MEFs was done using Amaxa nucleofactor kit (Lonza). Namely, MEFs were trypsinised and mixed with an appropriate amount of siRNA and nucleofactor reagent and placed into an amaxa cuvette. Electroporation was done with the appropriate programme using an amaxa nucleofactor and MEFs were immediately placed into pre-warmed media. Cells were transfected with siRNA for 72 hours prior to harvest. For FlagUBR5 ubiquitination assays, 293 cells were transfected using the calcium phosphate method (Promega). Namely, the appropriate amount of DNA and 2M CaCl2 were diluted in HBSS separately. CaCl2-HBSS mixture was added dropwise to DNA-HBSS while agitating the tube to allow proper mixing. The transfection mixture was incubated at room temperature for 30 minutes prior to addition to cells. The cell medium was changed prior to transfection and again 24 hours after transfection. Cells were harvested 48 hours after transfection for analysis.

2.5.3.3 Cell infection

For Cre mediated deletion of floxed alleles (e.g. *atmin*$^{f/f}$), primary MEF cells were infected at passage two with Adeno-Cre-GFP virus (Gene Transfer Vector Core, Iowa University). Cells were passaged into one day before infection to achieve 50% confluency. 10ul of Adeno-Cre-GFP or Adeno-GFP was added to the cells and the medium was replaced after 48 hours. Cells were then left for another 48 hours before being used. Infection efficiency was estimated by quantifying the percentage of GFP expressing cells and the efficiency of recombination assessed by genotyping from the isolated DNA for the floxed and delta alleles. All infection steps were carried out in a Category II Containment Suite.

For retroviral infection of primary or immortalized MEFs, phoenix cells were first transfected with the retroviral construct for viral packaging. Phoenix cells were seeded 24 hours beforehand and transfected with Lipofectamine 2000 as

mentioned above. On the same day, the MEFs were passaged to ensure sub-confluent density. 24 hours post-transfection, the media was removed from the phoenix cells and passed through a 0.45um filter. Polybrene was supplemented at 10ng/ml to the filtered media, which was then added to the MEFs. MEFs were incubated overnight with virus-containing media then allowed to recover for 3-4 hours in fresh media, before another round of infection. The MEFs were infected for 3-4 days repeatedly and finally split into selection media or sorted for GFP expression by FACS.

2.5.3.4 Cell treatments

Irradiation:

For cell culture experiments, IR was carried out using a Cs137 Gamma Irradiator at 2.1Gy/min. Cells and mice were irradiated at the indicated doses and harvested after 3 minutes or 2 hours respectively, unless otherwise stated.

Osmotic shock:

Cells were washed once with ddH2O and incubated with pre-warmed osmotic shock buffer for 60 minutes.

H2O2:

Cells were washed once with PBS and incubated treated with 250uM H2O2 (Fisher scientific, BP2633-500) diluted in DMEM for 30 minutes, prepared fresh from a stock solution immediately prior to use.

Neocarzinostatin:

Cells were treated with Neocarzinostatin (Sigma, N9162) at diluted to 200ng/ml in DMEM for 20 minutes prior to harvest.

Aphidicolin:

Cells were treated with aphidicolin (Sigma, A4487) diluted to 2uM in DMEM for 18 hours prior to harvest. HeLa lacO stable cells were treated with 0.2uM of aphidicolin for 18 hours prior to harvest. Control cells were mock treated with DMSO.

Small-molecule inhibitors:

Cells were treated with ATM inhibitor Ku-55933 (Calbiochem, 118500) at a final concentration of 10uM. DNA-PK inhibitor (Millipore, LY293646) was used a final concentration of 50uM. Caffeine was used at a final concentration of 3mM. All inhibitors were added one hour prior to other DNA damage treatments.

Cycloheximide:

Cells were treated with a final concentration of 10ug/ml cycloheximide (Sigma, C4859) for the indicated times prior to harvest.

Proteasome inhibitor:

MG132 (Sigma, C2211) was diluted in media 1:1000 at a final concentration of 10uM and added to cells for four hours prior to other treatments or harvest.

2.5.3.5 FACS analysis - BrdU and sub-G1

Cells were treated with 10uM BrdU (Sigma, B5002) diluted in DMEM for the indicated times and trypsinised and washed once with cold PBS. The cell pellet was fixed in cold 70% ethanol with gentle vortexing and left at 4°C for at least 4 hours. The fixed cells were washed twice in PBS and resuspended in 2M HCl at room temperature for 30 minutes. The cell pellet was washed twice with PBS and incubated with 2ul BrdU antibody (Beckton Dickson) at 20 minutes in the dark. Cells were washed once with PBST and incubated with 50 µl secondary antibody (made up 1 in 10 in PBST) for 20 minutes at room temperature in the dark. After another PBS wash, cells were treat with 50 µl ribonuclease and 150µl propidium iodide at room temperature in the dark for at least 30 minutes prior to analysis by FACS on LSRII Flow Cytometer (BD) and the data was analysed using Flow Jo. For cell cycle and sub-G1 analysis, cells were treated with 20Gy IR and fixed after indicated times and washed twice with PBS by centrifugation. The cell pellet was treated with 50ul ribonuclease A (stock at 100ug/ml) and after washing, stained with 200ul of prodidium iodide (50ug/ml).

2.5.3.6 Immunofluorescence

Cells were adhered onto slides, treated as indicated and fixed with 4%PFA at room temperature for 10 minutes or ice-cold methanol-acetone (1:1) at -20°C for 2 hours. For PFA fixation, cells were permeabilised with 0.5% Triton/PBS for 5 minutes. Cells were then blocked with blocking buffer at room temperature for 1 hour before addition of the indicated primary antibody diluted in blocking buffer overnight. Cells were then washed three times with PBS followed by the addition of secondary antibody in blocking buffer for 1 h at room temperature. Cells were washed with PBS and incubated with DAPI before mounting in DAKO. For immunofluorescence of suspension cells, cells were plated onto poly-L-lysine

coated coverslips for 1 hour prior to fixation with 4% PFA and immunofluorescence.

2.5.3.7 Immunohistochemistry

Mice were euthanised by cervical dislocation and small intestine was prepared for histology as described before [20]. Sections were cut at 4 μm for H&E staining, 53BP1 and MCM6 stainings. To quantify the 53BP1-positive cells per crypt, 100 full crypts were scored.

2.5.3.8 The G2 trap assay and clonogenic survival assay

To assess G2/M checkpoint function, cells were irradiated For the G2/M checkpoint assay, cells were transfected with the indicated DNA constructs and irradiated after 24 hours. Nocodazole was added immediately after IR at 100nM and cells were fixed after 18 hours in cold 70% ethanol. Fixed cells were stained with phospho-Histone3 antibody and analysed using a BD Biosciences FACScan. For post-IR colony formation assay, MEFs were irradiated at the indicated doses, after which they were trypsinised cell numbers counted using a Vi-Cell XR cell counter (Beckman Coulter). By serial dilutions, cells were diluted to 250cells/ml and 1000cell/ml and 1ml of each was seeded onto 6cm plates in triplicates. After seven days, the cells were stained with crystal violet and the number of colonies on each plate was manually counted and scored as a fraction of unirradiated controls.

2.5.3.9 β-galactosidase senescence assay

Cellular senescence was measured using the Senescent cells histochemical staining kit (Sigma, CS0030). Cells were fixed with fixation buffer for 6 minutes at room temperature. After washing twice in PBS, the cells were incubated in a sealed environment in staining mixture at 37°C overnight. After staining, the cells were washed three times with PBS and analysed under a light microcope for cells that stain blue.

2.5.3.10 Detection of reactive oxygen species using H_2DCFDA

H_2DCFDA, a cell-permeable fluorescein, was used as a ROS indicator in cells. Upon oxidation within cells, the dye emits fluorescence around 530nm that can be

measured by FACS. The dye was reconstituted in DMSO immediately before use and added to the cells, which were trypsinised and resuspended in pre-warmed PBS, at a final concentration of 10uM for 30 minutes at 37°C in the dark. After incubation, cells were centrifuged and cell pellet washed once in PBS, and immediately analysed using a LSRII Flow Cytometer (BD). Unlabelled control sample and luperox treated sample were used a negative and positive controls respectively.

2.5.4 Mouse studies

The following transgenic mouse lines were used for this study:

atmin$^{\Delta/\Delta}$	Kanu et al., 2007
atmin$^{f/f}$	Kanu et al., 2010
nbs1$^{f/f}$	Frappart et al., 2005
Rosa26-LSL-YFP	Srinivas et al., 2004
Villin-CreERT	el Marjou et al., 2004

2.5.4.1 Tamoxifen injection

For the results from Chapter 1, mice were injected intraperitoneally with three consecutive daily tamoxifen injections (5ul/g body weight of 20mg/ml stock, dissolved in peanut oil). Villin-CreERT deletion efficiency and genotyping of mice was determined using a PCR based assay using primers specific for the floxed exon 4, deleted exon 4 and WT *atmin* alleles; as well as for the floxed exon 6, deleted exon 6 and WT *nbs1* alleles. For irradiation experiments, mice were subjected to whole-body exposure to gamma irradiation from a 137Cs source (1.7 Gy/min) and were sacrificed at intervals after exposure as specified. Animals were maintained and bred in the LRI Biological Resources. All animal experiments were performed in accordance with UK Home Office and institutional guidelines.

2.5.4.2 Generation of primary mouse embryonic fibroblasts

For the isolation of primary MEFs, embryos were removed at E12.5 and transferred into cold sterile PBS. Under a dissecting microscope, the placenta, yolk sac, heat, liver and lungs were removed. The head and tail were removed for

subsequent genotyping. The remaining embryo was placed in a 6-well plate containing 4ml of pre-warmed DMEM and passed through a 18-gauge needle at least 10 times to dissociate the tissue.

2.5.4.3 Extraction of intestinal tissue

Mice were culled by cervical dislocation and the intestine was removed and placed into cold PBS. The colon and small intestine were flushed with cold PBS to remove waste and then cut into three sections. A small section was removed for protein extraction. The remaining intestine tissue was placed on a gut roller and cut open longitudinally on a piece of Whatman paper. The intestine tissue was fixed in 10% NBF (Neutral-buffer formalin) overnight and then transferred into 70% ethanol. To extract epithelial cells from the intestine for protein extraction, intestinal tissue was incubated on ice in 30mM EDTA for several hours with vortexing. The remaining gut tissue was removed and epithelial cells were pelleted by centrifugation at 1500rpm. The cell pellet, which contains villi and crypt cells were used for western blot analysis.

2.5.4.4 Histology

Tissue embedding in paraffin and staining were performed by the Experimental Histopathology Service at LRI. Fixed tissue was serially dehydrated through 30 minutes in 70% ethanol, 1 hour in 85% ethanol, 1 hour in 95% ethanol and finally 1 hour in 100% ethanol. The dehydrated tissue was cleared in xylene three times at 40°C for one hour and immersed in paraffin wax and cooled for 30 minutes at 4°C. 4um thick sections were cut by a microtome and mounted onto glass slides.

2.5.4.5 Haematoxylin and eosin staining

Haematoxylin is used to stain basophilic structures such as nucleic acids and ribosome while eosin is used to stain eosinophilic structures including proteins. Paraffin-embedded sections were dewaxed by incubation in xylene for three minutes. Sections were hydrated in decreasing ethanol concentration and stained in Harris' haematoxylin for five minutes and then washed under running water for five minutes, followed by a differentiation step for five seconds in 1% HCl-70% ethanol. Sections were then stained in 1% eosin Y for five minutes and washed again under running water for five minutes. Finally, sections were dehydrated in

increasing ethanol concentration, prior to clearing in xylene and mounting on slides using DAKO.

2.5.4.6 Immunohistochemistry

Paraffin embedded sections were first cleared by immersing in xylene, then hydrated by an decreasing ethanol concentration to finally in water. For antigen retrieval, sections were incubated in pre-heated citrate buffer and heated in a microwave for another 10 minutes. After cooling to room temperature, sections were incubated in 1.6% H_2O_2/PBS for ten minutes and washed three times with PBS. After blocking with blocking buffer for one hour, sections were incubated with primary antibody diluted in blocking buffer overnight at 4°C. The next day, sections were washed three times with PBS and incubated with biotin-tagged secondary antibodies diluted in blocking buffer for one hour at room temperature. After another three washes with PBS, sections were incubated in diaminibenzidine/H_2O_2 (DAB solution, Biogenex) for three to five minutes. The staining reaction was terminated by washing the sections in ddH_2O. Sections were counter stained with Mayer's haematoxylin for five minutes. The sections were then dehydrated by washing twice in 70% ethanol and twice in 100% ethanol, and cleared with two three-minute immersions in xylene prior to mounting in DPX mounting medium.

2.5.5 Statistics

Statistical evaluation was performed using the Student's two-tailed t test. Data is presented as mean ± s.e.m. and $p \leq 0.05$ was considered statistically significant.

2.5.6 Genome screen

Library and cells preparation: The Dharmacon human cDNA library was aliquoted into 96-well plates, in triplicates, using an automated robot to achieve a final siRNA concentration of 37.5nM per well. A total of 801 plates were used for the primary screen. HeLa Ohio cells were expanded into 50 x 175cm^2 Flasks and incubated at 37ºC, 10% CO_2 for three days to let the cells reach 80-90% confluency.

Cell transfection: Library plates were allowed to thaw at room temperature for 30 minutes and centrifuged for one minute. Control siRNAs were diluted and pipetted into the first two columns of each plate using a automatic multichannel pipette. 10ul of lullaby transfection reagent diluted (0.2ul in 10ul) in optimem were added to each well of the assay plates using WellMate. Plates are gently tapped to mix the reagents and incubated at room temperature for 20 minutes. Meanwhile, cells were trypsinised and diluted to 5 $x10^4$ cells/ml in DMEM. 80ul was added to each well using WellMate to achieve a final concentration of $4x10^3$ cells/well. Cells were incubated with the transfection mixture at 37°C, 10% CO_2 for 3 days. Transfection was carried out in batches of 200 plates.

Treatment with Aphidicolin: After 48 hours of transfection, the culture media was aspirated using a plate washer and 100ul/well of 2uM aphidicolin was added using WellMate. Cells were incubated at 37°C, 10% CO_2 overnight.

Cell fixation and staining: The culture media was aspirated using a plate washer and 100ul/well of cold methanol was added using WellMate. Plates were sealed and stored at -20°C. Prior to staining, the plates were thawed briefly at room temperature and washed three times in PBS using a plate washer. 50ul/well of blocking buffer was added using WellMate and plates were incubated at room temperature for 30 minutes. Blocking buffer was then aspirated and 30ul/well of primary antibody solution (diluted 1:400 in blocking buffer) was added using WellMate and left to incubate at room temperature for two hours. After three washes of PBS, 30ul/well of secondary antibody diluted (1:400 in blocking buffer) was added using WellMate and left at room temperature in the dark for a further two hours. After another three washes of PBS, 40ul/well of DAPI solution diluted (1:10000) in PBS was added and left to incubate in the dark for one hour, prior to a final PBS wash and plates were added with 30ul of PBS, sealed and stored at 4 °C prior to analysis.

Analysis by Cellomics Arrayscan High-content Analysis reader: At least 15 images were acquired in each of the three channels: DAPI, pATM (Alexa-fluor488), 53BP1 (Alexa-fluor647). A threshold was established from previous optimisation to determine the range of detection of foci. Average number of foci

was primarily used as the perimeter in hits selection, and average foci intensity and total foci area were also used as control criteria. The z-score for the primary screen was calculated using CellHTS2 software. The score for each well is normalised as: normalised well score = (raw well data value - median of sample wells on plate) / median absolute deviation of sample wells on plate. The final z-score from the three replicates was a median of the three z-scores from the triplications. The median of plate samples was used because within the primary screen, the assumption is that the majority of the siRNAs will not have an effect and therefore can act as a background reference. For the secondary and deconvolution screens, due to the preselected hits, it cannot be assumed that the majority of siRNAs will not have an effect. Thus a standard percent of control calculation was used for both of these screens, normalised to a negative control such as RISC-free.

Chapter 3. ATMIN competes with NBS1 for ATM binding

This work has been a collaboration with Kay Penicud from the lab and has been published in Cell Reports (Zhang et al., 2012).

3.1 ATMIN overexpression impairs ATM signalling after IR

As a cofactor of ATM, ATMIN shares a conserved C-terminal ATM interaction motif with NBS1 (Figure 4). This leads to the hypothesis that that ATMIN may compete with NBS1 for ATM binding, thus the protein level and strength of interaction of ATMIN and NBS1 could influence ATM pathway choice. In order to test this hypothesis, I overexpressed increasing amounts of ATMIN and observed a dose-dependent decrease in ATM signalling, thus suggesting that ATMIN level could affect ATM signalling after IR (Figure 11A). To test if ATM signalling was impaired due to increase in ATMIN levels, proteasome inhibitor (MG132) was used which itself led to a decrease in ATM signalling. Adding proteasome inhibitor (MG132) in addition to ATMIN overexpression further impaired ATM signalling (Figure 11B), suggesting that the effect could be due to further increase in ATMIN protein levels due to MG132, or that MG132 and ATMIN could act in parallel pathways to impair ATM signalling. The MG132-dependent impairment to ATM signalling after IR was also seen by immunofluorescence staining for phospho-SMC1, a phosphorylation substrate of ATM (Figure 11C). However, if ATMIN is depleted by siRNA, the PI effect on ATM signalling is rescued and more cells stained positive for pSMC1. This suggests that proteasome inhibition could impinge upon ATM signalling via ATMIN, however this does not rule out that there are other substrates whose ubiquitin-dependent turnover may be essential for robust ATM signalling.

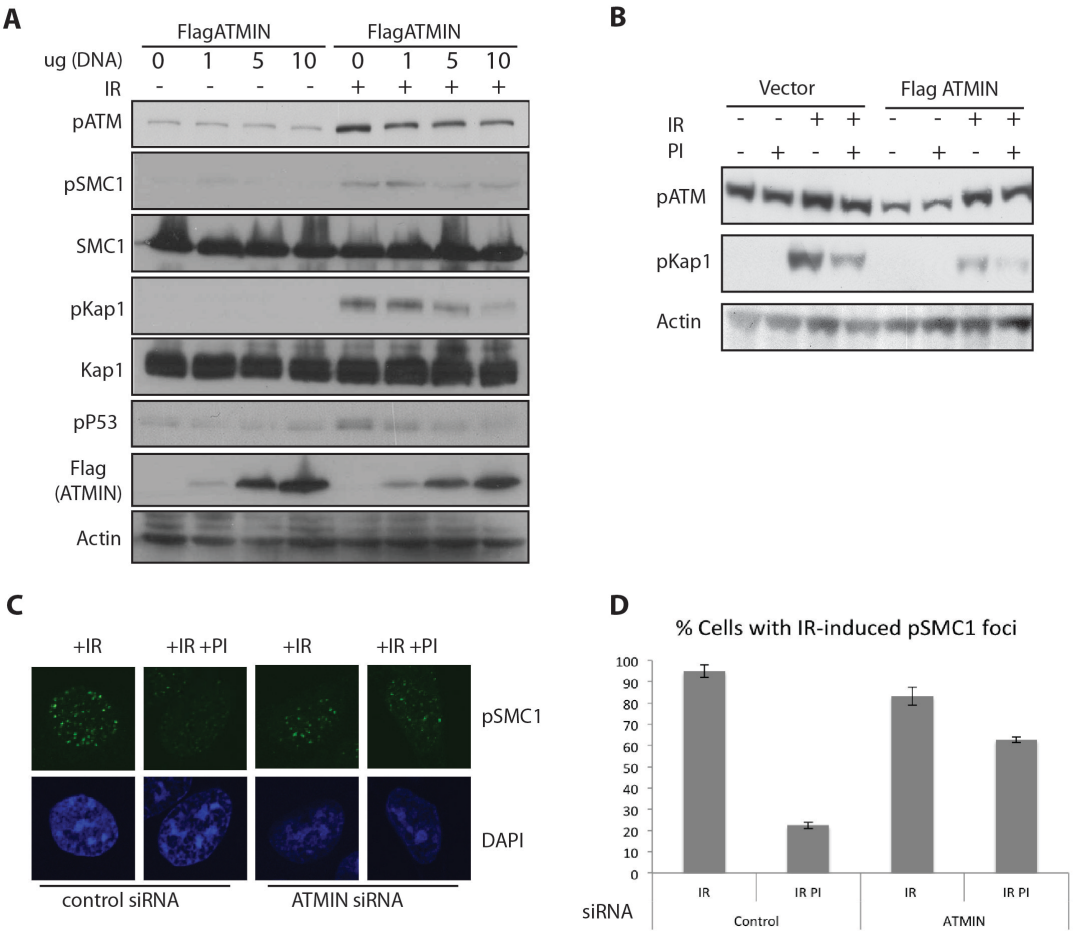

Figure 11. ATMIN overexpression impairs ATM signalling after IR.

(A) 293T cells were transfected with the indicated amounts of FlagATMIN or vector plasmid for 24 hours and treated with IR (2Gy). Whole cell lysate was harvested after 30 minutes for western blot analysis. (B) 293T cells were transfected with FlagATMIN or vector control for 24 hours, treated with or without MG132 (4 hours) and then irradiated (2Gy). Whole cell lysate was harvested for western blotting. (C) Immunofluorescence of pSMC1 on 293A cells transfected with siATMIN or siControl for 72 hours and treated with IR (2Gy) prior to fixation. (D) Quantification of percentage of cells positive for pSMC1 foci. Cells were scored as positive if they harboured more than 10 foci.

3.2 The ATM interaction motif of ATMIN is required to impair ATM signalling after IR

To further analyse the function of ATMIN, the N-terminus (ATMINΔC) or C-terminus (ATMINΔN) of ATMIN was used for overexpression, with the latter bearing the ATM-interaction motif (Figure 12A). While the C-terminus of ATMIN has a similar effect as full length ATMIN in impairing ATM signalling after IR, the N-terminus had less significant effect on ATM substrate phosphorylation either by immunofluorescence of 53BP1 as a substrate of ATM pathway or by ATM-phosphorylation of KAP1 (Figure 12B-D). In addition, overexpression of full length ATMIN or the C-terminus also abrogated NBS1 recruitment into foci after IR, while γH2AX foci formation was unaffected (Figure 12B,C), suggesting that the amount of damage is not altered by ATMIN overexpression. This also supports the hypothesis that ATMIN, if upregulated, could counteract the interaction of NBS1 with pATM, and that this is dependent on the ATM-interaction motif of ATMIN. Furthermore, the effect of ATMIN overexpression could be overcome by co-overexpressing NBS1, which suggests a titration effect of NBS1 to rescue ATM signalling (Figure 12E).

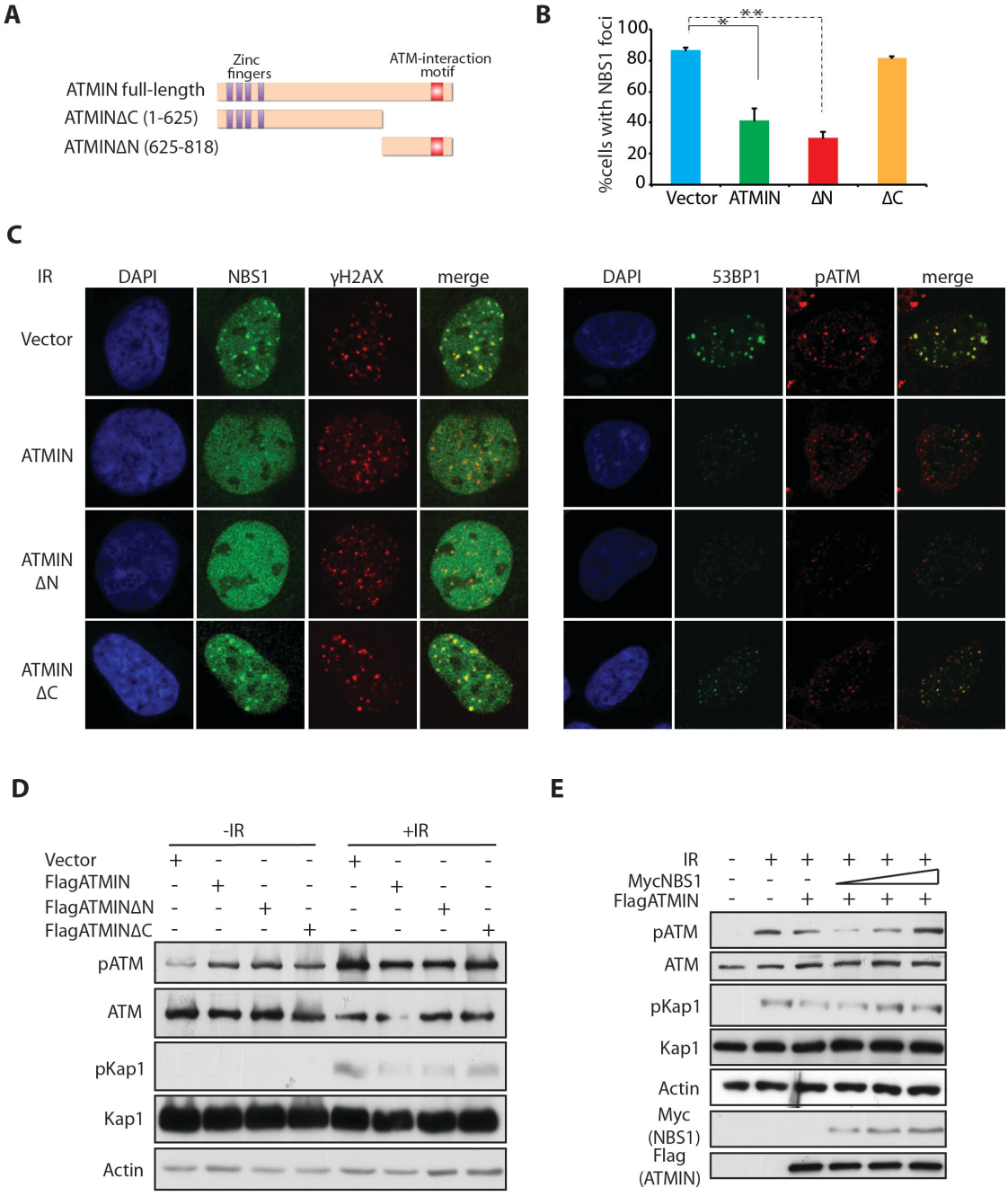

Figure 12. ATMIN-dependent impairment of ATM signalling requires the ATM-interaction motif.

(A) Scheme of ATMIN full-length, N- and C-terminal fragments used for overexpression studies. (B) Quantification of immunofluorescence staining of NBS1 foci in 293A cells (C) after transfection with the indicated ATMIN constructs and irradiation (2Gy). Cells were also stained for γH2AX, 53BP1 and pATM after the same treatment. (D) 293T cells transfected with the indicated constructs were irradiated (2Gy) and whole cell lysate harvested for western blot analysis. (E) 293T cells were transfected with FlagATMIN and increasing amount of MycNBS1 or vector and irradiated prior to harvest of whole cell lysate for western blot analysis.

3.3 Loss of ATMIN augments ATM signalling after IR

While increasing ATMIN levels decreased canonical ATM signalling, I wanted to test if decreasing ATMIN levels has the opposite effect. I generated immortalised *atmin*$^{F/F}$; cre-ERT mouse embryonic fibroblasts (MEFs) and immortalised the latter with large T antigen. Subsequently, ATMIN deletion was induced in vitro by adding 4-hydroxy-tamoxifen. The deletion was confirmed by genoptyping PCR for genomic region of *atmin*, QPCR for *atmin* transcript and western blotting for ATMIN protein level (Figure 13A). The resulting *atmin*-deficient MEFs, compared to *atmin*$^{F/F}$ wildtype, showed increased ATM signalling after low doses of IR (Figure 13B). This was validated using HeLa cells in which ATMIN was transiently silenced by siRNA, and resulted in an increase in pATM foci intensity as quantified by high-throughput microscopy, as well as increased NBS1 recruitment (Figure 13B,C). Hence, these data further show that ATMIN plays a role in regulating ATM signalling after IR.

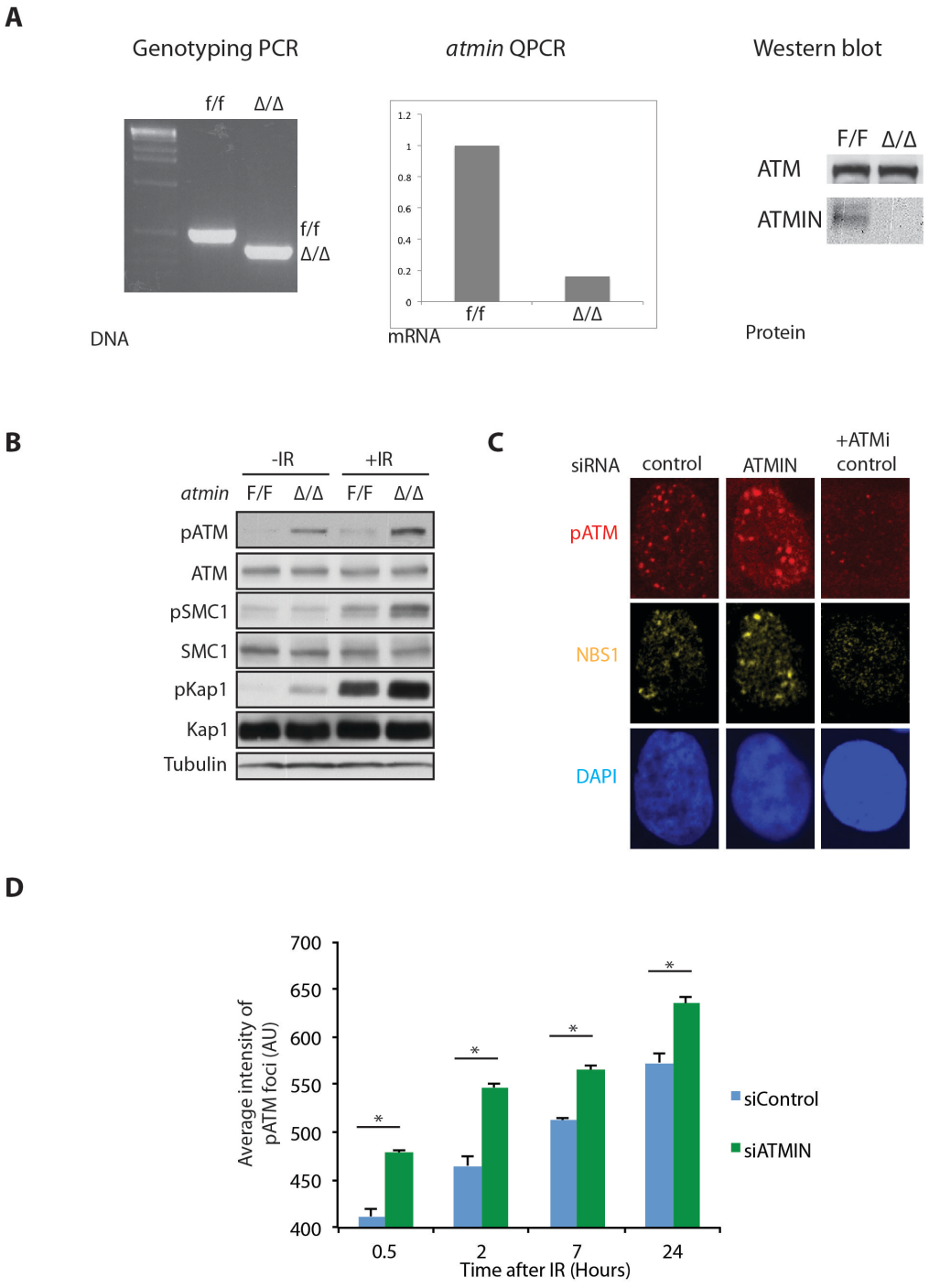

Figure 13. Loss of ATMIN increases NBS1-dependent ATM activation.

(A) Confirmation of endogenous ATMIN deletion by genotyping PCR on genomic DNA, QPCR using primers against the 3' UTR of ATMIN mRNA, and western blot to detect ATMIN protein from MEF whole cell lysate. (B) *atmin*$^{f/f}$ or *atmin*$^{\Delta/\Delta}$ MEFs were treated with IR and irradiated (1Gy) prior to harvest of whole cell lysate for western blot analysis. (C) Immunofluorescence of pATM and NBS1 on HeLa cells after treatment with siATMIN or siControl and treated with IR (1Gy). (D) Quantification of average pATM foci intensity on HeLa cells treated as in (B) by Arrayscan High-Content Analysis reader. Cells were fixed after IR at the indicated time points. (*= $p<0.05$)

The upregulation of ATM signalling after IR after loss of ATMIN can also be observed in vivo. *atmin*$^{f/f}$; *villin-creERT* mice were generated (see methods) and intestine-specific deletion of ATMIN was induced at 4 weeks of age by intra-peritoneal injection of tamoxifen. This led to efficient deletion of ATMIN in the intestine (*atmin*$^{\Delta G/\Delta G}$) confirmed by western blotting for total ATMIN protein level in gut lysate, as well as checking for YFP reporter expression after cre-mediated recombination. (Figure 14A,B). *atmin*$^{f/f}$ or *atmin*$^{\Delta G/\Delta G}$ mice were subjected to whole-body irradiation and the intestinal villi and crypts were harvested for western blotting. Gut lysate from *atmin*$^{\Delta G/\Delta G}$ mice showed an increase in ATM signalling two hours post IR (Figure 14C), which is corroborated by increased 53BP1 foci in the villus cells by immunohistochemistry (Figure 14D,E). Hence, both *in vitro* and *in vivo,* the flux through the ATM-NBS1 pathway is increased in the absence of ATMIN.

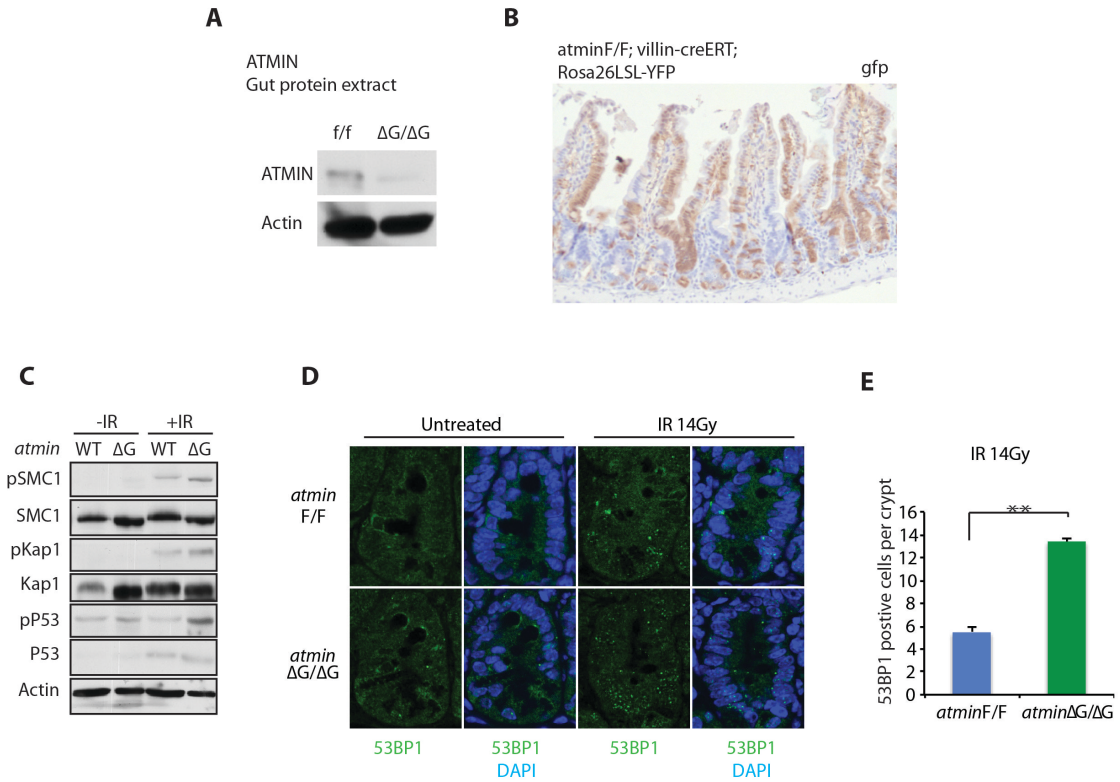

Figure 14. Loss of ATMIN in the intestine augments ATM signalling *in vivo*.

(A) Small intestine tissue lysate was prepared from *atmin*$^{f/f}$ and *atmin*$^{\Delta G/\Delta G}$ mice and analysed by western blotting for ATMIN protein level. (B) Immunohistochemistry staining of YFP reporter in the small intestine of *atmin*$^{f/f}$*; villin-creERT; Rosa26-LSL-YFP* animals showing efficiency of recombination two weeks after tamoxifen-induced *atmin* deletion. Brown staining indicates YFP expression. (C) *atmin*$^{f/f}$ and *atmin*$^{\Delta G/\Delta G}$ mice were irradiated with IR (14 Gy) and sacrificed after 2 hours. Small intestine tissue was homogenised in RIPA buffer supplemented with protease and phosphatase inhibitors and analysed by SDS-PAGE. (D) Immunofluorescence of fixed paraffin-embedded intestine tissue showing 53BP1 foci in representative crypts of the indicated genotypes taken at a similar time-point as for western analysis. (E) Quantification of 53BP1-positive cells by IHC-IF in *atmin*$^{f/f}$ (n=5) and *atmin*$^{\Delta G/\Delta G}$ (N=6) mice in intestinal crypts. ***p=0.003.*

3.4 ATMIN directly competes with NBS1 for ATM interaction

To study if ATMIN has any effect on the direct interaction of ATM and NBS1, ATM was immunoprecipitated from cell lysate with overexpressed ATMIN. NBS1 co-immunoprecipitated with ATM after IR, and this interaction was decreased in the presence of ATMIN overexpression (Figure 15A) together with decreased ATM autophosphorylation. This was also confirmed by immunoprecipitation using a pATM-specific antibody, which pulled down significantly lower amounts of total ATM protein in ATMIN overexpressing cells. NBS1 was efficiently immunoprecipitated by the pATM antibody, confirming a previous report that NBS1 specifically associates with pATM (Uziel et al., 2003). ATMIN overexpression also resulted in less NBS1 being pulled down by pATM antibody, showing reduced pATM–NBS1 interaction. Hence, ATMIN interferes with IR-induced ATM signalling by competing with NBS1 for ATM binding.

To investigate if ATMIN directly competes with NBS1 for ATM binding and to rule out other factors that might play a role such as RAD50 and MRE11, an in vitro translation approach was used to probe the interactions between ATM, NBS1 and ATMIN further. Given the large molecular weight of these proteins, especially ATM, a transcription coupled translation system was used instead of purifying recombinant proteins. Equal amounts of GFP-ATM and Myc-Nbs1 plasmid DNA together with increasing amounts of Flag-ATMIN plasmid DNA were translated in vitro using the TNT® coupled wheat-germ extract system. Using this system, a stronger western blot band was detected for NBS1 than ATMIN, suggesting that NBS1 protein could be expressed more than ATMIN given that both antibodies produce approximately equal signal intensity when used on whole-cell lysates. GFP-ATM was immunoprecipitated before blotting for Myc-Nbs1 and Flag-ATMIN. Under this circumstance, less NBS1 and more ATMIN was pulled down with ATM as the amount of ATMIN DNA was increased (Figure 15B). Since Mre11 and Rad50 are not present in the extract, this supports the hypothesis that ATMIN could compete with NBS1 for ATM binding. Nevertheless, it is impossible to rule out that in the cellular context, additional indirect effects are also responsible to

mediate the interaction with ATM in addition to the C-terminal interaction of ATMIN and NBS1.

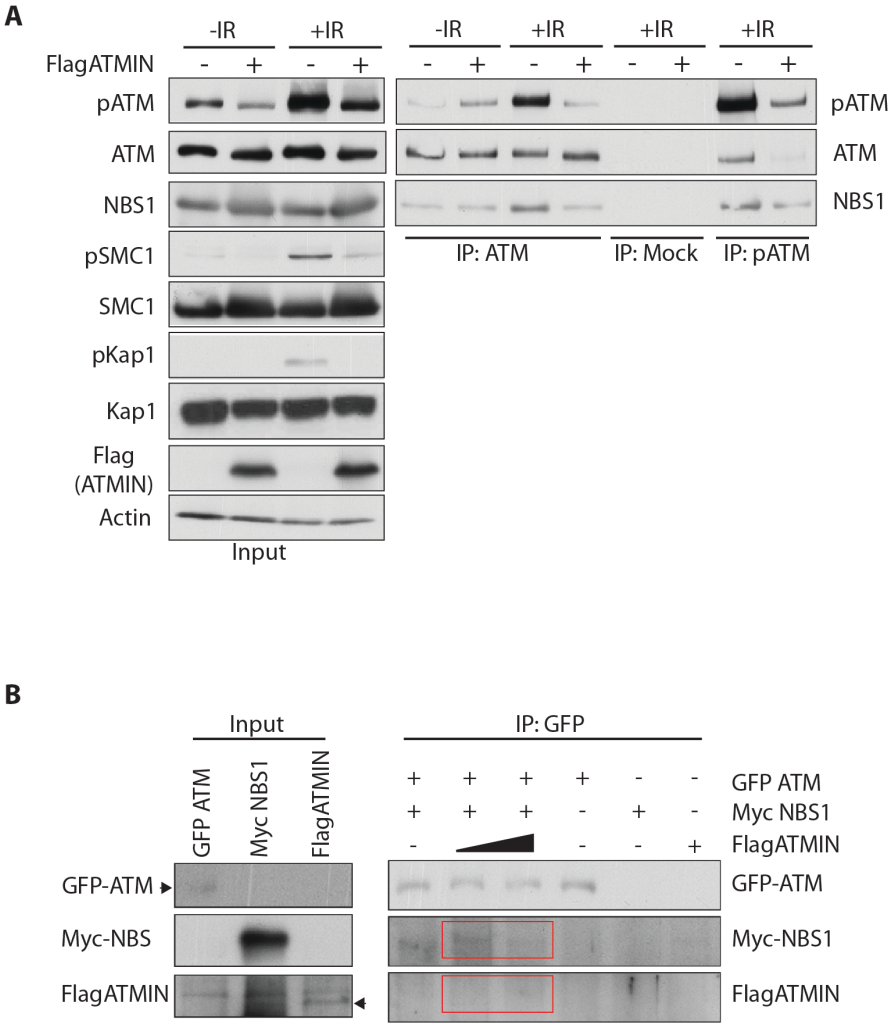

Figure 15. ATMIN overexpression impairs NBS1-ATM interaction.

(A) 293T cells transfected with full-length Flag-ATMIN were treated with IR (2 Gy) and whole cell lysate was used for ATM or pATM immunoprecipitation. (B) Equal amounts of GFP-ATM and Myc-Nbs1 plasmid DNA together with increasing amounts of Flag-ATMIN DNA were translated in vitro using the wheat-germ transcription-coupled translation system GFP-ATM was immunoprecipitated, and the mixture was analysed by western blotting for GFP, Myc and Flag.

3.5 Loss of ATMIN rescues proliferation arrest and senescence phenotypes in the absence of NBS1

While dysregulation of ATMIN perturbs NBS1-dependent canonical ATM signalling, the significance of this is unclear. Hence, in collaboration with Kay Penicud, *nbs1*$^{f/f}$, *atmin*$^{f/f}$ and compound floxed mice were generated to study the effect of ATMIN-dependent ATM signalling in nbs1-deficient background. While *nbs1*$^{\Delta/\Delta}$ cells have reduced IR-induced pKap1 and pp53 levels, the phosphorylation of p53 after hypotonic shock is slightly increased compared to wildtype, hence suggesting that NBS1 could also compete with ATMIN for ATM interaction after hypotonic shock (Figure 16A). NBS1 is required for proliferation and viability of MEFs (Yang et al., 2006). When NBS1 was acutely inactivated by adenoviral expression of cre recombinase in MEFs, *nbs1*$^{\Delta/\Delta}$ cells rapidly ceased to proliferate, as shown by cell number and BrdU incorporation (Figure 16B,C), and displayed signs of senescence even at low atmospheric oxygen levels (3%) at which wildtype MEFs do not undergo senescence, such as a flat enlarged morphology and cessation of proliferation at subconfluent densities. Senescence in these MEFs was confirmed by using senescence-associated β-galactosidase activity (Figure 16C,D). On the other hand, wildtype and *atmin*$^{\Delta/\Delta}$ MEFs proliferated normally and reached confluence. *atmin*$^{\Delta/\Delta}$*; nbs1*$^{\Delta/\Delta}$ double mutant MEFs partially rescued the proliferation defect and premature senescence of *nbs1*$^{\Delta/\Delta}$ MEFs, hence suggesting that the phenotypes observed in *nbs1*$^{\Delta/\Delta}$ cells could be due to increased ATMIN-mediated ATM signalling, which is ameliorated by concomitant loss of ATMIN.

In addition, ATMIN deletion can also rescue the loss of the progenitor pool in vivo in NBS1-depleted intestinal tissue. While nbs1 knock-out is embryonic lethal (Zhu et al., 2001), the acute deletion of nbs1 in the intestine of tamoxifen-treated nbs1F/F; villin-creERT (*nbs1*$^{\Delta G/\Delta G}$) mice results in disintegration of the intestinal mucosa. The phenotype is marked by loss of individual intact villus-crypt units and a depletion of progenitor cells marked by MCM6 at the bottom of crypts (Figure 16E,F) (Haigis et al., 2006). While *nbs1*∆*G/*∆*G* mice showed a substantial decrease in MCM6 positive cells, that in the double mutant mice were comparable

to wildtype. Hence, the loss of ATMIN rescues the progenitor cell depletion phenotype caused by NBS1 deficiency.

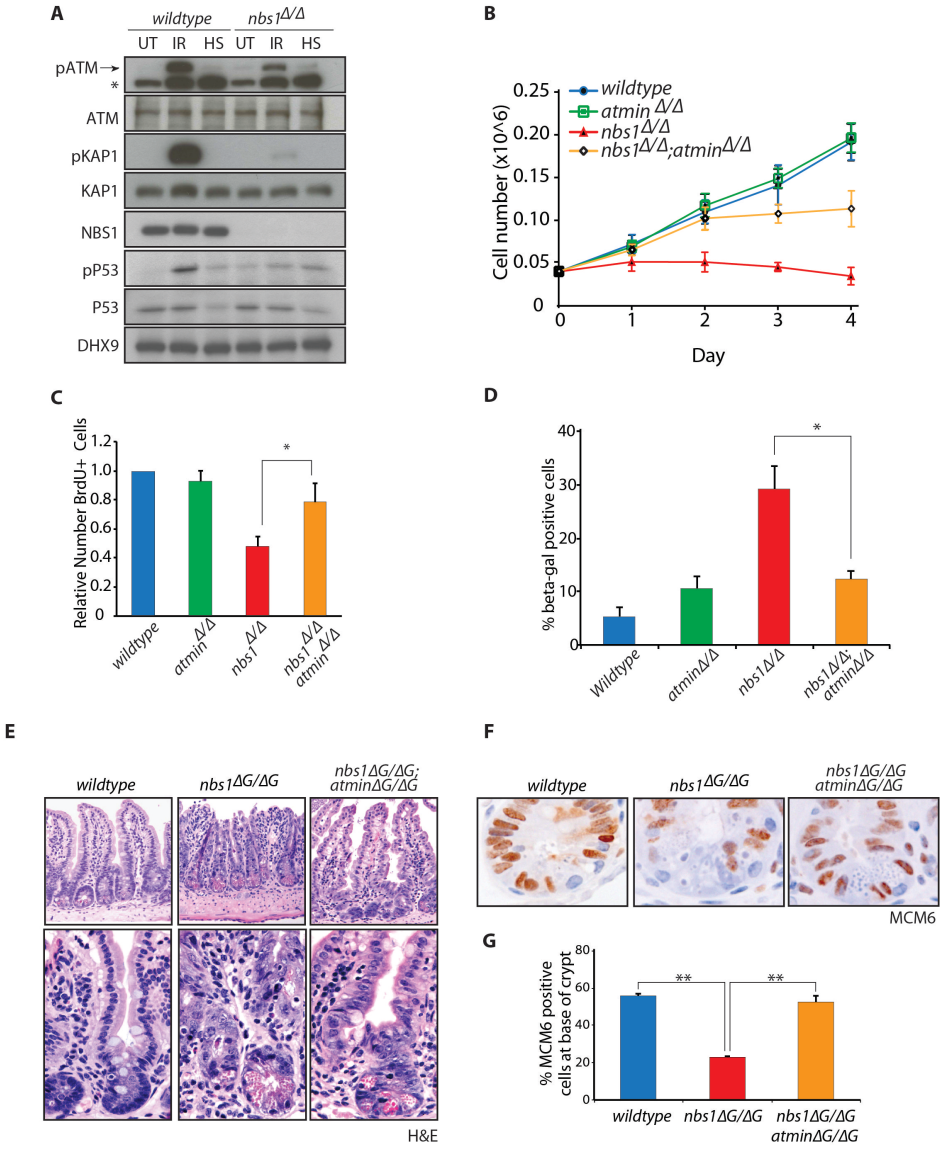

Figure 16. Co-deletion of *atmin* and *nbs1* rescues the lethality of *nbs1*Δ/Δ. (Kay Penicud)

(A) Wildtype and *nbs1*Δ/Δ MEFs were either untreated, treated with 135mOsm hypotonic shock buffer (HS) (1 hour) or IR (2Gy) and whole cell lysate harvested after fifteen minutes for western blotting with the indicated antibodies. (B) Primary MEFs were infected with AdenoCreGFP (*atmin*Δ/Δ, *nbs1*Δ/Δ and *nbs1*Δ/Δ*; atmin*Δ/Δ*)* for seven days and seeded at $4X10^4$ cells per well. Total cell number was counted after each day in triplicate over four days. (C) MEFs were treated with 10μM BrdU for 30min and analysed by FACS for BrdU incorporation, and shown as fraction of BrdU positive cells relative to wildtype. (*p=0.039) (D) Quantification of percentage of cells positive for b-galactosidase staining (*p=0.0028). (E) H&E staining on representative intestinal villi and crypts of mice with the indicated genotypes at 6 weeks of age. (F) Immunohistochemistry for MCM6-positive cells on representative intestines of mice with the indicated genotypes 5 days after VillinCre-ERT mediated deletion of *atmin* and *nbs1*. (G) Quantification of percentage of MCM6 positive cells in the crypt. (**p=0.0093)

3.6 *atmin*$^{\Delta/\Delta}$; *nbs1*$^{\Delta/\Delta}$ double mutant MEFs have more spontaneous DNA damage but fail to activate ATM in response to IR

In order to study the relative contribution of each cofactor to ATM activation, ATM signalling was examined in *atmin*$^{\Delta/\Delta}$, *nbs1*$^{\Delta/\Delta}$ or double mutant MEFs after spontaneous DNA damage and IR. In basal conditions, both *nbs1*Δ/Δ and *atmin*Δ/Δ mutant MEFs showed an increased percentage of cells with γH2Ax foci, in line with previous reports (Yang et al., 2006, Kanu et al., 2010) (Figure 17A), indicating that NBS1 and ATMIN are both required to protect against endogenous DNA damage. Moreover, spontaneous DNA damage was increased even further in *atmin*$^{\Delta/\Delta}$; *nbs1*$^{\Delta/\Delta}$ double mutant MEFs, indicating that NBS1 and ATMIN could act via different pathways due to the additive effect. While basal levels of pATM were detected by immunofluorescence in wildtype, *nbs1*$^{\Delta/\Delta}$ and *atmin*$^{\Delta/\Delta}$ single mutant MEFs, pATM was not detectable in *nbs1*$^{\Delta/\Delta}$; *atmin*$^{\Delta/\Delta}$ double mutant cells. The lack of ATM activation was confirmed by western blot, which shows no detectable pATM or ATM substrate phosphorylation after 5Gy IR, while ATM activation after oxidative stress was only slightly impaired (Figure 17B). This finding was also confirmed in vivo by immunohistochemistry staining of intestinal crypts in *nbs1*$^{\Delta/\Delta}$; *atmin*$^{\Delta/\Delta}$, which fail to form IR-induced 53BP1 foci and showed no pATM substrate phosphorylation after whole-body irradiation (Figure 17C,D). Thus, these data show that in the absence of both NBS1 and ATMIN, ATM cannot be activated and phosphorylate substrates after IR.

To address the physiological consequence of the heightened DNA damage and lack of ATM signalling in the absence of ATMIN and NBS1, NBS1/ATMIN double deficient MEFs and mice were irradiated. Double mutant MEFs showed an increased population of sub-G1 cells, a marker of radiosensitivity due to IR-induced apoptosis that persisted at 48 hours post IR (Figure 17E). While *nbs1*$^{\Delta G/\Delta G}$ mice are sensitive to whole-body irradiation, double-mutant mice were even more sensitive despite the improved structural integrity of the intestine prior to irradiation. In addition to the absence of 53BP1 foci formation and ATM substrate phosphorylation in the intestinal cells, histological staining showed massive radiation injury and cell loss in the double mutant mice intestine (data not

shown). Thus, ATMIN deficiency renders the *nbs1*-mutant cellular phenotype similar to the *atm*-mutant phenotype, which also display increased radiosensitivity. Hence, ATMIN and NBS1 cooperate to mediate ATM signalling and in the absence of both cofactors, there is no detectable ATM activity after IR. Hence, this argues for the hypothesis that, at least after some stimuli such as IR, ATMIN and NBS1 as the only cofactors that can activate ATM, as ATM can be activated in the absence of ATMIN and NBS1 by H_2O_2 treatment.

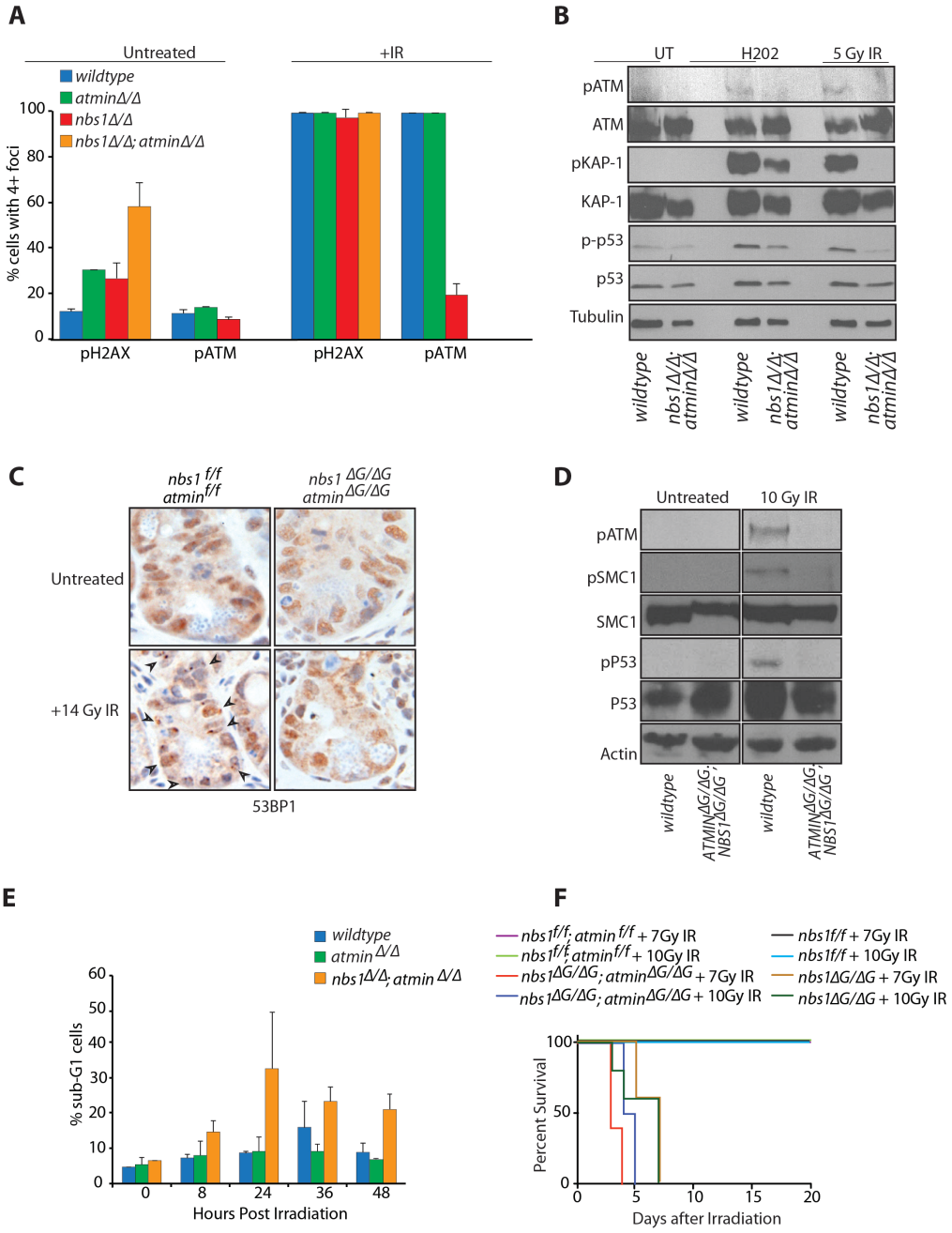

Figure 17. Loss of ATM signalling in the absence of both ATMIN and NBS1 (Kay Penicud).

(A) MEFs were infected with AdenoCreGFP (*atminΔ/Δ*, *nbs1Δ/Δ* and *nbs1Δ/Δ;atminΔ/Δ)* and cultured for seven days, prior to IR (5Gy) and fixation for immunofluorescence of pATM and γH2AX, quantified as percentage of cells positive for pATM or γH2AX foci. (B) MEFs were treated with either 250μm H_2O_2 or 5Gy IR prior to harvest of whole cell lysate for western blot analysis. (C) IHC of fixed paraffin-embedded intestine section showing 53BP1 foci in representative crypts after IR. Arrows indicate IR-induced 53BP1 foci. (D) Wildtype or *nbs1*$^{\Delta/\Delta}$*; atmin*$^{\Delta/\Delta}$*)* mice were irradiated with IR (10Gy) and tissue lysate was prepared from small intestine after 2 hours and analysed by western blotting. (E) Cells were treated with 20Gy irradiation

and fixed at the indicated time points post treatment. The percentage of sub-G1 cells was determined by FACS. (F) Four days after Villin-creERT-mediated deletion of *atmin* and *nbs1*, mice were treated with the indicated doses of irradiation (n = 5 mice per genotype per dose).

The *in vivo* data show that while the genetic deletion of ATMIN rescues the proliferation and premature senescence phenotypes of *nbs1*$^{\Delta/\Delta}$ MEFs, the rescue is not complete. This could be due to the role of NBS1 in localising MRE11 and RAD50 to the nucleus, as well as additional ATM-independent roles of the MRN complex (Deng et al., 2009, Dar et al., 2011, Williams et al., 2010). Hence, any other defects due to the loss of NBS1 will persist in *nbs1*$^{\Delta/\Delta}$; *atmin*$^{\Delta/\Delta}$ double-mutant cells. Moreover, the rescue of *nbs1*Δ/Δ phenotype by loss of ATMIN occurs despite greatly heightened level DNA damage in *nbs1*$^{\Delta/\Delta}$; *atmin*$^{\Delta/\Delta}$ double-mutant cells, suggesting that the phenotypes of NBS1-deficiency are not due to DNA damage *per se*; rather, the absence of ATMIN-mediated ATM signalling could ameliorate the cellular defects of *nbs1*$^{\Delta/\Delta}$ cells, such as due to increased p53 activity. This could be tested by co-deletion of *p53* together with *nbs1* whether the NBS1-deficiency phenotypes could also be rescued. Hence, while ATMIN and NBS1 compete for ATM interaction in vitro, they cooperate to activate ATM *in vivo* and a balance of NBS1- and ATMIN-mediated ATM signalling is required to maintain robust DNA damage signalling.

Chapter 4. UBR5 as an E3 ligase that modulates ATMIN function

4.1 Immunofluorescence-based screen for the E3 ligase that regulates ATMIN

Since ATMIN has important roles as a cofactor of ATM, and little is known about the regulation of its turnover and post-translational modifications, I wanted to investigate whether ATMIN could be regulated at the protein level. One hypothesis is that ATMIN could be regulated via proteasome-mediated degradation by an E3 ligase. It has been previously observed that ATM and ATMIN mutually stabilise each other and the instability due to loss of one partner could be rescued by proteasome inhibition (Kanu and Behrens, 2007). Moreover, endogenous and overexpressed ATMIN can also be stabilised by proteasome inhibition, as shown by western blot and immunofluorescence readouts. (Figure 18A,B) (Kanu and Behrens, 2007). These data suggests that ATMIN's interaction with ATM could stabilise it from ubiquitin-mediated degradation. A cycloheximide experiment showed that ATMIN protein has a half-life of approximately 3.5 hours (time taken for 50% reduction in signal intensity of ATMIN western blot) at basal conditions (Figure 18C,D).

In order to identify the E3 ligase that could act on ATMIN, I made a stable cell line expressing GFPATMIN by transfection and antibiotic selection. This cell line was sorted by FACS into 3 expression levels of GFPATMIN (H1, H2 and L3) and maintained for several passages while protein expression and GFP fluorescence was confirmed. L3 stable cell line showed the lowest expression level of GFPATMIN and highest fold increase after proteasome inhibitor treatment (Figure 18E). Previous data from our lab suggested that ATMIN levels could be destabilised in the absence of ATM. In the L3 stable cell line, silencing endogenous ATM led to decrease in GFPATMIN levels, which suggests that the GFPATMIN could be expressed at a more physiological level (Figure 18F). Hence this cell line was chosen for the screen. As a control, I also showed that adding proteasome inhibitor could increase the protein level and fluorescence intensity of GFPATMIN but not GFP alone (Figure 18G).

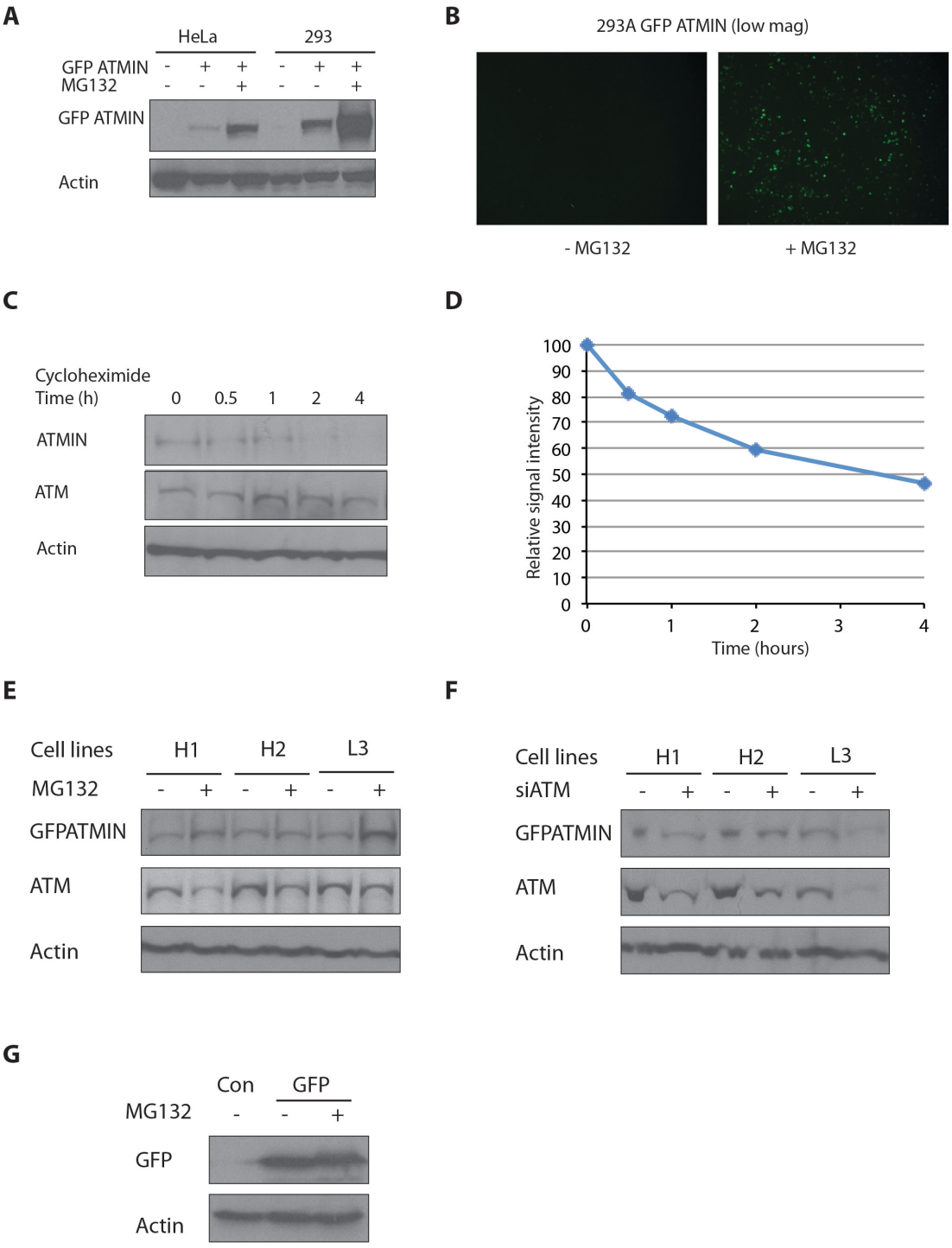

Figure 18. ATMIN is stabilised by proteasome inhibition.

(A) GFPATMIN was transiently overexpressed in HeLa or 293 cells and whole cell lysate harvested after 24 hours after proteasome inhibitor treatment where indicated. (B) Immunofluorescence of GFPATMIN overexpression in 293A cells before and after MG132 treatment. (C) Whole cell lysate of 293T cells showing ATMIN protein level after cycloheximide treatment at the indicated times, quantification of ATMIN immunoblot signal intensity normalised over actin shown in (D). (E) Three GFPATMIN expressing stable 293 cell lines, H1, H2 and L3 were treated with proteasome inhibitor and harvested for western blotting. (F) GFPATMIN expressing stable cell lines were treated with siRNA against ATM or control siRNA for 72 hours, before

harvesting of whole cell lysate for western blotting. (G) 293T cells were transfected with GFP vector and treated with proteasome inhibitor, before harvesting of whole cell lysate for western blotting.

In order to further validate the GFPATMIN stable cell lines, I tested the response to proteasome inhibitor treatment using GFP fluorescence measured by the high throughput cytometer Acumen, and observed that the L3 cell line had the greatest fold induction (3 fold) in GFP signal upon proteasome inhibitor treatment (Figure 19A). Furthermore, the GFP intensity was specific to the overexpression of ATMIN construct and not due to auto-fluorescence as the knockdown of ATMIN or GFP by siRNA reduced the GFP intensity (Figure 19B).

Hence, using GFPATMIN stabilisation as a readout, the screen was performed on a human library of 380 E3 ligases in order to identify if there is an E3 ligase that, when silenced, results in a similar increase in GFP fluorescence intensity as proteasome inhibition. With the help of High-throughput screening lab, optimisation of siRNA transfection efficiency and signal detection were performed. The L3 cell line was reverse transfected in a 96-well format with siRNA pools from Dharmacon and each sample was done in triplicate for consistency. In addition, two non-target siRNAs (OT-NT and RISC-free) and siRNA against ATMIN were used as negative controls. In addition to proteasome inhibitor treatment, siRNA against ubiquitin B (ubb) was also used as a positive control. 72 hours post-transfection, proteasome inhibitor (MG132) was added to the control wells for 4 hours prior to fixation and scanned on Acumen laser scanning cytometer for average percentage of GFP positive cells in each well. For analysis, each raw score was normalised to the median value for each plate, as well as to negative controls, to obtain a normalised z-score (Figure 19C).

As expected, proteasome inhibitor treatment resulted in the highest z-score in all the plates (z-score 8.88), as well as siRNA against ubiquitin (highest z-score 1.67). However, DMSO alone also increased the GFP fluorescence (highest z-score 2.53) as well as RISC-free control siRNA. The stabilisation effect of DMSO alone was not observed in previous tests, and the effect of RISC-free could only be speculated that it perhaps interfered with GFPATMIN degradation. ON-NT non-target control, however, behaved as expected without significant effect on GFP fluorescence, hence it was used as the negative control for normalisation.

Based on the z-score of average GFP intensity per well, four top hits were selected whose knockdown gave rise to the highest GFP fluorescence and the most reproducible result. These were, TRIM38 (z-score 2), SH3MD2 (z-score 1.52), TRIM67 (z-score 1.41) and HUWE1 (z-score 1.37).

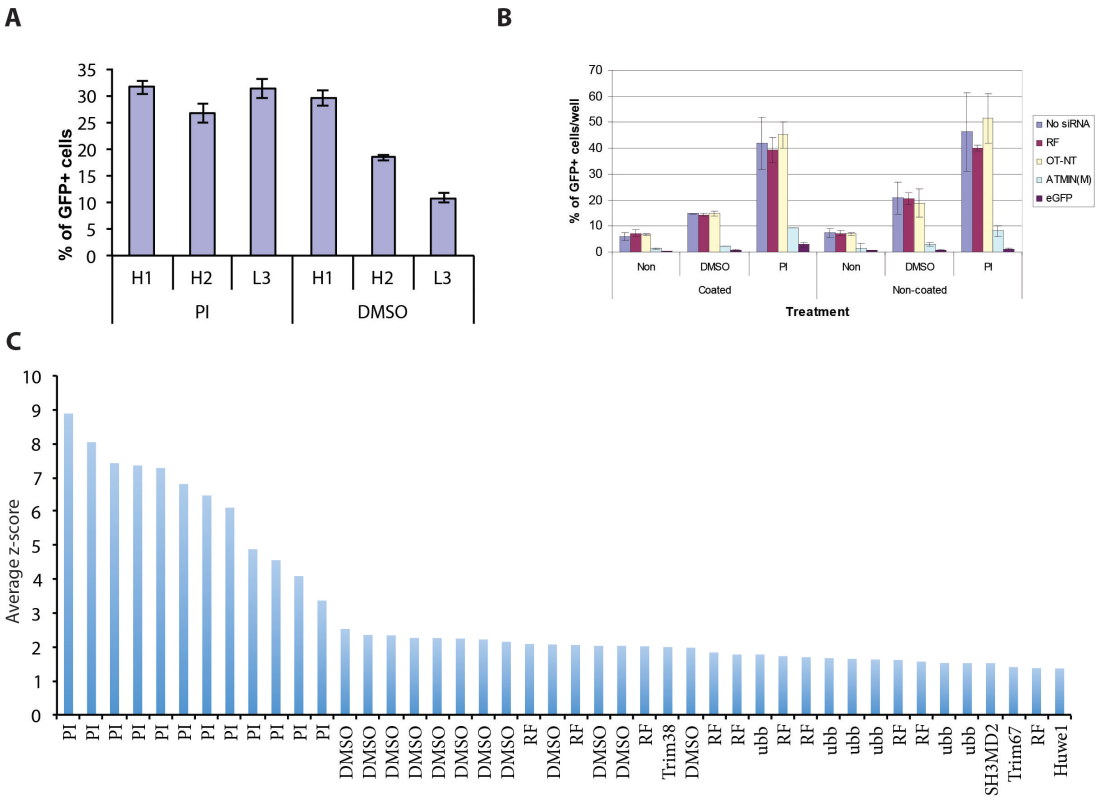

Figure 19. E3 ligase screen for regulators of ATMIN stability.

(A) GFPATMIN stable cell lines were treated with proteasome inhibitor or DMSO and analysed for GFP fluorescence by Acumen highthroughput cytometer. (B) GFPATMIN L3 cell line was transfected with siRNA against ATMIN, GFP or control siRNA for 72 hours, then treated with proteasome inhibitor or DMSO and analysed for GFP fluorescence as above. (C) Normalised z-score of top in hits from the screen, ranked in descending order. RF: risc-free control siRNA, OT-NT: Non-target control siRNA, ubb: siRNA against ubiquitin B.

TRIM38 has been recently described as an E3 ligase that has a role in the immune response (Xue et al., 2012). SH3MD2, also known as POSH, is a RING-finger containing E3 ligase that has been described as a negative regulator of death receptor mediated apoptosis through the modulation of caspase-8 activity (Christian et al., 2011). TRIM67 has been shown to regulate Ras signalling via degradation of 80K-H, which results in neural differentiation such as neuritogenesis (Yaguchi et al., 2012). HUWE1, a HECT domain E3 ligase, has been recently shown to play roles in cell proliferation and DNA damage response by regulating p53 levels (Chen et al., 2005), DNA polymerases β (Parsons et al., 2009) and Pol λ (Markkanen et al., 2012).

The four top hits from the screen were validated using siRNA pools from Dharmacon to silence the respective target genes in 293 cells, and checking the effect on ATMIN stabilization using both FlagATMIN and MycATMIN overexpression (Figure 20A-D). The efficiency of siRNA knockdown was also confirmed by quantitative PCR (Figure 20E). In addition, in order to validate if the hits have a functional role in regulating ATMIN function, I tested the effect of the knockdown on ATM signalling (Figure 20F). I have made the observation that ATMIN, when overexpressed, impairs ATM signalling after IR (Figure 11). Hence, if an E3 ligase negatively regulates ATMIN stability, its knockdown should also impair ATM signalling. However, of the four top hits, none of them reproducibly resulted in both endogenous ATMIN stabilisation and impaired ATM signalling. Some of the siRNA, such as siHUWE1, resulted in an increase in overexpressed ATMIN protein level. However, no consistent effect was observed on endogenous ATMIN. Hence, these hits did not fulfill the validation criteria and most likely do not regulate ATMIN function in vivo. However, in the end I chose to proceed with an alternative approach (Chapter 4.2). In retrospect, the screen could also have been repeated with IR to identify any E3 ligase activity that was augmented by IR or other stimuli.

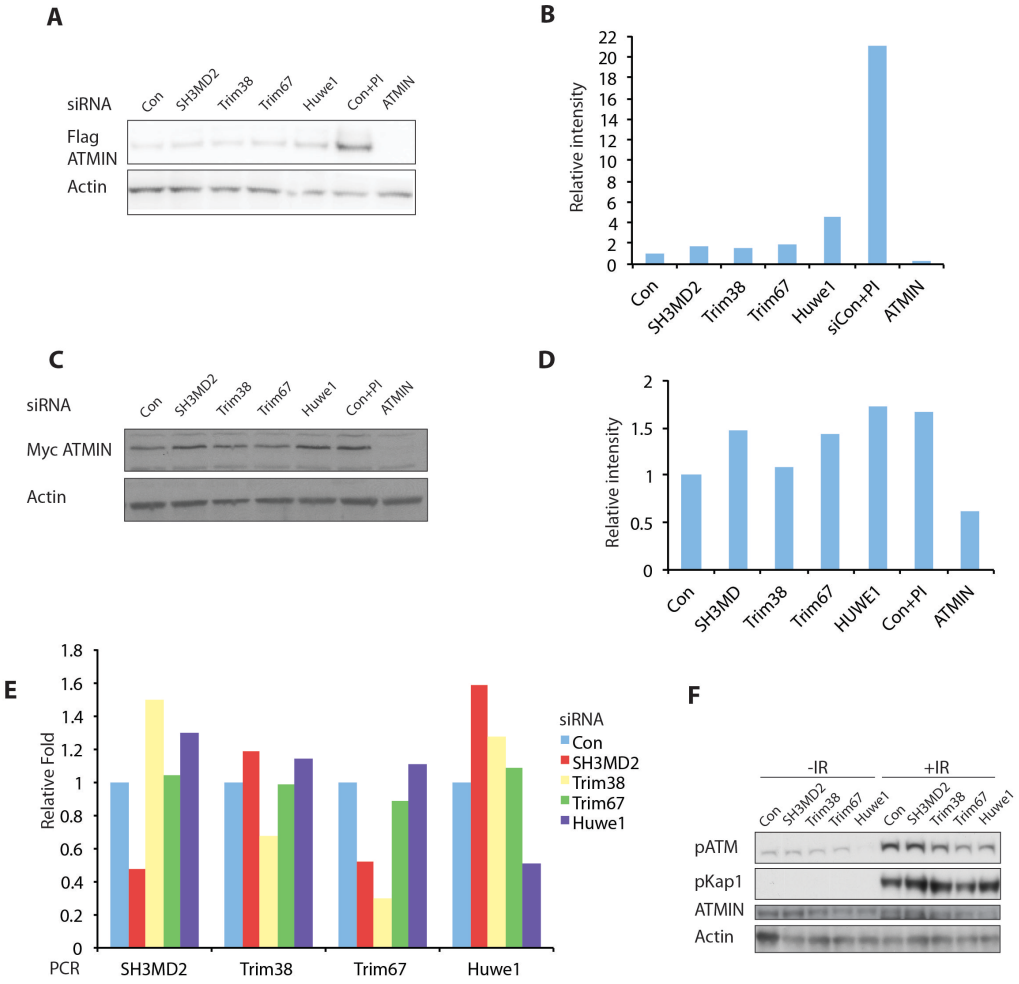

Figure 20. Validation of hits from E3 ligase screen.

(A, C) 293T cells were treated with siRNA against selected screen hits for 72 hours and FlagATMIN or MycATMIN was overexpressed during the last 48 hours. One sample was treated with proteasome inhibitor prior to harvest of WCL for western blotting. (B, D) Quantification of intensity of Flag- or MycATMIN western blot over actin. (E) QPCR showing mRNA levels after siRNA knockdown of selected hits for 72 hours. (F) 293T cells were treated with siRNA against selected hits for 72 hours, and treated with IR (2Gy) and harvested 30 minutes post-IR for western blotting using the indicated antibodies.

4.2 IP-MS screening using reconstituted MEFs

As an alternative, I used an immunoprecitation and mass spectrometry (IP-MS) approach to identify any ATMIN interactors including potential E3 ligases. In order to identify potential interactors, I used an ATMIN-deficient MEF cell line reconstituted with FlagATMIN, which is expressed at a higher level than endogenous ATMIN in vector reconstituted MEFs. By deleting the endogenous ATMIN, I would potentially enrich for the interactors pulled down by FlagATMIN. ATMIN-deficient MEFs were infected with retrovirus expressing FlagATMIN and sorted by FACS according to GFP expression from an IRES-GFP (Figure 21A). These MEFs were checked for their ATMIN protein levels by western blotting (Figure 21B), mRNA level after reconstitution (Figure 21D) as well as cre-mediated genomic deletion of floxed ATMIN allele (Figure 21E). In addition, expression of MycATMIN was able to partially rescue the defective ATM substrate phosphorylation after replication stress in ATMIN deficient MEFs (Figure 21C). These suggest that ATMIN function was partially rescued in the reconstituted MEFs and hence these cells were used for IP-MS experiments.

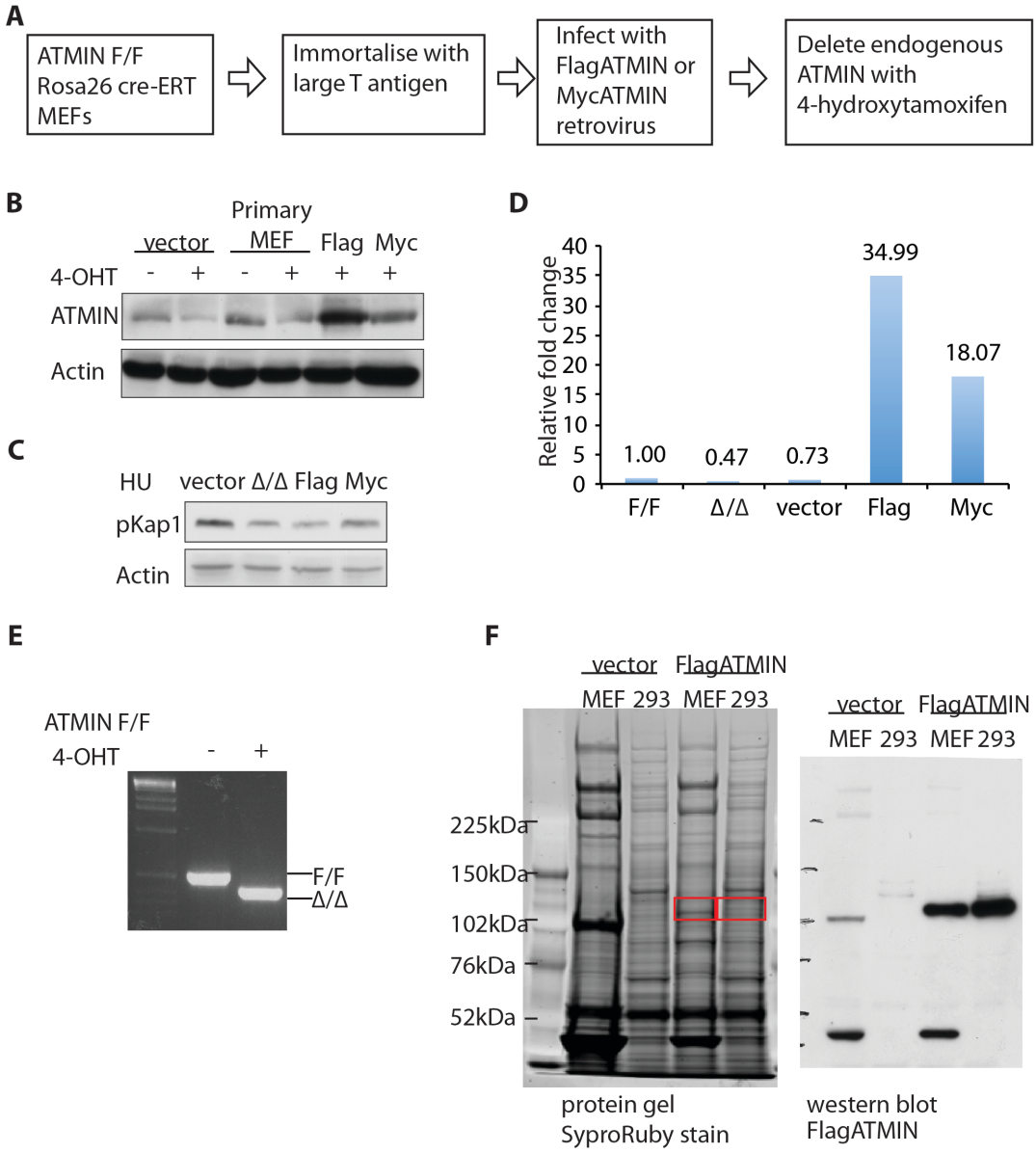

Figure 21. Reconstitution of ATMIN$^{f/f}$ MEFs for IP-MS.

(A) Scheme of ATMIN$^{f/f}$ MEF reconstitution. (B) Western blot of WCL showing ATMIN protein levels before and after tamoxifen treatment. (C) MEFs were treated for hydroxyurea for 4 hours and whole cell lysate harvested for western blotting using the indicated antibodies. (D) QPCR on MEFs showing ATMIN mRNA levels in each cell line. (E) Genomic DNA of MEFs before and after tamoxifen treatment were harvested for genotyping PCR using ATMIN flox, wildtype and delta primers. (F) Protein gel staining after flag immunoprecipitation showing FlagATMIN bands that were analysed by MS (left panel). Western blot showing corresponding position of FlagATMIN was used to confirm the pull down.

Using this approach, ATMIN was successfully identified through MS and from bands present in the ATMIN pull-down but not present in vector controls. Some interesting hits were consistently identified, such as ubiquitin activating enzyme E1 (Uba1) and ubiquitin carboxyl-terminal hydrolases. Hence, this supports the hypothesis that ATMIN could be regulated by ubiquitination. While ATMIN was consistently identified by mass spectrometry using both FlagATMIN reconstituted MEFs and 293 cells transiently transfected with 293T (Figure 21F), there were no E3 ligases amongst the proteins identified. Different treatment conditions such as replication stress, IR and proteasome inhibition were also used. An E1 enzyme, Uba1, was pulled down in three independent experiments. In addition, two deubiquitinases, Usp18 and UBP4, were also pulled down as interactors of ATMIN. This suggests that there is high probability of ubiquitination associated with ATMIN; however, the inability to pull down E3 ligases could be due to the latter's low abundance and relatively weak interaction with their substrates that make them difficult to detect using this approach. Hence, as the aim of the experiment was to identify E3 ligases that regulate ATMIN, the interactors were not followed up.

4.3 Identification of UBR5/EDD, an E3 ligase that interacts with ATMIN

Using a similar approach, a previous colleague from the lab, Janet Cronshaw, used a large-scale endogenous IP of ATMIN to identify interactors. Approximately 25 litres of 293T cells were used for the IP under basal or chloroquine treated conditions, and one E3 ligase was identified by mass spectrometry to interact with ATMIN under both of these conditions (Figure 22A). UBR5 is a HECT domain E3 ligase that was initially identified in *Drosophila melanogaster*, where its inactivation led to overgrowth of imaginal discs in larvae (Mansfield et al., 1994, Martin et al., 1977). As a member of the HECT domain family of E3 ligases, UBR5 is a large nuclear protein of 309kDa and the crystal structure of the C-loop of the HECT domain has been solved (Matta-Camacho et al., 2012). Moreover, UBR5 has been shown recently to play a role in the DNA damage response. UBR5

interacts with and ubiquitinates TOPBP1, targeting it for degradation (Honda et al., 2002). There is also evidence that it interacts with and is required for the activation of CHK2 (Henderson et al., 2006), and p53 (Ling and Lin, 2011), but this occurs independently of its E3 ligase activity.

The interaction between endogenous UBR5 and ATMIN was confirmed by co-immunoprecipitation (Janet Cronshaw, unpublished) as well as in an overexpression system (Figure 22B,C). Namely, FlagUBR5 and GFPATMIN were overexpressed separately in 293 cells and whole cell lysates were combined for co-IP. This was due to the observation that co-overexpression of both constructs in cells led to mutual stabilisation, which interferes with interpretation of data. Moreover, I also tried to map the ATMIN domain of interaction with UBR5, by cloning 4 overlapping ATMIN fragments for co-IP with FlagUBR5. All 4 fragments showed increased interaction when co-overexpressed in the presence of FlagUBR5, although there was some non-specific pull-down in the absence of FlagUBR5 (Figure 22D,E). Nevertheless, fragments A, B and D saw a higher enrichment over control IP than fragment C, suggesting that UBR5 most likely interacts with ATMIN over an extensive three-dimensional surface.

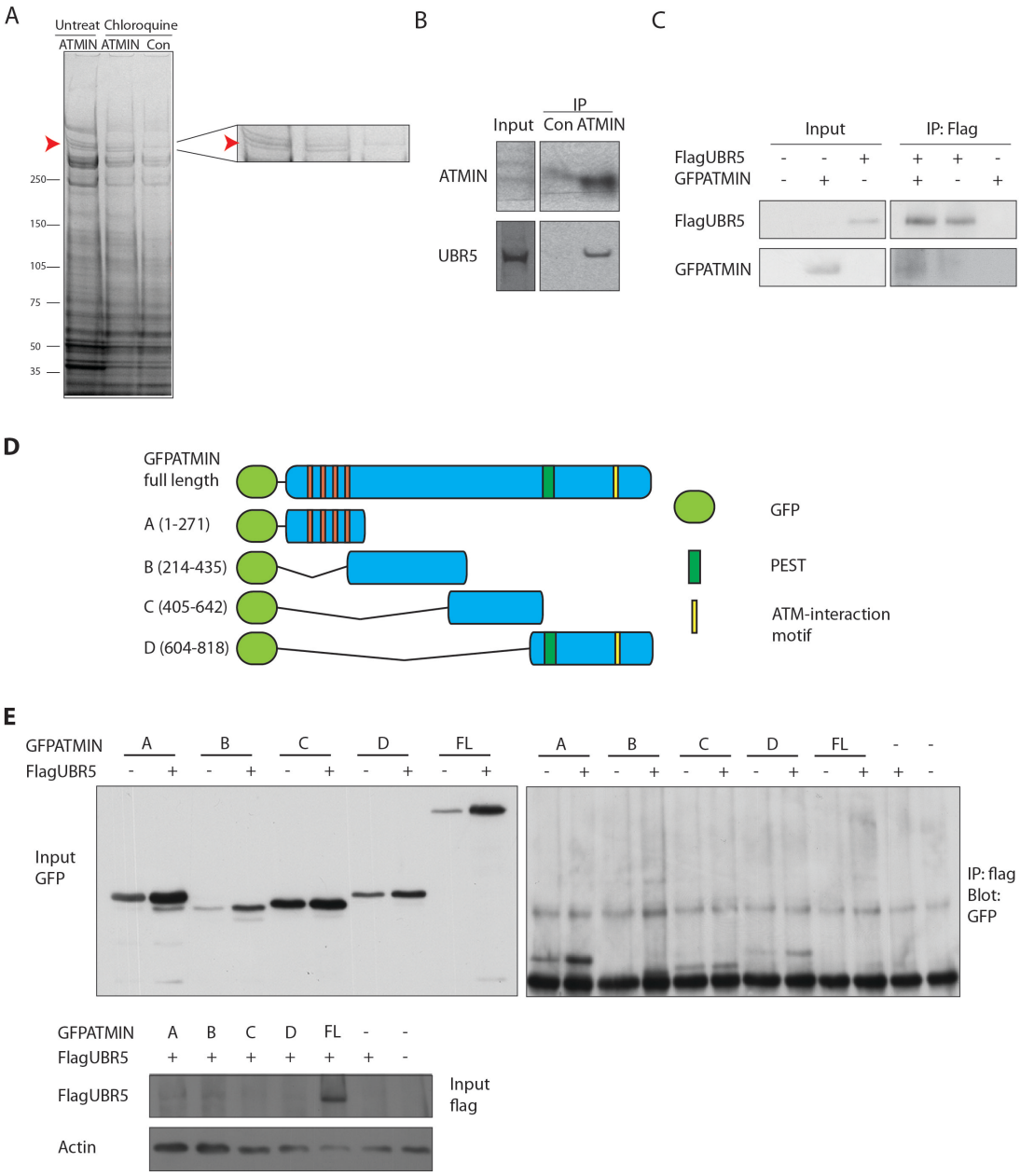

Figure 22. ATMIN interacts with UBR5.

(A) Gel stain after ATMIN immunoprecipitation using in-house ATMIN antibody, showing the bands that were analysed by MS, from which UBR5 was identified. (B) Endogenous ATMIN was immunoprecipitated using an in-house ATMIN antibody and probed with an antibody against UBR5. (C) GFPATMIN and FlagUBR5 were overexpressed separately in 293T cells. WCLs were harvested and mixed for 4 hours before flag pull-down. (D) Scheme of overlapping GFPATMIN fragments that were used to map interaction with UBR5. (E) GFPATMIN fragments (A-D) or full length (FL) were overexpressed with or without FlagUBR5 and WCL was used for flag IP and later blotted using GFP antibody.

Both ATMIN and UBR5 localise to the nucleus, under basal conditions and after IR. However, as they both show a diffuse pan-nuclear staining but no distinct foci formation, it is thus not possible to visualise any colocalisation with ATM after IR (Figure 23A). However, when UBR5 is silenced by siRNA, ATMIN protein level is not overall affected, after IR as well as by cycloheximide (Figure 23C). Hence, while UBR5 was identified as an ATMIN-interacting E3 ligase, silencing UBR5 does not change the ATMIN protein level appreciably, as would be expected for degradative ubiquitination. Moreover, it was observed that UBR5 knockdown decreases ATM and Kap1 phosphorylation after IR (Figure 23C). This will be discussed subsequently.

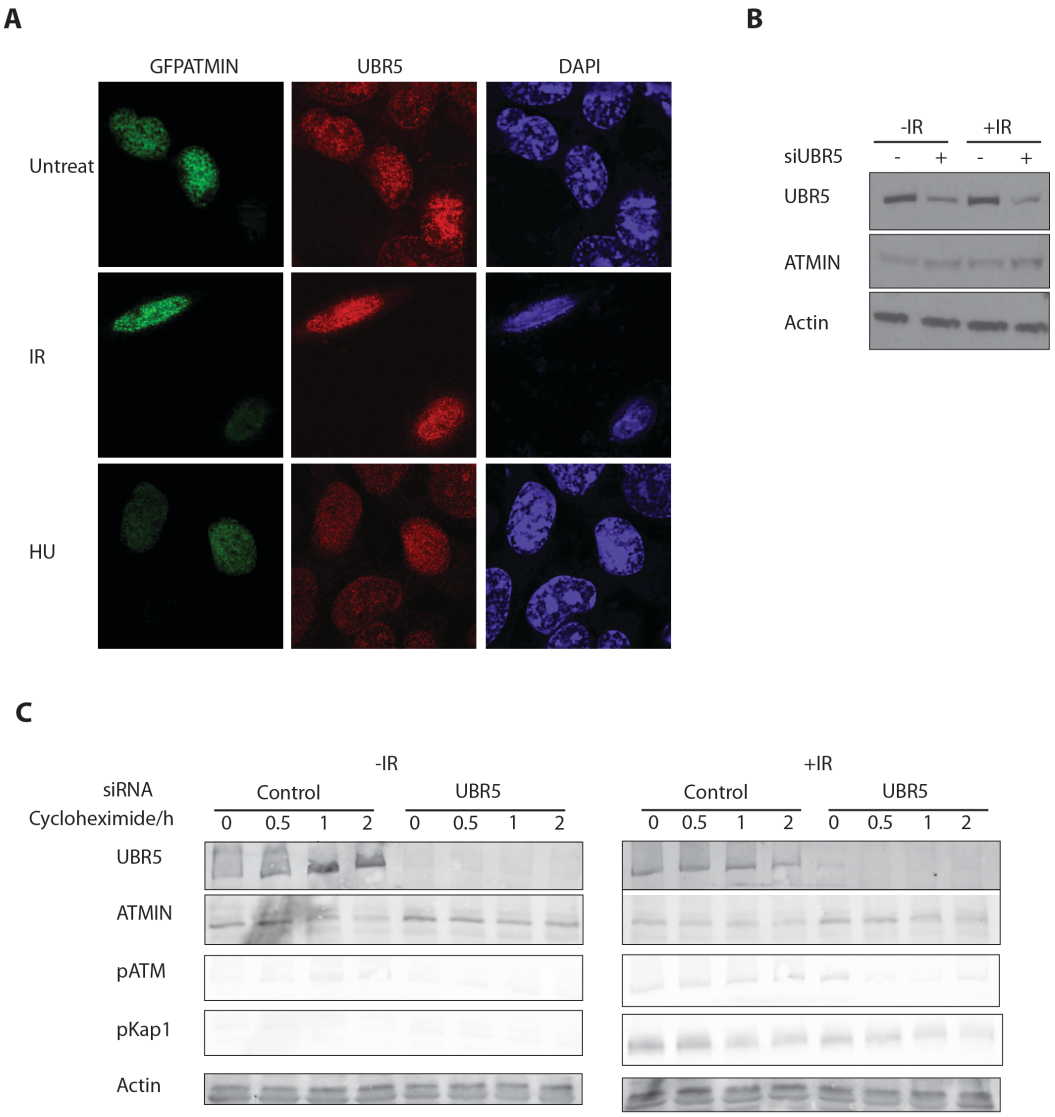

Figure 23. ATMIN and UBR5 localisation.

(A) GFPATMIN was overexpressed in 293A cells and treated with IR (2Gy) or HU 4 hours before fixation and staining for immunofluorescence. (B) Nuclear fraction of 293T cells before and after IR and fractions were analysed by SDS-PAGE and probed using the indicated antibodies. (C) 293T cells were transfected with siRNA against UBR5 for 72 hours and treated with IR (2Gy) before harvesting WCL for western blot. (D) Same as in (C), with the addition of cycloheximide immediately after IR (0 hr) and WCL was harvested at the indicated times after IR.

4.4 UBR5 ubiquitinates ATMIN in a stimulus dependent manner

To investigate whether ATMIN could be ubiquitinated endogenously, a His-ubiquitin pull-down was performed and endogenous ATMIN ubiquitination was detected after IR (Figure 24A). This ubiquitination was dependent on UBR5, since when UBR5 was silenced by siRNA, ATMIN ubiquitination as seen from a nickel NTA pull-down of His-ubiquitin decreased (Figure 24B). Conversely, when UBR5 was overexpressed, ATMIN ubiquitination increases drastically, suggesting that UBR5 is the E3 ligase that ubiquitinates ATMIN (Figure 12C). In addition, the ubiquitination of ATMIN is enhanced after IR, and can be consistently observed when the ubiquitin pull down was performed in the absence of proteasome inhibitor. Hence it is likely that the ubiquitination on ATMIN by UBR5 is non-degradative and induced in an IR-dependent manner. Since the most predominant ubiquitinated species appears as a single band around 8-10kDa higher than unmodified ATMIN, this suggests that the ubiquitination of ATMIN could be via a short mono- or di-ubiquitin modification.

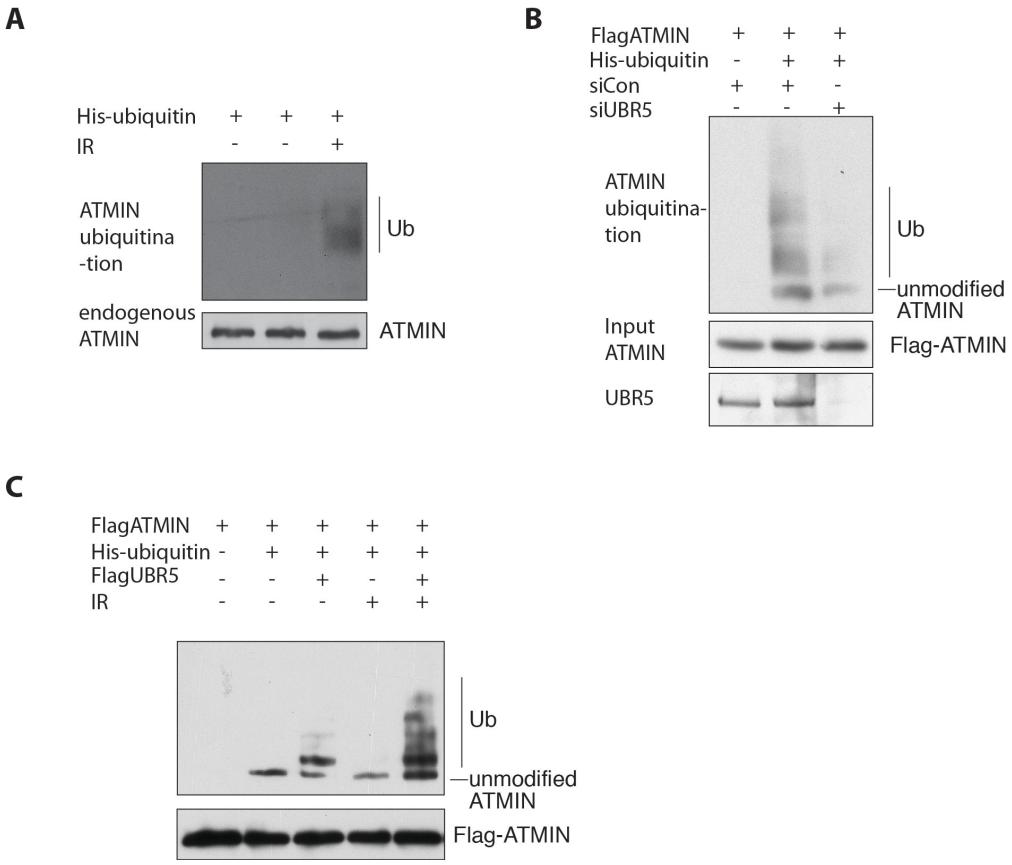

Figure 24. ATMIN ubiquitination by UBR5.

(A) Ubiquitin pulldown from 293T cells, showing ubiquitination of endogenous ATMIN. (B) Ubiquitin pulldown from 293T cells transfected with siRNA against UBR5 or control siRNA (siControl) followed by transfection with Flag-ATMIN and His-ubiquitin constructs. Cell were treated with IR (2Gy) and total cell lysate harvested after 30 minutes for Ni-NTA pulldown. His-ubiquitin was immunoprecipitated with Ni-NTA beads from lysates previously equilibrated for Flag-ATMIN input levels due to stabilisation of FlagATMIN in the presence of Flag-UBR5. (C) Ubiquitin pulldown from 293 cells expressing Flag-ATMIN and Flag-UBR5 and treated with or without IR (2Gy).

4.5 UBR5 ubiquitinates ATMIN in the N-terminus

Next, I went on to investigate the site of UBR5 ubiquitination of ATMIN. Firstly, I used the N- or C-terminus of ATMIN as a substrate in an *in vivo* ubiquitin assay. As observed previously, co-overexpression of UBR5 and many domains of ATMIN lead to mutual stabilisation, possibly due to tight interaction of UBR5 with ATMIN. I observed that the N-terminus (amino acids 1-352), but not the C-terminus (amino acid 625-818) of ATMIN was ubiquitinated, although both fragments were stabilised in the presence of UBR5 (Figure 25A). Furthermore, the ubiquitination of ATMIN N-terminus is dependent upon the E3 ligase activity of UBR5, as a C2768A catalytically dead mutant of UBR5 shows impaired ATMIN ubiquitination (Figure 25B).

Next, I used an IP-MS approach, whereby FlagATMIN N-terminus was immunoprecipitated following ubiquitination assay, and an additional gel band at the position of expected ATMIN ubiquitination was detected and analysed by mass spectrometry (Figure 25C). From this band, a single ubiquitination site was identified, lysine 238, in the presence of overexpressed UBR5. Protein sequence alignment showed that lys238 is conserved across species (Figure 25D). Importantly, when this residue was mutated to arginine and used as a substrate for in vivo ubiquitination assay, no ubiquitin modification was observed (Figure 25E). Since ATMIN ubiquitination is triggered by IR, I wanted to investigate whether any of DNA damage kinases of the PI3K family (ATM, ATR and DNA-PK) is responsible for UBR5 activation. When cells were treated with ATM inhibitor, or caffeine, which inhibits all PI3K family kinases (Sarkaria et al., 1999), IR-induced phosphorylation of ATM substrates were inhibited and ATMIN ubiquitination was reduced, whereas DNA PK inhibitor had little effect (Figure 25F). Thus efficient IR stimulation of ATMIN ubiquitination by UBR5 requires ATM activity.

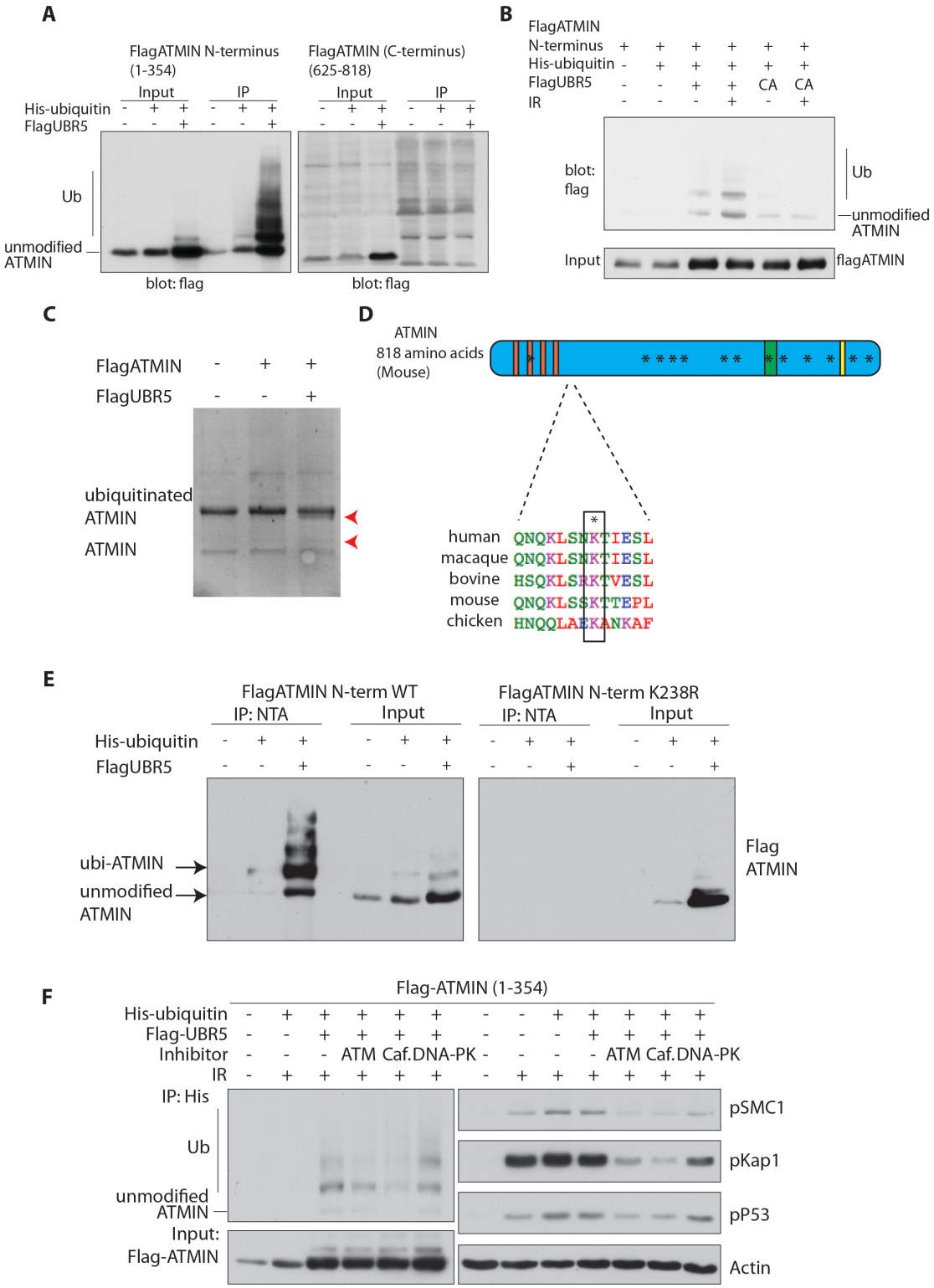

Figure 25. UBR5 ubiquitinates ATMIN in the N-terminus.

(A) Ubiquitin pulldown from 293T cells transfected with FlagATMIN N-terminus (amino acids 1-354) or C-terminus (625-818) and harvested after 48 hours. (B) Ubiquitin pulldown from 293T cells transfected with the indicated constructs and either wild type Flag-UBR5 (+) or C2768A mutant (E3 ligase-defective) Flag-UBR5 for 48 hours and treated with IR (2Gy). (C) Sypro ruby staining of SDS-PAGE gel of flag IP following in vivo ubiquitination of FlagATMIN N-terminus. (D) Scheme of ATMIN domains and conserved ubiquitination site Lys238. (E) Ubiquitin pulldown from 293T

cells transfected with FlagATMIN N-terminus wildtype or K238R mutant. (F) Ubiquitin pulldown (left) and western blots of whole cell lysates (right) from 293T cells transfected with the indicated constructs for 48 hours and treated with either ATM inhibitor, caffeine (Caf.) or DNA-PK inhibitor 1 hour before IR treatment (2Gy). Cells were harvested 30 minutes post-IR for Ni-NTA IP.

From the result of IPMS, it is likely that UBR5 mediates ATMIN ubiquitination on lys238. In addition to understanding the site of ubiquitination, I also investigated the type of ubiquitination linkage on ATMIN. Using an ubiquitin-K0 mutant that cannot be extended into chains in an in vivo ubiquitin assay, I also observed the mono-ubiquitination band similar to using wildtype ubiquitin (Figure 26A,B). Furthermore, the K0 ubiquitin resulted in an increase in the ATMIN mono-ubiquitination band intensity and a decrease in the higher molecular weight bands intensity, suggesting a shift to more ATMIN mono-ubiquitination (Figure 26B). In addition, the mono-ubiquitination band was also observed by using K48 and K63 ubiquitin mutants, which can only extend ubiquitin chain at K48 or K63 positions respectively due to mutation of all other lysines to arginines (Figure 26C). These data strongly suggest a mono-ubiquitination on ATMIN K238 by UBR5.

In order to confirm that the modification on ATMIN is indeed ubiquitination and not neddylation, an ubiquitin assay was performed in the presence of neddylation inhibitor (MLN4924), and this did not result in any reduction of ATMIN ubiquitination (Figure 26D). Though it is not possible to rule out other modifications that may occur subsequent to ATMIN ubiquitination, the major modification that is UBR5-dependent and triggered by IR is the mono-ubiquitination. Furthermore, to confirm that the full-length ATMIN also gets ubiquitinated in a manner that depends on the K238 residue, I performed an in vivo ubiquitination assay using wildtype or K238R full-length ATMIN, and observed that while full length wildtype ATMIN ubiquitination increases in the presence of FlagUBR5, that of mutant FlagATMIN does not increase when FlagUBR5 was added (Figure 26E) (We cannot rule out the presence of other E3 ligases that could target other lysine residues on ATMIN). Hence, it is likely that UBR5 ubiquitinates ATMIN only on K238 residue. Moreover, the increased UBR5-mediated ubiquitination of ATMIN appears to be specific to IR-stimulus because there is no change in ubiquitination after hypotonic shock (Figure 26F).

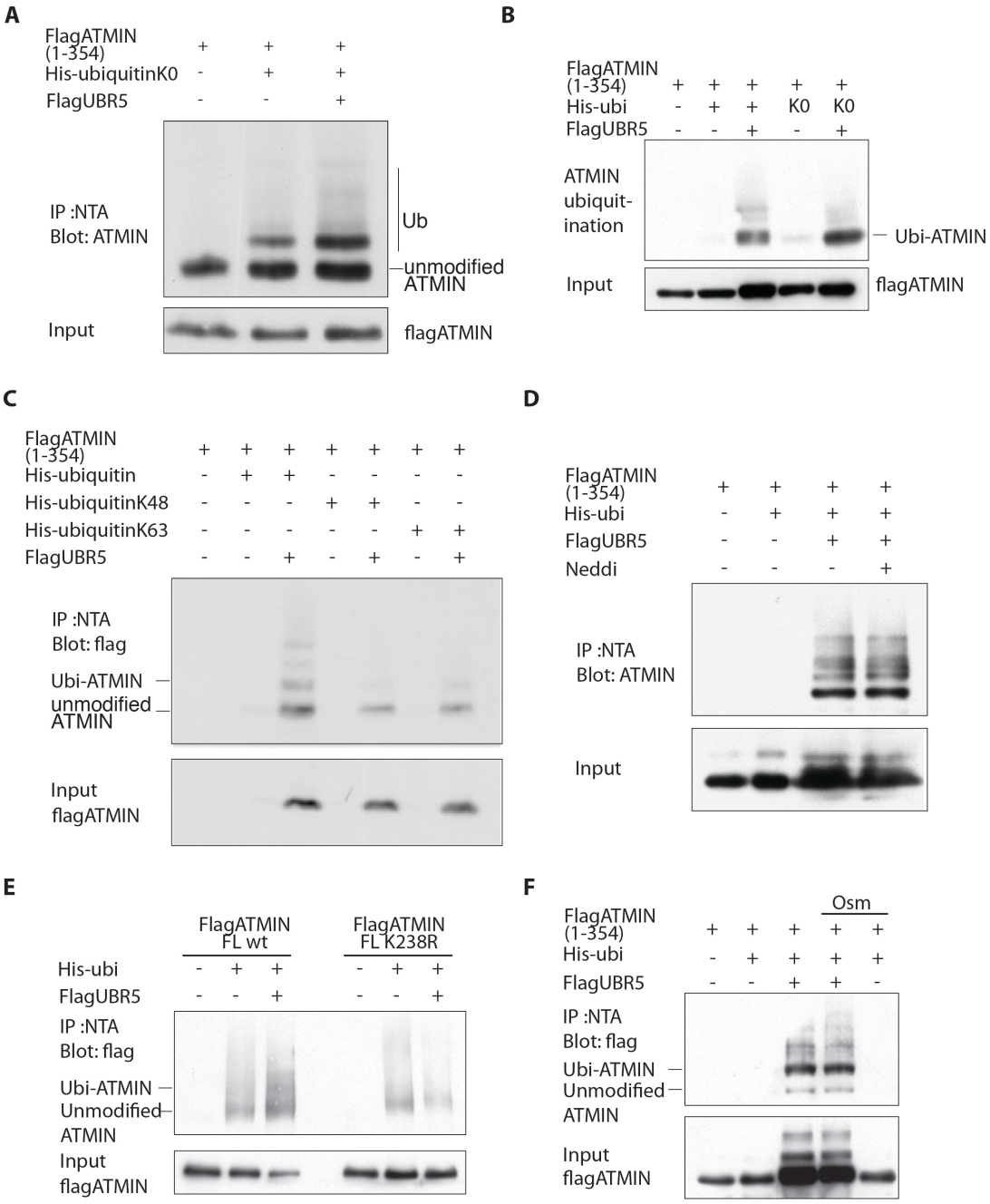

Figure 26. UBR5 catalyses ATMIN mono-ubiquitination.

(A,B) Ubiquitin pulldown following transfection of 293T cells with wildtype or K0-mutant ubiquitin. (C) Ubiquitin pulldown of 293T cells following transfection with wildtype, K48 or K63 ubiquitin mutants. (D) Ubiquitin pulldown of 293T cells after transfection with the indicated constructs and treatment with neddylation inhibitor MLN4924 (Neddi) for 4 hours prior to harvest. (E) Ubiquitin pulldown following transfection of 293T cells with wildtype full-length FlagATMIN or K238R full length FlagATMIN. (F) Ubiquitin pulldown following transfection of 293T cells with the indicated plasmids and treatment with or without hypotonic shock for 1 hour prior to harvest of whole cell lysate for immunoprecipitation.

4.6 Loss of UBR5 impairs ATM signalling after IR

UBR5 has been shown previously to regulate ATM-mediated phosphorylation of p53 (Ling and Lin, 2011) and activation of CHK2 after IR (Henderson et al., 2006). However, the regulation of CHK2 and p53 was not shown to be dependent on the E3 ligase activity of UBR5, furthermore no direct effect on ATM has been shown so far. I observed that silencing UBR5 impairs ATM signalling after IR, as seen by pKap1 and pSMC1 levels, indicating that ATM signalling partly depends on UBR5 (Figure 27A). Silencing UBR5 also diminishes IR-induced 53BP1 and pATM foci formation (Figure 27B,C). This is in agreement with previous data that overexpression of ATMIN competes with NBS1 for ATM binding and reduces NBS1 foci formation (Zhang et al., 2012). Since UBR5 ubiquitinates ATMIN on Lys238, I wanted to investigate whether this could be the mechanism by which UBR5 regulates ATM signalling. I overexpressed wildtype or K238R FlagATMIN (Lys238 mutated to Arg), with or without UBR5 knockdown, and checked the interaction of ATMIN with endogenous ATM by co-immunoprecipitation. Silencing UBR5 increases the interaction of wildtype FlagATMIN and ATM, and a similar pull-down was observed when FlagATMIN K238R was used regardless of UBR5 silencing (Figure 27D). Hence, this shows that ATMIN lysine 238 ubiquitination is required to regulate ATM-ATMIN interaction after IR, most likely by disrupting ATM-ATMIN complex to facilitate ATM-NBS1 interaction; a K238R mutant that is unable to be ubiquitinated binds strongly to ATM in a manner that is similar to loss of UBR5.

This model also predicts that knockdown of UBR5 should impair NBS1 interaction with ATM. Indeed, NBS1 foci formation following IR is impaired in the absence of UBR5 (Figure 27E,F). Hence, ATMIN overexpression and UBR5 knockdown have similar phenotypes in reducing NBS1-dependent ATM signalling.

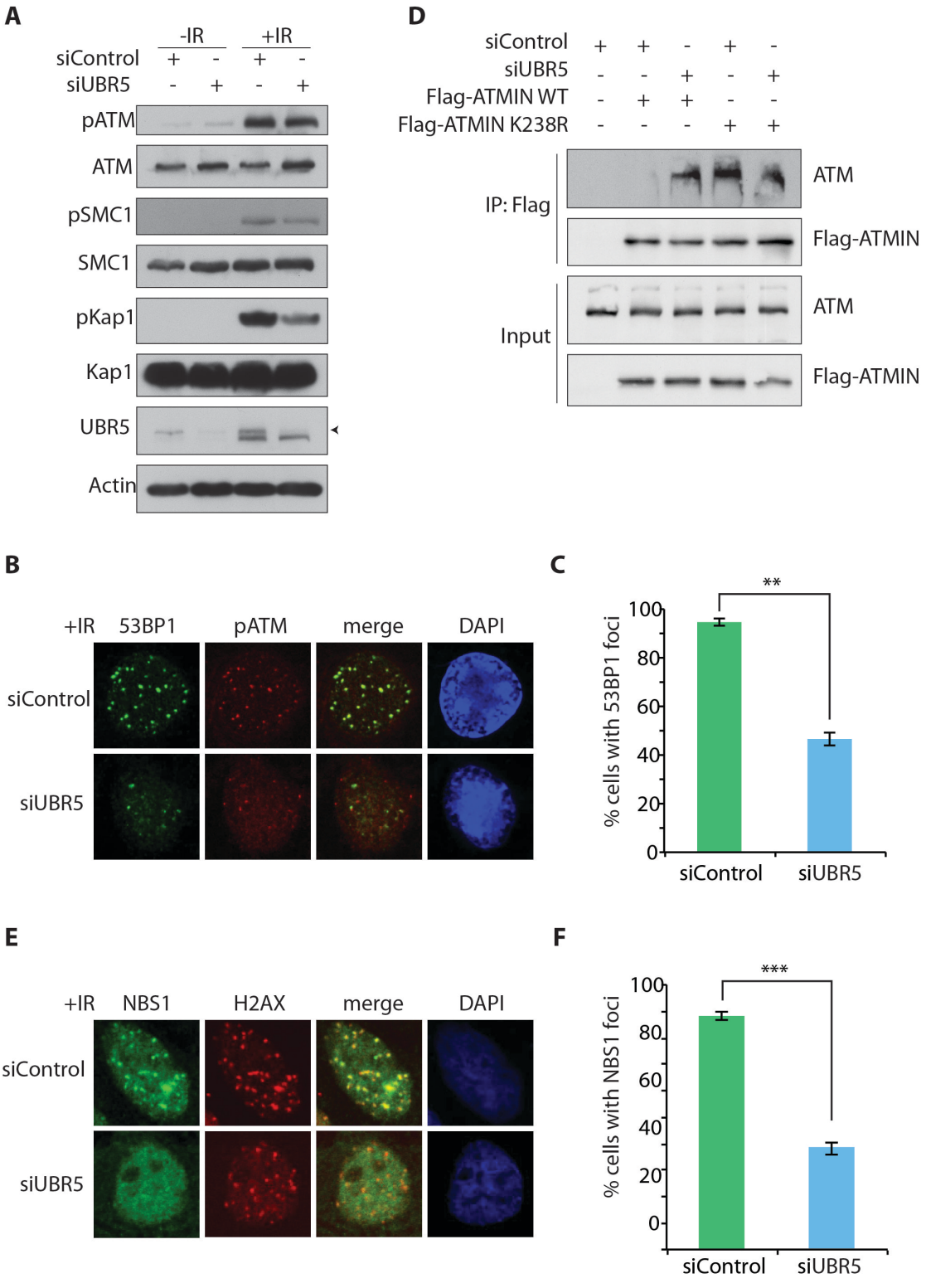

Figure 27. Loss of UBR5 impairs IR-induced NBS1-dependent ATM signalling.

(A) 293T cells were transfected with siUBR5 or siControl for 72 hours and treated with IR (2Gy) prior to harvest of WCL for western blotting. Arrow indicates the band that corresponds to UBR5 protein knockdown. (B) 293A cells were transfected with siUBR5 or siControl and treated with IR (2Gy) after 72 hours prior to fixation and immunofluorescence staining for 53BP1 and pATM. (C) Quantification of 53BP1 positive cells. Cells with at least 6 distinct foci were scored as positive. Error bars

represent s.e.m. (**p <0.01). (D) 293T cells were transfected with siUBR5 or siControl, and after 24 hours with Flag-ATMIN wild type or K238R mutant. Whole cell lysates were harvested 48 hours later for Flag IP. (E) 293A cells were transfected with siUBR5 or siControl for 72 hours and treated with IR (2Gy) prior to fixation and immunofluorescence staining for NBS1 and pH2AX. (F) Quantification of NBS1 positive cells. Cells with at least 5 distinct foci were scored as positive. Error bars represent s.e.m. (***p <0.005).

While silencing UBR5 impairs ATM signalling after IR, the defect can be partially rescued by concomitant loss of ATMIN (Figure 28A), suggesting that UBR5 acts via ATMIN to affect ATM signalling. The rescue is only partial, possibly because of reduced efficiency of knockdown using double siRNA. Similarly, using $ATMIN^{f/f}$ or $ATMIN^{\Delta/\Delta}$ MEFs, knock down of UBR5 only impairs ATM signalling in the presence of ATMIN (Figure 28B). Hence, ATMIN is required in UBR5-dependent impairment of ATM activation after IR.

Whilst ATMIN overexpression causes impairment in ATM signalling, when UBR5 was co-overexpressed with ATMIN, this rescued the ATMIN-dependent defect in ATM signalling, while overexpression of UBR5 alone has no effect (Figure 28C,D). These data imply that UBR5 and ATMIN could be acting in a complex whereby their levels must be regulated in order to ensure proper ATM activation after IR; an excess of ATMIN could titrate the activity of UBR5 and result in suppression of ATM activation, whilst an excess of UBR5 over ATMIN would have no effect as there would be no substrate to act on. To test this, I checked the IR-induced foci formation of 53BP1, pATM and NBS1. In agreement with western blot data, the co-overexpression of ATMIN and UBR5 rescued ATMIN-induced ATM signalling defect after IR, but does not affect the damage *per se* as shown by pH2AX staining (Figure 28D-G).

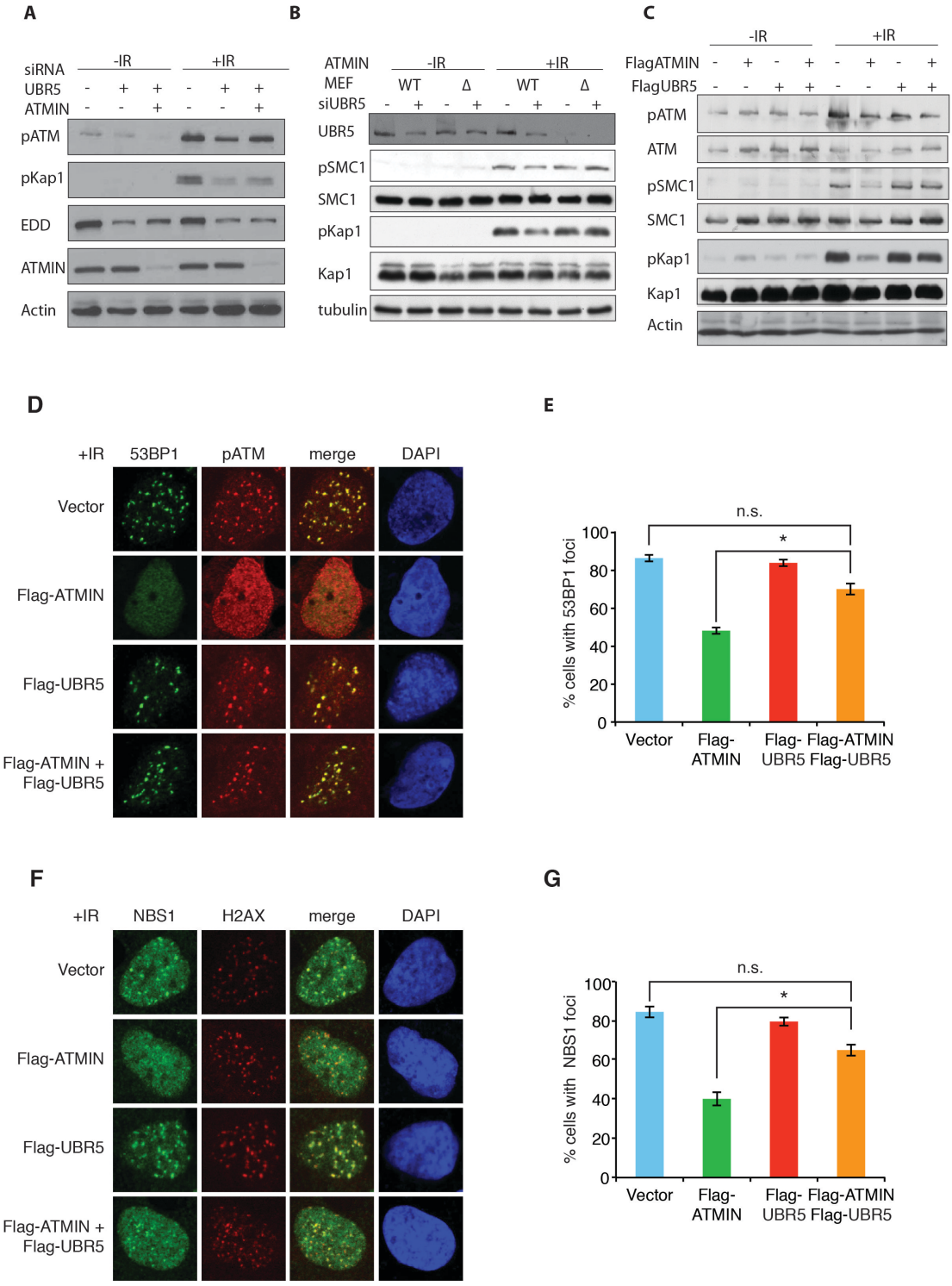

Figure 28. Overexpression of UBR5 rescues ATM signalling defect due to ATMIN competition.

(A) 293T cells were transfected with siUBR5, siATMIN or siControl for 72 hours and treated with IR (2Gy), prior to harvest for western blot. (B) ATMIN$^{f/f}$ (wild type) or ATMIN$^{\Delta/\Delta}$ MEFs were transfected with siUBR5 or siControl for 72 hours and treated with IR (2Gy), prior to harvest for western blot. (C) 293T cells were transfected with FlagUBR5, FlagATMIN or both for 48 hours and treated with IR (2Gy), prior to harvest for western blot. (D) 293A cells were transfected with Flag-ATMIN, Flag-UBR5 or both and irradiated after 48 hours, prior to fixation and immunostaining for 53BP1 and

pATM. (E) Quantification of 53BP1 positive cells. Cells with at least 6 distinct foci were scored as positive. Error bars represent s.e.m. (*p <0.05). (F) 293A cells were transfected with Flag-ATMIN, Flag-UBR5 or both and irradiated after 48 hours, prior to fixation and immunostaining for NBS1 and pH2AX. (G) Quantification of cells positive for NBS1 foci. Cell with at least 5 distinct foci were scored as positive. Error bars represent s.e.m. (*p <0.05). n.s., not significant.

4.7 ATMIN ubiquitination mutant has defective ATM signalling and checkpoint responses

If excess ATMIN-ATM interaction impairs ATM signalling, and ATMIN ubiquitination is required to disrupt ATM-ATMIN interaction, then ATMIN K238R mutant should also act as a dominant negative suppressor of ATM signalling after IR. ATM is required for cell cycle checkpoints, including the G2/M checkpoint in response to IR. In order to investigate the role of ATMIN K238 ubiquitination in the ATM-dependent DNA damage response, we measured IR-induced G2/M checkpoint activation in 293T cells expressing either wild-type ATMIN or the ATMIN-K238R mutant by detection of phosphorylated histone 3 (pH3) by FACS and using nocodazole to arrest cells that escape the G2/M checkpoint in mitosis.
When FlagATMIN K238R mutant is overexpressed in 293T cells, it abrogated the G2/M checkpoint after IR with a higher mitotic index than vector or FlagATMIN wildtype (Figure 29A). However, due to the presence of endogenous ATMIN, the defect may be less pronounced. Hence, I reconstituted ATMIN-null MEFs with wildtype or K238R FlagATMIN; specifically, *atmin*$^{f/f}$ cre-ERT MEFs were immortalised with large T antigen and infected with vector, FlagATMIN wildtype or FlagATMIN K238R expressing retrovirus and sorted by FACS.

The reconstituted MEFs were deleted for endogenous ATMIN by in vitro tamoxifen treatment, and vector-reconstituted (without tamoxifen treatment) was used as a control (Figure 29B). Deletion of endogenous ATMIN was checked by QPCR (Figure 29C) and expression level of ectopic wildtype or mutant ATMIN wildtype were comparable, as confirmed by western blot (Figure 29D). Upon IR treatment, ATMIN$^{\Delta/\Delta}$ reconstituted with K238R mutant ATMIN showed the greatest impairment in the ATM signalling compared to wildtype MEFs or ATMIN$^{\Delta/\Delta}$ MEFs reconstituted with wildtype ATMIN (Figure 29E).

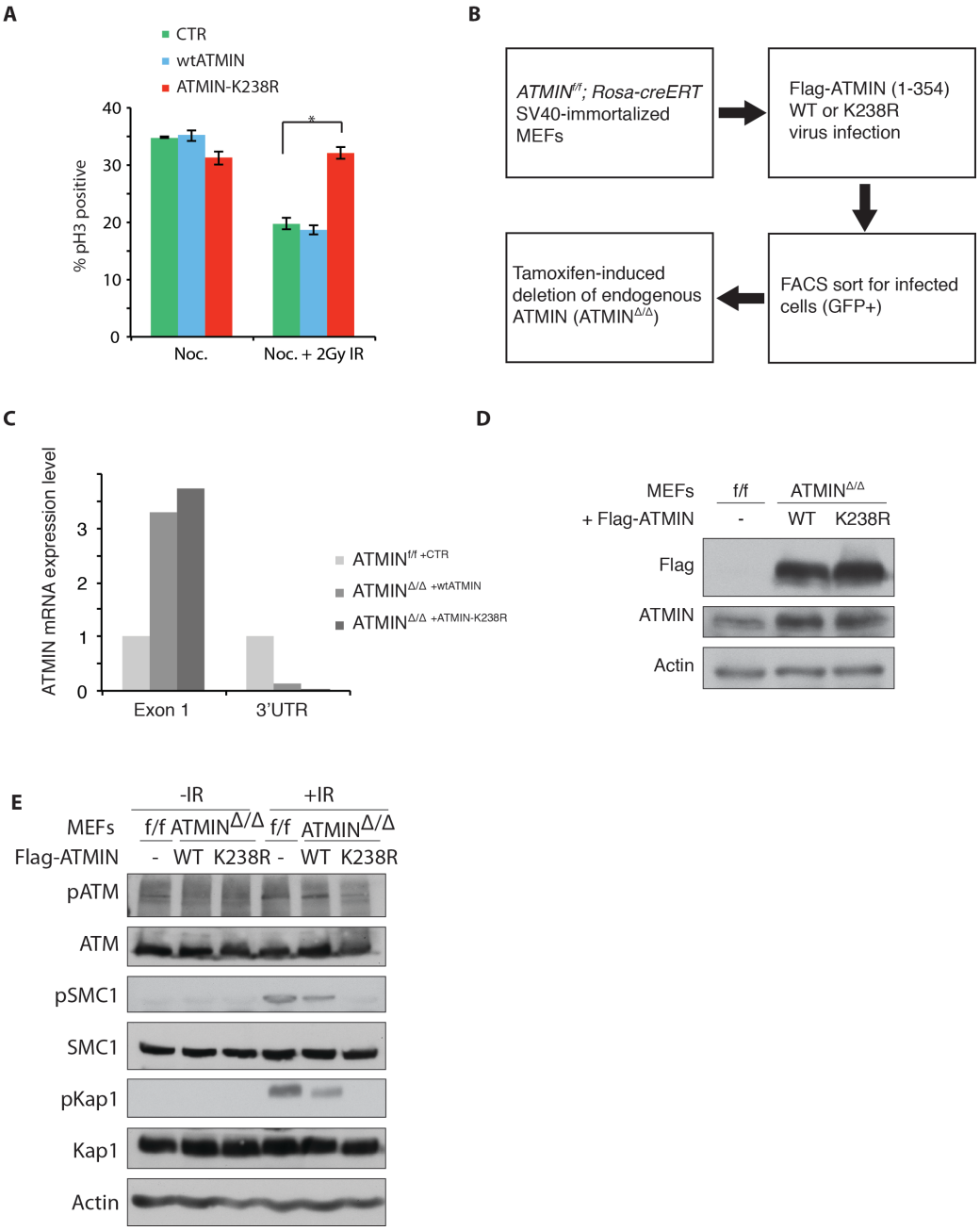

Figure 29. ATMIN ubiquitination is required for ATM signalling and function.

(A) G2/M trap and FACS analysis of mitotic index in 293T cells transfected with vector (CTR), Flag-ATMIN wild type (wtATMIN) or Flag-ATMIN K238R (ATMIN-K238R). Cells were irradiated 24hrs after transfection and nocodazole was immediately added to the media. After 18 hours, cells were harvested by trypsinization, fixed and stained for phospho-histone 3 (pH3) to indicate mitotic cells. (B) Scheme of FlagATMIN MEF reconstitution. (C) QPCR of reconstituted MEFs using ATMIN primer sets detecting exon 1 and the 3' UTR respectively. In *ATMIN*$^{F/F}$; *Rosa-creERT* cells, *ATMIN* (including the 3' UTR) is flanked by loxP sites and deleted upon tamoxifen-mediated cre activation (Kanu and Behrens, 2007). The reconstitution constructs do not contain *ATMIN* 3' UTR. (D) Western blots of whole cell lysates from reconstituted MEFs. (E) Western blot of wild-type MEFs transfected with empty vector (ATMIN$^{f/f+CTR}$) or ATMIN-null MEFs reconstituted with either wild type Flag-ATMIN full length (ATMIN$^{\Delta/\Delta\ +wtATMIN}$) or K238R mutant Flag-ATMIN full length (ATMIN$^{\Delta/\Delta\ +ATMIN-K238R}$). Cells were treated with IR and whole cell lysate harvested after 30 minutes.

Moreover, the ATMIN K238R reconstituted MEFs are also defective in 53BP1 and pATM foci formation after IR (Figure 30A,B). Consequently, these mutant MEFs are also radiosensitive, as seen by reduced colony-formation ability after IR (Figure 30C). Hence, this shows that ATMIN ubiquitination by UBR5 at Lys238 has an important role in mediating the full activation of ATM-dependent DNA damage response and loss of the E3 ligase or the ubiquitination site impairs ATM signalling and function after IR.

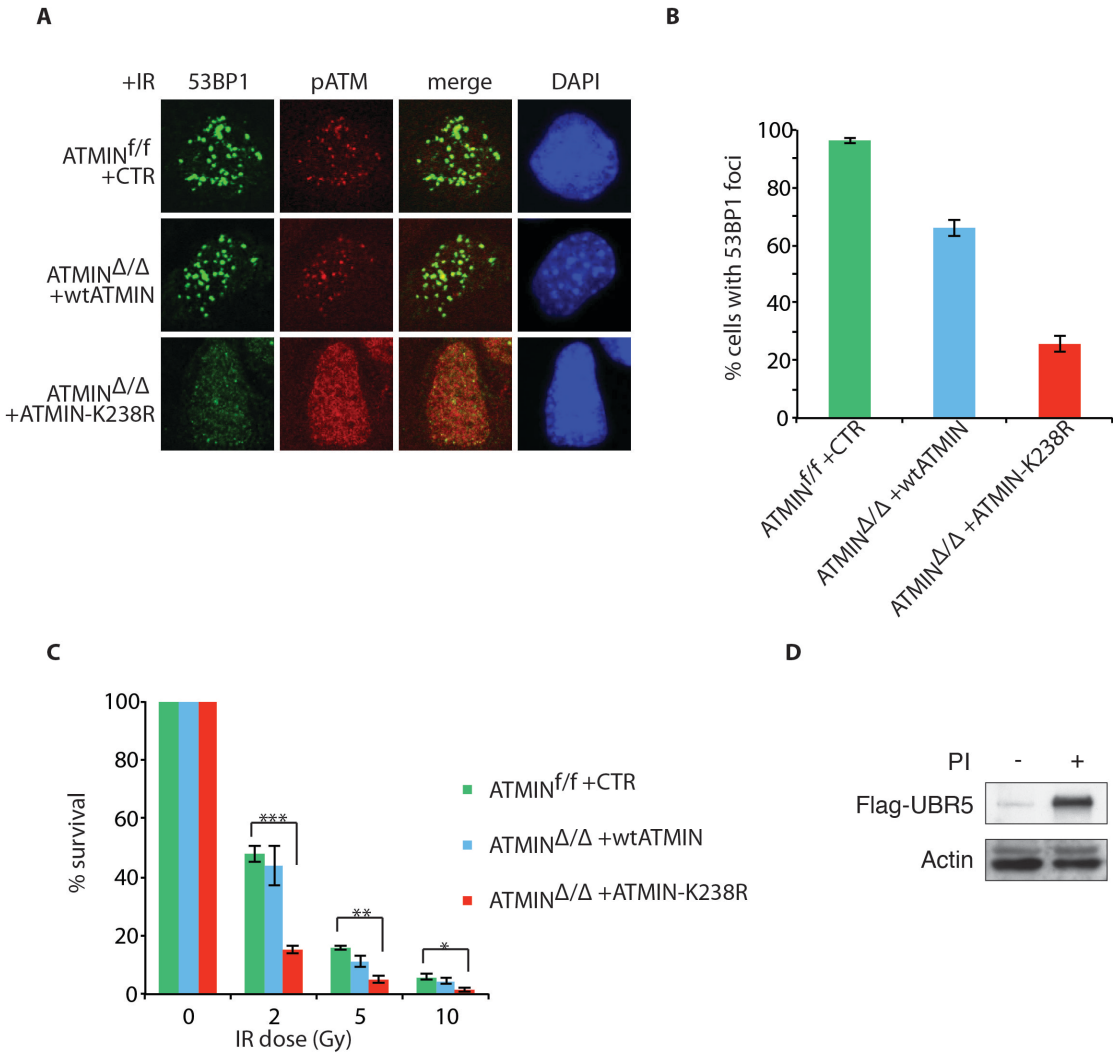

Figure 30. ATMIN ubiquitination is required for ATM signalling and function.

(A) Immunofluorescence staining of wild-type MEFs transfected with empty vector ($ATMIN^{f/f+CTR}$) or ATMIN-null MEFs reconstituted with either wild type Flag-ATMIN full length ($ATMIN^{\Delta/\Delta\ +wtATMIN}$) or K238R mutant Flag-ATMIN full length ($ATMIN^{\Delta/\Delta\ +ATMIN-K238R}$). Cells were treated with IR, and fixed after 30 minutes for 53BP1 and pATM staining. (B**)** Quantification of 53BP1 positive cells. Cells with at least 6 distinct foci were scored as positive. Error bars represent s.e.m. (C) Radiosensitivity assay of reconstituted MEFs, showing percentage of surviving colonies 7 days after the indicated dose of IR. Error bars represent s.e.m. (***p <0.005, **p<0.01). Error bars represent s.e.m. (D) Western blot of 293T cells transfected with FlagUBR5 for 48 hours and treated with proteasome inhibitor for 4 hours prior to harvest of WCL.

Since the E3 ligase activity of UBR5 appears to be augmented after IR, it is possible that UBR5 itself could undergo post-translational modifications that are required for its activation. Data from proteomics screens have shown that UBR5 has SQ/TQ sites (Mu et al., 2007, Matsuoka et al., 2007), which are potential targets for ATM and or ATR. Indeed, when cells were treated with ATM inhibitor or caffeine, decreased UBR5-dependent ATMIN ubiquitination was observed (Figure 25F). Another observation was that UBR5 protein level was destabilised after IR in the absence of ATMIN (ie. *atmin*$^{\Delta/\Delta}$ MEFs) (Figure 28B). It is possible that UBR5 could display auto-ubiquitination activity when its substrate is absent. This is supported by the stabilisation of overexpressed FlagUBR5 in the presence of proteasome inhibitor (Figure 30D). If this is correct, this suggests that UBR5 requires its substrate, ATMIN, to bind and become a substrate for its E3 ligase activity. In the absence of ATMIN, if UBR5 is activated post-IR, this will lead to UBR5 auto-ubiquitination and degradation.

In summary, UBR5 is activated post IR, perhaps by low levels of ATM and or ATR-mediated phosphorylation, and mono-ubiquitinates ATMIN on lys238. While the ubiquitination does not target ATMIN for degradation, it acts as a molecular switch to disrupt the basal ATMIN-ATM interaction and facilitate ATM-NBS1 interaction and subsequent ATM signalling post IR. This modification appears specific to IR but not to non-canonical stimuli of ATM activation such as osmotic stress. Loss of UBR5 or ATMIN mutant that cannot be ubiquitinated leads to impaired ATM signalling due to sequestering of ATM by ATMIN. Consequently, this leads to increased radiosensitivity and reduced viability of cells post IR. Hence, UBR5 is an important factor in ensuring the robust activation of ATM by contributing to the molecular decision favouring the ATM-NBS1 pathway over the ATM-ATMIN pathway after IR.

Chapter 5. The role of ATMIN in regulating ATM function after replication stress

Replication stress can be induced by external agents, such as drugs like aphidicolin and hydroxyurea, or internal natural barriers to replication, such as repetitive DNA sequences and DNA secondary structures. Following replication stress, replication stalls to preserve the integrity of the replication fork and allow time for replication restart once the stress is removed or internal barriers are overcome. However, under conditions of prolonged replication stress, the replication fork may collapse and forms a DSB due to endonuclease processing or due to ssDNA break. Sometimes, cells may progress to G2 with under-replicated DNA, which lead to the formation of anaphase bridges if the under-replicated DNA is segregated during mitosis. A sub-class of these anaphase bridges, called ultrafine anaphase bridges (UFBs) stain positively for BLM and PICH proteins but are DAPI-negative (Baumann et al., 2007) (Chan et al., 2007), which are believed to be progressively resolved during anaphase under normal conditions.

Another consequence of replication stress is the expression of chromosome fragile sites (CFS), which manifest as breaks on metaphase chromosomes following low level of replication stress by low doses of aphidicolin (Aph) (Glover et al., 1984). CFS represent regions of chromosome instability as they undergo sister chromatid exchange as well as translocations and deletions (Glover and Stein, 1987, Glover and Stein, 1988, Wang et al., 1993). ATR has been shown to regulate CFS stability; in the absence of ATR, cells show increased CFS following aphidicolin treatment and even under untreated conditions. (Casper et al., 2002) In addition to ATR, 53BP1 also has been shown to play a role in guarding genome stability. A recent study showed that 53BP1 forms nuclear bodies that accumulate after partial replication inhibition (low dose of aphidicolin 0.2uM) and act to protect under-replicated chromosome regions (such as fragile sites) that are not resolved by mitosis from further erosion (Lukas et al., 2011a, Harrigan et al., 2011). The recruitment of 53BP1 to underreplicated DNA is thought to depend on ATM, not ATR (Lukas et al., 2011a). Hence, in addition to ATR, ATM also has a role in suppressing chromosome instability arising from replication stress.

While the recruitment and activation of ATM at DSB via the MRN complex has been well characterised, its activation following replication stress is less well understood. Difilippantonio et al showed that ATM autophosphorylation and p53-Ser15 phosphorylation is unaffected in the absence of NBS1 (Difilippantonio et al., 2005). Hence, ATM may be recruited by an NBS1-independent mechanism after replication stress to fragile sites. Previous published data on ATMIN showed that it is required for ATM signalling after replication stress (Kanu and Behrens, 2007). In collaboration with Nnennaya Kanu, we wanted to investigate if ATMIN could act as a cofactor, akin to NBS1 after DSBs, which helps to localise ATM to sites of replication stress. While some of the biochemistry experiments were done by Nnennaya Kanu, I performed the immunofluorescence experiments and some additional biochemistry studies.

5.1 ATMIN is required for ATM signalling after replication stress

The possibility that ATMIN could play a role in replication stress stems from the defects observed in ATMIN deficient MEFs (*atmin*$^{\Delta/\Delta}$). Following aphidicolin treatment in wildtype MEFs, pATM and 53BP1 formed distinct foci that mostly colocalise. However, *atmin*$^{\Delta/\Delta}$ MEFs are defective in forming these foci after aphidicolin (Figure 31A,B). Moreover, blotting for pKap1, a downstream substrate of ATM, also shows a lower signal in *atmin*$^{\Delta/\Delta}$ MEFs, whilst that after IR is unaffected (Figure 31C). Using human lymphoblastoid cell lines, ATM wildtype cells increased 53BP1 foci and Kap1 phosphorylation whereas ATM knockout cells failed to do so (Figure 31D,E), suggesting that formation of 53BP1 foci and Kap1 phosphorylation upon Aph treatment are indeed ATM-dependent. In order to assess if ATMIN deficiency affected recovery and replication restart of cells, cells were arrested by hydroxyurea (HU) and then released into fresh medium containing BrdU and the cell cycle profiles were analysed. Compared with wildtype, *atmin*$^{\Delta/\Delta}$ MEFs had higher percentage of cells in S phase after release from HU (Figure 31F). A similar result was obtained by using Aph-induced arrest and release of 293T cells depleted of ATMIN by siRNA (Figure 31G). Hence, ATMIN-deficient MEFs have defective ATM signalling upon replication stress and slower recovery from replication stress.

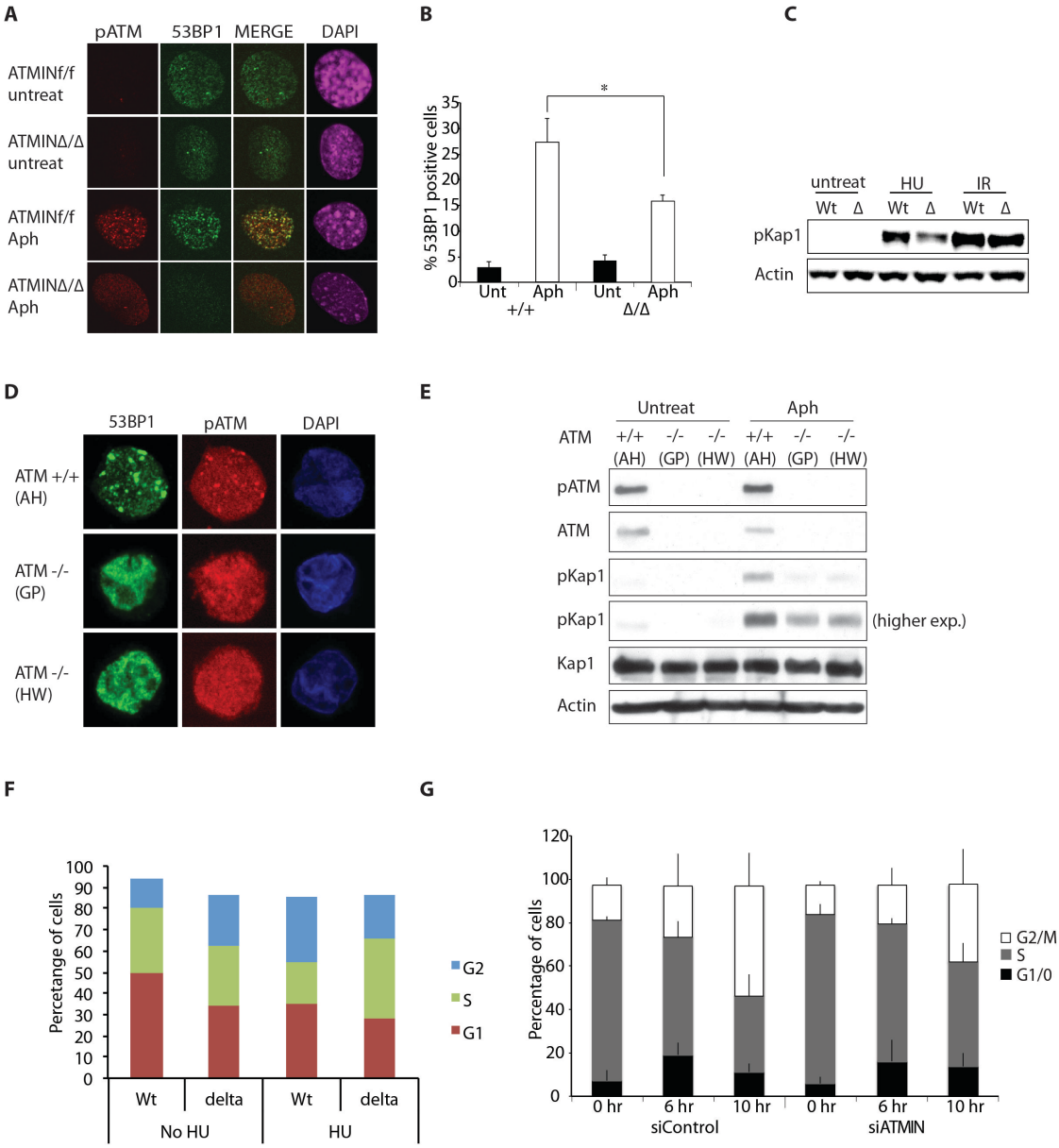

Figure 31. ATMIN is required for ATM signalling after replication stress.

(A) Immunofluorescence staining of pATM and 53BP1 on *atmin*$^{f/f}$ and *atmin*$^{\Delta/\Delta}$ MEFs. Cells were treated with aphidicolin 2uM for 18 hours prior to fixation. (B) Quantification of percentage of cells with 53BP1 foci. Cells with more than 10 foci are scored as positive. (*=P<0.05). (C) Whole cell lysate from *atmin*$^{f/f}$ and *atmin*$^{\Delta/\Delta}$ MEFs were harvested for western blotting after treatment with HU for 4 hours or IR (2Gy). (D) ATM wildtype (AH) or null (GP, HW) human lymphoblastoid cell lines were treated with Aph and stained for immunofluorescence using antibodies against the indicated proteins. (E) The same cells were treated with Aph or mock treated and whole cell lysate harvested for western blot analysis. (F) *atmin*$^{f/f}$ and *atmin*$^{\Delta/\Delta}$ MEFs were arrested with HU overnight or mock treated and released into fresh media containing BrdU for 6 hours, before fixation and analysis by FACS. (G) 293T cells were transfected with siATMIN or siControl for 72 hours and arrested by Aph overnight. Next, the cells were released into fresh media containing BrdU for 10 hours, before fixation and analysis of cell cycle profile by FACS.

5.2 WRNIP is a novel interactor of ATMIN and also interacts with RAD18

In order to dissect the mechanism by which ATMIN could play a role to localise ATM after replication stress, potential interactors were identified from earlier IP-MS studies using FlagATMIN (Janet Cronshaw, unpublished), including WRNIP1 (Werner helicase interacting protein1) as an interactor of ATMIN under basal conditions and after chloroquine treatment (Figure 32A). The interaction between ATMIN and WRNIP1 was confirmed by endogenous co-immunoprecipitation as well as by using overexpressed proteins (Figure 32B,C). FlagWRNIP was able to pull down MycATMIN in basal conditions as well as after aphidicolin. Colocalisation between pATM, 53BP1 and WRNIP foci could also be detected by immunofluorescence (IF) specifically after Aph (Figure 32D). Since ATMIN was found to associate with ATM after replication stress from previous work published from our lab (Kanu and Behrens, 2007), and WRNIP interacts with ATMIN and could form foci that colocalise with ATM, one hypothesis is that the formation of a WRNIP-ATMIN complex could be required to localise active ATM and its substrate 53BP1 after Aph. Unfortunately, due to the lack of suitable antibodies against ATMIN for IF, it was not possible to visualise directly a colocalisation between ATMIN and WRNIP in this study.

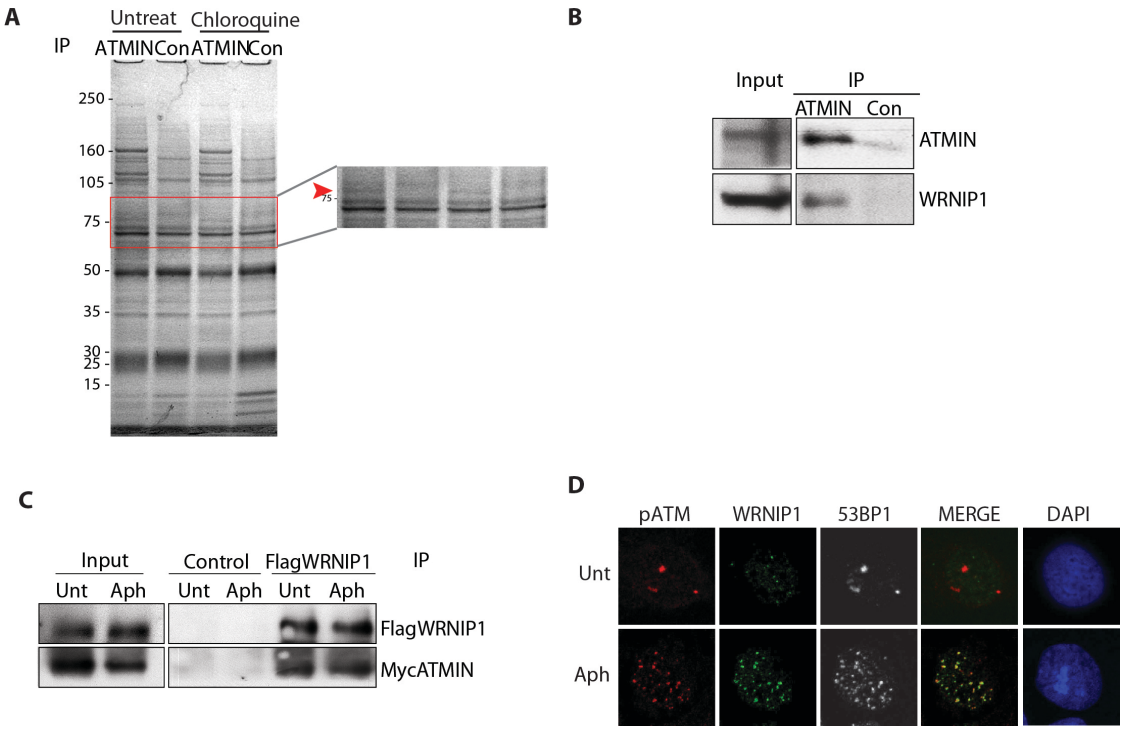

Figure 32. WRNIP1 as a novel interactor of ATMIN-ATM pathway.

(A) A large-scale IP was done on 293T cells treated with chloroquine for 4 hours or in untreated conditions, followed by SDS-PAGE and analysis by MS. Arrow indicates the band corresponding to WRNIP1 that is present in ATMIN pulldown but not in control IP. (Janet Cronshaw) (B) Endogenous co-IP was performed on 293T cells under basal conditions using an in-house ATMIN antibody. (Janet Cronshaw) (C) 293T cells were transfected with FlagWRNIP and MycATMIN for 24 hours and treated with or without Aph prior to harvest of WCL for co-IP. (Nnennaya Kanu) (D) Immunofluorescence of pATM, WRNIP and 53BP1 showing colocalisation after Aph treatment.

Mammalian WRNIP1 has been shown to localise in foci in replication factories marked by RPA, and responds by increasing the number of foci after treatments such as HU or UV that induce replication stalling, in a manner that depends on its UBZ domain (Crosetto et al., 2008). Furthermore, the yeast homologue of WRNIP, Mgs1, was shown to be recruited, via interactions between its UBZ domain and polyubiquitinated PCNA, to sites of replication stalling (Saugar et al., 2012). Similarly, human WRNIP1 can also interact with ubiquitinated PCNA in an NTA pull-down assay (Figure 33A) (Atanu Chakraborty). Since RAD18 is the E3 ligase that mono-ubiquitinates PCNA after replication stalling (Hoege et al., 2002), we wanted to test if Rad18 can interact with the ATMIN-WRNIP complex.

By immunofluorescence, WRNIP1 and RAD18 both form foci after Aph, the majority of which colocalise after Aph (Figure 33B). Moreover, overexpressed MycWRNIP could pull down FlagATMIN and FlagRAD18, suggesting that these three proteins could interact in a WAR complex (WRNIP1-ATMIN-RAD18) after replication stress (Figure 33D) (Nnennaya Kanu). In order to investigate the nature of these WRNIP1 and RAD18 foci, I co-stained with RPA, a marker for single-strand DNA (ssDNA) (Zou and Elledge, 2003), and observed colocalisation of both WRNIP1 and RAD18 with RPA foci after Aph, but not before. Hence, it is likely that WRNIP1 and RAD18 colocalise to stalled replication forks marked by RPA after Aph treatment (Figure 33E). In order to further probe the requirement for WRNIP1 and RAD18 foci formation, the genes were silenced individually. Silencing RAD18 by siRNA led to a reduction in the percentage of cells that were positive for WRNIP1 foci after Aph (Figure 33B, C), while knockdown of WRNIP1 does not significantly affect RAD18 foci formation. This shows that WRNIP1 foci formation after Aph is dependent upon RAD18, but not vice versa.

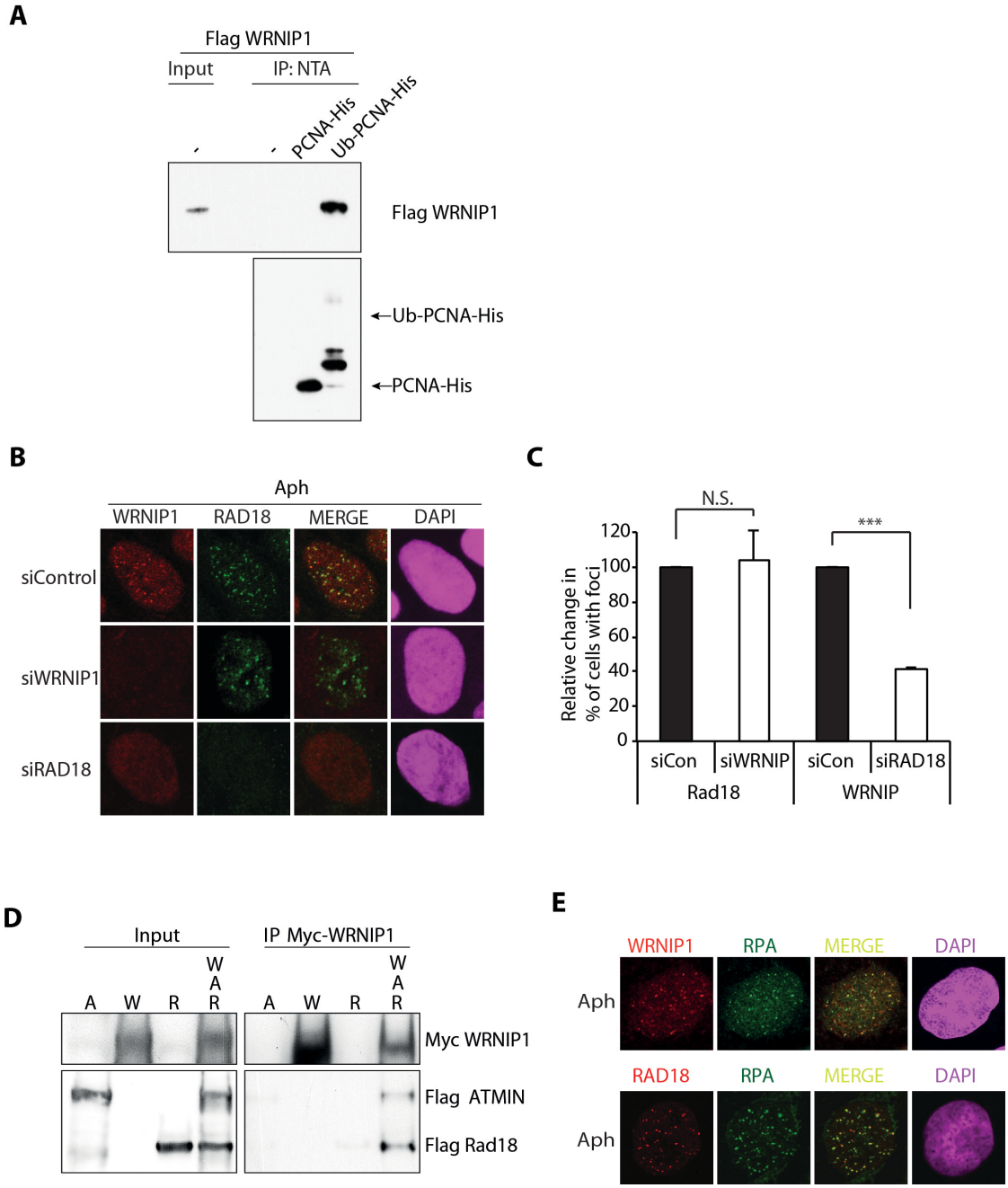

Figure 33. WRNIP1 and RAD18 colocalise to sites of replication stress

(A) Recombinant proteins FLAG-WRNIP was incubated with recombinant His-PCNA or ubiquitinated (Ub-) His-PCNA for 1 hr and mixture immunoprecipitated with Ni-NTA beads. (Atanu Chakraborty) (B) Immunofluorescence staining of WRNIP1 and RAD18 foci on 293A cells transfected with siWRNIP1, siRAD18 or siControl for 72 hours and treated with Aph prior to fixation and staining. (C) Quantification of percentage of cells with WRNIP1 and RAD18 foci normalised to siControl, cells were scored as positive if they harbour more than 6 foci. (N.S= not significant, ***=p<0.001) (D) 293T cells were transfected with MycWRNIP1, FlagATMIN and FlagRAD18 for 24 hours and whole cell lysate harvested for Myc IP. (Nnnenaya Kanu) (E) Immunofluorescence of WRNIP1, RPA and RAD18 colocalisation in 293A cells after treatment with Aph.

5.3 WRNIP1, ATMIN and RAD18 are all required for ATM signalling after replication stress, but not after IR

Since the loss of ATMIN impaired ATM signalling after replication stress, we wanted to investigate whether WRNIP1 or RAD18 has a similar phenotype. Knockdown of WRNIP, RAD18 and ATMIN all led to a decrease in pATM and 53BP1 foci after Aph (Figure 34A,B), with RAD18 having the strongest phenotype, followed by WRNIP, then ATMIN. Hence, ATMIN, WRNIP and RAD18 are all required to localise pATM and 53BP1 to sites of replication stress. This is further confirmed by western blotting for ATM substrate Kap1 and p53 phosphorylation (Figure 34C), both of which are impaired most strongly upon silencing WRNIP1 and RAD18. To check whether the loss of WAR complex affects ATM activity, I immunoprecipitated endogenous ATM after Aph treatment and performed in vitro kinase assay on GST-p53 substrate. In agreement with western blot data, ATM kinase activity is reduced most strongly in siRAD18 and siWRNIP1, and to a lesser extent after siATMIN (Figure 34D). While the loss of WAR impairs ATM substrate phosphorylation after Aph, the phosphorylation of CHK1, an ATR substrate, was not affected. Hence, the WAR complex is required for ATM signalling but not ATR signalling after replication stress (Figure 34C).

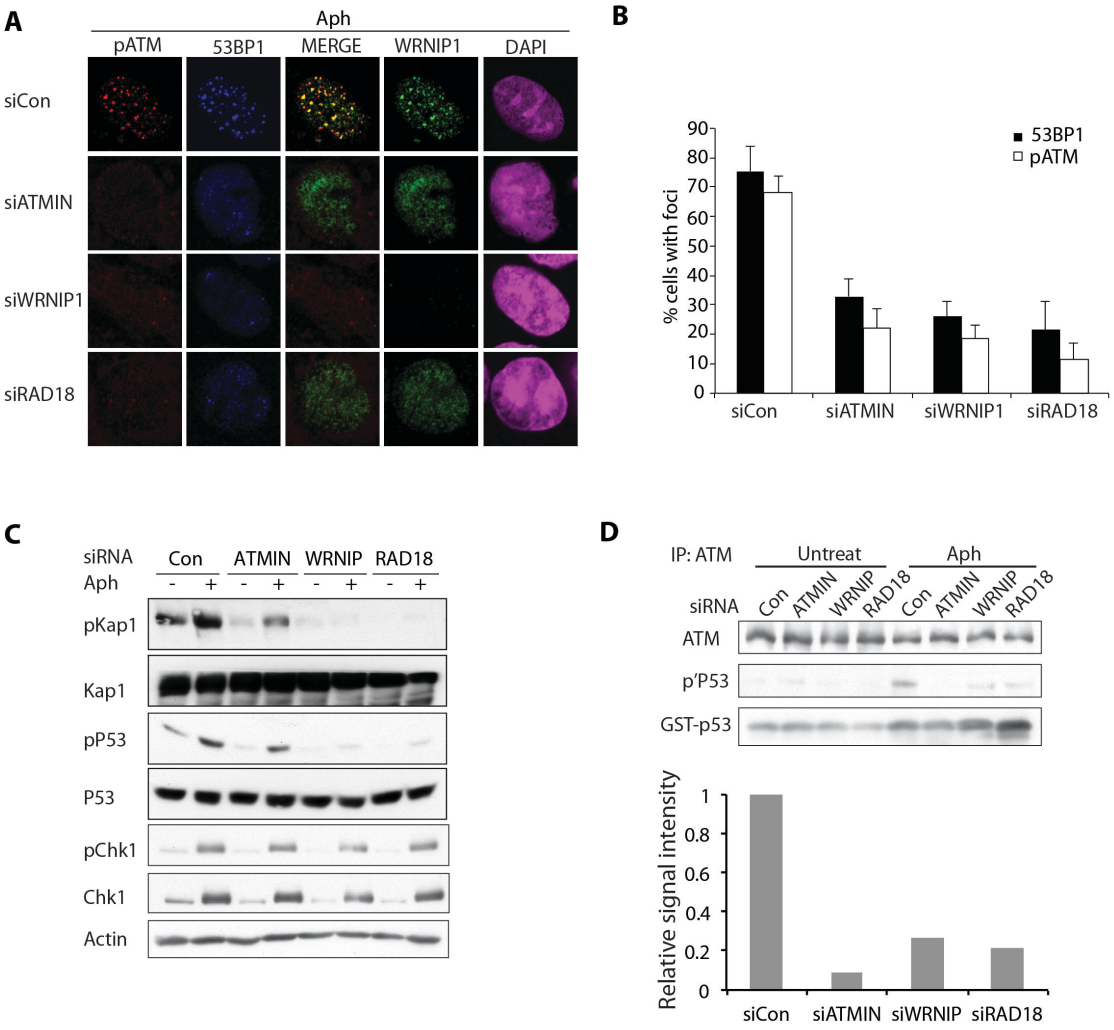

Figure 34. Loss of WAR complex impairs ATM signalling after Aph.

(A) 293A cells were transfected with siRNA against ATMIN, WRNIP1, RAD18 or Control siRNA for 72 hours and treated with Aph before fixation and staining for pATM, 53BP1 and WRNIP1 immunofluorescence. (B) Quantification of cells positive for 53BP1 or pATM foci from (A). Cells were scored as positive if they harboured more than 6 foci. (C) 293T cells were transfected with the indicated siRNAs for 72 hours and treated with Aph before harvesting of whole cell lysate for western blot analysis. (D) Total ATM was immunoprecipitated from whole cell lysate as in (C) and used for in vitro kinase assay with GST-p53 substrate. Graph shows the quantification of phospho-p53 western blot intensity relative to GST-p53.

While the WAR proteins are required for full ATM signalling after Aph, the knockdown of the WAR proteins had no appreciable effect on ATM signalling and foci formation after IR (Figure 35A,B) (Tianyi Zhang, Nnennaya Kanu). Hence, the WAR proteins are not required for ATM signalling after IR-induced canonical DSBs, but specifically after replication stress.

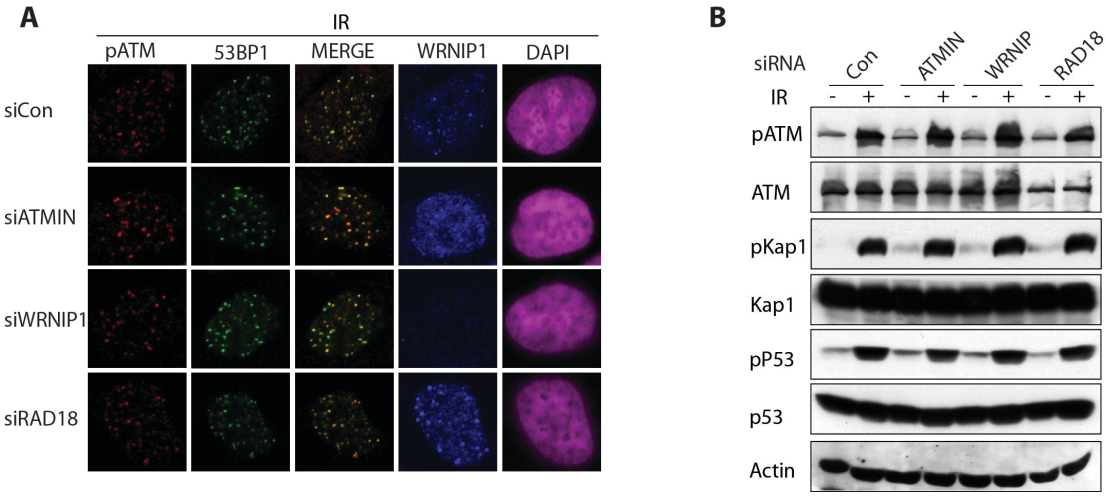

Figure 35. WAR complex is not required for IR-induced ATM signalling

(A) 293A cells were transfected with siRNA against ATMIN, WRNIP1, RAD18 or Control siRNA for 72 hours and treated with IR (2Gy) before fixation and staining for pATM, 53BP1 and WRNIP1 immunofluorescence. (B) 293T cells were transfected with the indicated siRNAs for 72 hours and treated with IR (2Gy) before harvesting of whole cell lysate for western blot analysis.

To confirm if pATM and 53BP1 localisation depends on the ability of WRNIP1 to interact with ubiquitin, we made use of an Ubiquitin Binding Zinc finger (UBZ) mutant of WRNIP1. Mutation to alanine of the highly conserved aspartate residue at position 37 of WRNIP1 (D37A) abolishes binding to both mono- and poly-ubiquitin (Crosetto et al., 2008). Endogenous WRNIP1 was first depleted using siRNAs directed against the *wrnip1* 3'UTR, achieving almost complete knockdown as seen by WRNIP1 immunofluorescence. Complementation with wild-type siRNA-resistant WRNIP1 rescued 53BP1 and pATM focus formation in WRNIP1-depleted cells. In contrast, complementing with D37A WRNIP1 mutant protein was unable to rescue pATM and 53BP1 focus formation (Figure 36A,B). This suggests that the UBZ domain of WRNIP1 is required to localise WRNIP1, pATM and 53BP1 to sites of replication stress.

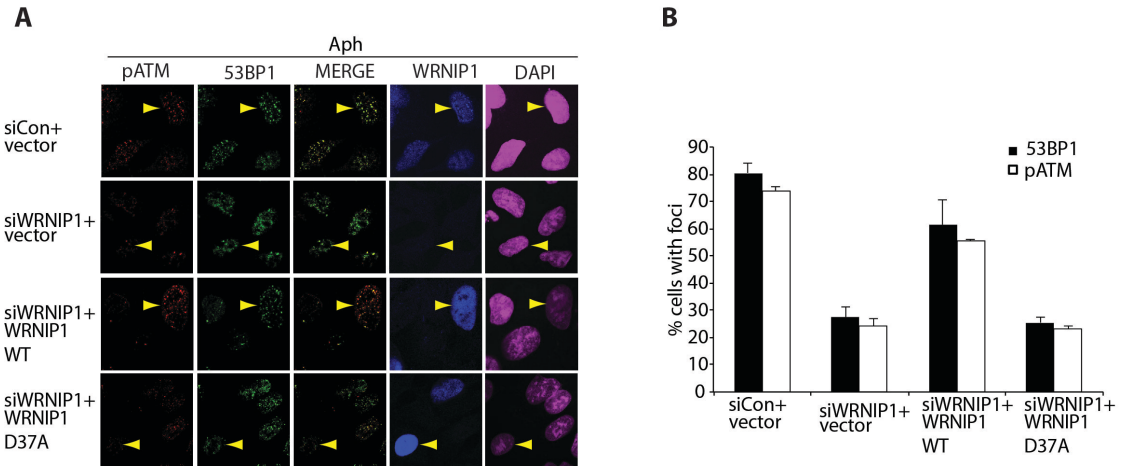

Figure 36. 53BP1 and pATM localisation depends on WRNIP ubiquitin-binding domain.

(A) 293A cells were transfected with siRNA targeting the 3'UTR of WRNIP1 for 48 hours, followed by transfection with either vector, FlagWRNIP1 wildtype or the D37A UBZ mutant for another 24 hours, and treatment with Aph overnight prior to fixation and staining for immunofluorescence. Arrowhead indicates cells that have WRNIP1 knockdown or re-expression. (B) Quantification of the percentage of WRNIP1 transfected cells with 53BP1 or pATM foci. Cells were scored as positive if they harboured more than 6 foci.

5.4 Knockdown of ATMIN increases ultrafine bridge formation during anaphase

Along with ATR, ATM has been implicated in promoting the recovery of collapsed replication forks and prevention of DSB accumulation (Trenz et al., 2006). Our data show that ATMIN could play a role in regulating ATM function after replication stress. A sub-class of anaphase bridges, called ultrafine anaphase bridges (UFBs), were recently identified to contain DNA and coated with PICH (Plk1-interacting checkpoint helicase) and BLM (Blooms syndrome DNA helicase), but they are DAPI-negative. (Chan et al., 2007, Baumann et al., 2007) UFBs are commonly found at fragile sites in human cells during mitosis, and are believed to represent catenated DNA from incomplete DNA replication (Chan et al., 2007, Chan et al., 2009, Rouzeau et al., 2012).

By co-staining with PICH and FANCD2, I observed a significant proportion of UFB formation (30% of all anaphases), as confirmed in both HCT116 and HeLa cell lines, in line with that of other published data (Chan et al., 2007) (Figure 25A). PICH, is believed to stabilise unresolved DNA under tension during anaphase and promote the resolution of concatenated DNA at anaphase. The frequency of UFB

formation was elevated upon silencing ATMIN to a similar extent as Aph treatment (Figure 25B). Moreover, treatment with Aph in addition to silencing ATMIN does not further increase UFB formation, suggesting that the loss of ATMIN induces replication stress that phenocopies Aph treatment and that ATMIN could act in the same pathway as Aph in up-regulating UFB formation.

To test whether UFB formation depends on ATM or ATR, cells were treated with either ATM inhibitor or siRNA against ATR and scored for UFBs. As expected, the loss of ATR increased UFB formation, presumably due to S phase checkpoint defect and failure to replicate unresolved DNA regions. The inhibition of ATM activity also increased UFB formation to a similar extent as ATR depletion (Figure 25C,D). Hence, this suggests that in addition to ATR, ATM could also function in the detection and/or resolution of intermediates of stalled replication fork. Knocking down both ATM and ATR increased UFB formation more than individual knockdown alone, suggesting that both kinases have non-overlapping roles in suppressing UFB formation. Moreover, this role of ATM in suppressing UFB formation is dependent upon ATMIN but not on NBS1, as the knockdown of NBS1 does not significantly increase UFB formation (Figure 25C). The knockdown of RAD18 also increases UFB frequency, similar to that of ATMIN knockdown, which supports that they could act in the same pathway. Furthermore, the knockdown of RAD18 in combination with ATM inhibition did not further increase UFB formation compared to siRAD18 alone, in line with the hypothesis that RAD18 functions in the same pathway as ATM. Hence, these data suggest that ATMIN, RAD18 and ATM could function in the same pathway in suppressing unresolved mitotic DNA structures as a result of replication stress.

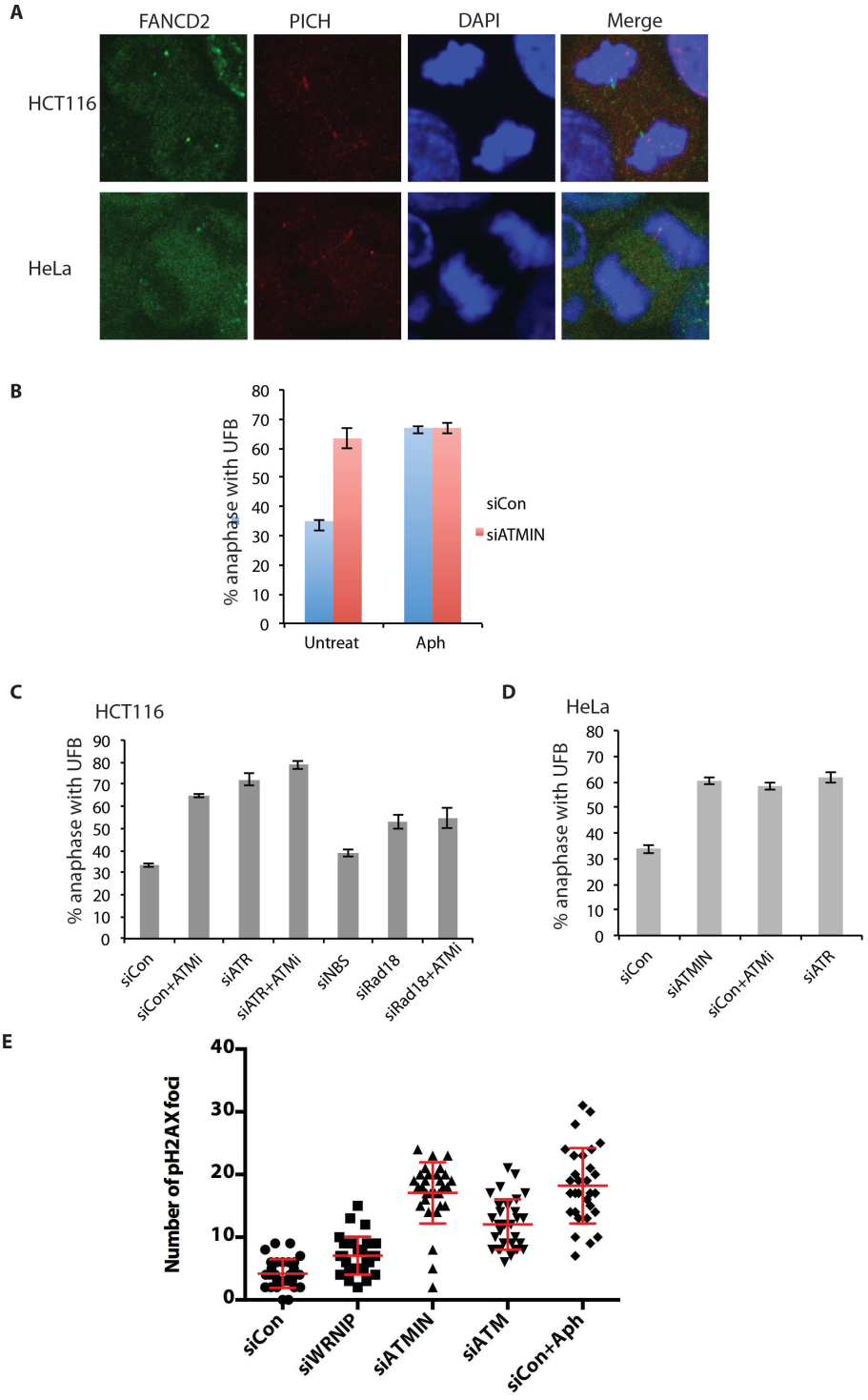

Figure 37. ATMIN-mediated ATM signalling suppresses UFB and γH2AX formation.

(A) Immunofluorescence of PICH and FANCD2 in HCT116 and HeLa cells, marking anaphase UFBs. (B-D) HCT116 or HeLa cells were transfected with the indicated siRNA for 72 hours and treated with Aph prior to fixation and immunofluorescence staining for PICH and FANCD2. Quantifications show the percentage of anaphases that display at least 1 UFB. (E) Quantification of total H2AX foci per metaphase after transfection of HCT116 with the indicated siRNA for 72 hours and treatment with Aph prior to fixation. Images were acquired as z-stacks in order to quantify all H2AX foci present.

In order to distinguish between the role of ATM in canonical DSB signalling versus signalling in response to replication stress, to show that the decrease in ATM signalling and foci formation is not due to a decrease in DSB formation, I investigated whether the knockdown of ATMIN or WRNIP affected γH2AX foci formation at metaphases. The loss of ATMIN or WRNIP increases, rather than decreases γH2AX formation, while ATM signalling is impaired (Figure 37E). This suggests that WAR-ATM pathway could be responding to another class of substrates, such as complex ssDNA-dsDNA or chicken-foot structures, which trigger ATM activation distinctly from the MRN-mediated DSB response.

5.5 ATM signalling after replication stress does not depend on ATR

Since ATR is the primary kinase that is recruited to ssDNA during replication stress, I wanted to investigate whether the ATM response is dependent upon ATR or if recruitment of both kinases occurs in parallel. The knockdown of ATR does not impair 53BP1 or RAD18 foci formation after Aph, hence suggesting that loss of ATR does not prevent RAD18 localising to sites of replication stress and that ATR is not required for ATM signalling after Aph (Figure 38A). Furthermore, the loss of ATR even upregulates ATM substrate phosphorylation after Aph compared to siControl by western blotting (Figure 38B), this could be due to the increased S phase damage in the absence of ATR. These data suggest that ATR and ATM are independently activated and recruited to sites of replication stress, and that ATR could even perhaps limit ATM activation until a later stage. One could speculate that early or prolonged activation of ATM in early S phase could direct cells to an apoptotic response, thus the activation of ATR in the first instance might inhibit ATM activation to allow the ATR-activated S phase checkpoint to resolve the replication problem, and only activating the ATM response if the barrier to replication persists after S/G2.

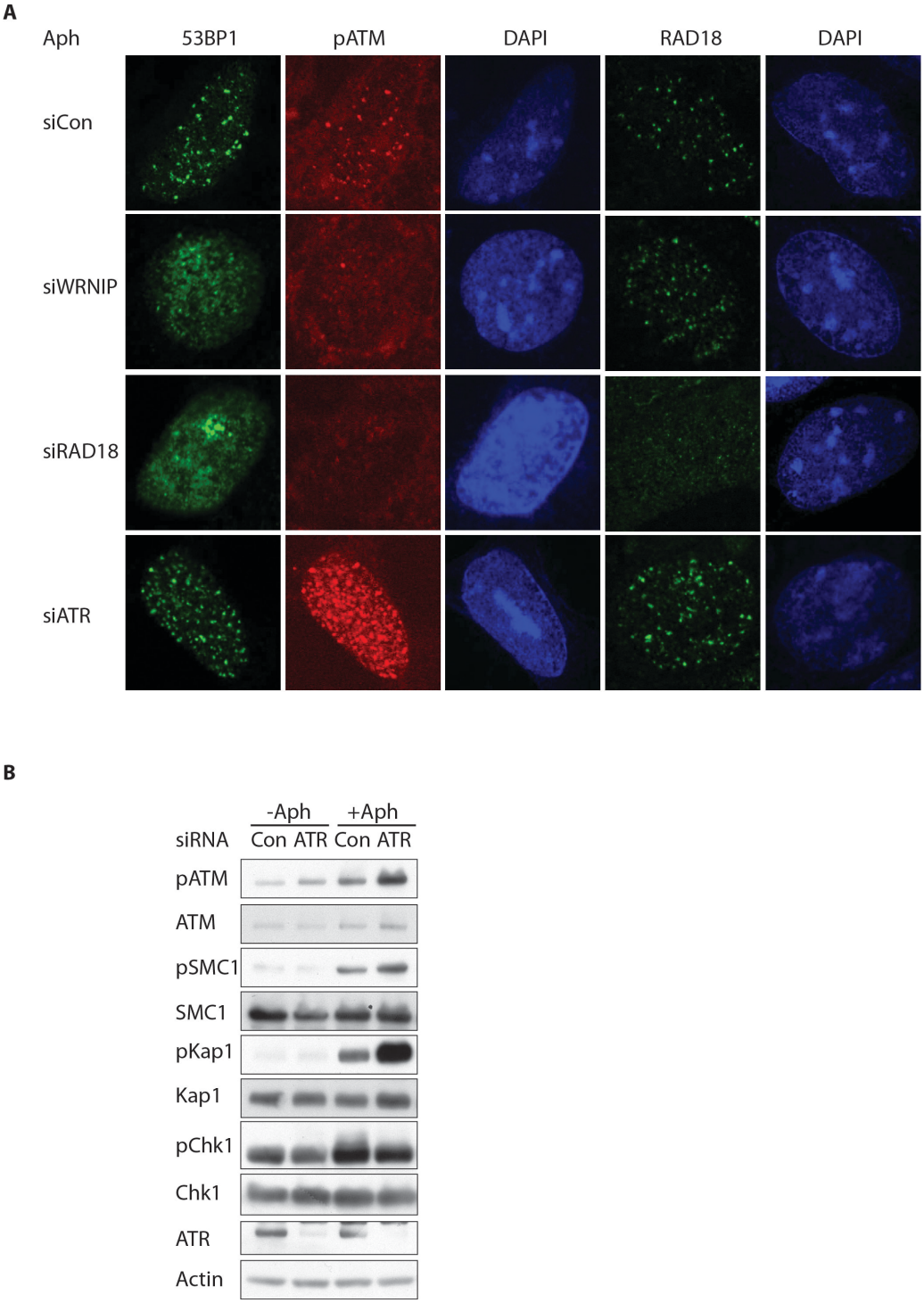

Figure 38. Knockdown of ATR does not impair ATM signalling after Aph.

(A) 293A cells were transfected with the indicated siRNA for 72 hours and treated with Aph, prior to fixation and immunofluorescence staining. (B) 293T cells were transfected with siControl or siATR for 72 hours and treated with Aph, prior to harvest of WCL for western blotting.

Together with the UFB data, this suggests a model whereby ATR, as the central kinase that responds to replication fork stalling during S phase, might act in concert with ATM to suppress UFB formation. While they are independently recruited to sites of replication stress, ATR could act in an early step to preserve the integrity of the replication fork and limit the activation of ATM. When the replication stalling is prolonged, ATM is subsequently activated via the WAR complex and possibly in response to specific DNA structures and continues to protect any ssDNA and recombination intermediates until they are repaired during the next G1 phase. In addition to ATR, ATM could have a role in sequestering any underreplicated DNA that arises from prolonged replication stress from breakage to form DSBs, and this most likely involves the activity of 53BP1, which shields the underreplicated DNA nuclear bodies until the next cell cycle.

Thus, ATMIN-mediated ATM signalling after replication stress is dependent on the WRNIP-ATMIN-RAD18 complex and could be activated by ubiquitinated PCNA along with other complex replication intermediate structures that is distinct from canonical IR-induced DSB stimuli. This could represent a novel mechanism of ATMIN-dependent ATM activation post-replication stress that is required for the protection of underreplicated DNA intermediates and maintenance of genomic stability.

Chapter 6. ATMIN genome screen for novel components of ATM-ATMIN pathway

ATMIN is required for ATM signalling after non-canonical stimuli such as replication stress, chloroquine and hypotonic stress (Kanu and Behrens, 2007). It is also required for pATM and 53BP1 localisation after replication stress (Figure 19A-C). In order to identify additional components of the ATM-ATMIN signalling pathway, we decided to use a genome-wide siRNA screening approach and immunofluorescence markers as readouts. The genome screen (primary and secondary screens) was carried out in collaboration with Joanna Loizou and the high-throughput screening facility at CRUK-LRI. I performed the deconvolution screen with the help of the high-throughput screening facility at CRUK-LRI and conducted the experiments to follow up the hits.

6.1 Screening approach, controls and optimisation

Initially, attempts were made at detecting endogenous ATMIN by immunofluorescence, using different in-house and commercial antibodies. However, while some of these antibodies gave nuclear foci stainings, there was no difference in staining observed in ATMIN wildtype or ATMIN-null MEFs (Figure 39A, Janet Cronshaw). Hence, due to the lack of good antibody for IF, it was not possible to screen for endogenous ATMIN foci formation. Next, I tried to overexpress GFP-ATMIN and look for foci formation after such as after Aph or MMS. Previously, it has been reported that GFPATMIN localises to foci after MMS treatment (McNees et al., 2005). However, only a small fraction of GFPATMIN foci colocalised with 53BP1 after MMS; most of the GFPATMIN was pan-nuclear. The latter also did not form discrete foci after Aph or colocalise with Aph-induced 53BP1 foci (Figure 39B). Moreover, the GFPATMIN foci, some of which partially colocalise with 53BP1 foci, were also observed in some cells in untreated conditions. Since the GFPATMIN foci formation did not appear to be stimulus specific possibly due to overexpression artefacts such as protein aggregation, as well as the low frequency of foci formation, it was not feasible to perform a genome screen with GFPATMIN as an immunofluorescence readout. Hence, an indirect approach was taken using pATM and 53BP1 foci, which could be visualised using commercial antibodies.

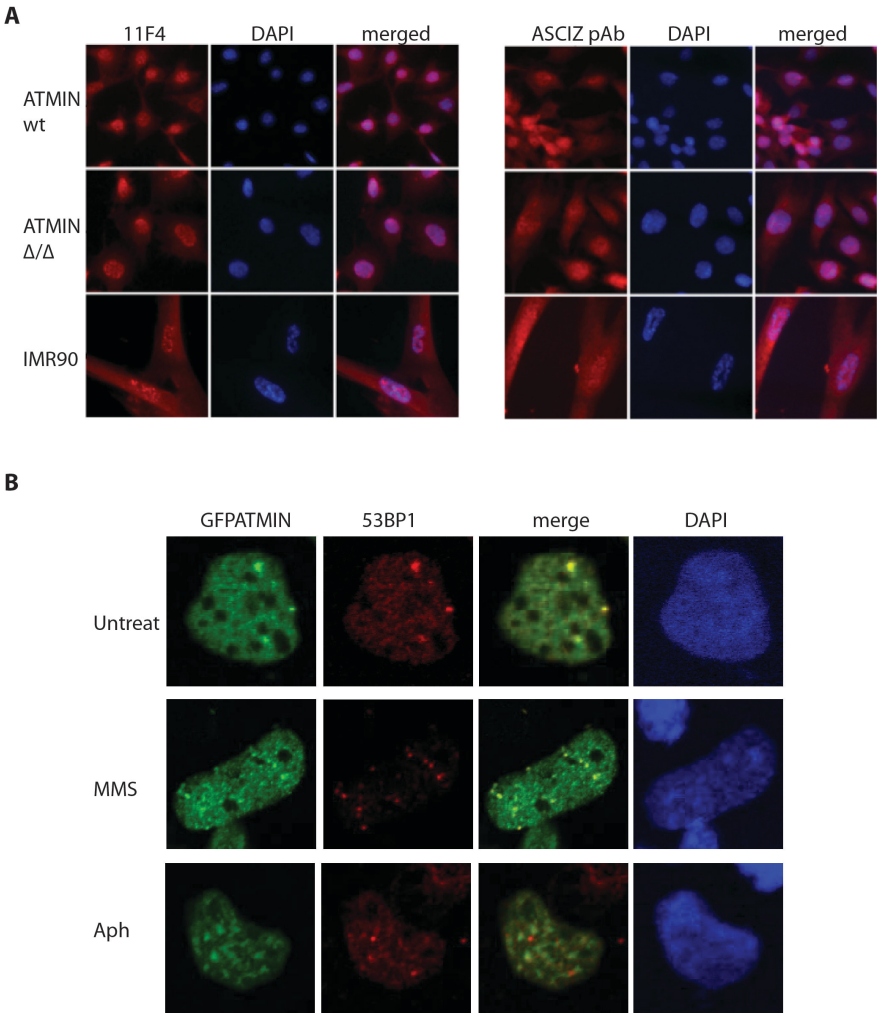

Figure 39. ATMIN immunofluorescence and localisation.

(A) Immunofluorescence of endogenous ATMIN using in-house ATMIN antibody or commercial ASCIZ antibody under basal conditions. (Janet Cronshaw) (B) GFPATMIN was overexpressed in 293A cells for 24 hours and treated with MMS or Aph for 4 hours prior to fixation and immunofluorescence staining.

In order to establish controls for the screen, several genes were chosen including ATMIN whose knockdown should result in decrease in pATM and 53BP1 foci after Aph, as evidenced by the ATMIN$^{\Delta/\Delta}$ MEF data (Figure 19). ATMIN siRNA was used as a positive control, the knockdown of which results in a three-fold reduction in pATM and 53BP1 foci after Aph (Figure 40, Figure 41A,B). The aim would be to look for genes whose knockdown gives a similar reduction in foci formation as ATMIN. In addition, 53BP1 and ATM siRNA were also used as positive controls, while si53BP1 led to an efficient reduction in 53BP1 foci, siATM did not produce a consistent reduction in pATM foci (Figure 41A). This could be due to the pATM antibody recognising other phospho-epitopes that are similar to pATM. Despite optimising several pATM antibodies, we did not find one that gave

a clean reduction upon knocking down ATM, although the knockdown was confirmed by western blotting for total ATM. Hence, we proceeded with the screen using a highly-specific 53BP1 antibody and a less specific pATM antibody and also used siATMIN+siATM double knockdown as another positive control, which results in a greater reduction in foci than ATM alone. As such, the results of the screen as discussed later will be mainly based on 53BP1 results and that of pATM is used a secondary guide.

RNF168 has been shown to play a role in amplifying the ubiquitination of chromatin around the DSB and in the retention of 53BP1 foci (Lukas et al., 2011a). Hence we also used RNF168 as a positive control. siRNF168 decreased 53BP1 foci formation after Aph, and to a lesser extent pATM (Figure 41A,B). Lastly, we also used Chk1 as a control, since the Chk1 has been shown to play a role in an ATR/ATM-independent checkpoint response (Rodriguez-Bravo et al., 2006) and its knockown increases apoptosis (Cho et al., 2005). The knockdown of Chk1 decreased foci formation but gave an intense pan-nuclear staining of pATM. Hence, hits that give a similar phenotype as siChk1 would be excluded. Using 53BP1, ATMIN, ATM, RNF168 and CHK1 as controls, the screen was carried out aiming to identify genes whose knockdown decreases 53BP1 and pATM foci, which could imply that they play a role in ATM-ATMIN signalling pathway.

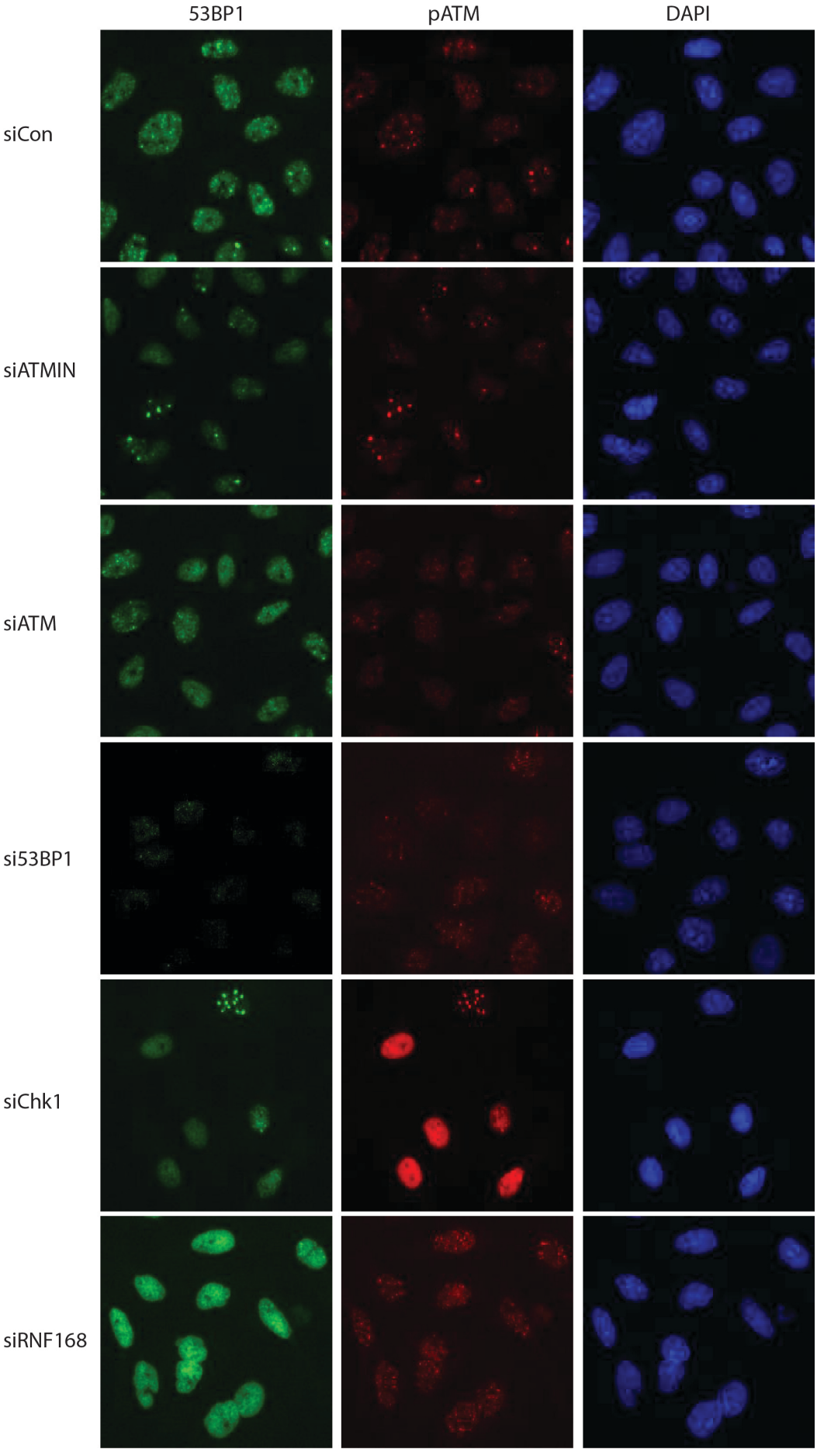
53BP1
pATM
DAPI
siCon
siATMIN
siATM
si53BP1
siChk1
siRNF168

Figure 40. Immunofluorescence on HeLa Ohio cells after transfection with siRNA against control genes for 72 hours and Aph treatment. Images were acquired on Arrayscan high content analysis reader.

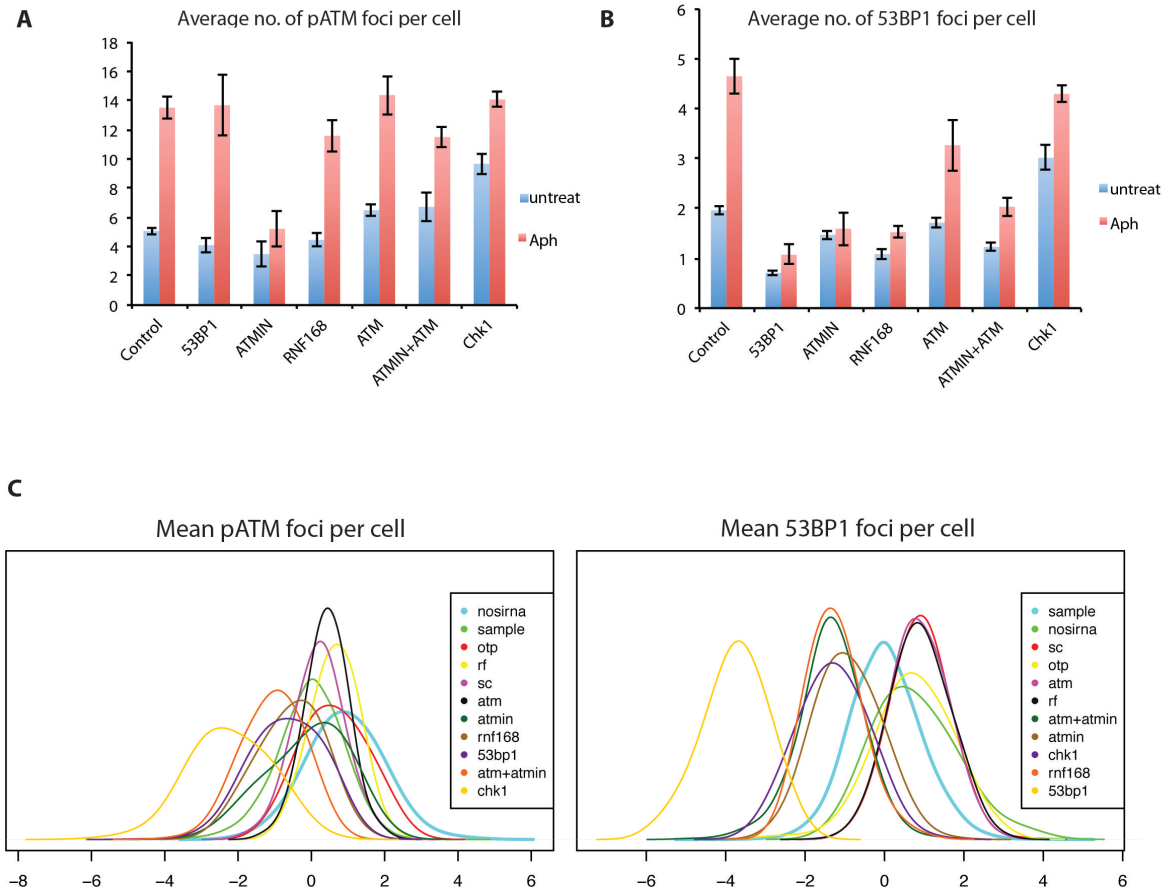

Figure 41. Screen controls optimisation and primary screen control siRNA distribution.

(A,B) pATM and 53BP1 foci were quantified by Arrayscan HCA reader after knockdown of control genes and treatment with Aph. (C) Distribution of control siRNA knockdown population mean z-score for pATM and 53BP1 after normalisation to correct for plate-to-plate variations. (OTP: Non-target control, rf: RISC-free control siRNA, sc: scrambled siRNA)

Optimisation was performed on a 96-well plate format to select the optimal transfection reagent, cell density and Aph treatment conditions. HeLa Ohio cells were chosen based on their adherent morphology to facilitate immunofluorescence staining and rapid proliferation. The cells were reverse transfected with the siRNA library for 72 hours and treated with Aph during the last 24 hours before fixation. Different fixation and staining methods were also compared to optimise signal-to-noise ratio. Through re-iterative optimisation with the help of the High-throughput Screening facility, we established a consistent

signal to noise ratio and set thresholds to quantify 53BP1 and pATM foci using a Thermo Scientific Cellomics Arrayscan High Content Analysis Reader. Foci that fall below or above a set intensity and size were excluded from the quantification. Using a 96-well format, the primary screen was performed against a Dharmacon human cDNA library of 21289 genes in triplicates (Figure 42A). For each sample well, 15 images were acquired by random sampling in each of the three channels, DAPI, 53BP1 and pATM, so that at least 300-500 cells were sampled for each well. The z-scores were calculated from the average number of foci per cell for each sample, normalised against the median value of control siRNA for each plate in order to correct for plate-to-plate variations. From the control distribution of mean foci count per cell across the whole population, knockdown of ATMIN decreased mean 53BP1 foci z-score but had less effect on pATM foci z-score compared to non-target siRNA control (OTP), scrambled siRNA (SC) or risk-free siRNA (RF) (Figure 41C). This could be due to variability of pATM antibody staining or that the effect of ATMIN knockdown on pATM foci formation is not always consistently observed across all the plates.

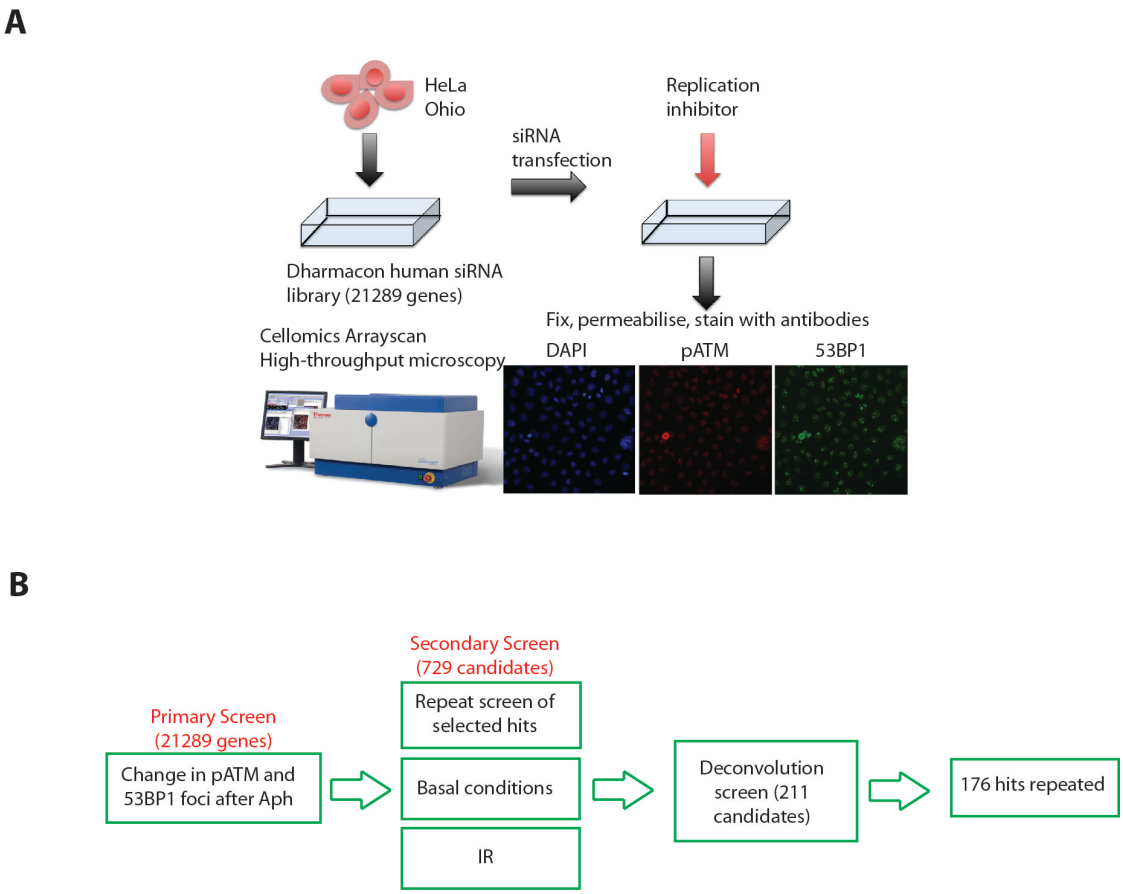

Figure 42. Scheme of genome-wide siRNA screen.

(A) Overview of screen strategy. HeLa Ohio cells were reverse transfected in 96-well format with human siRNA genome library for 72 hours, and Aph was added in the last 24 hours prior to fixation and staining for immunofluorescence. Plates were analysed by Cellomics Arrayscan HCS reader. (B) Scheme of screen approach. Primary screen was carried out on a genome-wide level, followed by a secondary screen using repeat conditions, untreated conditions and IR. Selected hits were taken through another round of deconvolution screen.

From the primary screen of 21289 genes, the 53BP1 and pATM z-scores were correlated to look for interesting hits that decreased both 53BP1 and pATM, increased both channels or decreased one channel but not the other (Figure 43A-C). To select initial hits, we used a lower cut-off of -1.86 for 53BP1, which corresponds to the effect of ATMIN siRNA, and -2 for pATM as a more stringent threshold, and z-score greater than 2 was used an upper cut-off. Hits that decreased cell numbers by more than z-score of 2 based on the number of DAPI positive cells scored were discarded. By classifying the hits according to different cut-off zones, we identified 729 interesting candidates as shown by the coloured regions in Figure 43C. Bioinformatics analysis using the PANTHER classification

system shows that a majority of these hits are involved in cell metabolic processes (Figure 43D). Functional categorisation of genes using DAVID database revealed that the most enriched group encode for proteins involved in transcription and DNA metabolic processes (Figure 42E), which suggests that the selected hits are of physiological relevance, as ATMIN has been implicated in these processes.

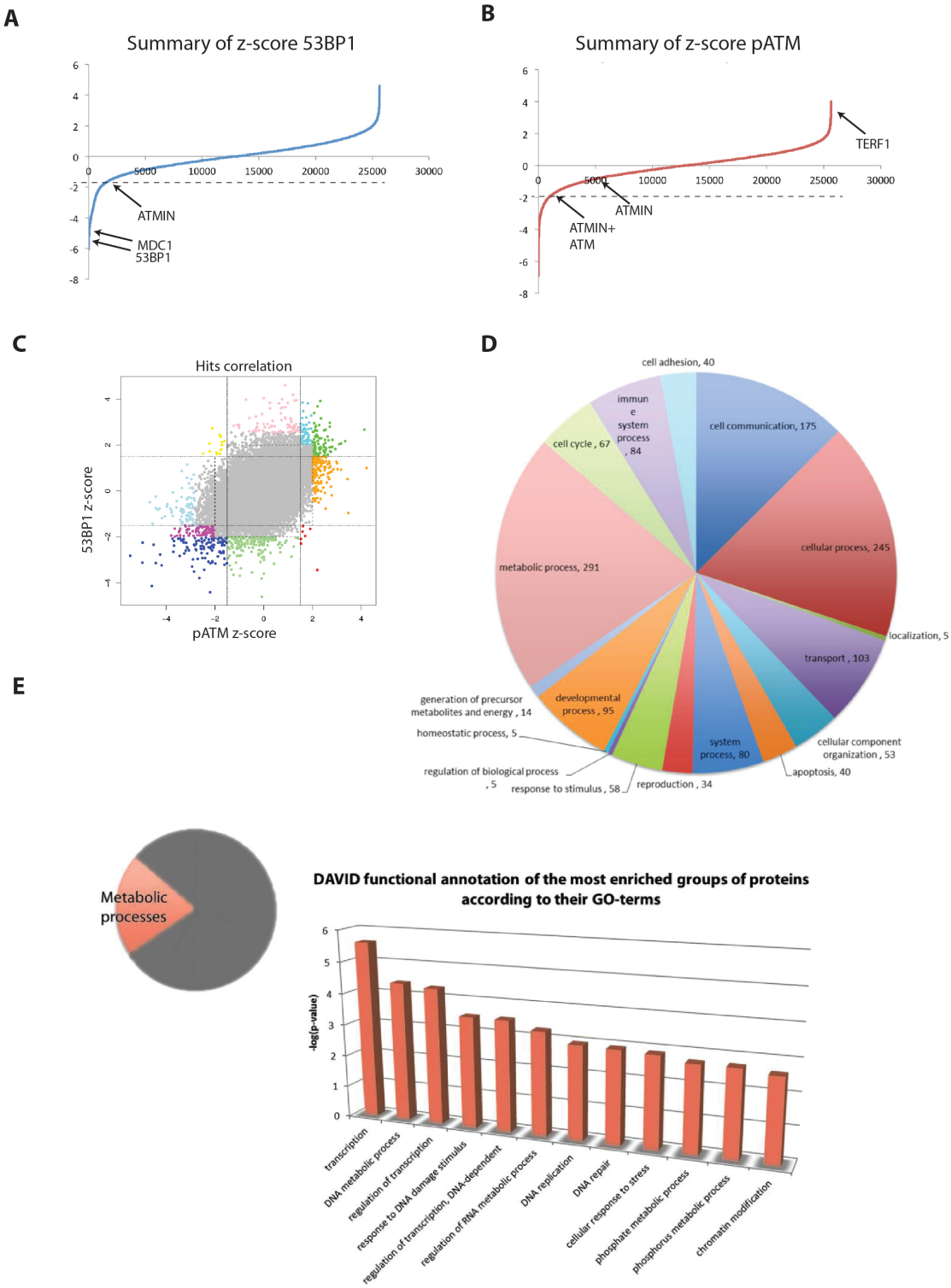

Figure 43. Analysis of primary screen hits.

(A,B) Scatter plot of z-scores from the primary screen for pATM and 53BP1 foci respectively. Arrows indicate the positions of controls and known genes such as MDC1 and TERF1. Dotted lines (-1.86 for 53BP1 and -2 for pATM) indicate thresholds used in the selection of hits. (C) Correlation of 53BP1 and pATM z-scores

and grouping of hits by category. Coloured regions represent the hits selected from the primary screen for further analysis. (D) PANTHER analysis of the selected hits for statistically significant sets according to their biological processes. The most significant categories of biological processes are represented in the pie chart (http://www.pantherdb.org). (E) Gene-ontology analysis using the DAVID database of genes from the most enriched group of biological processes (http://david.abcc.ncifcrf.gov).

6.2 Secondary screen and identification of hits

In order to further dissect the roles of these initial hits whose knockdown de-regulates 53BP1 and or pATM, a secondary screen was performed. For this screen, cells were treated with Aph, IR, or analysed under basal conditions (Figure 42B). Since ATMIN is not required for ATM signalling after IR, the secondary screen would reveal hits that are required strictly for ATM signalling pathway after Aph but not after IR and therefore may work with ATMIN, as well as any effects on ATM signalling under basal conditions. The secondary screen was repeated using the same conditions as before except for the addition of IR treated or untreated plates after siRNA transfection. 211 genes were selected from the secondary screen that successfully repeated the primary screen data. These were subsequently taken into a deconvolution screen using Aph treatment where an individual siRNA oligo was used instead of a pool of 4 siRNAs. 176 of the hits from the deconvolution screen were confirmed with at least 2 siRNA oligos showing a similar result as the pooled siRNA.

From the secondary screen, there were hits that increased foci in all three conditions, or decreased in all three conditions, and those that increased in one condition and decreased in another. Some hits were common to both IR and Aph pathways, such as RNF8 and MDC1, which have been shown to play a role in the IR-induced DSB signalling. RNF8 is recruited to DSB sites via its FHA domain with phosphorylated MDC1, and is required for histone H2A ubiquitination and subsequent 53BP1 and BRCA1 localisation (Huen et al., 2007, Mailand et al., 2007, Kolas et al., 2007). In line with published literature, knockdown of RNF8 decreases 53BP1 foci formation after IR. Interestingly, 53BP1 foci formation after Aph is also impaired. A similar result is observed for MDC1. Hence, this suggests that RNF8 and MDC1 are upstream in 53BP1 recruitment after both IR and Aph. Conversely, there were some hits such as RAD9A and RAD51 that decreased foci after Aph and increase foci after IR. These were similar to the phenotype after ATMIN knockdown, which slightly increases ATM signalling after IR (Zhang et al., 2012) and decreases foci formation after Aph. Hence, these hits are likely to play a similar role as ATMIN in regulating ATM signalling (Figure 44).

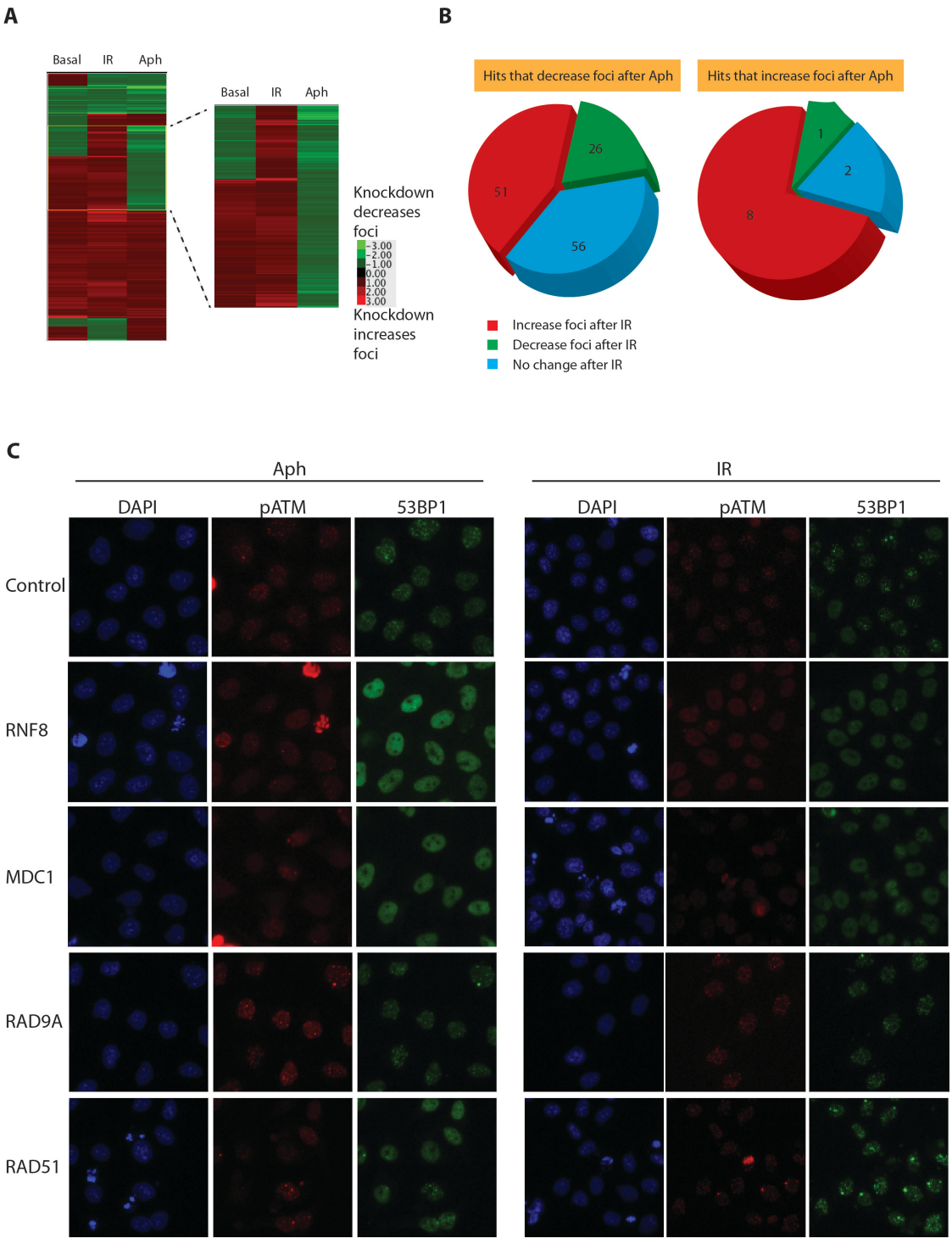

Figure 44. Summary of secondary screen results.

(A) Heat map showing fold change in 53BP1 foci compared to control siRNA under basal, Aph or IR conditions. Highlighted region represents hits of interest that decrease foci after Aph and increases after IR when depleted by siRNA. (B) Pie-chart showing number of hits from deconvolution screen and their effects after Aph and IR. (C) Representative images from the secondary screen showing hits that decrease foci after Aph and IR (RNF8, MDC1) and hits that decrease foci after Aph and increase after IR (RAD9A, RAD51).

Of the hits confirmed by deconvolution screen, we identified four genes that are involved in the protection against oxidative damage (Figure 45). OGG1, the DNA glycosylase that specifically removes 8-oxo-guanine (8-oxoG) from DNA, was identified as a top hit in reducing 53BP1 foci formation after Aph. Furthermore, loss of OGG1 has no effect on basal 53BP1 foci formation, and slightly increased foci formation after IR. Another highly related DNA glycosylase, MUTYH (MutY homolog), which cleaves the mismatched adenine from an A: 8-oxoG base pair, was also amongst the confirmed hits. Another enzyme of interest was NUDT1 (also known as MTH1), the nucleoside diphosphatase that cleaves oxidised purine triphosphate to monophosphates and thereby prevents the misincorporation of oxidised bases into DNA, was also identified as a positive hit after Aph. These three enzymes constitute the 8-oxoG system that prevents the incorporation of oxidised bases and initiates the base excision repair of oxidised lesions. In addition, another cytoplasmic enzyme, GSTM5 (Glutathione s-transferase mu 5) was also amongst the hits that decreased 53BP1 foci after replication stress. (For simplicity, these four genes will be collectively referred to as the 8-oxoG genes).

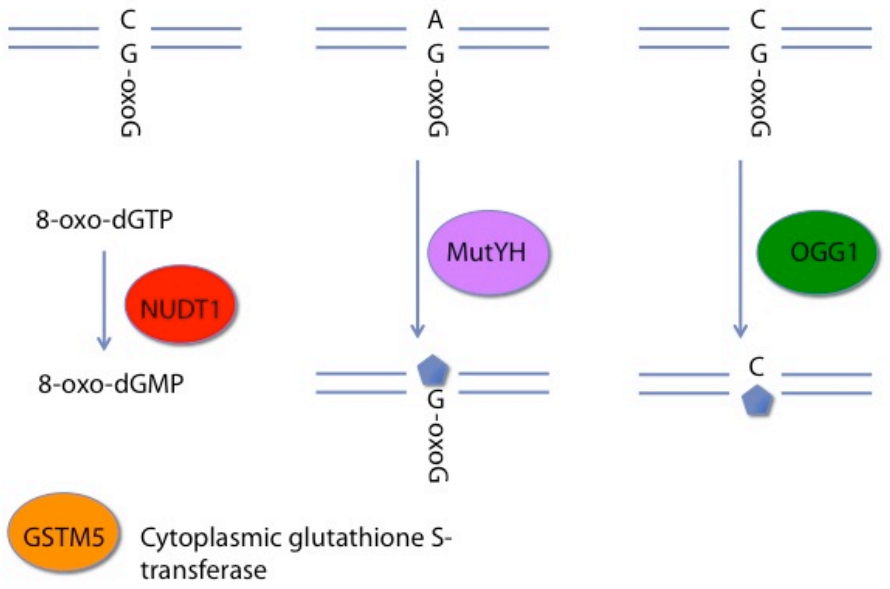

Figure 45. Components of the 8-oxoG system identified through the screen.

8-oxoG occurs at a frequency of approximately 1000-2000 lesions per human cell per day (van Loon et al., 2010), thus making it the most prevalent form of DNA oxidative damage. 8-oxo-G is also highly mutagenic due to its ability to mimic thymine and form a mismatch base pair with adenine, leading to C:G to A:T transversion mutations. C:G to A:T transversions have been reported to constitute one third of all somatic mutations in a small-cell lung cancer cell line (Pleasance et al., 2010b). Moreover, they have been identified as the second most prevalent mutational signature in melanoma cells in a study of somatic mutations from an individual cancer genome (Pleasance et al., 2010a). Ingenuity pathway analysis shows the biological networks in which these 8-oxoG genes have a known role, and there is no data showing any interaction with ATM (Figure 46). Despite no previous link with ATM, that the 8-oxoG system and oxidation protection enzymes were identified as top hits in the screen implies a hitherto unknown link between base excision repair and ATM signalling.

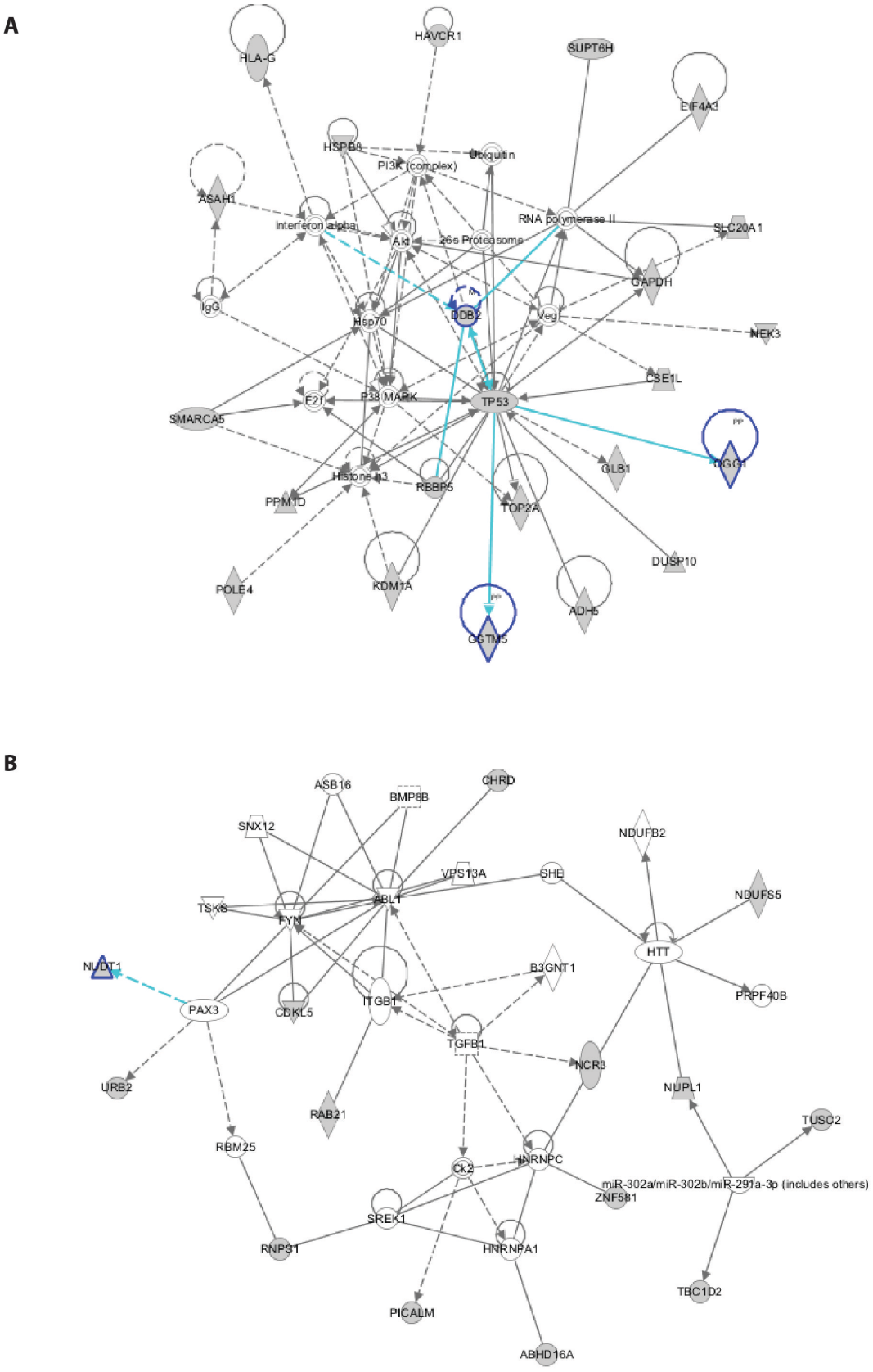

Figure 46. Ingenuity pathway analysis of OGG1, GSTM5, MUTYH and NUDT1 and their interaction networks respectively. Symbols that represent classes of genes and arrows that represent relationship are shown above and below.

C

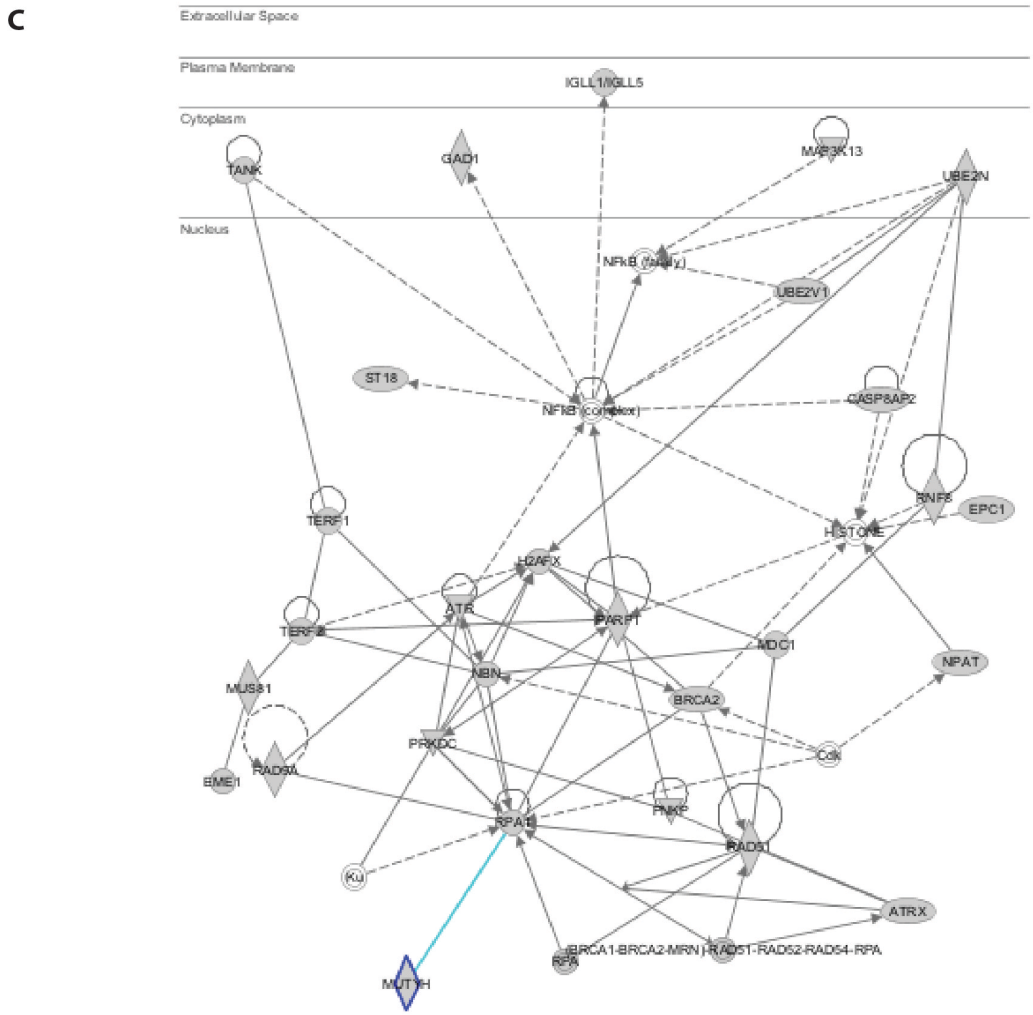
Extracellular Space
Plasma Membrane
Cytoplasm
Nucleus
IGLL1/IGLL5
TANK
GADD1
MAP3K13
UBE2N
NFkB (family)
UBE2V1
ST18
NFkB (complex)
CASP8AP2
RNF8
EPC1
TERF1
HISTONE
H2AFX
ATR
PARP1
TERF2
MDC1
NBN
NPAT
MUS81
BRCA2
PRKDC
CDK
EME1
RAD50
PNKP
RPA1
RAD51
Ku
ATRX
BRCA1-BRCA2-MRN-RAD51-RAD52-RAD54-RPA
RPA
MUTYH

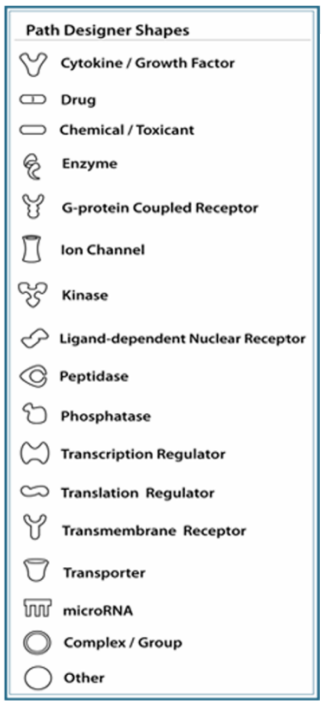
Path Designer Shapes
Cytokine / Growth Factor
Drug
Chemical / Toxicant
Enzyme
G-protein Coupled Receptor
Ion Channel
Kinase
Ligand-dependent Nuclear Receptor
Peptidase
Phosphatase
Transcription Regulator
Translation Regulator
Transmembrane Receptor
Transporter
microRNA
Complex / Group
Other

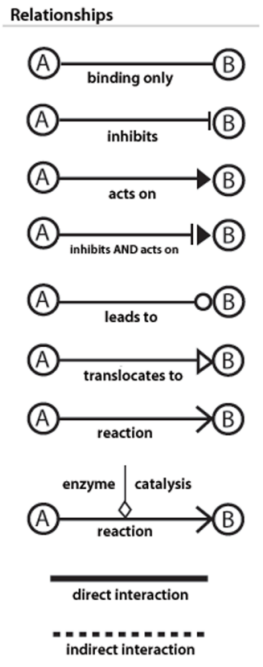
Relationships
A
B
binding only
inhibits
acts on
inhibits AND acts on
leads to
translocates to
reaction
enzyme
catalysis
reaction
direct interaction
indirect interaction

6.3 The knockdown of 8-oxoG genes impairs ATM signalling after replication stress, but not after IR

In order to validate the hits, siRNA experiments were repeated on a 24-well format with HeLa Ohio cells. As observed for the screen, the knockdown of 8-oxoG genes led to a decrease in 53BP1 and pATM foci formation upon Aph treatment (Figure 47). Some hits, such as NUDT1, have a greater effect, while others such as GSTM5 have a less dramatic phenotype. This could be due to specificity of action of some proteins and redundancy of others in the pathway, as such I also used MUTYH and OGG double siRNA knockdown to check for additive effects. The additive effect of combined knockdown of MUTYH and OGG1 implies that they could have redundant roles in the pathway.

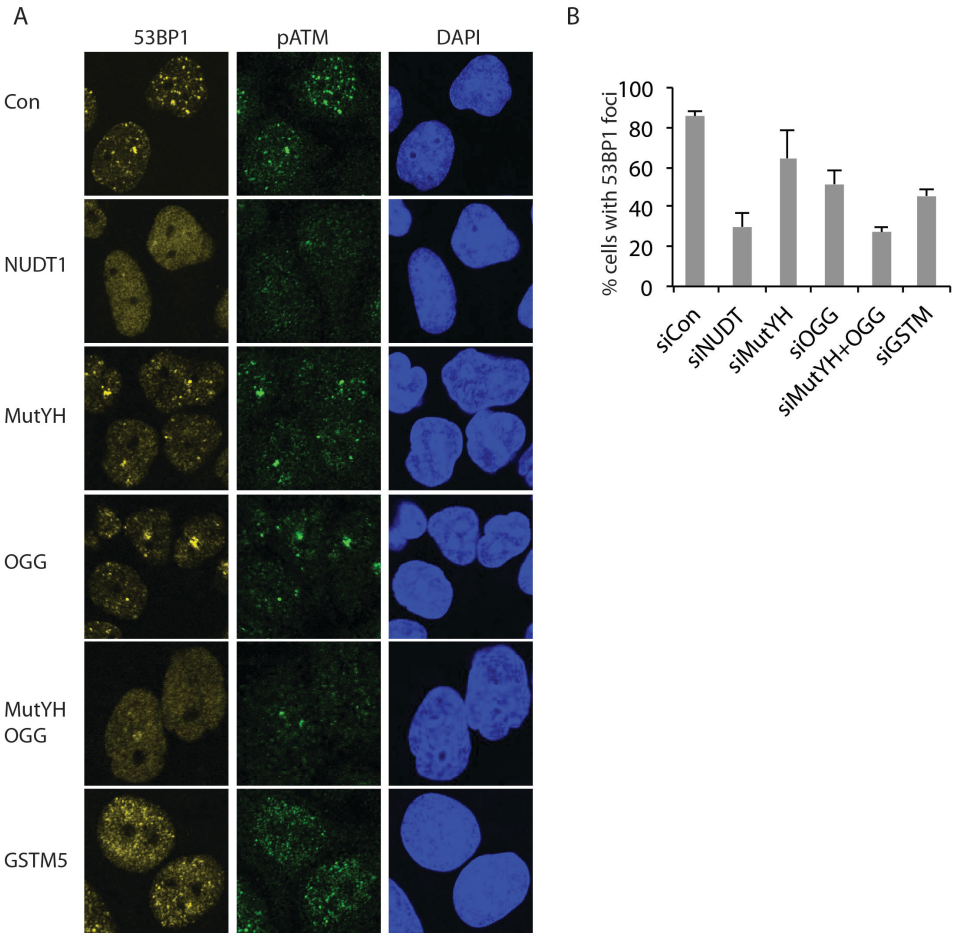

Figure 47. Loss of 8-oxoG genes impairs ATM signalling after Aph.

(A) Immunofluorescence of pATM and 53BP1 foci on HeLa Ohio cells after 72 hours transfection with the indicated siRNA and treated with Aph during the last 24 hours prior to fixation. (B) Quantification of percentage of cells positive for 53BP1 foci. Cells were scored as positive if they harboured more than 8 foci.

The immunofluorescence data was further validated in 293 cells, whereby knockdown of the 8-oxoG genes led to similar decreases in 53BP1 and pATM foci formation. To test whether the loss of foci depends on reactive oxygen species (ROS), a superoxide dismutase mimetic, TEMPOL (4-hydroxy-2,2,6,6-tetramethylpiperidin-1-oxyl), was used as a ROS scavenger, which has previously been shown to protect against H2O2-induced oxidative damage (Hahn et al., 1992, Hahn et al., 1997). Addition of TEMPOL rescued the 53BP1 and pATM foci formation after Aph in each 8-oxoG gene knockdown, with OGG and GSTM5 having the highest rescue to near wildtype levels (Figure 48A-C). This was also confirmed by western blot showing ATM substrate phosphorylation. While the knockdown of ROS genes led to decrease in phosphorylation of ATM substrates such as Kap1, SMC1 and p53, the addition of TEMPOL increased the phosphorylation levels for most 8-oxoG genes (Figure 48B). These data suggest that ATM signalling after Aph is impaired in the absence of 8-oxoG genes, and removal of oxidative stress by TEMPOL could augment ATM signalling in replication stress conditions.

To rule out any possible off-target effects of the siRNA, I also deconvoluted the siRNA pools against the hits of interest by cloning each siRNA sequence into an shRNA vector, and observed that the two best shRNAs gave a similar effect on ATM signalling as that seen in siRNA knockdowns (Figure 49A). Also, I verified that TEMPOL does not induce ATM signalling on its own, I compared ATM substrate phosphorylation by western blot after control siRNA treatment with or without TEMPOL treatment and saw no significant increase at basal conditions or after Aph. Hence, TEMPOL is able to exert its effect in augmenting ATM signalling only after 8-oxo-G dependent impairment in ATM signalling (Figure 49B).

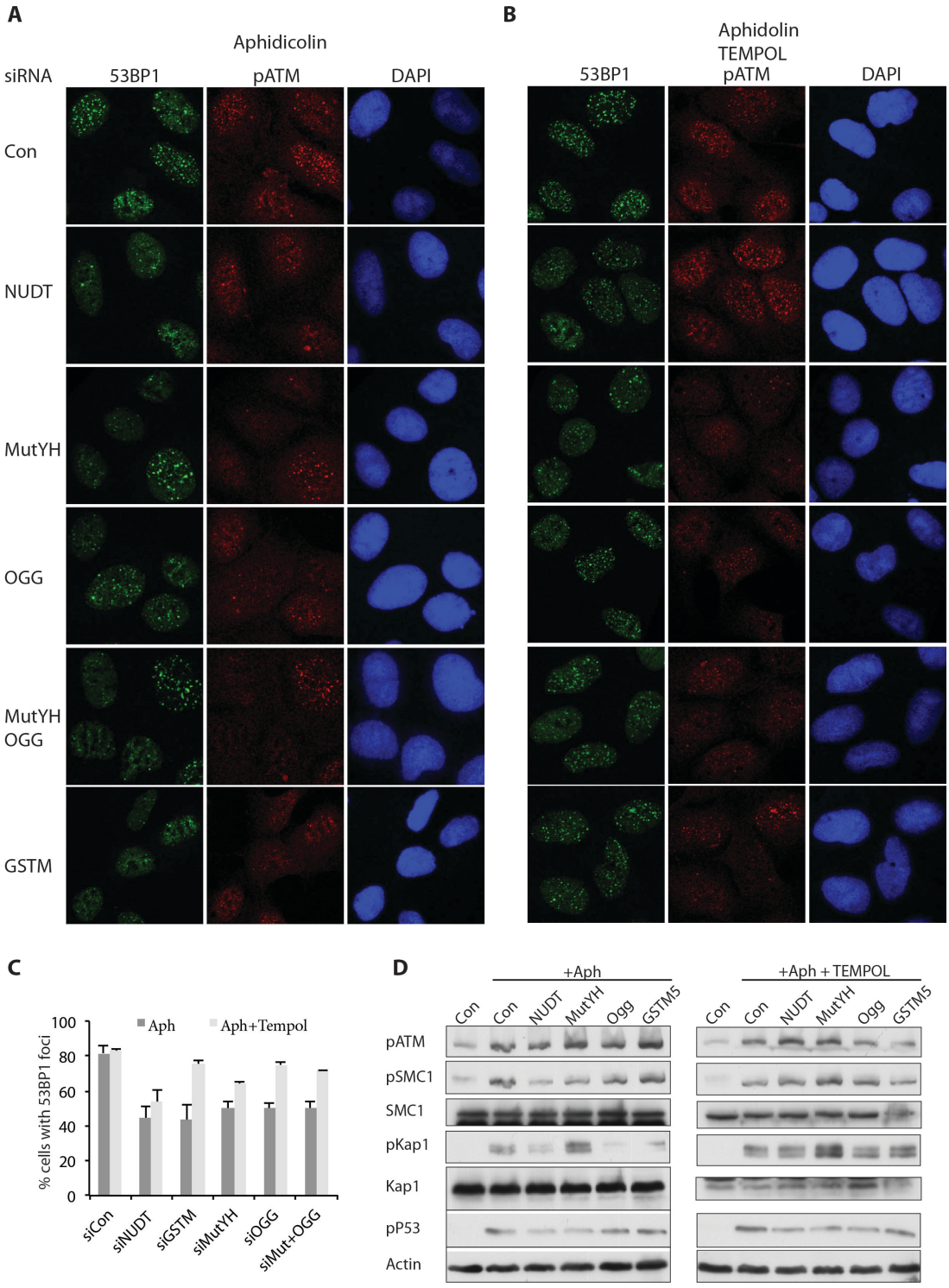

Figure 48. ROS scavenger TEMPOL rescues ATM signalling.

(A, B) Immunofluorescence of pATM and 53BP1 in 293A cells after 72 hours transfection with the indicated siRNA and Aph treatment prior to fixation, either with or without the addition of TEMPOL to the medium throughout the duration of the transfection. (C) Quantification of percentage of cells positive for 53BP1 foci. Cells were scored as positive if they harboured more than 8 foci. (D) 293T cells were transfected with the indicated siRNA with or without TEMPOL for 72 hours and treated with Aph in the last 24 hours prior to harvest of whole cell lysate for western blot analysis.

TEMPOL has been previously reported to protect cells against IR-induced chromosome aberrations such as dicentric, ring and triradial chromosomes and protect mice against whole body irradiation (Mitchell et al., 1991, Liebmann et al., 1994, Johnstone et al., 1995). Recently, it has also been shown to directly counteract the increase in oxidative DNA lesions such as 8-oxoG and sister chromatid exchange caused by vorinostat (histone deacetylase inhibitor) treatment (Alzoubi et al., 2013). Hence, the decrease in ATM signalling after Aph could be due to an increase in 8-oxoG lesions, which is rescued after treatment with TEMPOL.

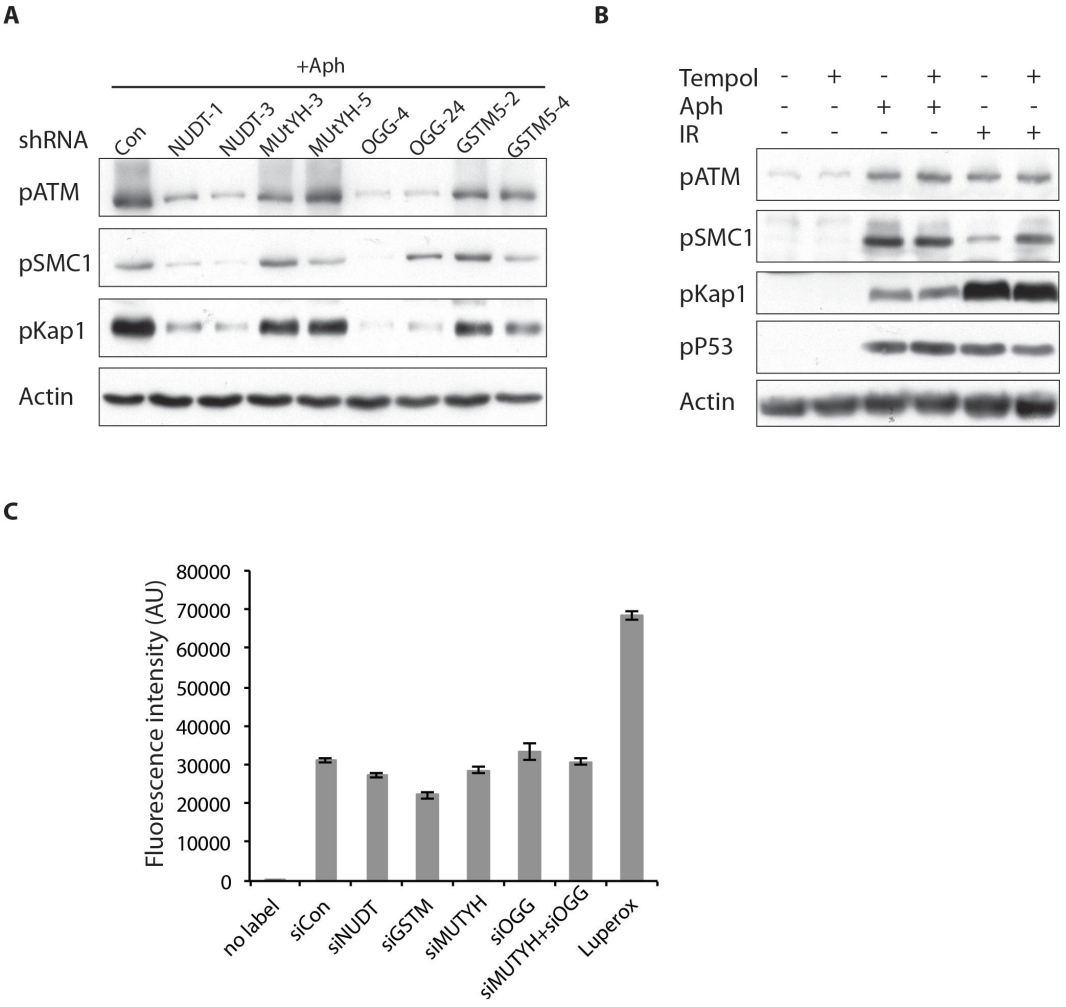

Figure 49. Deconvolution of screen hits and effect of TEMPOL on ATM signalling.

(A) 293T cells were transfected with the indicated shRNA constructs for 72 hours and treated with Aph prior to harvest of WCL for western blotting. (B) 293T cells were treated with or without TEMPOL for 72 hours and treated with Aph prior to harvest of WCL for western blotting. (C) 293T cells were transfected with the indicated siRNA for 72 hours prior to labelling with CM-H2DCFDA and total cellular ROS level was quantified by fluorescence intensity by FACS. Luperox treatment (1 hour, 10uM) was used as a positive control.

In order to test whether the effect on ATM signalling is due to changes in overall cellular ROS levels, or accumulation of oxidised nucleotides such as 8-oxoG, ROS labelling was performed to measure the ROS levels after knockdown of 8-oxoG genes. Using CM-H2DCFDA as a general ROS label and luperox (a highly active peroxide) treatment as a positive control, I observed that the knockdown of 8-oxoG genes did not change the overall ROS level appreciably compared to control (Figure 49C). Hence, the effects on ATM signalling is most likely due to other forms of oxidation such as 8-oxoG formation and not a change in overall ROS levels. However, a direct measurement of 8-oxoG level by immunofluorescence was not successful, this could be due to the epitope being too small to be detected by IF. Moreover, I also tried to validate the data using *ogg1*Δ/Δ primary MEFs isolated from *ogg1*Δ/Δ mice (Klungland et al., 1999). IF studies showed that *ogg*-null MEFs were still able to form 53BP1 and pATM foci after Aph compared to WT (Figure 50A). By western blot, both Ogg wildtype and knockout MEFs show ATM substrate phosphorylation after Aph, with even higher levels in the knockout, and knockdown of MUTYH in these MEFs also did not have any effect (Figure 50B). This discrepancy could be due to species-specific differences and redundancies in the GO pathway in mouse cells that are not present in human HeLa or 293 cells. Hence, the MEF system was not used any further for this study.

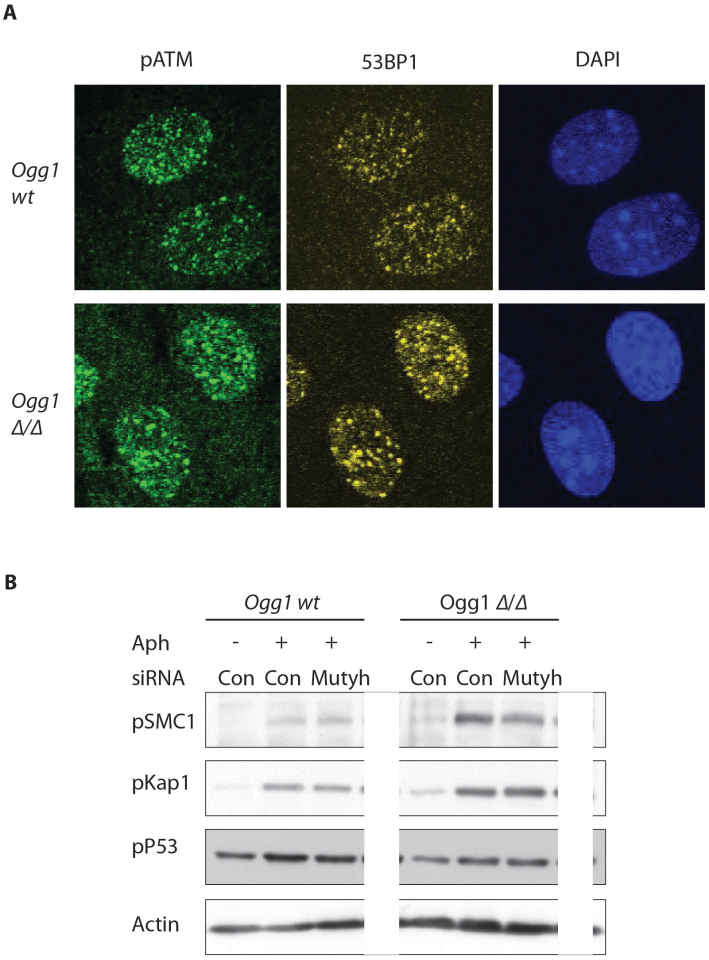

Figure 50. Validation using Ogg1 knockout MEFs.

(A) Immunofluorescence showing pATM and 53BP1 staining on *Ogg1* wildtype or knockout MEFs after treatment with Aph. (B) *Ogg1* wildtype or knockout MEFs were transfected with siMUTYH or siControl for 72 hours and treated with Aph prior to harvest of WCL for western blot analysis.

While the knockdown of 8-oxoG genes impaired ATM signalling after Aph, the ATM-mediated DSB response after IR was not affected, as judged by pATM and 53BP1 foci formation and ATM substrate phosphorylation (Figure 51). Hence, the effect of 8-oxoG genes on ATM signalling is specific to replication stress and does not affect MRN-dependent ATM activation after IR.

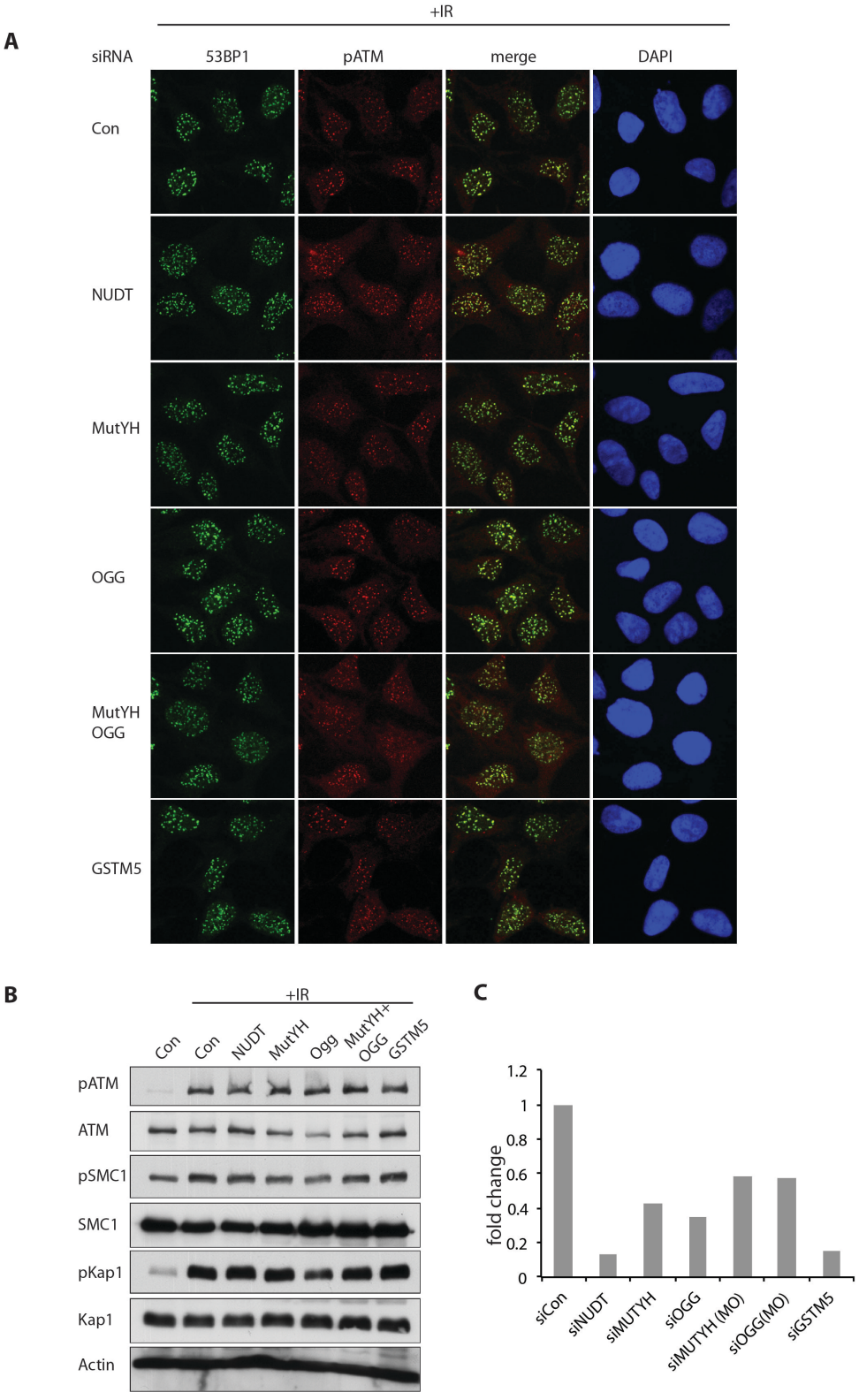

Figure 51. knockdown of 8-oxoG genes do not affect IR-induced ATM signalling.

(A) Immunofluorescence of pATM and 53BP1 in 293A cells after 72 hours transfection with the indicated siRNA and treatment with IR (2Gy) prior to fixation. (B) Western blot of 293T cells with the same treatment as in (A) and whole cell lysate harvested for western blot analysis. (C) QPCR of total mRNA from the same experiment as in (A) to show the siRNA knockdown efficiency of the indicated genes.

6.4 Loss of 8-oxoG genes impairs RAD18 foci formation after replication stress

Since we have previously shown that RAD18 is required to localise pATM and 53BP1 to sites of replication stress, I investigated whether the impairment in 53BP1 foci formation could be due to a defect in RAD18 recruitment. Indeed upon the knockdown of 8-oxoG genes, there was a reduction in RAD18 foci formation, which could be rescued to wildtype levels by addition of TEMPOL (Figure 52A,B). RAD18 has been previously reported to bind to forked DNA structures as well as ssDNA tails in vitro via its SAP (SAF-A/B, Acinus and PIAS) domain (Tsuji et al., 2008). A biotinylated DNA template with 40-mer dsDNA and 80-mer ssDNA was used in a pull down assay with recombinant human RAD18. While RAD18 was bound to the unmodified DNA template, oxidation of the DNA using H2O2 decreased the RAD18 interaction (Figure 52C, right panel). Published data showed that the lower concentration of H2O2 (3mM) was sufficient to generate 34.95nmol/mg 8-oxoG DNA as measured by gas-chromatography mass spectrometry (Whiteman et al., 2002), but was not high enough to degrade the DNA template as analysed by separating the DNA strands on a denaturing urea-PAGE (Figure 52C). Hence, the knockdown of 8-oxoG genes could affect RAD18 binding to ds-ssDNA junctions due to the oxidation of DNA. The SAP domain on RAD18 has a helix–extended-loop–helix structure that is homologous to that of PIAS, which is proposed to bind in the minor groove of DNA (Tsuji et al., 2008, Okubo et al., 2004). One could speculate that in the absence of functional 8-oxoG genes, the excessive base oxidation may distort the conformation of the DNA minor groove, thereby preventing RAD18 binding to ssDNA-dsDNA junctions at stalled replication sites.

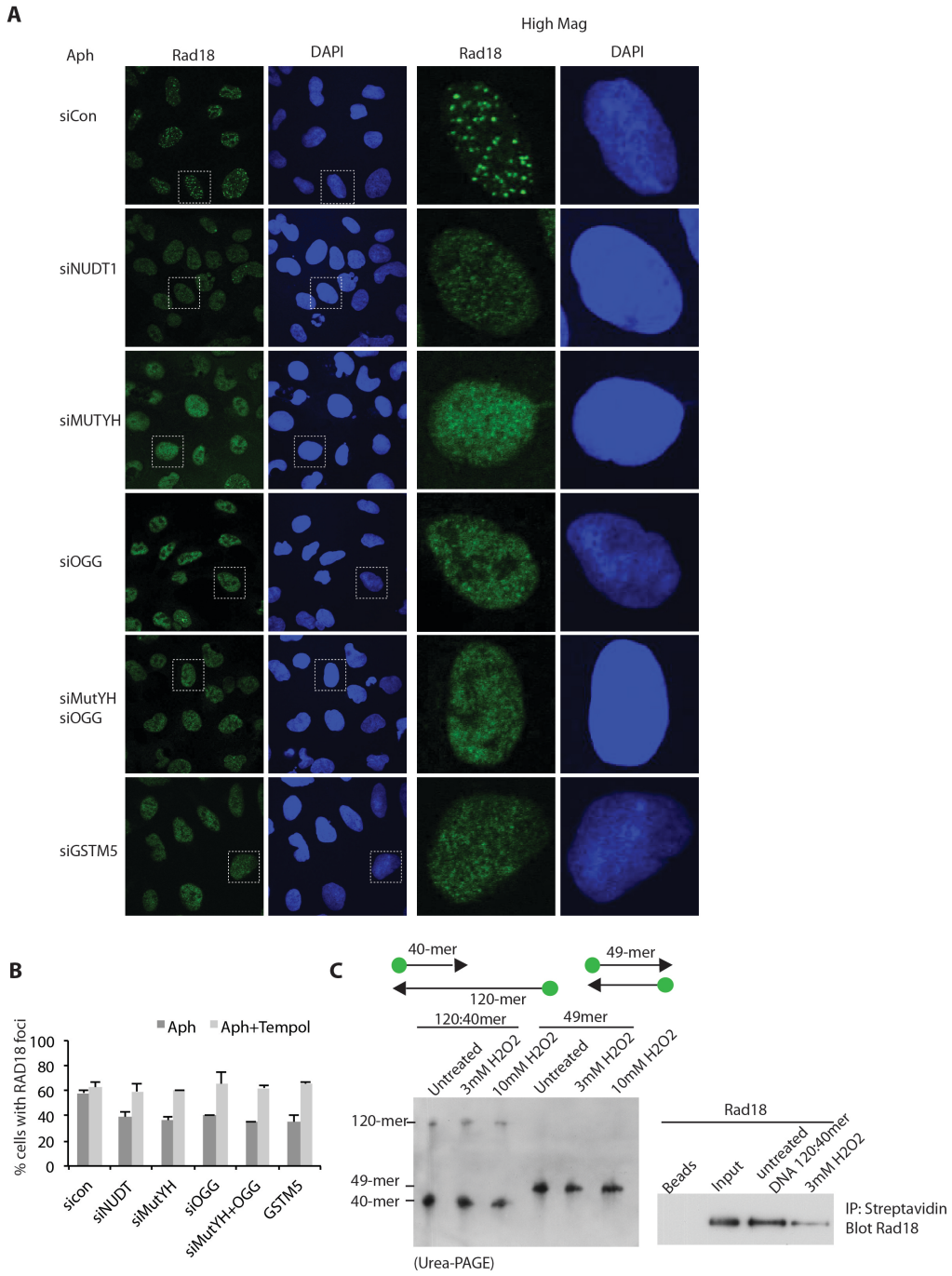

Figure 52. Knockdown of 8-oxoG genes and DNA oxidation impairs RAD18 binding to DNA.

(A) Immunofluorescence of RAD18 foci in 293A cells transfected with the indicated siRNA for 72 hours and treated with Aph prior to fixation. (B) Quantification of percentage of cells with RAD18 foci. Cells were scored as positive if they harbour more than 8 foci. (C) In vitro pull-down of RAD18 using biotinylated DNA oligos. Biotinylated annealed DNA oligos were oxidised in vitro with H2O2 or untreated and then incubated with recombinant RAD18 before immunoprecipitation with streptavidin beads and blotting against RAD18 (right panel). (Beads: no DNA oligo, Input: no beads or DNA oligo). An aliquot of DNA fragment was subjected to denaturing urea-PAGE (left panel) to check for presence of both strands.

6.5 Knockdown of 8-oxoG genes increases ultrafine bridge formation during anaphase

If the knockdown of 8-oxoG genes affects RAD18 localisation to sites of replication stress and thereby impairs 53BP1 foci formation, I wanted to investigate whether this has a similar functional consequence as the loss of ATMIN in anaphase bridge formation. Indeed, under basal conditions, the knockdown of 8-oxoG genes induces a heightened frequency of anaphase bridges coated with PICH and are sometimes DAPI-positive (Figure 53A,B). These anaphase bridges can also be suppressed with TEMPOL, which correlates with the rescue of foci and signalling. That the loss of 8-oxoG genes has a similar phenotype could be due to the increased barrier to replication posed by 8-oxo-G and other products of DNA oxidation, which also impairs RAD18 from binding DNA and downstream ATM activation.

A

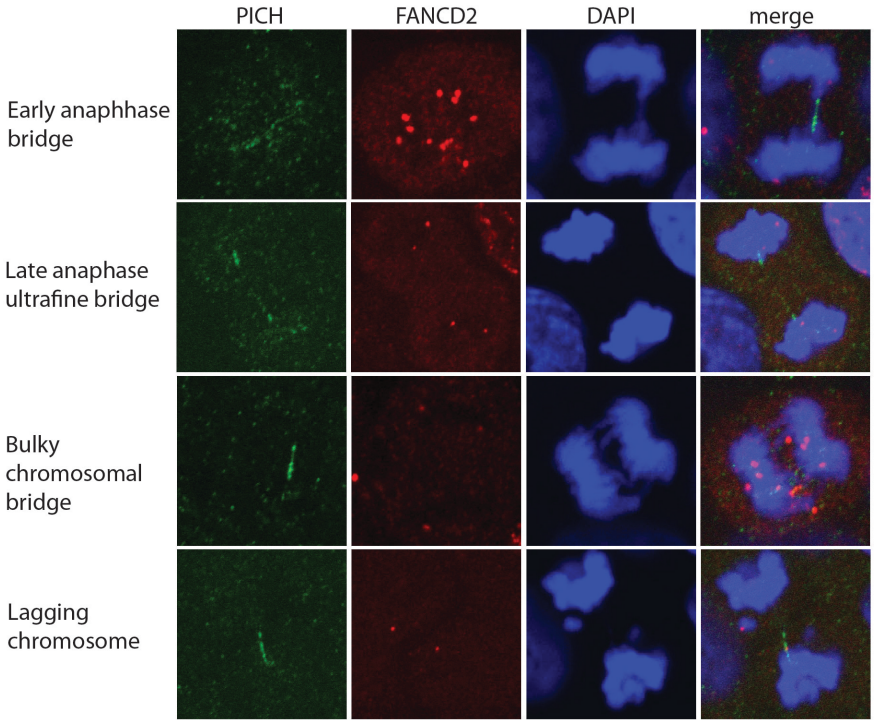

B

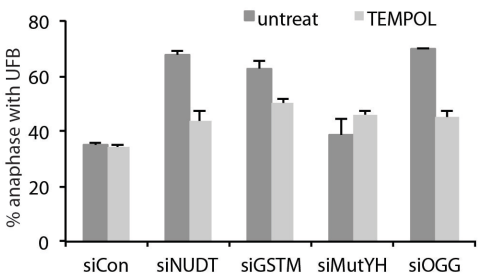

Figure 53. Knockdown of 8-oxoG genes increases anaphase bridge formation.

(A) Representative images of different types of anaphase bridges that can be observed in untreated HCT116 cells, marked by DAPI and/or FANCD2 and PICH immunofluorescence staining. (B) Quantification of percentage of anaphases that display at least one UFB. HCT116 cells were transfected with the indicated siRNA for 72 hours and fixed for PICH and FANCD2 immunofluorescence staining as in (A).

6.6 Knockdown of 8-oxoG genes reduces RAD18, ATM and 53BP1 localisation to induced fragile sites

In order to directly visualise the localisation of 53BP1 at replication stress site, I used a traceable *Lac* operator-harbouring cell line that has stable integration of 256 repeats of the *Lac* operator (*LacO*) site, followed by 18 nucleotide *ISce*I restriction site and 96 copies of the tetracycline response element *TetO* on chromosome 3 (Figure 54) (Soutoglou et al., 2007). It has been shown that, when combined with fluorescent lacR expression, the *lacO* site can act as an inducible fragile site that also undergoes UFB formation and stains positively for PICH (Jacome and Fernandez-Capetillo, 2011). Hence, this system represents a method of directly visualising protein localisation at an induced fragile site.

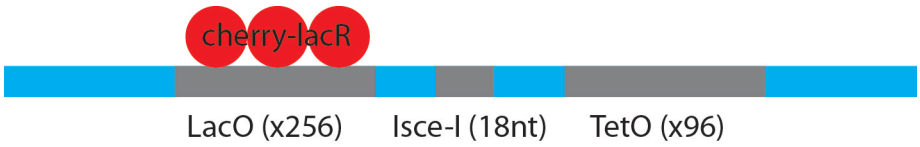

Figure 54. Schematic of the stable *lac* operator HeLa cell line. (Adapted from Soutoglou et al., 2007)

By using this system, I observed Rad18, 53BP1 and pATM colocalise with cherry-lacR foci when the latter is overexpressed (Figure 55A). Furthermore, the colocalisation with 53BP1 is enhanced upon Aph treatment (Figure 55B), which enhances fragile site expression. In agreement with data on 53BP1 foci formation and ATM signalling, the loss of 8-oxoG genes reduced the colocalisation of cherry-lacR with pATM and 53BP1 and this is most likely due to reduced RAD18 localisation to the site.

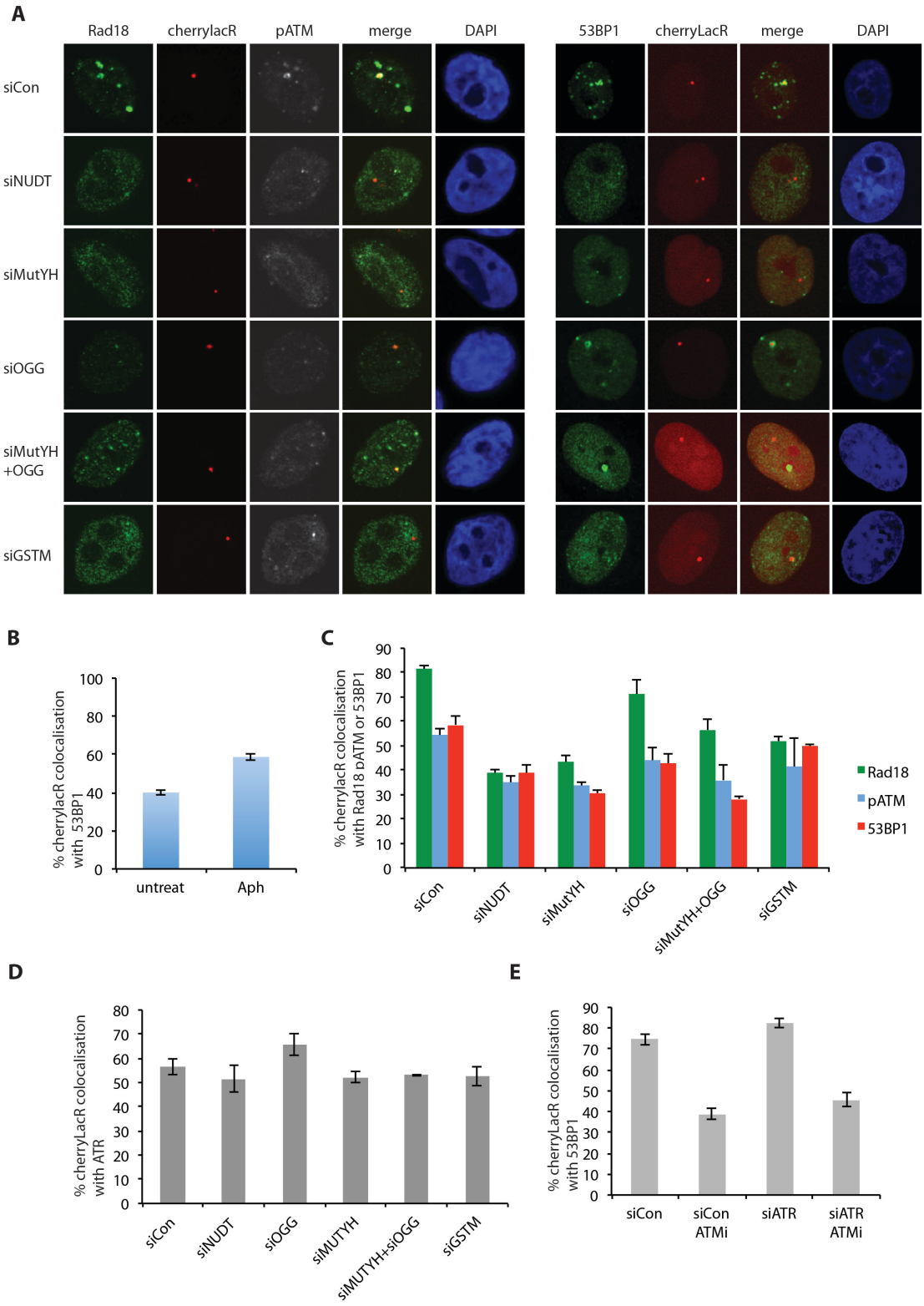

Figure 55. 8-oxoG genes are required for 53BP1 and pATM localisation to inducible fragile site cherrylacR.

(A) 293A cells were transfected with the indicated siRNA for 72 hours. After 24 hours, they were transfected with cherrylacR. In the last 24 hours, they were treated with Aph prior to fixation and immunofluorescence staining. (B) Quantification showing percentage of cherrylacR positive cells that also harbours a colocalised 53BP1 fous with or without Aph treatment. (C) Quantification of percentage of cells with

cherrylacR that also shows colocalisation with RAD18, pATM or 53BP1 from experiment in (A). At least 100 cells were scored for each treatment. (D) Quantification of percentage of cells with cherrylacR that also shows colocalisation with ATR after a similar experimental set-up as in (A). (E) Quantification of percentage of cells with cherrylacR that also shows colocalisation 53BP1. Cells were treated as in (A), with the exception of treatment with ATM inhibitor 1 hour prior to Aph treatment.

On the other hand, ATR recruitment to the inducible fragile site was not changed in the absence of 8-oxoG genes (Figure 55D). Since ATR recruitment depends on the RPA-ssDNA signal, it is most likely not affected by the loss of 8-oxoG genes. In order to understand the relative contribution of ATR and ATM to the GO phenotype, I checked the effect of ATR knockdown or ATM inhibition on cherrylacR-53BP1 colocalisation. While the inhibition of ATM activity decreased 53BP1 colocalisation with cherrylacR, the knockdown of ATR slightly increased 53BP1 it. Hence, the data suggest that the localisation of 53BP1 to the cherrylacR fragile site is dependent on the ATM pathway, but not ATR.

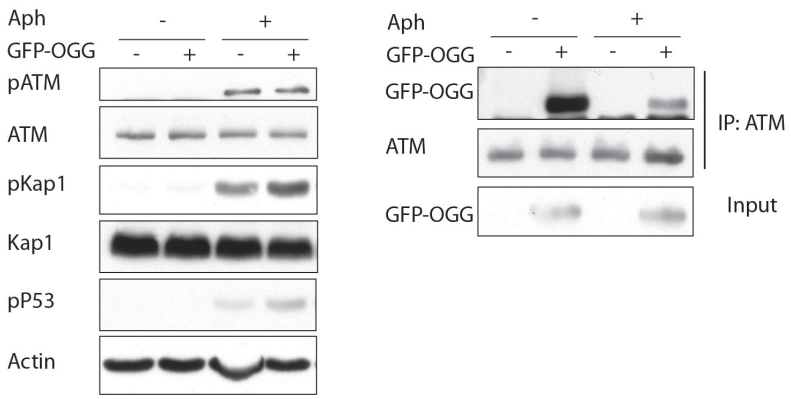

Figure 56. OGG1 interacts with ATM when overexpressed.

293T cells were transfected with GFP-OGG1 or vector for 24 hours and treated with Aph prior to harvest of WCL for ATM IP and western blot analysis.

In addition to affecting RAD18 foci formation, another mechanism by which OGG1 could contribute to ATM signalling could be by interacting with it. Using co-immunoprecipitation, I observed that GFP-OGG interacts with endogenous ATM under basal conditions and to a lesser extent after Aph (Figure 56). Furthermore, overexpression of OGG1 slightly increases ATM signalling after Aph as shown b y pKap1 and pP53 phosphorylations. One could speculate that as it scans the DNA for mismatched 8-oxo-G:C basepairs, OGG1 may form a signalling platform on which inactive ATM docks. This perhaps facilitates its activation on chromatin

where oxidative DNA lesions stall replication. Upon Aph treatment, the limiting pool of ATM would be activated via the WAR complex, thus leaving the OGG1 platform and leading to less OGG1-ATM interaction. Thus, it could be possible that in addition to its role in base excision repair, OGG1 positioning at strategic locations on the chromatin also facilitates the activation of ATM upon replication stress, as oxidised DNA could serve as an early signal of a replication problem. Recently, a novel interaction has been identified between OGG1 and PARP1, that OGG1 is required to facilitate PARP1 activity in DNA repair and can stimulate PARP1 activity in vitro (Noren Hooten et al., 2011). Hence, a similar mechanism could exist that facilitates ATM activation after oxidative or replication stress, making use of a protein that is specifically recruited to sites of oxidised DNA.

Chapter 7. Discussion

7.1 ATMIN NBS1 competition model

7.1.1 ATMIN can influence NBS1-dependent ATM signalling at DSBs by competition.

We have shown that altering ATMIN levels can directly impinge upon ATM signalling via the canonical MRN-dependent pathway. Increasing ATMIN by overexpression impairs ATM signalling and damage foci formation after IR, and reduces ATM-NBS1 interaction. Conversely, depleting ATMIN genetically or by siRNA leads to an increase in ATM signalling even in basal conditions. This most likely depends on the C-terminal ATM interaction motif of ATMIN, which is necessary and sufficient for the competition with NBS1. The ATMIN-dependent downregulation in ATM signalling can be rescued by overexpression of NBS1, which suggests a controlled stoichiometry is required to maintain the balance between these two cofactors. Hence, the protein level, localisation or affinity of ATMIN and NBS1 must be tightly regulated in the cell to ensure the correct balance and appropriate pathway of ATM activation.

Conversely, NBS1 can also influence, to some extent, ATMIN-dependent ATM signalling after osmotic stress. This suggests that the competition could act in both ways; although the effect of NBS1 on osmotic stress-induced ATM signalling is less dramatic, this could be due to additional mechanism on NBS1 that are required to regulate NBS1's interaction with ATM in addition to protein levels. For instance, it has been shown that ATM can still interact with the MRN in the absence of NBS1 C-terminal ATM interaction motif (Difilippantonio et al., 2007) and evidence from gel filtration experiments also showed that ATM can make contacts with MRE11/RAD50 in the absence of NBS1(Lee and Paull, 2004).

7.1.2 *nbs1*$^{\Delta/\Delta}$*; atmin*$^{\Delta/\Delta}$ double mutant cells have a similar phenotype as *atm*-/- cells

nbs1-null MEFs undergo premature senescence and have poor viability in culture, whereas *atm*-null MEFs are viable in culture. The loss of ATMIN rescues cell

viability and proliferation of *nbs1*-null cells, despite the high levels of endogenous DNA damage in the double knockout cells. This suggests that the phenotypes of *nbs1*-null cells cannot be ascribed solely to accumulation of DNA damage *per se*, rather the deleterious effects could be due to enhanced ATMIN-dependent ATM signalling, possibly via heightened activity of p53 or other ATM substrates.

In response to IR, *nbs1-/-; atmin-/-* double knockout cells are extremely radiosensitive owing to the complete absence of ATM signalling. Similarly, *atmin*ΔG/ΔG; *nbs1*ΔG/ΔG mice are extremely sensitive to whole-body irradiation; the intestines shows extensive DNA damage and cell loss, with no IR-induced 53BP1 foci formation and ATM signalling. As such, the concomitant loss of ATMIN and NBS1 shifts the cellular phenotype to that of ATM knockout. These data also implicate ATMIN and NBS1 as the only cofactors of ATM; in the absence of NBS1, the residual ATM signalling could be ATMIN-dependent. However, ATM activation by disulphide-crosslinking appears to be unaffected in the absence of NBS1 and ATMIN (Figure 17B). This could represent a mode of ATM activation that does not require any cofactor binding.

7.1.3 Future perspectives

The loss of ATMIN can rescue the embryonic lethality in NBS1-null mice, as well as the loss of the progenitor population in the intestinal crypts when NBS1 is deleted in the intestine by *villin-creERT*. It would be interesting to find out if deletion of ATMIN can also rescue the phenotypes in the humanised NBS1 mouse model (Difilippantonio et al., 2005), such as microcephaly, immunodeficiency, increased cancer predisposition and radiosensitivity. It is still unclear which of the NBS1 phenotypes is a direct consequence of NBS1-ATM signalling. If ATMIN loss can rescue some of these phenotypes, it could imply that competition with NBS1 in the regulation of NBS1-ATM signalling plays a key role *in vivo*.

One could speculate that the competition model could also have therapeutic potential in radiotherapy. In NBS1-proficient scenario, it has been reported that ATM signalling conferred protection against IR-induced enteritis in mice (Westphal et al., 1997). Hence, perhaps the specific downregulation of ATMIN in the

intestine could boost ATM signalling and hence reduce the side effects of enteritis in radiotherapy? Conversely, if ATMIN expression could be upregulated in tumour cells, this might reduce NBS1-dependent ATM signalling and make the latter more susceptible to IR-induced apoptosis at a lower dose that results in less damage to healthy tissue.

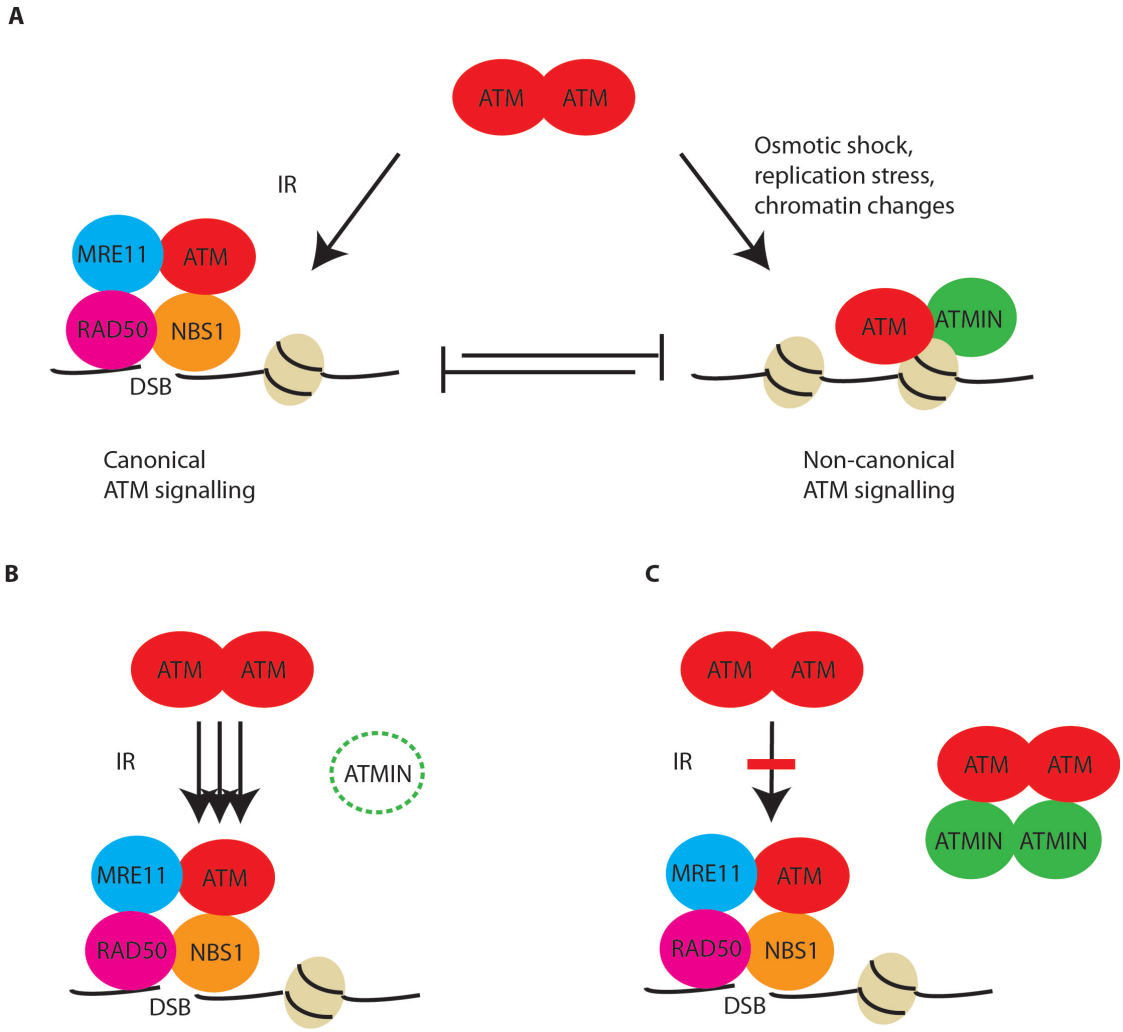

Figure 57. Competition between ATMIN and NBS1 regulates ATM signalling pathway choice.

(A) Under basal conditions, ATM exists predominantly as an inactive dimer. It is able to associate with either ATMIN or NBS1 as its cofactor depending on the stimuli. After IR, ATM preferentially interacts with NBS1, which lead to its activation. Upon osmotic shock, replication stress and other chromatin-modifying stimuli, ATM preferentially interacts with ATMIN and the non-canonical pathway is activated. (B) In the absence of ATMIN, ATM signalling after IR is augmented, resulting in greater intensity of foci formation and increased ATM substrate signalling. (C) Increase in ATMIN level impairs ATM-NBS1 interaction and dampens IR-induced ATM signalling.

7.2 UBR5-mediated ATMIN ubiquitination is required for IR-induced ATM signalling

While ATM associates with NBS1 or ATMIN under different stimuli, it is unclear how this change in interaction is regulated. If ATMIN is the cofactor that binds inactive ATM under basal conditions and contributes to the basal state of ATM signalling (Kanu and Behrens, 2007), how does ATM rapidly shift to interact with NBS1 upon IR? Our data suggests that UBR5 could be regulating ATMIN affinity for ATM by N-terminal ubiquitination on ATMIN, and this post-translational modification is required for canonical NBS1-dependent ATM activation.

7.2.1 ATMIN ubiquitination is required for IR-induced ATM signalling

UBR5 is a HECT domain E3 ligase that interacts constitutively with ATMIN in the nucleus, whose E3 activity is augmented rapidly after IR (Figure 24). However, the ubiquitination does not appear to affect ATMIN protein stability and loss of UBR5 has little effect on ATMIN levels. We showed that the ubiquitination occurs on the N-terminus of ATMIN (Lys238) and seems to be a mono-ubiquitination (Figure 25). In the absence of UBR5 we observed a reduction in ATM signalling and a concomitant increase in ATMIN-ATM interaction. This is phenocopied by using a mutant ATMIN that cannot be ubiquitinated. Hence, the ubiquitination could act as a molecular switch that regulates ATMIN's affinity for ATM. In the absence of this PTM on ATMIN, as shown by the ATMIN K238R reconstituted MEFs, ATM signalling and checkpoint functions are severely impaired (Figure 29).

Interestingly, given that ATMIN has many lysine residues, the site of ATMIN ubiquitination is separated by about 500 amino acids in primary amino acid sequence from the ATM interaction motif, a main point of ATMIN/ATM interaction (Kanu and Behrens, 2007, Zhang et al., 2012), raising the question of how ubiquitination is able to affect interaction with ATM. One could speculate that ATMIN ubiquitination may impair ATM binding by steric interference, or could induce an allosteric change in ATMIN that decreases affinity for ATM.

7.2.2 Regulation of UBR5 activity and stability

In response to IR, UBR5-mediated modification of ATMIN is stimulated, resulting in increased ATMIN ubiquitination. While it is possible that this is due to increased availability of the K238 site, or other changes, IR stimulation may also induce post-translational modification of UBR5 itself directly to increase its enzymatic activity. UBR5 is a heavily phosphorylated protein, and many phosphorylation sites on UBR5 have been reported in the literature, mostly identified by large scale proteomics studies. In particular, UBR5 was found to be phosphorylated on 9 SQ/TQ sites, predicted phosphorylation sites of ATM/ATR kinases, in response to DNA damage (Mu et al., 2007, Matsuoka et al., 2007). It is therefore conceivable that increased activity of UBR5 after IR is at least in part mediated by DNA damage-induced UBR5 phosphorylation. Our finding that inhibition of DNA damage-induced kinases reduced ATMIN ubiquitination (Figure 25E) supports this notion. While it may seem paradoxical that ATM is required for UBR5 activation and UBR5 is also required for ATM activation after IR, this could be due to a positive feedback mechanism that is common in DNA damage signalling to facilitate the rapid activation and recruitment of multiple factors to amplify the signalling cascade.

Whilst silencing UBR5 in cells does not change ATMIN levels appreciably, UBR5 levels greatly decrease in response to IR in *atmin*$^{\Delta/\Delta}$ cells (Figure 28), and ATMIN overexpression can significantly increases UBR5 protein levels (data not shown). Many E3 ubiquitin ligases regulate their protein levels by auto-ubiquitination, and that proteasome inhibition can stabilise UBR5 protein level (Figure 30D) suggests that this is also the case for UBR5. Owing to its large molecular weight, UBR5 ubiquitin assay was made technically difficult. Nevertheless, it is possible that if the preferred substrate ATMIN is not available, IR-induced UBR5 activity may result in auto-ubiquitination, and thus degradation.

7.2.3 Ubiquitination mediates the switch from ATMIN- to MRN-dependent ATM signalling

The MRN complex is responsible for the initial recognition of DSBs upon genotoxic stress and recruits ATM to DNA damage foci for its subsequent

activation (Lee and Paull, 2005). NBS1 is a key component of the MRN complex, which serves as a bridging factor for the interaction of Mre11 with ATM (Williams et al., 2007). Thus, NBS1 is central to the ability of the MRN complex to activate ATM.

Interestingly, NBS1 as well as ATMIN is modified by ubiquitination upon IR treatment. Recently, it has been shown that Skp2 E3 ligase is a critical regulator required for the recruitment of ATM by the MRN complex, and subsequent ATM activation in response to DSBs. Skp2 triggers K63-linked ubiquitination of NBS1, which increases NBS1 interaction with ATM, in turn facilitating activation and recruitment of ATM to DNA damage foci (Wu et al., 2012).

While ATMIN ubiquitination decreases its affinity for ATM, NBS1 ubiquitination increases its interaction with ATM, thereby mediating the switch from ATMIN- to MRN-dependent ATM signalling in response to IR. In addition, the competitive relationship between ATMIN and NBS1 implies that reduced interaction with ATMIN also contributes to this switch by making more active monomeric ATM available for interaction with MRN. Thus, the data suggest that IR-induced ubiquitination of two key molecules that determine ATM pathway choice, ATMIN and NBS1, is an essential mechanism in promoting ATM signalling at DSBs (Figure 42).

Given that the *Drosophila* homologue of UBR5 was initially identified as a tumour suppressor, it is somewhat surprising that in some human cancers including breast, ovarian and colon, more than 50% of cancers are associated with UBR5 gene copy number gains (COSMIC database). One hypothesis is that tumour cells may upregulate UBR5 expression to facilitate ATM signalling to protect against the increased DNA damage load or to gain resistance to radiotherapy. However, one cannot rule out other targets of UBR5 that could also play a role in tumourigenesis. Future studies using an in vivo conditional UBR5 mouse model will provide additional insight to its role in DNA damage signalling and during development.

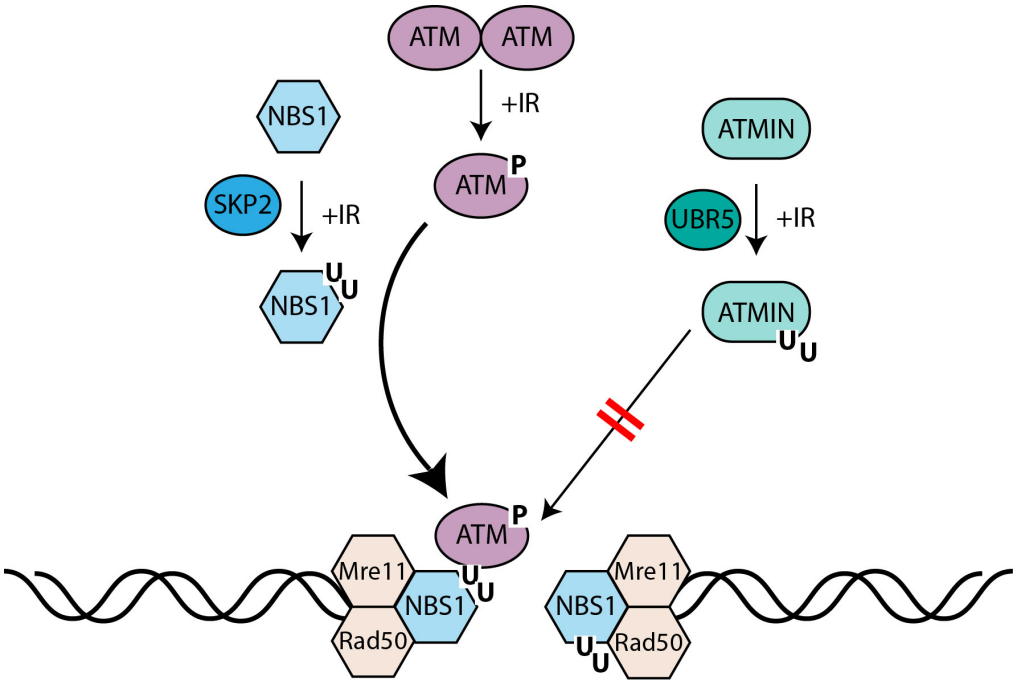

Figure 58. Model showing how ubiquitination of ATMIN and NBS1 facilitate ATM interaction with the MRN complex at DSBs.

Upon IR stimulation, ATM monomerises and can bind either NBS1 or ATMIN. IR-induced UBR5 E3 activity ubiquitinates ATMIN and decreases the interaction of the latter with ATM, while SKP2 ubiquitinates NBS1 and this promotes the NBS1-ATM interaction, thereby ensuring that ATM interacts with the correct cofactor after IR.

7.3 The WRNIP-ATMIN-RAD18 complex and ATM signalling after replication stress

7.3.1 ATMIN is required for ATM signalling after replication stress

We have shown that ATMIN is required as a cofactor of ATM for signalling in Aph conditions. The loss of ATMIN phenocopies the loss of ATM in failure to form 53BP1 foci and impairment in ATM substrate phosphorylation after replication stress (Figure 31). The loss of ATMIN results in increased DNA damage and chromosome segregation errors as seen by increased anaphase bridge formation (Figure 25). Furthermore, cells that have lost ATMIN also have difficulty recovering from replication stress (Figure 19F,G). Mechanistically, ATMIN interacts with WRNIP1, which, like its yeast homologue MGS1 (Saugar et al., 2012), can interact with ubiquitinated PCNA at sites of replication stress. WRNIP can also interact with RAD18, the E3 ligase that mono-ubiquitinates PCNA at Lys164 to activate translesion synthesis (Stelter and Ulrich, 2003, Kannouche et al., 2004, Watanabe et al., 2004). This is further supported by the data that 53BP1 and pATM foci formation depends on a functional UBZ domain on WRNIP1, as a mutant WRNIP1 that is unable to bind ubiquitinated proteins fails to rescue 53BP1 and pATM foci formation.

7.3.2 The WAR complex is specific for ATM signalling after Aph

WRNIP1, RAD18 and 53BP1 form foci, which colocalise at sites of replication stress after Aph, marked by RPA. While ATMIN, WRNIP1 and RAD18 are all required for 53BP1 foci formation and ATM substrate phosphorylation after Aph, they are not required for ATR-mediated phosphorylation of CHK1 (Figure 22). This suggests that the WAR complex is not required for ATR activation, which depends on ssDNA-RPA, the 9-1-1 complex and TOPBP1 (Cimprich and Cortez, 2008, Flynn and Zou, 2011). Moreover, the knockdown of ATR does not impair ATM activation by the WAR complex, hence suggesting that this pathway of ATM signalling does not seem to lie downstream of ATR (Figure 26).

Furthermore, the WAR complex is not required for canonical ATM signalling in response to IR-induced DSBs (Figure 23). This suggests that ATM activation by WAR could be intrinsically different from that mediated by the MRN complex. It cannot be ruled out that the MRN complex could also play a role during replication stress, as it was shown recently that NBS1 is required for an alternative pathway of ATR activation to phosphorylate RPA32 (Shiotani et al., 2013). The MRN complex has been reported to colocalise with PCNA during unperturbed S phase (Maser et al., 2001) and is required for S phase checkpoint following IR (Gatei et al., 2000b, Zhao et al., 2000, Wu et al., 2000, Lim et al., 2000). In addition to its role in ATM-dependent G2/M checkpoint following IR, NBS1 is also required for ATR-dependent and replication-independent checkpoint response to UV (Stiff et al., 2008).

However, there is also some evidence that NBS1 is dispensable for replication stress signalling by ATM. *nbs1*-null B cells show similar ATM and p53 phosphorylation after replication stress as wildtype cells (Difilippantonio et al., 2005). Furthermore, it has been shown recently using deficient cell lines, that ATM, Mre11, and Rad50, but not Nbs1 and H2AX, are required for cell survival and recovery from gemcitabine-induced stalled replication forks (Ewald et al., 2008). Hence, while the MRN complex contributes to ATR signalling after replication stress, it has not been shown to be required for ATM signalling after replication stress, which as our data suggests, depends on WRNIP1, ATMIN and RAD18. More biochemical evidence is required to fully dissect the involvement of the WAR complex in activation ATM in response to Aph. The identification of the DNA substrate responsible for ATM activation under Aph conditions, using techniques such as 2-D agarose gel electrophoresis, together with recombinant proteins or cell-free extracts would provide an in vitro approach to analyse the components required for ATM activation after replication stress.

7.3.3 WAR-dependent ATM signalling does not depend on ATR

ATR has been shown to be the primary kinase that responds to replication stress (Flynn and Zou, 2011) and ATM is believed to be activated following replication stress due to the DSBs formed when DNA polymerases encounter SSBs or basic sites. In addition, Stiff et al. showed that ATM autophosphorylation following UV or hydroxyurea is dependent on ATR, which could also phosphorylate ATM S1981

site *in vitro* (Stiff et al., 2006). Our data suggests that at least under Aph conditions, the transient knockdown of ATR does not decrease ATM autophosphorylation or substrate phosphorylation; ATM signalling and IRIF were increased compared to control (Figure 38). The difference could be due to the type and duration of drug treatment used (short treatment of hydroxyurea versus a prolonged treatment with aphidicolin), or cell type differences between hTERT-immortalised ATR-Seckel fibroblast and 293 cells. It could be possible that ATR is required for ATM activation at early time points immediately after replication stress, but during a prolonged replication stress, further ATM activation occurs independently of ATR via the WAR complex. Furthermore, treatment with either the ATM inhibitor or the knockdown of ATR increases UFB formation, and the combined treatment further increases UFB formation suggests ATR and ATM have non-overlapping roles in suppressing UFB formation (Figure 37).

Nevertheless, the WAR complex has physiological relevance as cells undergo increased anaphase bridges and segregation errors in its absence, similar to the effect of ATM deficiency. Recent evidence suggests a role of ATM in protecting fragile sites by regulating 53BP1 nuclear bodies (Lukas et al., 2011a, Harrigan et al., 2011). The G1 53BP1 nuclear bodies were proposed to shield unrepaired lesions against degradation left over from the previous cell cycle. It is possible that these 53BP1 nuclear bodies arise during S/G2 phase and progressively diminish as the majority of S phase damage is repaired. Only a few foci remain at sites of late or unreplicated DNA when the latter escape detection by cell cycle checkpoints by an unknown mechanism. However, it is unclear whether ATM and 53BP1 remains at fragile sites at mitosis, or come off and are reloaded onto fragile sites in the next cell cycle, as these proteins do not form any detectable foci during mitosis. Hence, the WAR complex mediated ATM signalling after Aph could represent a novel pathway of ATM function that link its recruitment to sites of replication stress to its role in protecting fragile sites from genomic instability.

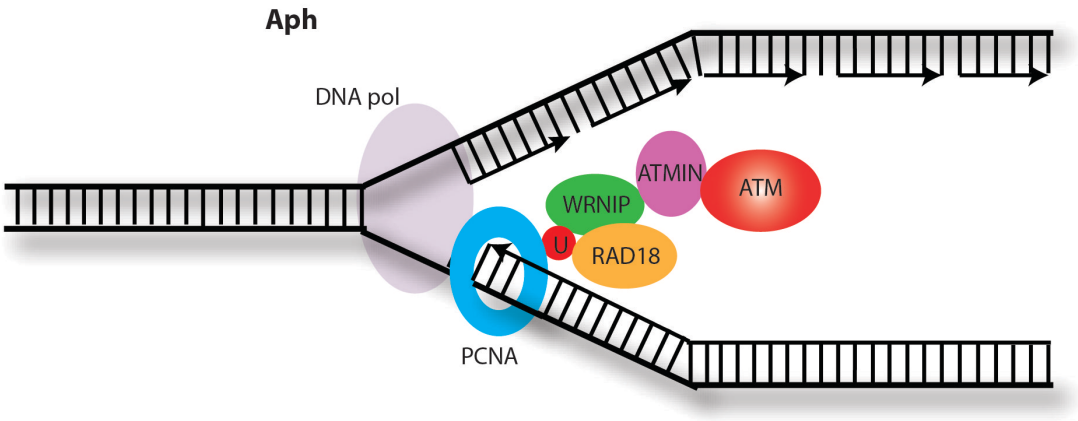

Figure 59. Model of ATM recruitment at stalled replication fork by the WAR complex.

Upon replication fork stalling, such as that induced by Aph, RAD18 mono-ubiquitinates PCNA on Lys164, and WRNIP1 could interact with ubiquitinated PCNA and RAD18 and gets recruited to the site. ATMIN could act as a bridging adaptor in bringing ATM to the stalled replication fork.

7.4 8-oxoG genes are required for ATM signalling after replication stress

7.4.1 The knockdown of 8-oxoG genes impairs ATM signalling after Aph

OGG1 was identified as the top hit in the genome screen for genes that affect 53BP1 foci formation after Aph, and similarly other proteins that function in the 8-oxoG repair pathway including NUDT1, MUTYH and GSTM5 were also required for 53BP1 foci formation after replication stress. While the data could be validated in different cell lines, it is not clear how the consequent increase in base oxidation in the absence of these genes would decrease ATM signalling. One hypothesis would be that in the absence of OGG1, MUTYH or both enzymes, there is reduced cleavage of oxidised bases and less fewer apurinic/apyrimidinic sites would be formed, which could potentially reduce the number of ssDNA gaps that need to be filled by DNA polymerases and hence replication stress to trigger ATM signalling. However, this does not explain why the loss of NUDT1 or GSTM5 also have a similar impairment in 53BP1 foci formation and ATM signalling, as they increase nucleotide oxidation with no known effect on the repair of 8-oxoG. Furthermore, from the screen results, the loss of 8-oxoG genes does not significantly change 53BP1 and pATM foci formation in basal conditions. Hence, it is unlikely that the loss of ATM signalling is due to a decrease in SSBs formed.

A second scenario would be that the presence of 8-oxoG at sites of replication stalling directly impairs ATM signalling. Our data suggest a model whereby WRNIP-ATMIN-RAD18 forms a complex that activates ATM independently of ATR upon Aph, and the presence of 8-oxoG could inhibit the interaction of the WAR complex with DNA. This is supported by *in vitro* data that RAD18 binding to primer-template DNA decreases when the DNA is oxidised, as well as decreased RAD18 recruitment to induced cherrylacR fragile site after the knockdown of 8-oxoG genes. It has also been shown that the MRN complex is less able to bind DNA in the presence of H_2O_2 and therefore defective in activating ATM in vitro under oxidative conditions. (Guo et al., 2010a). As a result of impaired RAD18 recruitment, it could be possible that the signal for ATM activation under Aph is diminished. Following up this study, this hypothesis could be tested by artificially tethering RAD18 to the lacO-tetO site by overexpression of a RAD18-GFP-TetR

fusion protein, and this should be able to rescue the ATM signalling if the hypothesis is true. DNA oxidation could also impair the E3 ligase activity of RAD18, thus reducing PCNA monoubiquitination. This hypothesis would require an *in vitro* ubiquitination assay to study RAD18 E ligase activity as the changes in in vivo PCNA monoubiquitination of mammalian cells were difficult to detect (data not shown).

Similarly to the knockdown of the WAR complex, the knockdown of 8-oxoG genes increases UFB formation but does not affect ATM signalling after IR. This also suggests that the 8-oxoG genes could function in the same pathway as WAR in regulating ATM signalling after Aph. While the knockdown of 8-oxoG genes affect ATM signalling, both ATR signalling and foci recruitment to cherrylacR sites are not impaired. This suggests that base oxidation does not affect the formation of ssDNA-RPA and ATR activation during S phase. Hence, the effect of 8-oxoG genes on ATM signalling does not act via ATR signalling.

In addition, one could speculate that some of the 8-oxoG components such as OGG1 could form a complex with ATM and directly facilitate its recruitment to G:C rich regions, which are prone to both replication stalling and base oxidation. A preliminary experiment suggests that overexpressed OGG1 could interact with ATM under basal conditions and after Aph. It would be interesting to test for any interaction between the 8-oxoG proteins and with ATM. Furthermore, by knocking down both the WAR complex and 8-oxoG genes, it could potentially reveal any epistatic relationship between the two pathways. However, the reduced transfection efficiency of multiple siRNAs could make it technically difficult to test this hypothesis.

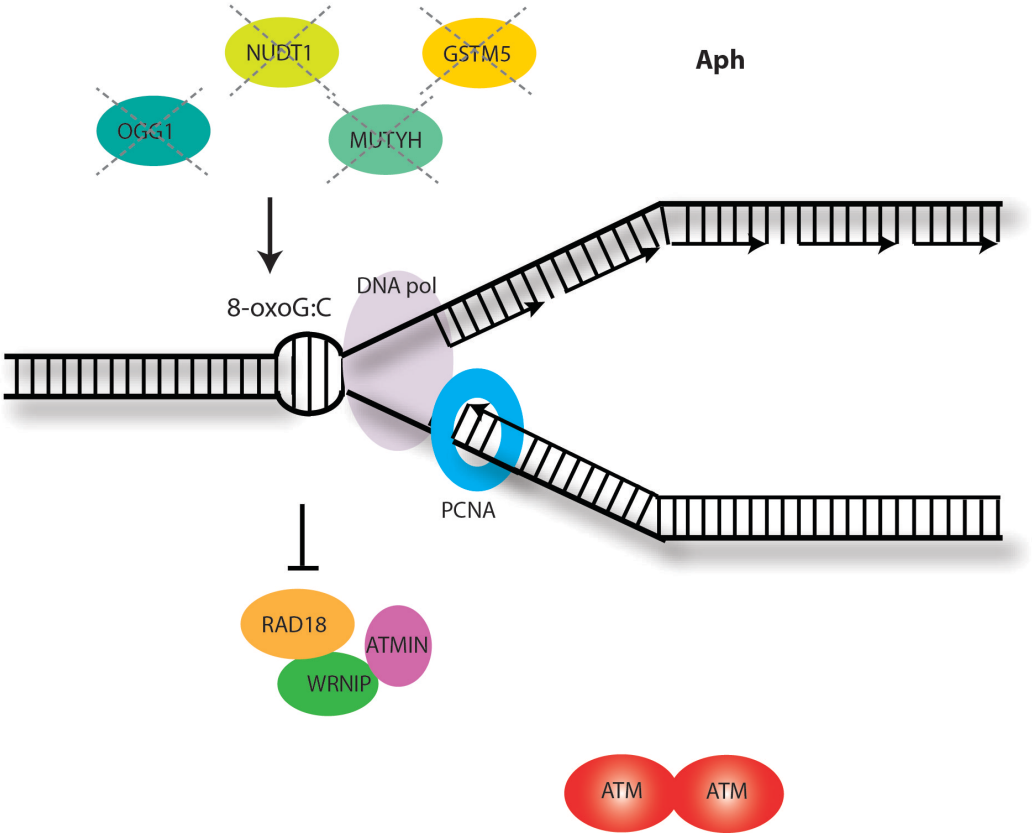

Figure 60. Possible model of the GO pathway regulating ATM signalling at a replication stalled fork via the WAR complex.

7.4.2 TEMPOL rescues ATM signalling in the absence of 8-oxoG genes

Another interesting question is how TEMPOL rescues ATM signalling in the absence of 8-oxoG genes after Aph treatment. TEMPOL can act as a superoxide dismutase mimetic by quenching superoxide anions to form hydrogen peroxide. It has been reported to function as a much better ROS scavenger than other antioxidants such as N-acetylcysteine or vitamin C, and has also been used extensively to rescue oxidative stress in animal models and even lengthen the lifespan of animals and reduce tumour incidence (Mitchell et al., 2003, Wilcox, 2010). At the cellular levels, TEMPOL rescued ATM signalling, RAD18 foci formation at fragile sites and suppress UFB formation after the knockdown of 8-oxoG genes. However, it does not seem to increase ATM signalling in control wildtype cells, suggesting that its effect is only prominent when base oxidation is elevated. One could speculate that a threshold of 8-oxoG accumulation needs to be reached prior to ATM activity being stimulated by TEMPOL and this threshold

could be sensed by the binding of 8-oxoG genes such as OGG1 for instance. It would also be interesting to investigate if TEMPOL affects OGG1-ATM interaction or has any effect on the activity of OGG1 directly through in vitro assays.

7.4.3 ATM signalling after replication stress requires a functional 8-oxoG system, the WAR complex, but does not depend on ATR

Data from Chapters 4 and 5 showed that ATM signalling was impaired after the knockdown of the WAR complex or that of 8-oxoG system under Aph conditions. On the other hand, ATR-mediated Chk1 phosphorylation was unaffected after the knockdown of the WAR complex and ATR recruitment to the induced cherrylacR fragile site was also unaffected by the knockdown of 8-oxoG genes. Conversely, the knockdown of ATR increases ATM signalling after replication stress, possibly due to the increase in conversion of SSBs into DSBs in the absence of ATR-mediated checkpoint function, or that ATR suppresses ATM activation possibly by competing with ATM binding at the sites of replication stress. It is possible that there is a DNA substrate/intermediate generated during replication stress that serves as the stimulus for ATM signalling and 53BP1 localisation and whose formation does not depend on ATR. Since both RPA and γH2AX localises to cherrylacR foci, the DNA substrate could be a complex ssDNA-dsDNA intermediate that could recruit RAD18 and activate ATM distinctly from the canonical MRN-dependent activation of ATM after IR-induced DSBs. This is also supported by the evidence that the knockdown of NBS1 does not increase UFB formation, unlike the knockdown of ATM or ATMIN (Figure 37C).

7.4.4 Future validation in mouse models

As discussed in the introduction, single knockout mouse models of the GO pathway do not manifest severe phenotypes until 1.5 years of age. Double knockout *mutyh-/-* and *ogg-/-* mice show accumulation of 8-oxoG in tissues, but still have a relatively long latency of tumourigenesis (10months) (Xie et al., 2004). It would be interesting to investigate whether the loss of a tumour suppressor gene such as p53 would accelerate the tumour formation in the *mutyh-/-* and *ogg-/-* knockout mice. Given the possible link between BER and ATM signalling in vitro, one would expect that ATM signalling after replication stress would be

impaired in *ogg-/- ; mutyh-/-* double knockout mice. Similarly, any defect in the recruitment and function of RAD18 in these double knockout mice would also confirm the in vitro data. Furthermore, if ATM signalling is impaired in the *ogg-/- ; mutyh-/-* double knockout mice, it would be interesting to assess the function of ATM signalling after replication stress in vivo, whether it would promote chromosome segregation errors and genome instability especially in tissues with high cell turnover such as the skin and intestine.

7.5 Concluding remarks

In summary, in this thesis I have elucidated four mechanisms that influence ATM-ATMIN signalling. I have shown that ATMIN can compete with NBS1 for ATM interaction and thereby influence the MRN-dependent ATM signalling after IR. I have also shown that ATMIN can be ubiquitinated by UBR5 in an IR-dependent manner, which modulates the affinity of ATMIN for ATM and allow the latter to be activated via the MRN-dependent pathway.

Moreover, I have investigated the mechanism by which ATMIN could contribute to ATM signalling after replication stress via WRNIP1 and RAD18-mediated ubiquitination of PCNA. Through a genome screen approach, I have identified a novel link between the 8-oxoG system and ATMIN-dependent ATM signalling. I have shown that genes involved in 8-oxoG removal are required for RAD18 recruitment and ATM signalling after replication stress. I have shown that ATMIN is an important interactor of ATM and loss of ATMIN can lead to deleterious effects in cells.

Chapter 8. Reference list

ALZOUBI, K. H., KHABOUR, O. F., JABER, A. G., AL-AZZAM, S. I., MHAIDAT, N. M. & MASADEH, M. M. 2013. Tempol prevents genotoxicity induced by vorinostat: role of oxidative DNA damage. *Cytotechnology*.

AMOUROUX, R., CAMPALANS, A., EPE, B. & RADICELLA, J. P. 2010. Oxidative stress triggers the preferential assembly of base excision repair complexes on open chromatin regions. *Nucleic Acids Res,* 38**,** 2878-90.

ARAI, T., KELLY, V. P., MINOWA, O., NODA, T. & NISHIMURA, S. 2006. The study using wild-type and Ogg1 knockout mice exposed to potassium bromate shows no tumor induction despite an extensive accumulation of 8-hydroxyguanine in kidney DNA. *Toxicology,* 221**,** 179-86.

ARAVIND, L., WALKER, D. R. & KOONIN, E. V. 1999. Conserved domains in DNA repair proteins and evolution of repair systems. *Nucleic Acids Res,* 27**,** 1223-42.

ASPINWALL, R., ROTHWELL, D. G., ROLDAN-ARJONA, T., ANSELMINO, C., WARD, C. J., CHEADLE, J. P., SAMPSON, J. R., LINDAHL, T., HARRIS, P. C. & HICKSON, I. D. 1997. Cloning and characterization of a functional human homolog of Escherichia coli endonuclease III. *Proc Natl Acad Sci U S A,* 94**,** 109-14.

BAKKENIST, C. J. & KASTAN, M. B. 2003. DNA damage activates ATM through intermolecular autophosphorylation and dimer dissociation. *Nature,* 421**,** 499-506.

BALL, H. L. & CORTEZ, D. 2005. ATRIP oligomerization is required for ATR-dependent checkpoint signaling. *J Biol Chem,* 280**,** 31390-6.

BALL, H. L., MYERS, J. S. & CORTEZ, D. 2005. ATRIP binding to replication protein A-single-stranded DNA promotes ATR-ATRIP localization but is dispensable for Chk1 phosphorylation. *Mol Biol Cell,* 16**,** 2372-81.

BARLOW, C., HIROTSUNE, S., PAYLOR, R., LIYANAGE, M., ECKHAUS, M., COLLINS, F., SHILOH, Y., CRAWLEY, J. N., RIED, T., TAGLE, D. & WYNSHAW-BORIS, A. 1996. Atm-deficient mice: a paradigm of ataxia telangiectasia. *Cell,* 86**,** 159-71.

BARTEK, J. & LUKAS, J. 2003. Chk1 and Chk2 kinases in checkpoint control and cancer. *Cancer Cell,* 3**,** 421-9.

BARZILAI, A., ROTMAN, G. & SHILOH, Y. 2002. ATM deficiency and oxidative stress: a new dimension of defective response to DNA damage. *DNA Repair (Amst),* 1**,** 3-25.

BAUMANN, C., KORNER, R., HOFMANN, K. & NIGG, E. A. 2007. PICH, a centromere-associated SNF2 family ATPase, is regulated by Plk1 and required for the spindle checkpoint. *Cell,* 128**,** 101-14.

BEAUSOLEIL, S. A., JEDRYCHOWSKI, M., SCHWARTZ, D., ELIAS, J. E., VILLEN, J., LI, J., COHN, M. A., CANTLEY, L. C. & GYGI, S. P. 2004. Large-scale characterization of HeLa cell nuclear phosphoproteins. *Proc Natl Acad Sci U S A,* 101**,** 12130-5.

BEKKER-JENSEN, S., RENDTLEW DANIELSEN, J., FUGGER, K., GROMOVA, I., NERSTEDT, A., LUKAS, C., BARTEK, J., LUKAS, J. & MAILAND, N. 2010. HERC2 coordinates ubiquitin-dependent assembly of DNA repair factors on damaged chromosomes. *Nat Cell Biol,* 12**,** 80-6; sup pp 1-12.

BENCOKOVA, Z., KAUFMANN, M. R., PIRES, I. M., LECANE, P. S., GIACCIA, A. J. & HAMMOND, E. M. 2009. ATM activation and signaling under hypoxic conditions. *Mol Cell Biol,* 29**,** 526-37.

BERMUDEZ, V. P., LINDSEY-BOLTZ, L. A., CESARE, A. J., MANIWA, Y., GRIFFITH, J. D., HURWITZ, J. & SANCAR, A. 2003. Loading of the human 9-1-1 checkpoint complex onto DNA by the checkpoint clamp loader hRad17-replication factor C complex in vitro. *Proc Natl Acad Sci U S A,* 100**,** 1633-8.

BHAKAT, K. K., MOKKAPATI, S. K., BOLDOGH, I., HAZRA, T. K. & MITRA, S. 2006. Acetylation of human 8-oxoguanine-DNA glycosylase by p300 and its role in 8-oxoguanine repair in vivo. *Mol Cell Biol,* 26**,** 1654-65.

BJORAS, M., SEEBERG, E., LUNA, L., PEARL, L. H. & BARRETT, T. E. 2002. Reciprocal "flipping" underlies substrate recognition and catalytic activation by the human 8-oxo-guanine DNA glycosylase. *J Mol Biol,* 317**,** 171-7.

BOLDOGH, I., MILLIGAN, D., LEE, M. S., BASSETT, H., LLOYD, R. S. & MCCULLOUGH, A. K. 2001. hMYH cell cycle-dependent expression, subcellular localization and association with replication foci: evidence suggesting replication-coupled repair of adenine:8-oxoguanine mispairs. *Nucleic Acids Res,* 29**,** 2802-9.

BOTHMER, A., ROBBIANI, D. F., DI VIRGILIO, M., BUNTING, S. F., KLEIN, I. A., FELDHAHN, N., BARLOW, J., CHEN, H. T., BOSQUE, D., CALLEN, E., NUSSENZWEIG, A. & NUSSENZWEIG, M. C. 2011. Regulation of DNA end joining, resection, and immunoglobulin class switch recombination by 53BP1. *Mol Cell,* 42**,** 319-29.

BOTHMER, A., ROBBIANI, D. F., FELDHAHN, N., GAZUMYAN, A., NUSSENZWEIG, A. & NUSSENZWEIG, M. C. 2010. 53BP1 regulates DNA resection and the choice between classical and alternative end joining during class switch recombination. *J Exp Med,* 207**,** 855-65.

BOTUYAN, M. V., LEE, J., WARD, I. M., KIM, J. E., THOMPSON, J. R., CHEN, J. & MER, G. 2006. Structural basis for the methylation state-specific recognition of histone H4-K20 by 53BP1 and Crb2 in DNA repair. *Cell,* 127**,** 1361-73.

BOUWMAN, P., ALY, A., ESCANDELL, J. M., PIETERSE, M., BARTKOVA, J., VAN DER GULDEN, H., HIDDINGH, S., THANASOULA, M., KULKARNI, A., YANG, Q., HAFFTY, B. G., TOMMISKA, J., BLOMQVIST, C., DRAPKIN, R., ADAMS, D. J., NEVANLINNA, H., BARTEK, J., TARSOUNAS, M., GANESAN, S. & JONKERS, J. 2010. 53BP1 loss rescues BRCA1 deficiency and is associated with triple-negative and BRCA-mutated breast cancers. *Nat Struct Mol Biol,* 17**,** 688-95.

BOVERIS, A., VALDEZ, L. B., ZAOBORNYJ, T. & BUSTAMANTE, J. 2006. Mitochondrial metabolic states regulate nitric oxide and hydrogen peroxide diffusion to the cytosol. *Biochim Biophys Acta,* 1757**,** 535-42.

BROOKS, C. L., LI, M., HU, M., SHI, Y. & GU, W. 2007. The p53--Mdm2--HAUSP complex is involved in p53 stabilization by HAUSP. *Oncogene,* 26**,** 7262-6.

BRUNER, S. D., NORMAN, D. P. & VERDINE, G. L. 2000. Structural basis for recognition and repair of the endogenous mutagen 8-oxoguanine in DNA. *Nature,* 403**,** 859-66.

BUNTING, S. F., CALLEN, E., WONG, N., CHEN, H. T., POLATO, F., GUNN, A., BOTHMER, A., FELDHAHN, N., FERNANDEZ-CAPETILLO, O., CAO, L., XU, X., DENG, C. X., FINKEL, T., NUSSENZWEIG, M., STARK, J. M. & NUSSENZWEIG, A. 2010. 53BP1 inhibits homologous recombination in Brca1-deficient cells by blocking resection of DNA breaks. *Cell,* 141**,** 243-54.

BYRD, P. J., COOPER, P. R., STANKOVIC, T., KULLAR, H. S., WATTS, G. D., ROBINSON, P. J. & TAYLOR, M. R. 1996. A gene transcribed from the bidirectional ATM promoter coding for a serine rich protein: amino acid sequence, structure and expression studies. *Hum Mol Genet,* 5**,** 1785-91.

BYUN, T. S., PACEK, M., YEE, M. C., WALTER, J. C. & CIMPRICH, K. A. 2005. Functional uncoupling of MCM helicase and DNA polymerase activities activates the ATR-dependent checkpoint. *Genes Dev,* 19**,** 1040-52.

CAI, J. P., ISHIBASHI, T., TAKAGI, Y., HAYAKAWA, H. & SEKIGUCHI, M. 2003. Mouse MTH2 protein which prevents mutations caused by 8-oxoguanine nucleotides. *Biochem Biophys Res Commun,* 305**,** 1073-7.

CALLAGHAN, M. J., RUSSELL, A. J., WOOLLATT, E., SUTHERLAND, G. R., SUTHERLAND, R. L. & WATTS, C. K. 1998. Identification of a human HECT family protein with homology to the Drosophila tumor suppressor gene hyperplastic discs. *Oncogene,* 17**,** 3479-91.

CALSOU, P., DELTEIL, C., FRIT, P., DROUET, J. & SALLES, B. 2003. Coordinated assembly of Ku and p460 subunits of the DNA-dependent protein kinase on DNA ends is necessary for XRCC4-ligase IV recruitment. *J Mol Biol,* 326**,** 93-103.

CALSOU, P., FRIT, P., HUMBERT, O., MULLER, C., CHEN, D. J. & SALLES, B. 1999. The DNA-dependent protein kinase catalytic activity regulates DNA end processing by means of Ku entry into DNA. *J Biol Chem,* 274**,** 7848-56.

CAO, L., XU, X., BUNTING, S. F., LIU, J., WANG, R. H., CAO, L. L., WU, J. J., PENG, T. N., CHEN, J., NUSSENZWEIG, A., DENG, C. X. & FINKEL, T. 2009. A selective requirement for 53BP1 in the biological response to genomic instability induced by Brca1 deficiency. *Mol Cell,* 35**,** 534-41.

CARSON, C. T., SCHWARTZ, R. A., STRACKER, T. H., LILLEY, C. E., LEE, D. V. & WEITZMAN, M. D. 2003. The Mre11 complex is required for ATM activation and the G2/M checkpoint. *EMBO J,* 22**,** 6610-20.

CASPER, A. M., NGHIEM, P., ARLT, M. F. & GLOVER, T. W. 2002. ATR regulates fragile site stability. *Cell,* 111**,** 779-89.

CHAGRAOUI, J., HEBERT, J., GIRARD, S. & SAUVAGEAU, G. 2011. An anticlastogenic function for the Polycomb Group gene Bmi1. *Proc Natl Acad Sci U S A,* 108**,** 5284-9.

CHAN, K. L., NORTH, P. S. & HICKSON, I. D. 2007. BLM is required for faithful chromosome segregation and its localization defines a class of ultrafine anaphase bridges. *EMBO J,* 26**,** 3397-409.

CHAN, K. L., PALMAI-PALLAG, T., YING, S. & HICKSON, I. D. 2009. Replication stress induces sister-chromatid bridging at fragile site loci in mitosis. *Nat Cell Biol,* 11**,** 753-60.

CHAPMAN, J. R., BARRAL, P., VANNIER, J. B., BOREL, V., STEGER, M., TOMAS-LOBA, A., SARTORI, A. A., ADAMS, I. R., BATISTA, F. D. & BOULTON, S. J. 2013. RIF1 is essential for 53BP1-dependent nonhomologous end joining and suppression of DNA double-strand break resection. *Mol Cell,* 49**,** 858-71.

CHAPMAN, J. R. & JACKSON, S. P. 2008. Phospho-dependent interactions between NBS1 and MDC1 mediate chromatin retention of the MRN complex at sites of DNA damage. *EMBO Rep,* 9**,** 795-801.

CHEN, D., KON, N., LI, M., ZHANG, W., QIN, J. & GU, W. 2005. ARF-BP1/Mule is a critical mediator of the ARF tumor suppressor. *Cell,* 121**,** 1071-83.

CHEN, L., TRUJILLO, K., SUNG, P. & TOMKINSON, A. E. 2000. Interactions of the DNA ligase IV-XRCC4 complex with DNA ends and the DNA-dependent protein kinase. *J Biol Chem,* 275**,** 26196-205.

CHO, S. H., TOOULI, C. D., FUJII, G. H., CRAIN, C. & PARRY, D. 2005. Chk1 is essential for tumor cell viability following activation of the replication checkpoint. *Cell Cycle,* 4**,** 131-9.

CHRISTIAN, P. A., FIANDALO, M. V. & SCHWARZE, S. R. 2011. Possible role of death receptor-mediated apoptosis by the E3 ubiquitin ligases Siah2 and POSH. *Mol Cancer,* 10**,** 57.

CIMPRICH, K. A. & CORTEZ, D. 2008. ATR: an essential regulator of genome integrity. *Nat Rev Mol Cell Biol,* 9**,** 616-27.

CLANCY, J. L., HENDERSON, M. J., RUSSELL, A. J., ANDERSON, D. W., BOVA, R. J., CAMPBELL, I. G., CHOONG, D. Y., MACDONALD, G. A., MANN, G. J., NOLAN, T., BRADY, G., OLOPADE, O. I., WOOLLATT, E., DAVIES, M. J., SEGARA, D., HACKER, N. F., HENSHALL, S. M., SUTHERLAND, R. L. & WATTS, C. K. 2003. EDD, the human orthologue of the hyperplastic discs tumour suppressor gene, is amplified and overexpressed in cancer. *Oncogene,* 22**,** 5070-81.

COLEMAN, K. A. & GREENBERG, R. A. 2011. The BRCA1-RAP80 complex regulates DNA repair mechanism utilization by restricting end resection. *J Biol Chem,* 286**,** 13669-80.

COOPER, E. M., CUTCLIFFE, C., KRISTIANSEN, T. Z., PANDEY, A., PICKART, C. M. & COHEN, R. E. 2009. K63-specific deubiquitination by two JAMM/MPN+ complexes: BRISC-associated Brcc36 and proteasomal Poh1. *EMBO J,* 28**,** 621-31.

CORTEZ, D., GUNTUKU, S., QIN, J. & ELLEDGE, S. J. 2001. ATR and ATRIP: partners in checkpoint signaling. *Science,* 294**,** 1713-6.

COSTANZO, V. & GAUTIER, J. 2003. Single-strand DNA gaps trigger an ATR- and Cdc7-dependent checkpoint. *Cell Cycle,* 2**,** 17.

COUCH, F. B., BANSBACH, C. E., DRISCOLL, R., LUZWICK, J. W., GLICK, G. G., BETOUS, R., CARROLL, C. M., JUNG, S. Y., QIN, J., CIMPRICH, K. A. & CORTEZ, D. 2013. ATR phosphorylates SMARCAL1 to prevent replication fork collapse. *Genes Dev,* 27**,** 1610-23.

CROSETTO, N., BIENKO, M., HIBBERT, R. G., PERICA, T., AMBROGIO, C., KENSCHE, T., HOFMANN, K., SIXMA, T. K. & DIKIC, I. 2008. Human Wrnip1 is localized in replication factories in a ubiquitin-binding zinc finger-dependent manner. *J Biol Chem,* 283**,** 35173-85.

D'AMOURS, D. & JACKSON, S. P. 2001. The yeast Xrs2 complex functions in S phase checkpoint regulation. *Genes Dev,* 15**,** 2238-49.

DANIEL, J. A., PELLEGRINI, M., LEE, J. H., PAULL, T. T., FEIGENBAUM, L. & NUSSENZWEIG, A. 2008. Multiple autophosphorylation sites are dispensable for murine ATM activation in vivo. *J Cell Biol,* 183**,** 777-83.

DANTZER, F., LUNA, L., BJORAS, M. & SEEBERG, E. 2002. Human OGG1 undergoes serine phosphorylation and associates with the nuclear matrix and mitotic chromatin in vivo. *Nucleic Acids Res,* 30**,** 2349-57.

DAR, I., YOSHA, G., ELFASSY, R., GALRON, R., WANG, Z. Q., SHILOH, Y. & BARZILAI, A. 2011. Investigation of the functional link between ATM and NBS1 in the DNA damage response in the mouse cerebellum. *J Biol Chem,* 286**,** 15361-76.

DART, D. A., ADAMS, K. E., AKERMAN, I. & LAKIN, N. D. 2004. Recruitment of the cell cycle checkpoint kinase ATR to chromatin during S-phase. *J Biol Chem,* 279**,** 16433-40.

DAUB, H., OLSEN, J. V., BAIRLEIN, M., GNAD, F., OPPERMANN, F. S., KORNER, R., GREFF, Z., KERI, G., STEMMANN, O. & MANN, M. 2008. Kinase-selective enrichment enables quantitative phosphoproteomics of the kinome across the cell cycle. *Mol Cell,* 31**,** 438-48.

DE JAGER, M., VAN NOORT, J., VAN GENT, D. C., DEKKER, C., KANAAR, R. & WYMAN, C. 2001. Human Rad50/Mre11 is a flexible complex that can tether DNA ends. *Mol Cell,* 8**,** 1129-35.

DE SOUZA-PINTO, N. C., MAYNARD, S., HASHIGUCHI, K., HU, J., MUFTUOGLU, M. & BOHR, V. A. 2009. The recombination protein RAD52 cooperates with the excision repair protein OGG1 for the repair of oxidative lesions in mammalian cells. *Mol Cell Biol,* 29**,** 4441-54.

DELACROIX, S., WAGNER, J. M., KOBAYASHI, M., YAMAMOTO, K. & KARNITZ, L. M. 2007. The Rad9-Hus1-Rad1 (9-1-1) clamp activates checkpoint signaling via TopBP1. *Genes Dev,* 21**,** 1472-7.

DENG, Y., GUO, X., FERGUSON, D. O. & CHANG, S. 2009. Multiple roles for MRE11 at uncapped telomeres. *Nature,* 460**,** 914-8.

DEO, R. C., SONENBERG, N. & BURLEY, S. K. 2001. X-ray structure of the human hyperplastic discs protein: an ortholog of the C-terminal domain of poly(A)-binding protein. *Proc Natl Acad Sci U S A,* 98**,** 4414-9.

DESAI-MEHTA, A., CEROSALETTI, K. M. & CONCANNON, P. 2001. Distinct functional domains of nibrin mediate Mre11 binding, focus formation, and nuclear localization. *Mol Cell Biol,* 21**,** 2184-91.

DHENAUT, A., BOITEUX, S. & RADICELLA, J. P. 2000. Characterization of the hOGG1 promoter and its expression during the cell cycle. *Mutat Res,* 461**,** 109-18.

DI VIRGILIO, M., CALLEN, E., YAMANE, A., ZHANG, W., JANKOVIC, M., GITLIN, A. D., FELDHAHN, N., RESCH, W., OLIVEIRA, T. Y., CHAIT, B. T., NUSSENZWEIG, A., CASELLAS, R., ROBBIANI, D. F. & NUSSENZWEIG, M. C. 2013. Rif1 prevents resection of DNA breaks and promotes immunoglobulin class switching. *Science,* 339**,** 711-5.

DIFILIPPANTONIO, S., CELESTE, A., FERNANDEZ-CAPETILLO, O., CHEN, H. T., REINA SAN MARTIN, B., VAN LAETHEM, F., YANG, Y. P., PETUKHOVA, G. V., ECKHAUS, M., FEIGENBAUM, L., MANOVA, K., KRUHLAK, M., CAMERINI-OTERO, R. D., SHARAN, S., NUSSENZWEIG, M. & NUSSENZWEIG, A. 2005. Role of Nbs1 in the activation of the Atm kinase revealed in humanized mouse models. *Nat Cell Biol,* 7**,** 675-85.

DIFILIPPANTONIO, S., CELESTE, A., KRUHLAK, M. J., LEE, Y., DIFILIPPANTONIO, M. J., FEIGENBAUM, L., JACKSON, S. P., MCKINNON, P. J. & NUSSENZWEIG, A. 2007. Distinct domains in Nbs1 regulate irradiation-induced checkpoints and apoptosis. *J Exp Med,* 204**,** 1003-11.

DIFILIPPANTONIO, S., GAPUD, E., WONG, N., HUANG, C. Y., MAHOWALD, G., CHEN, H. T., KRUHLAK, M. J., CALLEN, E., LIVAK, F., NUSSENZWEIG, M. C., SLECKMAN, B. P. & NUSSENZWEIG, A. 2008. 53BP1 facilitates long-range DNA end-joining during V(D)J recombination. *Nature,* 456**,** 529-33.

DIGWEED, M. & SPERLING, K. 2004. Nijmegen breakage syndrome: clinical manifestation of defective response to DNA double-strand breaks. *DNA Repair (Amst),* 3**,** 1207-17.

DIMITROVA, N., CHEN, Y. C., SPECTOR, D. L. & DE LANGE, T. 2008. 53BP1 promotes non-homologous end joining of telomeres by increasing chromatin mobility. *Nature,* 456**,** 524-8.

DOIL, C., MAILAND, N., BEKKER-JENSEN, S., MENARD, P., LARSEN, D. H., PEPPERKOK, R., ELLENBERG, J., PANIER, S., DUROCHER, D., BARTEK, J., LUKAS, J. & LUKAS, C. 2009. RNF168 binds and amplifies ubiquitin conjugates on damaged chromosomes to allow accumulation of repair proteins. *Cell,* 136**,** 435-46.

DROST, R., BOUWMAN, P., ROTTENBERG, S., BOON, U., SCHUT, E., KLARENBEEK, S., KLIJN, C., VAN DER HEIJDEN, I., VAN DER GULDEN, H., WIENTJENS, E., PIETERSE, M., CATTEAU, A., GREEN, P., SOLOMON, E., MORRIS, J. R. & JONKERS, J. 2011. BRCA1 RING function is essential for tumor suppression but dispensable for therapy resistance. *Cancer Cell,* 20**,** 797-809.

DUPRE, A., BOYER-CHATENET, L. & GAUTIER, J. 2006. Two-step activation of ATM by DNA and the Mre11-Rad50-Nbs1 complex. *Nat Struct Mol Biol,* 13**,** 451-7.

DURKIN, S. G. & GLOVER, T. W. 2007. Chromosome fragile sites. *Annu Rev Genet,* 41**,** 169-92.

DUURSMA, A. M., DRISCOLL, R., ELIAS, J. E. & CIMPRICH, K. A. 2013. A role for the MRN complex in ATR activation via TOPBP1 recruitment. *Mol Cell,* 50**,** 116-22.

EINOLF, H. J. & GUENGERICH, F. P. 2001. Fidelity of nucleotide insertion at 8-oxo-7,8-dihydroguanine by mammalian DNA polymerase delta. Steady-state and pre-steady-state kinetic analysis. *J Biol Chem,* 276**,** 3764-71.

ELLISON, V. & STILLMAN, B. 2003. Biochemical characterization of DNA damage checkpoint complexes: clamp loader and clamp complexes with specificity for 5' recessed DNA. *PLoS Biol,* 1**,** E33.

ESCRIBANO-DIAZ, C., ORTHWEIN, A., FRADET-TURCOTTE, A., XING, M., YOUNG, J. T., TKAC, J., COOK, M. A., ROSEBROCK, A. P., MUNRO, M., CANNY, M. D., XU, D. & DUROCHER, D. 2013. A cell cycle-dependent regulatory circuit composed of 53BP1-RIF1 and BRCA1-CtIP controls DNA repair pathway choice. *Mol Cell,* 49**,** 872-83.

EWALD, B., SAMPATH, D. & PLUNKETT, W. 2008. ATM and the Mre11-Rad50-Nbs1 complex respond to nucleoside analogue-induced stalled replication forks and contribute to drug resistance. *Cancer Res,* 68**,** 7947-55.

FALCK, J., COATES, J. & JACKSON, S. P. 2005. Conserved modes of recruitment of ATM, ATR and DNA-PKcs to sites of DNA damage. *Nature,* 434**,** 605-11.

FEIJOO, C., HALL-JACKSON, C., WU, R., JENKINS, D., LEITCH, J., GILBERT, D. M. & SMYTHE, C. 2001. Activation of mammalian Chk1 during DNA replication arrest: a role for Chk1 in the intra-S phase checkpoint monitoring replication origin firing. *J Cell Biol,* 154**,** 913-23.

FENG, L., FONG, K. W., WANG, J., WANG, W. & CHEN, J. 2013. RIF1 counteracts BRCA1-mediated end resection during DNA repair. *J Biol Chem,* 288**,** 11135-43.

FERNANDES, N., SUN, Y., CHEN, S., PAUL, P., SHAW, R. J., CANTLEY, L. C. & PRICE, B. D. 2005. DNA damage-induced association of ATM with its target proteins requires a protein interaction domain in the N terminus of ATM. *J Biol Chem,* 280**,** 15158-64.

FLYNN, R. L. & ZOU, L. 2011. ATR: a master conductor of cellular responses to DNA replication stress. *Trends Biochem Sci,* 36**,** 133-40.

FORTINI, P., PARLANTI, E., SIDORKINA, O. M., LAVAL, J. & DOGLIOTTI, E. 1999. The type of DNA glycosylase determines the base excision repair pathway in mammalian cells. *J Biol Chem,* 274**,** 15230-6.

FROMME, J. C., BANERJEE, A., HUANG, S. J. & VERDINE, G. L. 2004. Structural basis for removal of adenine mispaired with 8-oxoguanine by MutY adenine DNA glycosylase. *Nature,* 427**,** 652-6.

FROMME, J. C., BRUNER, S. D., YANG, W., KARPLUS, M. & VERDINE, G. L. 2003. Product-assisted catalysis in base-excision DNA repair. *Nat Struct Biol,* 10**,** 204-11.

FURUICHI, M., YOSHIDA, M. C., ODA, H., TAJIRI, T., NAKABEPPU, Y., TSUZUKI, T. & SEKIGUCHI, M. 1994. Genomic structure and chromosome location of the human mutT homologue gene MTH1 encoding 8-oxo-dGTPase for prevention of A:T to C:G transversion. *Genomics,* 24**,** 485-90.

FURUYA, K., POITELEA, M., GUO, L., CASPARI, T. & CARR, A. M. 2004. Chk1 activation requires Rad9 S/TQ-site phosphorylation to promote association with C-terminal BRCT domains of Rad4TOPBP1. *Genes Dev,* 18**,** 1154-64.

GATEI, M., SCOTT, S. P., FILIPPOVITCH, I., SORONIKA, N., LAVIN, M. F., WEBER, B. & KHANNA, K. K. 2000a. Role for ATM in DNA damage-induced phosphorylation of BRCA1. *Cancer Res,* 60**,** 3299-304.

GATEI, M., YOUNG, D., CEROSALETTI, K. M., DESAI-MEHTA, A., SPRING, K., KOZLOV, S., LAVIN, M. F., GATTI, R. A., CONCANNON, P. & KHANNA, K. 2000b. ATM-dependent phosphorylation of nibrin in response to radiation exposure. *Nat Genet,* 25**,** 115-9.

GATTI, M., PINATO, S., MASPERO, E., SOFFIENTINI, P., POLO, S. & PENENGO, L. 2012. A novel ubiquitin mark at the N-terminal tail of histone H2As targeted by RNF168 ubiquitin ligase. *Cell Cycle,* 11**,** 2538-44.

GILAD, S., KHOSRAVI, R., SHKEDY, D., UZIEL, T., ZIV, Y., SAVITSKY, K., ROTMAN, G., SMITH, S., CHESSA, L., JORGENSEN, T. J., HARNIK, R., FRYDMAN, M., SANAL, O., PORTNOI, S., GOLDWICZ, Z., JASPERS, N. G., GATTI, R. A., LENOIR, G., LAVIN, M. F., TATSUMI, K., WEGNER, R. D., SHILOH, Y. & BAR-SHIRA, A. 1996. Predominance of null mutations in ataxia-telangiectasia. *Hum Mol Genet,* 5**,** 433-9.

GINJALA, V., NACERDDINE, K., KULKARNI, A., OZA, J., HILL, S. J., YAO, M., CITTERIO, E., VAN LOHUIZEN, M. & GANESAN, S. 2011. BMI1 is recruited to DNA breaks and contributes to DNA damage-induced H2A ubiquitination and repair. *Mol Cell Biol,* 31**,** 1972-82.

GLOVER, T. W., BERGER, C., COYLE, J. & ECHO, B. 1984. DNA polymerase alpha inhibition by aphidicolin induces gaps and breaks at common fragile sites in human chromosomes. *Hum Genet,* 67**,** 136-42.

GLOVER, T. W. & STEIN, C. K. 1987. Induction of sister chromatid exchanges at common fragile sites. *Am J Hum Genet,* 41**,** 882-90.

GLOVER, T. W. & STEIN, C. K. 1988. Chromosome breakage and recombination at fragile sites. *Am J Hum Genet,* 43**,** 265-73.

GOODARZI, A. A., KURKA, T. & JEGGO, P. A. 2011. KAP-1 phosphorylation regulates CHD3 nucleosome remodeling during the DNA double-strand break response. *Nat Struct Mol Biol,* 18**,** 831-9.

GOODARZI, A. A., NOON, A. T., DECKBAR, D., ZIV, Y., SHILOH, Y., LOBRICH, M. & JEGGO, P. A. 2008. ATM signaling facilitates repair of DNA double-strand breaks associated with heterochromatin. *Mol Cell,* 31**,** 167-77.

GREENMAN, C., STEPHENS, P., SMITH, R., DALGLIESH, G. L., HUNTER, C., BIGNELL, G., DAVIES, H., TEAGUE, J., BUTLER, A., STEVENS, C., EDKINS, S., O'MEARA, S., VASTRIK, I., SCHMIDT, E. E., AVIS, T., BARTHORPE, S., BHAMRA,

G., BUCK, G., CHOUDHURY, B., CLEMENTS, J., COLE, J., DICKS, E., FORBES, S., GRAY, K., HALLIDAY, K., HARRISON, R., HILLS, K., HINTON, J., JENKINSON, A., JONES, D., MENZIES, A., MIRONENKO, T., PERRY, J., RAINE, K., RICHARDSON, D., SHEPHERD, R., SMALL, A., TOFTS, C., VARIAN, J., WEBB, T., WEST, S., WIDAA, S., YATES, A., CAHILL, D. P., LOUIS, D. N., GOLDSTRAW, P., NICHOLSON, A. G., BRASSEUR, F., LOOIJENGA, L., WEBER, B. L., CHIEW, Y. E., DEFAZIO, A., GREAVES, M. F., GREEN, A. R., CAMPBELL, P., BIRNEY, E., EASTON, D. F., CHENEVIX-TRENCH, G., TAN, M. H., KHOO, S. K., TEH, B. T., YUEN, S. T., LEUNG, S. Y., WOOSTER, R., FUTREAL, P. A. & STRATTON, M. R. 2007. Patterns of somatic mutation in human cancer genomes. *Nature,* 446**,** 153-8.

GUDJONSSON, T., ALTMEYER, M., SAVIC, V., TOLEDO, L., DINANT, C., GROFTE, M., BARTKOVA, J., POULSEN, M., OKA, Y., BEKKER-JENSEN, S., MAILAND, N., NEUMANN, B., HERICHE, J. K., SHEARER, R., SAUNDERS, D., BARTEK, J., LUKAS, J. & LUKAS, C. 2012. TRIP12 and UBR5 suppress spreading of chromatin ubiquitylation at damaged chromosomes. *Cell,* 150**,** 697-709.

GUO, Z., DESHPANDE, R. & PAULL, T. T. 2010a. ATM activation in the presence of oxidative stress. *Cell Cycle,* 9**,** 4805-11.

GUO, Z., KOZLOV, S., LAVIN, M. F., PERSON, M. D. & PAULL, T. T. 2010b. ATM activation by oxidative stress. *Science,* 330**,** 517-21.

HAHN, S. M., MITCHELL, J. B. & SHACTER, E. 1997. Tempol inhibits neutrophil and hydrogen peroxide-mediated DNA damage. *Free Radic Biol Med,* 23**,** 879-84.

HAHN, S. M., TOCHNER, Z., KRISHNA, C. M., GLASS, J., WILSON, L., SAMUNI, A., SPRAGUE, M., VENZON, D., GLATSTEIN, E., MITCHELL, J. B. & ET AL. 1992. Tempol, a stable free radical, is a novel murine radiation protector. *Cancer Res,* 52**,** 1750-3.

HAIGIS, K., SAGE, J., GLICKMAN, J., SHAFER, S. & JACKS, T. 2006. The related retinoblastoma (pRb) and p130 proteins cooperate to regulate homeostasis in the intestinal epithelium. *J Biol Chem,* 281**,** 638-47.

HAMMOND, E. M., KAUFMANN, M. R. & GIACCIA, A. J. 2007. Oxygen sensing and the DNA-damage response. *Curr Opin Cell Biol,* 19**,** 680-4.

HARRIGAN, J. A., BELOTSERKOVSKAYA, R., COATES, J., DIMITROVA, D. S., POLO, S. E., BRADSHAW, C. R., FRASER, P. & JACKSON, S. P. 2011. Replication stress induces 53BP1-containing OPT domains in G1 cells. *J Cell Biol,* 193**,** 97-108.

HAYASHI, H., TOMINAGA, Y., HIRANO, S., MCKENNA, A. E., NAKABEPPU, Y. & MATSUMOTO, Y. 2002. Replication-associated repair of adenine:8-oxoguanine mispairs by MYH. *Curr Biol,* 12**,** 335-9.

HEFFERNAN, T. P., SIMPSON, D. A., FRANK, A. R., HEINLOTH, A. N., PAULES, R. S., CORDEIRO-STONE, M. & KAUFMANN, W. K. 2002. An ATR- and Chk1-dependent S checkpoint inhibits replicon initiation following UVC-induced DNA damage. *Mol Cell Biol,* 22**,** 8552-61.

HENDERSON, M. J., MUNOZ, M. A., SAUNDERS, D. N., CLANCY, J. L., RUSSELL, A. J., WILLIAMS, B., PAPPIN, D., KHANNA, K. K., JACKSON, S. P., SUTHERLAND, R. L. & WATTS, C. K. 2006. EDD mediates DNA damage-induced activation of CHK2. *J Biol Chem,* 281**,** 39990-40000.

HILBERT, T. P., CHAUNG, W., BOORSTEIN, R. J., CUNNINGHAM, R. P. & TEEBOR, G. W. 1997. Cloning and expression of the cDNA encoding the human homologue of the DNA repair enzyme, Escherichia coli endonuclease III. *J Biol Chem,* 272**,** 6733-40.

HOEGE, C., PFANDER, B., MOLDOVAN, G. L., PYROWOLAKIS, G. & JENTSCH, S. 2002. RAD6-dependent DNA repair is linked to modification of PCNA by ubiquitin and SUMO. *Nature,* 419**,** 135-41.

HONDA, Y., TOJO, M., MATSUZAKI, K., ANAN, T., MATSUMOTO, M., ANDO, M., SAYA, H. & NAKAO, M. 2002. Cooperation of HECT-domain ubiquitin ligase hHYD and DNA topoisomerase II-binding protein for DNA damage response. *J Biol Chem,* 277**,** 3599-605.

HOPFNER, K. P., KARCHER, A., CRAIG, L., WOO, T. T., CARNEY, J. P. & TAINER, J. A. 2001. Structural biochemistry and interaction architecture of the DNA double-strand break repair Mre11 nuclease and Rad50-ATPase. *Cell,* 105**,** 473-85.

HU, J., IMAM, S. Z., HASHIGUCHI, K., DE SOUZA-PINTO, N. C. & BOHR, V. A. 2005. Phosphorylation of human oxoguanine DNA glycosylase (alpha-OGG1) modulates its function. *Nucleic Acids Res,* 33**,** 3271-82.

HU, Y., SCULLY, R., SOBHIAN, B., XIE, A., SHESTAKOVA, E. & LIVINGSTON, D. M. 2011. RAP80-directed tuning of BRCA1 homologous recombination function at ionizing radiation-induced nuclear foci. *Genes Dev,* 25**,** 685-700.

HUEN, M. S., GRANT, R., MANKE, I., MINN, K., YU, X., YAFFE, M. B. & CHEN, J. 2007. RNF8 transduces the DNA-damage signal via histone ubiquitylation and checkpoint protein assembly. *Cell,* 131**,** 901-14.

HUERTAS, P. 2010. DNA resection in eukaryotes: deciding how to fix the break. *Nat Struct Mol Biol,* 17**,** 11-6.

HUERTAS, P. & JACKSON, S. P. 2009. Human CtIP mediates cell cycle control of DNA end resection and double strand break repair. *J Biol Chem,* 284**,** 9558-65.

IKEDA, S., BISWAS, T., ROY, R., IZUMI, T., BOLDOGH, I., KUROSKY, A., SARKER, A. H., SEKI, S. & MITRA, S. 1998. Purification and characterization of human NTH1, a homolog of Escherichia coli endonuclease III. Direct identification of Lys-212 as the active nucleophilic residue. *J Biol Chem,* 273**,** 21585-93.

ISMAIL, I. H., ANDRIN, C., MCDONALD, D. & HENDZEL, M. J. 2010. BMI1-mediated histone ubiquitylation promotes DNA double-strand break repair. *J Cell Biol,* 191**,** 45-60.

ITAKURA, E., SAWADA, I. & MATSUURA, A. 2005. Dimerization of the ATRIP protein through the coiled-coil motif and its implication to the maintenance of stalled replication forks. *Mol Biol Cell,* 16**,** 5551-62.

JACKSON, S. P. & DUROCHER, D. 2013. Regulation of DNA damage responses by ubiquitin and SUMO. *Mol Cell,* 49**,** 795-807.

JACOME, A. & FERNANDEZ-CAPETILLO, O. 2011. Lac operator repeats generate a traceable fragile site in mammalian cells. *EMBO Rep,* 12**,** 1032-8.

JAZAYERI, A., BALESTRINI, A., GARNER, E., HABER, J. E. & COSTANZO, V. 2008. Mre11-Rad50-Nbs1-dependent processing of DNA breaks generates oligonucleotides that stimulate ATM activity. *EMBO J,* 27**,** 1953-62.

JIANG, X., SUN, Y., CHEN, S., ROY, K. & PRICE, B. D. 2006. The FATC domains of PIKK proteins are functionally equivalent and participate in the Tip60-dependent activation of DNA-PKcs and ATM. *J Biol Chem,* 281**,** 15741-6.

JOHNSTONE, P. A., DEGRAFF, W. G. & MITCHELL, J. B. 1995. Protection from radiation-induced chromosomal aberrations by the nitroxide Tempol. *Cancer,* 75**,** 2323-7.

JOUGHIN, B. A., TIDOR, B. & YAFFE, M. B. 2005. A computational method for the analysis and prediction of protein:phosphopeptide-binding sites. *Protein Sci,* 14**,** 131-9.

JUANG, Y. C., LANDRY, M. C., SANCHES, M., VITTAL, V., LEUNG, C. C., CECCARELLI, D. F., MATEO, A. R., PRUNEDA, J. N., MAO, D. Y., SZILARD, R. K., ORLICKY, S., MUNRO, M., BRZOVIC, P. S., KLEVIT, R. E., SICHERI, F. & DUROCHER, D. 2012. OTUB1 co-opts Lys48-linked ubiquitin recognition to suppress E2 enzyme function. *Mol Cell,* 45**,** 384-97.

JURADO, S., CONLAN, L. A., BAKER, E. K., NG, J. L., TENIS, N., HOCH, N. C., GLEESON, K., SMEETS, M., IZON, D. & HEIERHORST, J. 2012a. ATM substrate Chk2-interacting Zn2+ finger (ASCIZ) Is a bi-functional transcriptional activator and feedback sensor in the regulation of dynein light chain (DYNLL1) expression. *J Biol Chem,* 287**,** 3156-64.

JURADO, S., GLEESON, K., O'DONNELL, K., IZON, D. J., WALKLEY, C. R., STRASSER, A., TARLINTON, D. M. & HEIERHORST, J. 2012b. The Zinc-finger protein ASCIZ regulates B cell development via DYNLL1 and Bim. *J Exp Med,* 209**,** 1629-39.

JURADO, S., SMYTH, I., VAN DENDEREN, B., TENIS, N., HAMMET, A., HEWITT, K., NG, J. L., MCNEES, C. J., KOZLOV, S. V., OKA, H., KOBAYASHI, M., CONLAN, L. A., COLE, T. J., YAMAMOTO, K., TANIGUCHI, Y., TAKEDA, S., LAVIN, M. F. & HEIERHORST, J. 2010. Dual functions of ASCIZ in the DNA base damage response and pulmonary organogenesis. *PLoS Genet,* 6**,** e1001170.

KAIDI, A. & JACKSON, S. P. 2013. KAT5 tyrosine phosphorylation couples chromatin sensing to ATM signalling. *Nature,* 498**,** 70-4.

KAKUMA, T., NISHIDA, J., TSUZUKI, T. & SEKIGUCHI, M. 1995. Mouse MTH1 protein with 8-oxo-7,8-dihydro-2'-deoxyguanosine 5'-triphosphatase activity that prevents transversion mutation. cDNA cloning and tissue distribution. *J Biol Chem,* 270**,** 25942-8.

KANG, J., BRONSON, R. T. & XU, Y. 2002. Targeted disruption of NBS1 reveals its roles in mouse development and DNA repair. *EMBO J,* 21**,** 1447-55.

KANNOUCHE, P. L., WING, J. & LEHMANN, A. R. 2004. Interaction of human DNA polymerase eta with monoubiquitinated PCNA: a possible mechanism for the polymerase switch in response to DNA damage. *Mol Cell,* 14**,** 491-500.

KANU, N. & BEHRENS, A. 2007. ATMIN defines an NBS1-independent pathway of ATM signalling. *EMBO J,* 26**,** 2933-41.

KANU, N., PENICUD, K., HRISTOVA, M., WONG, B., IRVINE, E., PLATTNER, F., RAIVICH, G. & BEHRENS, A. 2010. The ATM cofactor ATMIN protects against oxidative stress and accumulation of DNA damage in the aging brain. *J Biol Chem,* 285**,** 38534-42.

KIM, S. T., LIM, D. S., CANMAN, C. E. & KASTAN, M. B. 1999. Substrate specificities and identification of putative substrates of ATM kinase family members. *J Biol Chem,* 274**,** 37538-43.

KITAGAWA, R., BAKKENIST, C. J., MCKINNON, P. J. & KASTAN, M. B. 2004. Phosphorylation of SMC1 is a critical downstream event in the ATM-NBS1-BRCA1 pathway. *Genes Dev,* 18**,** 1423-38.

KLAUNIG, J. E. & KAMENDULIS, L. M. 2004. The role of oxidative stress in carcinogenesis. *Annu Rev Pharmacol Toxicol,* 44**,** 239-67.

KLUNGLAND, A., ROSEWELL, I., HOLLENBACH, S., LARSEN, E., DALY, G., EPE, B., SEEBERG, E., LINDAHL, T. & BARNES, D. E. 1999. Accumulation of premutagenic DNA lesions in mice defective in removal of oxidative base damage. *Proc Natl Acad Sci U S A,* 96**,** 13300-5.

KOBLIAKOVA IU, V., KIREEV, II, STEFANOVA, V. N., ZATSEPINA, O. V. & POLIAKOV, V. 2001. [Differential decondensation of mitotic chromosomes in SPEV tissue cultured cells induced by repeated hypotonic shock]. *Tsitologiia,* 43**,** 462-70.

KOLAS, N. K., CHAPMAN, J. R., NAKADA, S., YLANKO, J., CHAHWAN, R., SWEENEY, F. D., PANIER, S., MENDEZ, M., WILDENHAIN, J., THOMSON, T. M., PELLETIER, L., JACKSON, S. P. & DUROCHER, D. 2007. Orchestration of the DNA-damage response by the RNF8 ubiquitin ligase. *Science,* 318**,** 1637-40.

KOMANDER, D., CLAGUE, M. J. & URBE, S. 2009. Breaking the chains: structure and function of the deubiquitinases. *Nat Rev Mol Cell Biol,* 10**,** 550-63.

KOMANDER, D. & RAPE, M. 2012. The ubiquitin code. *Annu Rev Biochem,* 81**,** 203-29.

KONDO, T., WAKAYAMA, T., NAIKI, T., MATSUMOTO, K. & SUGIMOTO, K. 2001. Recruitment of Mec1 and Ddc1 checkpoint proteins to double-strand breaks through distinct mechanisms. *Science,* 294**,** 867-70.

KOZLOV, S. V., GRAHAM, M. E., JAKOB, B., TOBIAS, F., KIJAS, A. W., TANUJI, M., CHEN, P., ROBINSON, P. J., TAUCHER-SCHOLZ, G., SUZUKI, K., SO, S., CHEN, D. & LAVIN, M. F. 2011. Autophosphorylation and ATM activation: additional sites add to the complexity. *J Biol Chem,* 286**,** 9107-19.

KOZLOV, S. V., GRAHAM, M. E., PENG, C., CHEN, P., ROBINSON, P. J. & LAVIN, M. F. 2006. Involvement of novel autophosphorylation sites in ATM activation. *EMBO J,* 25**,** 3504-14.

KUBOTA, Y., NASH, R. A., KLUNGLAND, A., SCHAR, P., BARNES, D. E. & LINDAHL, T. 1996. Reconstitution of DNA base excision-repair with purified human

proteins: interaction between DNA polymerase beta and the XRCC1 protein. *EMBO J,* 15**,** 6662-70.

KULATHU, Y. & KOMANDER, D. 2012. Atypical ubiquitylation - the unexplored world of polyubiquitin beyond Lys48 and Lys63 linkages. *Nat Rev Mol Cell Biol,* 13**,** 508-23.

KUMAGAI, A., LEE, J., YOO, H. Y. & DUNPHY, W. G. 2006. TopBP1 activates the ATR-ATRIP complex. *Cell,* 124**,** 943-55.

LAN, J., LI, W., ZHANG, F., SUN, F. Y., NAGAYAMA, T., O'HORO, C. & CHEN, J. 2003. Inducible repair of oxidative DNA lesions in the rat brain after transient focal ischemia and reperfusion. *J Cereb Blood Flow Metab,* 23**,** 1324-39.

LAVIN, M. F., KOZLOV, S., GUEVEN, N., PENG, C., BIRRELL, G., CHEN, P. & SCOTT, S. 2005. Atm and cellular response to DNA damage. *Adv Exp Med Biol,* 570**,** 457-76.

LEE, J., KUMAGAI, A. & DUNPHY, W. G. 2007. The Rad9-Hus1-Rad1 checkpoint clamp regulates interaction of TopBP1 with ATR. *J Biol Chem,* 282**,** 28036-44.

LEE, J. H., GOODARZI, A. A., JEGGO, P. A. & PAULL, T. T. 2010. 53BP1 promotes ATM activity through direct interactions with the MRN complex. *EMBO J,* 29**,** 574-85.

LEE, J. H., MAND, M. R., DESHPANDE, R. A., KINOSHITA, E., YANG, S. H., WYMAN, C. & PAULL, T. T. 2013. Ataxia telangiectasia-mutated (ATM) kinase activity is regulated by ATP-driven conformational changes in the Mre11/Rad50/Nbs1 (MRN) complex. *J Biol Chem,* 288**,** 12840-51.

LEE, J. H. & PAULL, T. T. 2004. Direct activation of the ATM protein kinase by the Mre11/Rad50/Nbs1 complex. *Science,* 304**,** 93-6.

LEE, J. H. & PAULL, T. T. 2005. ATM activation by DNA double-strand breaks through the Mre11-Rad50-Nbs1 complex. *Science,* 308**,** 551-4.

LI, W., LUO, Y., ZHANG, F., SIGNORE, A. P., GOBBEL, G. T., SIMON, R. P. & CHEN, J. 2006. Ischemic preconditioning in the rat brain enhances the repair of endogenous oxidative DNA damage by activating the base-excision repair pathway. *J Cereb Blood Flow Metab,* 26**,** 181-98.

LIEBMANN, J., DELUCA, A. M., EPSTEIN, A., STEINBERG, S. M., MORSTYN, G. & MITCHELL, J. B. 1994. Protection from lethal irradiation by the combination of stem cell factor and tempol. *Radiat Res,* 137**,** 400-4.

LIM, D. S., KIM, S. T., XU, B., MASER, R. S., LIN, J., PETRINI, J. H. & KASTAN, M. B. 2000. ATM phosphorylates p95/nbs1 in an S-phase checkpoint pathway. *Nature,* 404**,** 613-7.

LING, S. & LIN, W. C. 2011. EDD inhibits ATM-mediated phosphorylation of p53. *J Biol Chem,* 286**,** 14972-82.

LIU, H., TAKEDA, S., KUMAR, R., WESTERGARD, T. D., BROWN, E. J., PANDITA, T. K., CHENG, E. H. & HSIEH, J. J. 2010. Phosphorylation of MLL by ATR is required for execution of mammalian S-phase checkpoint. *Nature,* 467**,** 343-6.

LIU, Q., GUNTUKU, S., CUI, X. S., MATSUOKA, S., CORTEZ, D., TAMAI, K., LUO, G., CARATTINI-RIVERA, S., DEMAYO, F., BRADLEY, A., DONEHOWER, L. A. & ELLEDGE, S. J. 2000. Chk1 is an essential kinase that is regulated by Atr and required for the G(2)/M DNA damage checkpoint. *Genes Dev,* 14**,** 1448-59.

LIU, S., SHIOTANI, B., LAHIRI, M., MARECHAL, A., TSE, A., LEUNG, C. C., GLOVER, J. N., YANG, X. H. & ZOU, L. 2011. ATR autophosphorylation as a molecular switch for checkpoint activation. *Mol Cell,* 43**,** 192-202.

LIU, X. & ROY, R. 2002. Truncation of amino-terminal tail stimulates activity of human endonuclease III (hNTH1). *J Mol Biol,* 321**,** 265-76.

LLOYD, J., CHAPMAN, J. R., CLAPPERTON, J. A., HAIRE, L. F., HARTSUIKER, E., LI, J., CARR, A. M., JACKSON, S. P. & SMERDON, S. J. 2009. A supramodular FHA/BRCT-repeat architecture mediates Nbs1 adaptor function in response to DNA damage. *Cell,* 139**,** 100-11.

LOBRICH, M. & JEGGO, P. A. 2005. Harmonising the response to DSBs: a new string in the ATM bow. *DNA Repair (Amst),* 4**,** 749-59.

LOIZOU, J. I., SANCHO, R., KANU, N., BOLLAND, D. J., YANG, F., RADA, C., CORCORAN, A. E. & BEHRENS, A. 2011. ATMIN is required for maintenance of genomic stability and suppression of B cell lymphoma. *Cancer Cell,* 19**,** 587-600.

LUKAS, C., SAVIC, V., BEKKER-JENSEN, S., DOIL, C., NEUMANN, B., PEDERSEN, R. S., GROFTE, M., CHAN, K. L., HICKSON, I. D., BARTEK, J. & LUKAS, J. 2011a. 53BP1 nuclear bodies form around DNA lesions generated by mitotic transmission of chromosomes under replication stress. *Nat Cell Biol,* 13**,** 243-53.

LUKAS, J., LUKAS, C. & BARTEK, J. 2011b. More than just a focus: The chromatin response to DNA damage and its role in genome integrity maintenance. *Nat Cell Biol,* 13**,** 1161-9.

MAHUT, M., LEITNER, M., EBNER, A., LAMMERHOFER, M., HINTERDORFER, P. & LINDNER, W. 2012. Time-resolved chloroquine-induced relaxation of supercoiled plasmid DNA. *Anal Bioanal Chem,* 402**,** 373-80.

MAILAND, N., BEKKER-JENSEN, S., FAUSTRUP, H., MELANDER, F., BARTEK, J., LUKAS, C. & LUKAS, J. 2007. RNF8 ubiquitylates histones at DNA double-strand breaks and promotes assembly of repair proteins. *Cell,* 131**,** 887-900.

MANSFIELD, E., HERSPERGER, E., BIGGS, J. & SHEARN, A. 1994. Genetic and molecular analysis of hyperplastic discs, a gene whose product is required for regulation of cell proliferation in Drosophila melanogaster imaginal discs and germ cells. *Dev Biol,* 165**,** 507-26.

MARKKANEN, E., VAN LOON, B., FERRARI, E., PARSONS, J. L., DIANOV, G. L. & HUBSCHER, U. 2012. Regulation of oxidative DNA damage repair by DNA polymerase lambda and MutYH by cross-talk of phosphorylation and ubiquitination. *Proc Natl Acad Sci U S A,* 109**,** 437-42.

MARTIN, P., MARTIN, A. & SHEARN, A. 1977. Studies of l(3)c43hs1 a polyphasic, temperature-sensitive mutant of Drosophila melanogaster with a variety of imaginal disc defects. *Dev Biol,* 55**,** 213-32.

MASER, R. S., MIRZOEVA, O. K., WELLS, J., OLIVARES, H., WILLIAMS, B. R., ZINKEL, R. A., FARNHAM, P. J. & PETRINI, J. H. 2001. Mre11 complex and DNA replication: linkage to E2F and sites of DNA synthesis. *Mol Cell Biol,* 21**,** 6006-16.

MATSUOKA, S., BALLIF, B. A., SMOGORZEWSKA, A., MCDONALD, E. R., 3RD, HUROV, K. E., LUO, J., BAKALARSKI, C. E., ZHAO, Z., SOLIMINI, N., LERENTHAL, Y., SHILOH, Y., GYGI, S. P. & ELLEDGE, S. J. 2007. ATM and ATR substrate analysis reveals extensive protein networks responsive to DNA damage. *Science,* 316**,** 1160-6.

MATTA-CAMACHO, E., KOZLOV, G., MENADE, M. & GEHRING, K. 2012. Structure of the HECT C-lobe of the UBR5 E3 ubiquitin ligase. *Acta Crystallogr Sect F Struct Biol Cryst Commun,* 68**,** 1158-63.

MATTIROLI, F., VISSERS, J. H., VAN DIJK, W. J., IKPA, P., CITTERIO, E., VERMEULEN, W., MARTEIJN, J. A. & SIXMA, T. K. 2012. RNF168 ubiquitinates K13-15 on H2A/H2AX to drive DNA damage signaling. *Cell,* 150**,** 1182-95.

MAZZEI, F., VIEL, A. & BIGNAMI, M. 2013. Role of MUTYH in human cancer. *Mutat Res,* 743-744**,** 33-43.

MCGOWAN, C. H. 2002. Checking in on Cds1 (Chk2): A checkpoint kinase and tumor suppressor. *Bioessays,* 24**,** 502-11.

MCNEES, C. J., CONLAN, L. A., TENIS, N. & HEIERHORST, J. 2005. ASCIZ regulates lesion-specific Rad51 focus formation and apoptosis after methylating DNA damage. *EMBO J,* 24**,** 2447-57.

MCVEY, M. & LEE, S. E. 2008. MMEJ repair of double-strand breaks (director's cut): deleted sequences and alternative endings. *Trends Genet,* 24**,** 529-38.

MELO, J. A., COHEN, J. & TOCZYSKI, D. P. 2001. Two checkpoint complexes are independently recruited to sites of DNA damage in vivo. *Genes Dev,* 15**,** 2809-21.

MIMITOU, E. P. & SYMINGTON, L. S. 2009. DNA end resection: many nucleases make light work. *DNA Repair (Amst),* 8**,** 983-95.

MINOWA, O., ARAI, T., HIRANO, M., MONDEN, Y., NAKAI, S., FUKUDA, M., ITOH, M., TAKANO, H., HIPPOU, Y., ABURATANI, H., MASUMURA, K., NOHMI, T., NISHIMURA, S. & NODA, T. 2000. Mmh/Ogg1 gene inactivation results in accumulation of 8-hydroxyguanine in mice. *Proc Natl Acad Sci U S A,* 97**,** 4156-61.

MIRZOEVA, O. K. & PETRINI, J. H. 2001. DNA damage-dependent nuclear dynamics of the Mre11 complex. *Mol Cell Biol,* 21**,** 281-8.

MITCHELL, J. B., DEGRAFF, W., KAUFMAN, D., KRISHNA, M. C., SAMUNI, A., FINKELSTEIN, E., AHN, M. S., HAHN, S. M., GAMSON, J. & RUSSO, A. 1991. Inhibition of oxygen-dependent radiation-induced damage by the nitroxide superoxide dismutase mimic, tempol. *Arch Biochem Biophys,* 289**,** 62-70.

MITCHELL, J. B., XAVIER, S., DELUCA, A. M., SOWERS, A. L., COOK, J. A., KRISHNA, M. C., HAHN, S. M. & RUSSO, A. 2003. A low molecular weight antioxidant decreases weight and lowers tumor incidence. *Free Radic Biol Med,* 34**,** 93-102.

MO, J. Y., MAKI, H. & SEKIGUCHI, M. 1992. Hydrolytic elimination of a mutagenic nucleotide, 8-oxodGTP, by human 18-kilodalton protein: sanitization of nucleotide pool. *Proc Natl Acad Sci U S A,* 89**,** 11021-5.

MORDES, D. A., GLICK, G. G., ZHAO, R. & CORTEZ, D. 2008. TopBP1 activates ATR through ATRIP and a PIKK regulatory domain. *Genes Dev,* 22**,** 1478-89.

MOSHOUS, D., CALLEBAUT, I., DE CHASSEVAL, R., CORNEO, B., CAVAZZANA-CALVO, M., LE DEIST, F., TEZCAN, I., SANAL, O., BERTRAND, Y., PHILIPPE, N., FISCHER, A. & DE VILLARTAY, J. P. 2001. Artemis, a novel DNA double-strand break repair/V(D)J recombination protein, is mutated in human severe combined immune deficiency. *Cell,* 105**,** 177-86.

MOYNAHAN, M. E., PIERCE, A. J. & JASIN, M. 2001. BRCA2 is required for homology-directed repair of chromosomal breaks. *Mol Cell,* 7**,** 263-72.

MU, J. J., WANG, Y., LUO, H., LENG, M., ZHANG, J., YANG, T., BESUSSO, D., JUNG, S. Y. & QIN, J. 2007. A proteomic analysis of ataxia telangiectasia-mutated (ATM)/ATM-Rad3-related (ATR) substrates identifies the ubiquitin-proteasome system as a regulator for DNA damage checkpoints. *J Biol Chem,* 282**,** 17330-4.

MURRAY, J. M., STIFF, T. & JEGGO, P. A. 2012. DNA double-strand break repair within heterochromatic regions. *Biochem Soc Trans,* 40**,** 173-8.

NAKABEPPU, Y., KAJITANI, K., SAKAMOTO, K., YAMAGUCHI, H. & TSUCHIMOTO, D. 2006. MTH1, an oxidized purine nucleoside triphosphatase, prevents the cytotoxicity and neurotoxicity of oxidized purine nucleotides. *DNA Repair (Amst),* 5**,** 761-72.

NAKADA, S., TAI, I., PANIER, S., AL-HAKIM, A., IEMURA, S., JUANG, Y. C., O'DONNELL, L., KUMAKUBO, A., MUNRO, M., SICHERI, F., GINGRAS, A. C., NATSUME, T., SUDA, T. & DUROCHER, D. 2010. Non-canonical inhibition of DNA damage-dependent ubiquitination by OTUB1. *Nature,* 466**,** 941-6.

NAKAMOTO, H., KANEKO, T., TAHARA, S., HAYASHI, E., NAITO, H., RADAK, Z. & GOTO, S. 2007. Regular exercise reduces 8-oxodG in the nuclear and mitochondrial DNA and modulates the DNA repair activity in the liver of old rats. *Exp Gerontol,* 42**,** 287-95.

NEW, J. H., SUGIYAMA, T., ZAITSEVA, E. & KOWALCZYKOWSKI, S. C. 1998. Rad52 protein stimulates DNA strand exchange by Rad51 and replication protein A. *Nature,* 391**,** 407-10.

NICASSIO, F., CORRADO, N., VISSERS, J. H., ARECES, L. B., BERGINK, S., MARTEIJN, J. A., GEVERTS, B., HOUTSMULLER, A. B., VERMEULEN, W., DI FIORE, P. P. & CITTERIO, E. 2007. Human USP3 is a chromatin modifier required for S phase progression and genome stability. *Curr Biol,* 17**,** 1972-7.

NICK MCELHINNY, S. A., SNOWDEN, C. M., MCCARVILLE, J. & RAMSDEN, D. A. 2000. Ku recruits the XRCC4-ligase IV complex to DNA ends. *Mol Cell Biol,* 20**,** 2996-3003.

NOON, A. T., SHIBATA, A., RIEF, N., LOBRICH, M., STEWART, G. S., JEGGO, P. A. & GOODARZI, A. A. 2010. 53BP1-dependent robust localized KAP-1 phosphorylation

is essential for heterochromatic DNA double-strand break repair. *Nat Cell Biol,* 12**,** 177-84.

NOREN HOOTEN, N., KOMPANIEZ, K., BARNES, J., LOHANI, A. & EVANS, M. K. 2011. Poly(ADP-ribose) polymerase 1 (PARP-1) binds to 8-oxoguanine-DNA glycosylase (OGG1). *J Biol Chem,* 286**,** 44679-90.

OKA, H., SAKAI, W., SONODA, E., NAKAMURA, J., ASAGOSHI, K., WILSON, S. H., KOBAYASHI, M., YAMAMOTO, K., HEIERHORST, J., TAKEDA, S. & TANIGUCHI, Y. 2008. DNA damage response protein ASCIZ links base excision repair with immunoglobulin gene conversion. *Biochem Biophys Res Commun,* 371**,** 225-9.

OKUBO, S., HARA, F., TSUCHIDA, Y., SHIMOTAKAHARA, S., SUZUKI, S., HATANAKA, H., YOKOYAMA, S., TANAKA, H., YASUDA, H. & SHINDO, H. 2004. NMR structure of the N-terminal domain of SUMO ligase PIAS1 and its interaction with tumor suppressor p53 and A/T-rich DNA oligomers. *J Biol Chem,* 279**,** 31455-61.

OLCINA, M., LECANE, P. S. & HAMMOND, E. M. 2010. Targeting hypoxic cells through the DNA damage response. *Clin Cancer Res,* 16**,** 5624-9.

OLSEN, J. V., BLAGOEV, B., GNAD, F., MACEK, B., KUMAR, C., MORTENSEN, P. & MANN, M. 2006. Global, in vivo, and site-specific phosphorylation dynamics in signaling networks. *Cell,* 127**,** 635-48.

OPPERMANN, F. S., GNAD, F., OLSEN, J. V., HORNBERGER, R., GREFF, Z., KERI, G., MANN, M. & DAUB, H. 2009. Large-scale proteomics analysis of the human kinome. *Mol Cell Proteomics,* 8**,** 1751-64.

PAN, M. R., PENG, G., HUNG, W. C. & LIN, S. Y. 2011. Monoubiquitination of H2AX protein regulates DNA damage response signaling. *J Biol Chem,* 286**,** 28599-607.

PARKER, A., GU, Y., MAHONEY, W., LEE, S. H., SINGH, K. K. & LU, A. L. 2001. Human homolog of the MutY repair protein (hMYH) physically interacts with proteins involved in long patch DNA base excision repair. *J Biol Chem,* 276**,** 5547-55.

PARKER, A. R., O'MEALLY, R. N., SAHIN, F., SU, G. H., RACKE, F. K., NELSON, W. G., DEWEESE, T. L. & ESHLEMAN, J. R. 2003. Defective human MutY phosphorylation exists in colorectal cancer cell lines with wild-type MutY alleles. *J Biol Chem,* 278**,** 47937-45.

PARSONS, J. L., TAIT, P. S., FINCH, D., DIANOVA, II, EDELMANN, M. J., KHORONENKOVA, S. V., KESSLER, B. M., SHARMA, R. A., MCKENNA, W. G. & DIANOV, G. L. 2009. Ubiquitin ligase ARF-BP1/Mule modulates base excision repair. *EMBO J,* 28**,** 3207-15.

PASCUCCI, B., MAGA, G., HUBSCHER, U., BJORAS, M., SEEBERG, E., HICKSON, I. D., VILLANI, G., GIORDANO, C., CELLAI, L. & DOGLIOTTI, E. 2002. Reconstitution of the base excision repair pathway for 7,8-dihydro-8-oxoguanine with purified human proteins. *Nucleic Acids Res,* 30**,** 2124-30.

PAZ-ELIZUR, T., SEVILYA, Z., LEITNER-DAGAN, Y., ELINGER, D., ROISMAN, L. C. & LIVNEH, Z. 2008. DNA repair of oxidative DNA damage in human carcinogenesis: potential application for cancer risk assessment and prevention. *Cancer Lett,* 266**,** 60-72.

PLEASANCE, E. D., CHEETHAM, R. K., STEPHENS, P. J., MCBRIDE, D. J., HUMPHRAY, S. J., GREENMAN, C. D., VARELA, I., LIN, M. L., ORDONEZ, G. R., BIGNELL, G. R., YE, K., ALIPAZ, J., BAUER, M. J., BEARE, D., BUTLER, A., CARTER, R. J., CHEN, L., COX, A. J., EDKINS, S., KOKKO-GONZALES, P. I., GORMLEY, N. A., GROCOCK, R. J., HAUDENSCHILD, C. D., HIMS, M. M., JAMES, T., JIA, M., KINGSBURY, Z., LEROY, C., MARSHALL, J., MENZIES, A., MUDIE, L. J., NING, Z., ROYCE, T., SCHULZ-TRIEGLAFF, O. B., SPIRIDOU, A., STEBBINGS, L. A., SZAJKOWSKI, L., TEAGUE, J., WILLIAMSON, D., CHIN, L., ROSS, M. T., CAMPBELL, P. J., BENTLEY, D. R., FUTREAL, P. A. & STRATTON, M. R. 2010a. A comprehensive catalogue of somatic mutations from a human cancer genome. *Nature,* 463**,** 191-6.

PLEASANCE, E. D., STEPHENS, P. J., O'MEARA, S., MCBRIDE, D. J., MEYNERT, A., JONES, D., LIN, M. L., BEARE, D., LAU, K. W., GREENMAN, C., VARELA, I., NIK-ZAINAL, S., DAVIES, H. R., ORDONEZ, G. R., MUDIE, L. J., LATIMER, C., EDKINS, S., STEBBINGS, L., CHEN, L., JIA, M., LEROY, C., MARSHALL, J., MENZIES, A., BUTLER, A., TEAGUE, J. W., MANGION, J., SUN, Y. A., MCLAUGHLIN, S. F., PECKHAM, H. E., TSUNG, E. F., COSTA, G. L., LEE, C. C., MINNA, J. D., GAZDAR, A., BIRNEY, E., RHODES, M. D., MCKERNAN, K. J., STRATTON, M. R., FUTREAL, P. A. & CAMPBELL, P. J. 2010b. A small-cell lung cancer genome with complex signatures of tobacco exposure. *Nature,* 463**,** 184-90.

PODLUTSKY, A. J., DIANOVA, II, PODUST, V. N., BOHR, V. A. & DIANOV, G. L. 2001. Human DNA polymerase beta initiates DNA synthesis during long-patch repair of reduced AP sites in DNA. *EMBO J,* 20**,** 1477-82.

POSPELOVA, T. V., DEMIDENKO, Z. N., BUKREEVA, E. I., POSPELOV, V. A., GUDKOV, A. V. & BLAGOSKLONNY, M. V. 2009. Pseudo-DNA damage response in senescent cells. *Cell Cycle,* 8**,** 4112-8.

RAPALI, P., GARCIA-MAYORAL, M. F., MARTINEZ-MORENO, M., TARNOK, K., SCHLETT, K., ALBAR, J. P., BRUIX, M., NYITRAY, L. & RODRIGUEZ-CRESPO, I. 2011. LC8 dynein light chain (DYNLL1) binds to the C-terminal domain of ATM-interacting protein (ATMIN/ASCIZ) and regulates its subcellular localization. *Biochem Biophys Res Commun,* 414**,** 493-8.

REID, L. J., SHAKYA, R., MODI, A. P., LOKSHIN, M., CHENG, J. T., JASIN, M., BAER, R. & LUDWIG, T. 2008. E3 ligase activity of BRCA1 is not essential for mammalian cell viability or homology-directed repair of double-strand DNA breaks. *Proc Natl Acad Sci U S A,* 105**,** 20876-81.

RIBALLO, E., KUHNE, M., RIEF, N., DOHERTY, A., SMITH, G. C., RECIO, M. J., REIS, C., DAHM, K., FRICKE, A., KREMPLER, A., PARKER, A. R., JACKSON, S. P., GENNERY, A., JEGGO, P. A. & LOBRICH, M. 2004. A pathway of double-strand break rejoining dependent upon ATM, Artemis, and proteins locating to gamma-H2AX foci. *Mol Cell,* 16**,** 715-24.

ROBERTS, S. A., STRANDE, N., BURKHALTER, M. D., STROM, C., HAVENER, J. M., HASTY, P. & RAMSDEN, D. A. 2010. Ku is a 5'-dRP/AP lyase that excises nucleotide damage near broken ends. *Nature,* 464**,** 1214-7.

RODRIGUEZ-BRAVO, V., GUAITA-ESTERUELAS, S., FLORENSA, R., BACHS, O. & AGELL, N. 2006. Chk1- and claspin-dependent but ATR/ATM- and Rad17-independent DNA replication checkpoint response in HeLa cells. *Cancer Res,* 66**,** 8672-9.

ROUZEAU, S., CORDELIERES, F. P., BUHAGIAR-LABARCHEDE, G., HURBAIN, I., ONCLERCQ-DELIC, R., GEMBLE, S., MAGNAGHI-JAULIN, L., JAULIN, C. & AMOR-GUERET, M. 2012. Bloom's syndrome and PICH helicases cooperate with topoisomerase IIalpha in centromere disjunction before anaphase. *PLoS One,* 7**,** e33905.

RUSSO, M. T., DE LUCA, G., DEGAN, P., PARLANTI, E., DOGLIOTTI, E., BARNES, D. E., LINDAHL, T., YANG, H., MILLER, J. H. & BIGNAMI, M. 2004. Accumulation of the oxidative base lesion 8-hydroxyguanine in DNA of tumor-prone mice defective in both the Myh and Ogg1 DNA glycosylases. *Cancer Res,* 64**,** 4411-4.

SAKAMOTO, K., TOMINAGA, Y., YAMAUCHI, K., NAKATSU, Y., SAKUMI, K., YOSHIYAMA, K., EGASHIRA, A., KURA, S., YAO, T., TSUNEYOSHI, M., MAKI, H., NAKABEPPU, Y. & TSUZUKI, T. 2007. MUTYH-null mice are susceptible to spontaneous and oxidative stress induced intestinal tumorigenesis. *Cancer Res,* 67**,** 6599-604.

SAKUMI, K., TOMINAGA, Y., FURUICHI, M., XU, P., TSUZUKI, T., SEKIGUCHI, M. & NAKABEPPU, Y. 2003. Ogg1 knockout-associated lung tumorigenesis and its suppression by Mth1 gene disruption. *Cancer Res,* 63**,** 902-5.

SARKARIA, J. N., BUSBY, E. C., TIBBETTS, R. S., ROOS, P., TAYA, Y., KARNITZ, L. M. & ABRAHAM, R. T. 1999. Inhibition of ATM and ATR kinase activities by the radiosensitizing agent, caffeine. *Cancer Res,* 59**,** 4375-82.

SATO, K., SUNDARAMOORTHY, E., RAJENDRA, E., HATTORI, H., JEYASEKHARAN, A. D., AYOUB, N., SCHIESS, R., AEBERSOLD, R., NISHIKAWA, H., SEDUKHINA, A. S., WADA, H., OHTA, T. & VENKITARAMAN, A. R. 2012. A DNA-damage selective role for BRCA1 E3 ligase in claspin ubiquitylation, CHK1 activation, and DNA repair. *Curr Biol,* 22**,** 1659-66.

SAUGAR, I., PARKER, J. L., ZHAO, S. & ULRICH, H. D. 2012. The genome maintenance factor Mgs1 is targeted to sites of replication stress by ubiquitylated PCNA. *Nucleic Acids Res,* 40**,** 245-57.

SAUNDERS, D. N., HIRD, S. L., WITHINGTON, S. L., DUNWOODIE, S. L., HENDERSON, M. J., BIBEN, C., SUTHERLAND, R. L., ORMANDY, C. J. & WATTS, C. K. 2004. Edd, the murine hyperplastic disc gene, is essential for yolk sac vascularization and chorioallantoic fusion. *Mol Cell Biol,* 24**,** 7225-34.

SAVITSKY, K., SFEZ, S., TAGLE, D. A., ZIV, Y., SARTIEL, A., COLLINS, F. S., SHILOH, Y. & ROTMAN, G. 1995. The complete sequence of the coding region of the ATM gene reveals similarity to cell cycle regulators in different species. *Hum Mol Genet,* 4**,** 2025-32.

SCHAR, P., FASI, M. & JESSBERGER, R. 2004. SMC1 coordinates DNA double-strand break repair pathways. *Nucleic Acids Res,* 32**,** 3921-9.

SHAKYA, R., REID, L. J., RECZEK, C. R., COLE, F., EGLI, D., LIN, C. S., DEROOIJ, D. G., HIRSCH, S., RAVI, K., HICKS, J. B., SZABOLCS, M., JASIN, M., BAER, R. & LUDWIG, T. 2011. BRCA1 tumor suppression depends on BRCT phosphoprotein binding, but not its E3 ligase activity. *Science,* 334**,** 525-8.

SHANBHAG, N. M., RAFALSKA-METCALF, I. U., BALANE-BOLIVAR, C., JANICKI, S. M. & GREENBERG, R. A. 2010. ATM-dependent chromatin changes silence transcription in cis to DNA double-strand breaks. *Cell,* 141**,** 970-81.

SHAO, G., LILLI, D. R., PATTERSON-FORTIN, J., COLEMAN, K. A., MORRISSEY, D. E. & GREENBERG, R. A. 2009. The Rap80-BRCC36 de-ubiquitinating enzyme complex antagonizes RNF8-Ubc13-dependent ubiquitination events at DNA double strand breaks. *Proc Natl Acad Sci U S A,* 106**,** 3166-71.

SHIBATA, A., BARTON, O., NOON, A. T., DAHM, K., DECKBAR, D., GOODARZI, A. A., LOBRICH, M. & JEGGO, P. A. 2010. Role of ATM and the damage response mediator proteins 53BP1 and MDC1 in the maintenance of G(2)/M checkpoint arrest. *Mol Cell Biol,* 30**,** 3371-83.

SHINOHARA, A. & OGAWA, T. 1998. Stimulation by Rad52 of yeast Rad51-mediated recombination. *Nature,* 391**,** 404-7.

SHIOTANI, B., NGUYEN, H. D., HAKANSSON, P., MARECHAL, A., TSE, A., TAHARA, H. & ZOU, L. 2013. Two distinct modes of ATR activation orchestrated by Rad17 and Nbs1. *Cell Rep,* 3**,** 1651-62.

SIEBER, O. M., HOWARTH, K. M., THIRLWELL, C., ROWAN, A., MANDIR, N., GOODLAD, R. A., GILKAR, A., SPENCER-DENE, B., STAMP, G., JOHNSON, V., SILVER, A., YANG, H., MILLER, J. H., ILYAS, M. & TOMLINSON, I. P. 2004. Myh deficiency enhances intestinal tumorigenesis in multiple intestinal neoplasia (ApcMin/+) mice. *Cancer Res,* 64**,** 8876-81.

SMITS, V. A., REAPER, P. M. & JACKSON, S. P. 2006. Rapid PIKK-dependent release of Chk1 from chromatin promotes the DNA-damage checkpoint response. *Curr Biol,* 16**,** 150-9.

SO, S., DAVIS, A. J. & CHEN, D. J. 2009. Autophosphorylation at serine 1981 stabilizes ATM at DNA damage sites. *J Cell Biol,* 187**,** 977-90.

SORENSEN, C. S., SYLJUASEN, R. G., FALCK, J., SCHROEDER, T., RONNSTRAND, L., KHANNA, K. K., ZHOU, B. B., BARTEK, J. & LUKAS, J. 2003. Chk1 regulates the S phase checkpoint by coupling the physiological turnover and ionizing radiation-induced accelerated proteolysis of Cdc25A. *Cancer Cell,* 3**,** 247-58.

SOUTOGLOU, E., DORN, J. F., SENGUPTA, K., JASIN, M., NUSSENZWEIG, A., RIED, T., DANUSER, G. & MISTELI, T. 2007. Positional stability of single double-strand breaks in mammalian cells. *Nat Cell Biol,* 9**,** 675-82.

SOUTOGLOU, E. & MISTELI, T. 2008. Activation of the cellular DNA damage response in the absence of DNA lesions. *Science,* 320**,** 1507-10.

SOWD, G. A., LI, N. Y. & FANNING, E. 2013. ATM and ATR activities maintain replication fork integrity during SV40 chromatin replication. *PLoS Pathog,* 9**,** e1003283.

SRIVASTAVA, D. K., BERG, B. J., PRASAD, R., MOLINA, J. T., BEARD, W. A., TOMKINSON, A. E. & WILSON, S. H. 1998. Mammalian abasic site base excision repair. Identification of the reaction sequence and rate-determining steps. *J Biol Chem,* 273**,** 21203-9.

STELTER, P. & ULRICH, H. D. 2003. Control of spontaneous and damage-induced mutagenesis by SUMO and ubiquitin conjugation. *Nature,* 425**,** 188-91.

STEWART, G. S., PANIER, S., TOWNSEND, K., AL-HAKIM, A. K., KOLAS, N. K., MILLER, E. S., NAKADA, S., YLANKO, J., OLIVARIUS, S., MENDEZ, M., OLDREIVE, C., WILDENHAIN, J., TAGLIAFERRO, A., PELLETIER, L., TAUBENHEIM, N., DURANDY, A., BYRD, P. J., STANKOVIC, T., TAYLOR, A. M. & DUROCHER, D. 2009. The RIDDLE syndrome protein mediates a ubiquitin-dependent signaling cascade at sites of DNA damage. *Cell,* 136**,** 420-34.

STEWART, G. S., STANKOVIC, T., BYRD, P. J., WECHSLER, T., MILLER, E. S., HUISSOON, A., DRAYSON, M. T., WEST, S. C., ELLEDGE, S. J. & TAYLOR, A. M. 2007. RIDDLE immunodeficiency syndrome is linked to defects in 53BP1-mediated DNA damage signaling. *Proc Natl Acad Sci U S A,* 104**,** 16910-5.

STIFF, T., CEROSALETTI, K., CONCANNON, P., O'DRISCOLL, M. & JEGGO, P. A. 2008. Replication independent ATR signalling leads to G2/M arrest requiring Nbs1, 53BP1 and MDC1. *Hum Mol Genet,* 17**,** 3247-53.

STIFF, T., WALKER, S. A., CEROSALETTI, K., GOODARZI, A. A., PETERMANN, E., CONCANNON, P., O'DRISCOLL, M. & JEGGO, P. A. 2006. ATR-dependent phosphorylation and activation of ATM in response to UV treatment or replication fork stalling. *EMBO J,* 25**,** 5775-82.

STUCKI, M., CLAPPERTON, J. A., MOHAMMAD, D., YAFFE, M. B., SMERDON, S. J. & JACKSON, S. P. 2005. MDC1 directly binds phosphorylated histone H2AX to regulate cellular responses to DNA double-strand breaks. *Cell,* 123**,** 1213-26.

SUGIMURA, H., KOHNO, T., WAKAI, K., NAGURA, K., GENKA, K., IGARASHI, H., MORRIS, B. J., BABA, S., OHNO, Y., GAO, C., LI, Z., WANG, J., TAKEZAKI, T., TAJIMA, K., VARGA, T., SAWAGUCHI, T., LUM, J. K., MARTINSON, J. J., TSUGANE, S., IWAMASA, T., SHINMURA, K. & YOKOTA, J. 1999. hOGG1 Ser326Cys polymorphism and lung cancer susceptibility. *Cancer Epidemiol Biomarkers Prev,* 8**,** 669-74.

SUN, Y., JIANG, X., CHEN, S., FERNANDES, N. & PRICE, B. D. 2005. A role for the Tip60 histone acetyltransferase in the acetylation and activation of ATM. *Proc Natl Acad Sci U S A,* 102**,** 13182-7.

SUN, Y., XU, Y., ROY, K. & PRICE, B. D. 2007. DNA damage-induced acetylation of lysine 3016 of ATM activates ATM kinase activity. *Mol Cell Biol,* 27**,** 8502-9.

SUNG, P. 1997. Function of yeast Rad52 protein as a mediator between replication protein A and the Rad51 recombinase. *J Biol Chem,* 272**,** 28194-7.

TAKAGI, Y., SETOYAMA, D., ITO, R., KAMIYA, H., YAMAGATA, Y. & SEKIGUCHI, M. 2012. Human MTH3 (NUDT18) protein hydrolyzes oxidized forms of guanosine and deoxyguanosine diphosphates: comparison with MTH1 and MTH2. *J Biol Chem,* 287**,** 21541-9.

TAUCHI, H., KOBAYASHI, J., MORISHIMA, K., MATSUURA, S., NAKAMURA, A., SHIRAISHI, T., ITO, E., MASNADA, D., DELIA, D. & KOMATSU, K. 2001. The forkhead-associated domain of NBS1 is essential for nuclear foci formation after irradiation but not essential for hRAD50[middle dot]hMRE11[middle dot]NBS1 complex DNA repair activity. *J Biol Chem,* 276**,** 12-5.

TAYLOR, A. M., GROOM, A. & BYRD, P. J. 2004. Ataxia-telangiectasia-like disorder (ATLD)-its clinical presentation and molecular basis. *DNA Repair (Amst),* 3**,** 1219-25.

THEUNISSEN, J. W., KAPLAN, M. I., HUNT, P. A., WILLIAMS, B. R., FERGUSON, D. O., ALT, F. W. & PETRINI, J. H. 2003. Checkpoint failure and chromosomal instability without lymphomagenesis in Mre11(ATLD1/ATLD1) mice. *Mol Cell,* 12**,** 1511-23.

TRENZ, K., SMITH, E., SMITH, S. & COSTANZO, V. 2006. ATM and ATR promote Mre11 dependent restart of collapsed replication forks and prevent accumulation of DNA breaks. *EMBO J,* 25**,** 1764-74.

TSAI, C. J., KIM, S. A. & CHU, G. 2007. Cernunnos/XLF promotes the ligation of mismatched and noncohesive DNA ends. *Proc Natl Acad Sci U S A,* 104**,** 7851-6.

TSUJI, Y., WATANABE, K., ARAKI, K., SHINOHARA, M., YAMAGATA, Y., TSURIMOTO, T., HANAOKA, F., YAMAMURA, K., YAMAIZUMI, M. & TATEISHI, S. 2008. Recognition of forked and single-stranded DNA structures by human RAD18 complexed with RAD6B protein triggers its recruitment to stalled replication forks. *Genes Cells,* 13**,** 343-54.

TSUZUKI, T., EGASHIRA, A., IGARASHI, H., IWAKUMA, T., NAKATSURU, Y., TOMINAGA, Y., KAWATE, H., NAKAO, K., NAKAMURA, K., IDE, F., KURA, S., NAKABEPPU, Y., KATSUKI, M., ISHIKAWA, T. & SEKIGUCHI, M. 2001a. Spontaneous tumorigenesis in mice defective in the MTH1 gene encoding 8-oxo-dGTPase. *Proc Natl Acad Sci U S A,* 98**,** 11456-61.

TSUZUKI, T., EGASHIRA, A. & KURA, S. 2001b. Analysis of MTH1 gene function in mice with targeted mutagenesis. *Mutat Res,* 477**,** 71-8.

UZIEL, T., LERENTHAL, Y., MOYAL, L., ANDEGEKO, Y., MITTELMAN, L. & SHILOH, Y. 2003. Requirement of the MRN complex for ATM activation by DNA damage. *EMBO J,* 22**,** 5612-21.

VAN DER KEMP, P. A., THOMAS, D., BARBEY, R., DE OLIVEIRA, R. & BOITEUX, S. 1996. Cloning and expression in Escherichia coli of the OGG1 gene of Saccharomyces cerevisiae, which codes for a DNA glycosylase that excises 7,8-dihydro-8-oxoguanine and 2,6-diamino-4-hydroxy-5-N-methylformamidopyrimidine. *Proc Natl Acad Sci U S A,* 93**,** 5197-202.

VAN LOON, B., MARKKANEN, E. & HUBSCHER, U. 2010. Oxygen as a friend and enemy: How to combat the mutational potential of 8-oxo-guanine. *DNA Repair (Amst),* 9**,** 604-16.

VILENCHIK, M. M. & KNUDSON, A. G. 2003. Endogenous DNA double-strand breaks: production, fidelity of repair, and induction of cancer. *Proc Natl Acad Sci U S A,* 100**,** 12871-6.

WALKER, J. R., CORPINA, R. A. & GOLDBERG, J. 2001. Structure of the Ku heterodimer bound to DNA and its implications for double-strand break repair. *Nature,* 412**,** 607-14.

WALTES, R., KALB, R., GATEI, M., KIJAS, A. W., STUMM, M., SOBECK, A., WIELAND, B., VARON, R., LERENTHAL, Y., LAVIN, M. F., SCHINDLER, D. & DORK, T. 2009. Human RAD50 deficiency in a Nijmegen breakage syndrome-like disorder. *Am J Hum Genet,* 84**,** 605-16.

WANG, B. & ELLEDGE, S. J. 2007. Ubc13/Rnf8 ubiquitin ligases control foci formation of the Rap80/Abraxas/Brca1/Brcc36 complex in response to DNA damage. *Proc Natl Acad Sci U S A,* 104**,** 20759-63.

WANG, N. D., TESTA, J. R. & SMITH, D. I. 1993. Determination of the specificity of aphidicolin-induced breakage of the human 3p14.2 fragile site. *Genomics,* 17**,** 341-7.

WATANABE, K., TATEISHI, S., KAWASUJI, M., TSURIMOTO, T., INOUE, H. & YAMAIZUMI, M. 2004. Rad18 guides poleta to replication stalling sites through physical interaction and PCNA monoubiquitination. *EMBO J,* 23**,** 3886-96.

WEISER, T., GASSMANN, M., THOMMES, P., FERRARI, E., HAFKEMEYER, P. & HUBSCHER, U. 1991. Biochemical and functional comparison of DNA polymerases alpha, delta, and epsilon from calf thymus. *J Biol Chem,* 266**,** 10420-8.

WERTZ, I. E., O'ROURKE, K. M., ZHOU, H., EBY, M., ARAVIND, L., SESHAGIRI, S., WU, P., WIESMANN, C., BAKER, R., BOONE, D. L., MA, A., KOONIN, E. V. & DIXIT, V. M. 2004. De-ubiquitination and ubiquitin ligase domains of A20 downregulate NF-kappaB signalling. *Nature,* 430**,** 694-9.

WESTPHAL, C. H., ROWAN, S., SCHMALTZ, C., ELSON, A., FISHER, D. E. & LEDER, P. 1997. atm and p53 cooperate in apoptosis and suppression of tumorigenesis, but not in resistance to acute radiation toxicity. *Nat Genet,* 16**,** 397-401.

WHITEMAN, M., HONG, H. S., JENNER, A. & HALLIWELL, B. 2002. Loss of oxidized and chlorinated bases in DNA treated with reactive oxygen species: implications for assessment of oxidative damage in vivo. *Biochem Biophys Res Commun,* 296**,** 883-9.

WIEDERHOLD, L., LEPPARD, J. B., KEDAR, P., KARIMI-BUSHERI, F., RASOULI-NIA, A., WEINFELD, M., TOMKINSON, A. E., IZUMI, T., PRASAD, R., WILSON, S. H., MITRA, S. & HAZRA, T. K. 2004. AP endonuclease-independent DNA base excision repair in human cells. *Mol Cell,* 15**,** 209-20.

WIENER, R., ZHANG, X., WANG, T. & WOLBERGER, C. 2012. The mechanism of OTUB1-mediated inhibition of ubiquitination. *Nature,* 483**,** 618-22.

WILCOX, C. S. 2010. Effects of tempol and redox-cycling nitroxides in models of oxidative stress. *Pharmacol Ther,* 126**,** 119-45.

WILLIAMS, B. R., MIRZOEVA, O. K., MORGAN, W. F., LIN, J., DUNNICK, W. & PETRINI, J. H. 2002. A murine model of Nijmegen breakage syndrome. *Curr Biol,* 12**,** 648-53.

WILLIAMS, G. J., LEES-MILLER, S. P. & TAINER, J. A. 2010. Mre11-Rad50-Nbs1 conformations and the control of sensing, signaling, and effector responses at DNA double-strand breaks. *DNA Repair (Amst),* 9**,** 1299-306.

WILLIAMS, J. R., ZHANG, Y., RUSSELL, J., KOCH, C. & LITTLE, J. B. 2007. Human tumor cells segregate into radiosensitivity groups that associate with ATM and TP53 status. *Acta Oncol,* 46**,** 628-38.

WILLIAMS, R. S., DODSON, G. E., LIMBO, O., YAMADA, Y., WILLIAMS, J. S., GUENTHER, G., CLASSEN, S., GLOVER, J. N., IWASAKI, H., RUSSELL, P. &

TAINER, J. A. 2009. Nbs1 flexibly tethers Ctp1 and Mre11-Rad50 to coordinate DNA double-strand break processing and repair. *Cell,* 139**,** 87-99.

WILLIAMS, R. S., MONCALIAN, G., WILLIAMS, J. S., YAMADA, Y., LIMBO, O., SHIN, D. S., GROOCOCK, L. M., CAHILL, D., HITOMI, C., GUENTHER, G., MOIANI, D., CARNEY, J. P., RUSSELL, P. & TAINER, J. A. 2008. Mre11 dimers coordinate DNA end bridging and nuclease processing in double-strand-break repair. *Cell,* 135**,** 97-109.

WU, C. Y., KANG, H. Y., YANG, W. L., WU, J., JEONG, Y. S., WANG, J., CHAN, C. H., LEE, S. W., ZHANG, X., LAMOTHE, B., CAMPOS, A. D., DARNAY, B. G. & LIN, H. K. 2011a. Critical role of monoubiquitination of histone H2AX protein in histone H2AX phosphorylation and DNA damage response. *J Biol Chem,* 286**,** 30806-15.

WU, J., CHEN, Y., LU, L. Y., WU, Y., PAULSEN, M. T., LJUNGMAN, M., FERGUSON, D. O. & YU, X. 2011b. Chfr and RNF8 synergistically regulate ATM activation. *Nat Struct Mol Biol,* 18**,** 761-8.

WU, J., ZHANG, X., ZHANG, L., WU, C. Y., REZAEIAN, A. H., CHAN, C. H., LI, J. M., WANG, J., GAO, Y., HAN, F., JEONG, Y. S., YUAN, X., KHANNA, K. K., JIN, J., ZENG, Y. X. & LIN, H. K. 2012. Skp2 E3 ligase integrates ATM activation and homologous recombination repair by ubiquitinating NBS1. *Mol Cell,* 46**,** 351-61.

WU, L. & HICKSON, I. D. 2006. DNA helicases required for homologous recombination and repair of damaged replication forks. *Annu Rev Genet,* 40**,** 279-306.

WU, X., RANGANATHAN, V., WEISMAN, D. S., HEINE, W. F., CICCONE, D. N., O'NEILL, T. B., CRICK, K. E., PIERCE, K. A., LANE, W. S., RATHBUN, G., LIVINGSTON, D. M. & WEAVER, D. T. 2000. ATM phosphorylation of Nijmegen breakage syndrome protein is required in a DNA damage response. *Nature,* 405**,** 477-82.

WYATT, H. D., SARBAJNA, S., MATOS, J. & WEST, S. C. 2013. Coordinated Actions of SLX1-SLX4 and MUS81-EME1 for Holliday Junction Resolution in Human Cells. *Mol Cell,* 52**,** 234-47.

XIA, F., TAGHIAN, D. G., DEFRANK, J. S., ZENG, Z. C., WILLERS, H., ILIAKIS, G. & POWELL, S. N. 2001. Deficiency of human BRCA2 leads to impaired homologous recombination but maintains normal nonhomologous end joining. *Proc Natl Acad Sci U S A,* 98**,** 8644-9.

XIA, Y., PAO, G. M., CHEN, H. W., VERMA, I. M. & HUNTER, T. 2003. Enhancement of BRCA1 E3 ubiquitin ligase activity through direct interaction with the BARD1 protein. *J Biol Chem,* 278**,** 5255-63.

XIE, Y., YANG, H., CUNANAN, C., OKAMOTO, K., SHIBATA, D., PAN, J., BARNES, D. E., LINDAHL, T., MCILHATTON, M., FISHEL, R. & MILLER, J. H. 2004. Deficiencies in mouse Myh and Ogg1 result in tumor predisposition and G to T mutations in codon 12 of the K-ras oncogene in lung tumors. *Cancer Res,* 64**,** 3096-102.

XUE, Q., ZHOU, Z., LEI, X., LIU, X., HE, B., WANG, J. & HUNG, T. 2012. TRIM38 negatively regulates TLR3-mediated IFN-beta signaling by targeting TRIF for degradation. *PLoS One,* 7**,** e46825.

YAGUCHI, H., OKUMURA, F., TAKAHASHI, H., KANO, T., KAMEDA, H., UCHIGASHIMA, M., TANAKA, S., WATANABE, M., SASAKI, H. & HATAKEYAMA, S. 2012. TRIM67 protein negatively regulates Ras activity through degradation of 80K-H and induces neuritogenesis. *J Biol Chem,* 287**,** 12050-9.

YANG, Y. G., SAIDI, A., FRAPPART, P. O., MIN, W., BARRUCAND, C., DUMON-JONES, V., MICHELON, J., HERCEG, Z. & WANG, Z. Q. 2006. Conditional deletion of Nbs1 in murine cells reveals its role in branching repair pathways of DNA double-strand breaks. *EMBO J,* 25**,** 5527-38.

YIN, Z., MENENDEZ, D., RESNICK, M. A., FRENCH, J. E., JANARDHAN, K. S. & JETTEN, A. M. 2012. RAP80 is critical in maintaining genomic stability and suppressing tumor development. *Cancer Res,* 72**,** 5080-90.

YOO, S. & DYNAN, W. S. 1999. Geometry of a complex formed by double strand break repair proteins at a single DNA end: recruitment of DNA-PKcs induces inward translocation of Ku protein. *Nucleic Acids Res,* 27**,** 4679-86.

YOSHIDA, M., YOSHIDA, K., KOZLOV, G., LIM, N. S., DE CRESCENZO, G., PANG, Z., BERLANGA, J. J., KAHVEJIAN, A., GEHRING, K., WING, S. S. & SONENBERG, N. 2006. Poly(A) binding protein (PABP) homeostasis is mediated by the stability of its inhibitor, Paip2. *EMBO J,* 25**,** 1934-44.

YOU, Z., BAILIS, J. M., JOHNSON, S. A., DILWORTH, S. M. & HUNTER, T. 2007. Rapid activation of ATM on DNA flanking double-strand breaks. *Nat Cell Biol,* 9**,** 1311-8.

YOU, Z., CHAHWAN, C., BAILIS, J., HUNTER, T. & RUSSELL, P. 2005. ATM activation and its recruitment to damaged DNA require binding to the C terminus of Nbs1. *Mol Cell Biol,* 25**,** 5363-79.

YU, X., FU, S., LAI, M., BAER, R. & CHEN, J. 2006. BRCA1 ubiquitinates its phosphorylation-dependent binding partner CtIP. *Genes Dev,* 20**,** 1721-6.

ZHANG, J., WILLERS, H., FENG, Z., GHOSH, J. C., KIM, S., WEAVER, D. T., CHUNG, J. H., POWELL, S. N. & XIA, F. 2004. Chk2 phosphorylation of BRCA1 regulates DNA double-strand break repair. *Mol Cell Biol,* 24**,** 708-18.

ZHANG, T., PENICUD, K., BRUHN, C., LOIZOU, J. I., KANU, N., WANG, Z. Q. & BEHRENS, A. 2012. Competition between NBS1 and ATMIN controls ATM signaling pathway choice. *Cell Rep,* 2**,** 1498-504.

ZHAO, H. & PIWNICA-WORMS, H. 2001. ATR-mediated checkpoint pathways regulate phosphorylation and activation of human Chk1. *Mol Cell Biol,* 21**,** 4129-39.

ZHAO, S., WENG, Y. C., YUAN, S. S., LIN, Y. T., HSU, H. C., LIN, S. C., GERBINO, E., SONG, M. H., ZDZIENICKA, M. Z., GATTI, R. A., SHAY, J. W., ZIV, Y., SHILOH, Y. & LEE, E. Y. 2000. Functional link between ataxia-telangiectasia and Nijmegen breakage syndrome gene products. *Nature,* 405**,** 473-7.

ZHOU, B. B. & ELLEDGE, S. J. 2000. The DNA damage response: putting checkpoints in perspective. *Nature,* 408**,** 433-9.

ZHU, J., PETERSEN, S., TESSAROLLO, L. & NUSSENZWEIG, A. 2001. Targeted disruption of the Nijmegen breakage syndrome gene NBS1 leads to early embryonic lethality in mice. *Curr Biol,* 11**,** 105-9.

ZIMMERMANN, M., LOTTERSBERGER, F., BUONOMO, S. B., SFEIR, A. & DE LANGE, T. 2013. 53BP1 regulates DSB repair using Rif1 to control 5' end resection. *Science,* 339**,** 700-4.

ZIV, Y., BIELOPOLSKI, D., GALANTY, Y., LUKAS, C., TAYA, Y., SCHULTZ, D. C., LUKAS, J., BEKKER-JENSEN, S., BARTEK, J. & SHILOH, Y. 2006. Chromatin relaxation in response to DNA double-strand breaks is modulated by a novel ATM- and KAP-1 dependent pathway. *Nat Cell Biol,* 8**,** 870-6.

ZOU, L., CORTEZ, D. & ELLEDGE, S. J. 2002. Regulation of ATR substrate selection by Rad17-dependent loading of Rad9 complexes onto chromatin. *Genes Dev,* 16**,** 198-208.

ZOU, L. & ELLEDGE, S. J. 2003. Sensing DNA damage through ATRIP recognition of RPA-ssDNA complexes. *Science,* 300**,** 1542-8.